

COASTFOOC

COAstal Surveillance Through Observation of Ocean Colour

Funded by:

European Commission, 4th RTD FP Environment & Climate
Contract N° ENV4-CT96-0310

Co-Funded by:

European Space Agency

Final Report, 3 January 2000



WeW



Carl v. Ossietzky
UNIVERSITÄT
OLDENBURG





0. EXECUTIVE SUMMARY	1
0.1. PARTNERSHIP	1
0.2. HIGHLIGHTS	1
0.3. RATIONALE	2
0.4. OBJECTIVES (<i>as initially stated in the Work Programme</i>)	2
0.5. ACHIEVEMENTS	3
0.6. EVALUATION	3
0.7. EXPLOITATION PLAN	3
0.8. RELATED PUBLICATIONS	4
0.9. CONCLUSIONS	5
1. INTRODUCTION	5
1.1. OBJECTIVES (<i>as initially stated</i>)	5
1.2. CONTEXT	6
1.3. PRESENTATION OF THE CONSORTIUM	7
2. WORK ACHIEVED AND RESULTS	10
2.1. OVERVIEW.....	10
2.2. FIELD WORK	12
2.2.1. <i>Sampling platforms and Field Campaigns</i>	12
2.2.2. <i>Measurements</i>	32
2.2.3. <i>Data processing</i>	38
2.2.3.1. Processing chain for multiple instruments system: Methodology and tool description	38
2.2.3.1.1. Methodology.....	39
2.2.3.1.1.1. Packet validation	39
2.2.3.1.1.2. Time stamping	39
2.2.3.1.1.3. Depth stamping	40
2.2.3.1.1.4. Depth merging	40
2.2.3.1.1.5. Global processing flow	40
2.2.3.1.2. Filters	41
2.2.3.1.3. Recommendations	44
2.2.3.1.3.1. Data collection protocol	44
2.2.3.1.3.2. Surface data computation	44
2.2.3.1.3.3. Self sufficient instruments	44
2.2.3.1.3.4. A User Interface to provide easy quality control	45
2.2.3.1.3.5. Reminder of the different hurdles to pass	45
2.2.3.2. Interpretation of the vertical profiles and outputs for a surface data base	46
2.2.3.2.1. SADAM – The SATLANTIC Data Manager	46
2.2.3.2.1.1. Requirements	47
2.2.3.2.1.2. Post-processing of raw data	47
2.2.3.2.1.3. Depth merging and binning	48
2.2.3.2.1.4. Surface extrapolation	48
2.2.3.2.2. IDL tool for interpretation of absorption, attenuation and backscattering coefficients profiles	53
2.2.3.3. Data bases	60
2.2.3.3.1. The Database	60
2.2.3.3.2. The www video server	60
2.2.3.3.3. Perspectives for future	62
2.3. PARAMETERISATION OF IOPS	62
2.3.1. <i>Bacteria</i>	62
2.3.1.1. Instrument Description	63
2.3.1.2. Methodology and Processing Description	64
2.3.1.3. Data analysis and classification	64
2.3.1.4. Results	64
2.3.2. <i>Phytoplankton species composition</i>	66
2.3.2.1. Notes on cell counts from COAST/OOC campaigns	67
2.3.2.1.1. Method	67
2.3.2.1.2. Discussion of error sources	67



2.3.2.2. Results on a campaign basis	68
2.3.3. Phytoplankton pigments	71
2.3.4. DOC vs. CDOM relationship, POC	77
2.3.5. Particle absorption spectra measured in the laboratory.....	80
2.3.6. Chl, Y and SPM variability	81
2.3.7. IOP variability	85
2.3.8. IOP variability as determined from the measurements performed using the Oldenburg instrument package	96
2.3.8.1. Material and Methods	96
2.3.8.1.1. Multi-channel fluorometer:.....	96
2.3.8.1.2. Polychromatic daylight radiometer.....	96
2.3.8.1.3. Transmissometer Polychromatic transmissometer PAAL.....	96
2.3.8.1.4. CTD: Meerestechnik Elektronik, OTS 1500.....	96
2.3.8.2. Regions.....	98
2.3.8.2.1. Seine	98
2.3.8.2.2. Humber	102
2.3.8.2.3. German Bight.....	104
2.3.8.2.4. Rhone.....	106
2.4. REFLECTANCE MODELLING.....	110
2.4.1. Proposed Model	110
2.4.1.1. Remotely sensed layer.....	110
2.4.1.2. Water constituents	110
2.4.1.3. Vertical distribution.....	112
2.4.1.4. Inherent optical properties of water and its constituents.....	112
2.4.1.4.1. Pure sea water and phytoplankton	113
2.4.1.4.2. Non-chlorophyllous suspended sediments and gelbstoff	115
2.4.1.4.3. $f(\lambda)$ lookup table calculation.....	116
2.4.1.5. Warning concerning the use of the model: State-of-the-Art and uncertainties	118
2.4.1.6. References	120
2.4.2. Validation.....	120
2.5. ALGORITHM DEVELOPMENT.....	129
2.5.1. Algorithms	129
2.5.1.1. NIOZ band-ratio algorithm.....	129
2.5.1.1.1. Introduction	129
2.5.1.1.2. Instrument description	130
2.5.1.1.2.1. PR650 Spectrascan Spectracolorimeter	130
2.5.1.1.2.2. Satlantic Radiometer	131
2.5.1.1.3. Data collection and processing	131
2.5.1.1.4. Incident spectral irradiance correction	131
2.5.1.1.5. Sun/sky glint correction	133
2.5.1.1.6. Coastal Colour algorithms	135
2.5.1.1.7. Suspended Particulate Matter	135
2.5.1.1.8. Chlorophyll.....	137
2.5.1.1.9. Conclusions and recommendations	139
2.5.1.2. PML band-ratio algorithm	140
2.5.1.2.1. Development of a Reflectance Model	140
2.5.1.2.1.1. The Forward Model	140
2.5.1.2.1.2. Application of The Forward Model to Band Ratio Algorithms	140
2.5.1.2.1.3. Relationship of Band Ratios and IOPs	141
2.5.1.2.2. Development of Novel Band Ratio Algorithms	141
2.5.1.2.2.1. Case I Parameterisation	141
2.5.1.2.2.2. Case II Parameterisation and Retrieval	141
2.5.1.2.2.3. Implementation of the Model	142
2.5.1.2.2.4. Results	142
2.5.1.2.3. Applications	143
2.5.1.2.4. Conclusions	143
2.5.1.2.5. References	152
2.5.1.3. SAI neural network approach	152
2.5.1.4. GKSS Neural Network Algorithm	157
2.5.1.4.1. Overview of activities	157



2.5.1.4.2. GKSS team	157
2.5.1.4.3. Acknowledgements.....	158
2.5.1.4.4. Overview of field activities.....	158
2.5.1.4.5. Retrieval of water constituents from water leaving radiance reflectances by inverse modelling.....	159
2.5.1.4.5.1. Outline of the procedure.....	159
2.5.1.4.5.2. Results of training	162
2.5.1.4.5.3. Tests using MOS scenes.....	163
2.5.1.4.5.4. Summary and Conclusions	168
2.5.1.5. Sun-Induced Chlorophyll Fluorescence algorithm	169
2.5.2. <i>Level 2 ground segment prototype (simulator) adapted to the CASI data</i>	169
2.5.2.1. CASI operations carried out during the COAST/OOC campaigns #3, #4, and #6.....	169
2.5.2.1.1. Objectives	169
2.5.2.1.2. The "Compact Airborne Spectrographic Imager" (CASI)	170
2.5.2.1.3. Calibration of CASI.....	170
2.5.2.1.4. Use of CASI.....	172
2.5.2.1.5. Adaptation of the LPCM MERIS breadboard prototype to CASI specificities.....	173
2.5.2.1.6. Integration of the prototypes corresponding to ATBDs 2.5, 2.6, 2.8, and 2.12.....	174
2.5.2.1.7. The problem of surface roughness	175
2.5.2.1.8. Post-processing of the <i>in situ</i> data : from diffuse reflectances to water-leaving radiances	175
2.5.2.1.8.1. Accounting for changes in solar elevation.....	175
2.5.2.1.8.2. Accounting for the bi-directionality of the diffuse reflectance	176
2.5.2.1.8.3. Accounting for the surface effects.....	177
2.5.2.1.8.4. The downwelling irradiance above the sea surface.....	178
2.5.2.1.9. Application to CASI images (COAST/OOC #3, #4, and #6)	178
2.5.2.1.10. Mapping of the sampling areas	179
2.5.2.1.11. Results in terms of recovery of the spectral reflectance above the sea surface	179
2.5.2.1.12. Results in terms of "CASI-derived" <i>versus in situ</i> geophysical parameters	180
2.5.2.2. Conclusions and perspectives.....	181
2.5.2.3. Notations	199
2.5.2.4. References.....	201
3. DELIVERABLES.....	201
4. DEPARTURE FROM THE WORK PLAN	202
5. CONCLUSIONS & EXPLOITATION PLAN	204
6. ANNEXES	205
6.1. SUN-INDUCED CHLOROPHYLL FLUORESCENCE ALGORITHM	205
6.2. COMPARISON BETWEEN MEASUREMENTS PERFORMED WITH THE CORE INSTRUMENT PACKAGE AND THE PML INSTRUMENTS DURING COAST/OOC-6.	226
6.2.1. <i>Introduction</i>	226
6.2.2. <i>In-situ Fieldwork</i>	226
6.2.2.1. Helicopter Campaign.....	226
6.2.2.2. PML Sampling	226
6.2.3. <i>PML Data Processing</i>	228
6.2.4. <i>Comparison between PML and Helicopter Data</i>	228
6.3. PUBLICATIONS.....	231
6.3.1. <i>Papers</i>	231
6.3.2. <i>Theses</i>	232
6.3.3. <i>Conference papers and abstracts</i>	232
6.4. FORMATION	233
6.5. DATA CDS.....	233

0. EXECUTIVE SUMMARY

0.1. PARTNERSHIP

ACRI	ACRI S. A., France
LPCM	Laboratoire de Physique et Chimie Marines (LPCM), Université Pierre et Marie Curie et Unité Associée CNRS, France
JRC	Space Application Institute, Joint Research Centre (JRC), Italy
U. Oldenburg	University of Oldenburg, Germany
NIOZ	Netherlands Institute for Sea Research, Netherlands
GKSS	GKSS-Forschungszentrum Geesthacht GmbH, Institute of Hydrophysics, Germany
FUB	Free University of Berlin , Germany
U. Trondheim	University of Trondheim, Norway
PML	Plymouth Marine Laboratory, United Kingdom

0.2. HIGHLIGHTS

- COAST/OOC aimed at gathering data on optical properties of coastal waters in order to elaborate algorithms for the interpretation of remotely sensed ocean colour.
- COAST/OOC innovated by using helicopter as sampling platform; technical developments were achieved to adapt instrument deployment and water sampling. It allowed a more efficient and appropriate sampling.
- A total of 424 stations were visited along coasts of the Mediterranean Sea, Adriatic Sea, Baltic Sea, North Sea, English Channel and Atlantic ocean.
- A database has been developed. It contains for all stations, inherent and apparent optical properties of seawater measured *in situ* using optical profilers, as well as a set of variables determined on surface water samples.
- Parameterisations of the inherent optical properties of optically significant seawater constituents were derived.
- A seawater reflectance model was proposed.

*ACRI - LPCM - SAI - U. Oldenburg
 NIOZ - U. Trondheim - FUB - PML - GKSS*

- Development and improvement of ocean colour algorithms was achieved.

0.3. RATIONALE

In marine water studies, satellite remote-sensing represents the most suitable technique for large-scale monitoring. It provides, on a daily basis, synoptic view of the spatial distribution of different biological, chemical and physical variables essential in oceanographic and environmental studies, as well as for resource management. Although processing of remotely-sensed data is typically complex and, therefore, reserved to specialists, the resulting products under the simple form of coloured maps can be easily used by neophytes for qualitative interpretations.

Among information provided by satellite sensors on seawater qualities, ocean colour represents the main tool for monitoring optically significant material. In open ocean, it has been successfully used to produce large-scale maps of phytoplankton biomass distribution and, using bio-optical models, the 3-D distribution of primary production (rate of carbon fixation) at local and global scales. Such products are currently used in environmental programmes such as the Joint Global Ocean Flux Study (JGOFS, IGBP), which aims at determining the role of ocean in the global carbon cycle and related green house effect.

Ocean colour remote-sensing is a well adapted tool for monitoring coastal systems where highly contrasted structures evolve quickly in time and space. However, the exploitation of ocean colour data in coastal waters has greatly been impeded by the incapability to deal with their peculiar optical behaviour and complexity. New ocean colour sensors will allow to deal with this complexity if our knowledge of marine optics in coastal waters is good enough. It opens the way to new perspectives in the issue of surveying and monitoring such zones which are of great economical, environmental and social importance.

COAST/OOC was timely because it aimed at fulfilling well identified gaps in marine optics and ocean colour remote sensing, while several new and improved ocean colour sensors are becoming available with the potential of providing data in real time on a daily basis, at high spatial resolution and with a global coverage. COAST/OOC was mainly motivated by the urgent need for managing coastal zones in regard to coastal management, industrial and urban pollution, fisheries and aquaculture management (*e.g.* red tides), tourism mutual relationship with the environment, etc.

0.4. OBJECTIVES (as initially stated in the Work Programme)

- To produce a large data set of the inherent optical properties of the main classes of optically significant substances in European coastal waters.
- To determine quantitatively the effect of red tides on ocean colour.
- To produce optimised algorithms using the new acquired optical data set, which will allow to produce maps of the main optically significant sea water components (including red tides) using the future ocean colour sensors (new spectral bands).

- To provide operational ocean colour algorithms for specific ocean colour sensors.
- To implement ocean colour analysis into a video server frame, allowing a wide field of users to exploit this information for economically and socially important applications.

COAST/OOC was a 3-year project that started on October 1st, 1996.

0.5. ACHIEVEMENTS

- Database including apparent and inherent optical properties of European coastal waters, together with data processing tools
- Database including water leaving reflectance data measured from an airborne platform simultaneously with *in situ* measurements of optical properties
- IOPs parameterisations for coastal waters
- Reflectance models
- Ocean colour Band-ratio and inverse modelling algorithms valid for European waters
- Simulator of ocean colour satellite sensors including algorithms developed previously during the present study
- A new sampling platform
- Dissemination and training

0.6. EVALUATION

COAST/OOC has been especially successful in supporting the development and improvement of ocean colour algorithms dedicated to coastal waters. The most concrete benefit for users will be the availability of coastal products derived from the processing of the ESA MERIS sensor, which will be launched on June 2001 (see <http://envisat.estec.esa.nl/>).

The COAST/OOC data base will certainly be an important research tool during the next years for the whole international community working on coastal ocean colour remote sensing. This contribution makes COAST/OOC a very successful project.

0.7. EXPLOITATION PLAN

The COAST/OOC data set will be made available to the public on October 1st, 2001. The ocean colour algorithms improved using COAST/OOC data will be definitively implemented within the MERIS processing during year 2000.

*ACRJ - LPCM - SAI - U. Oldenburg
NIOZ - U. Trondheim - FUB - PML - GKSS*

0.8. RELATED PUBLICATIONS

Claustre, H., Fell, F., Oubelkheir, K., Prieur, L., Sciandra, A., Gentilli, B. and M. Babin. 1999. Continuous monitoring of surface optical properties across a geostrophic front: biogeochemical inferences. *Limnology and Oceanography, In press.*

Tassan, S., G. M. Ferrari, A. Bricaud and M. Babin. 1999. Variability of the amplification factor of light absorption by filter-retained aquatic particles in the coastal environment. *Journal of Plankton Res. In press.*

Giovanni M. Ferrari. 2000. The relationship between Chromophoric Dissolved Organic Carbon in European Atlantic Coastal Areas and in West-Mediterranean Sea (Gulf of Lions). *Marine Chemistry, In press.*

Johnsen, Geir & Samset, O. Bio-optical taxonomy in phytoplankton: Field and laboratory studies of potential harmful algal blooms. *In preparation.*

Johnsen, G., Chauton, M. Ferrari, M., Fell, F. Bio-optical and pigment signature as a function fresh water run off and phytoplankton distribution. *In preparation.*

Babin, M., Ferrari, M., Fell, F., Obolensky, G., Fournier-Sicre, V. & Claustre H. Parameterisation of the absorption coefficient in coastal waters. *In preparation.*

Babin, M., Fell, F., Obolensky, G. & Fournier-Sicre, V. Parametrerisation of the scattering coefficient in coastal waters. *In preparation.*

Babin, M., Fell, F., Antoine, D., Ferrari, M., Montagner, F. & Morel, A. A reflectance model for coastal waters. *In preparation.*

Barth, H. 1999. Substanzspezifische Analyse spektraler Attenuationskoeffizienten und ihr Einfluß auf das Strahlungsfeld im Meer. PhD Thesis, Carl von Ossietzky Universität Oldenburg

Schröder, M. 1999. Beiträge durch Fluoreszenz und Raman- Streuung zum Spektrum des Tageslichtes im Ozean. Diploma Thesis, Carl von Ossietzky Universität Oldenburg.

Loisel, H. 1999. Contribution à l'étude des propriétés bio-optiques et du transfert radiatif dans l'océan: applications. Doctorate Thesis, Université Pierre et Marie Curie.

Obolensky, G. 1997. Etude du coefficient de rétrodiffusion de l'eau de mer et de ses variations en fonction de la concentration en particules. Diplôme d'Etudes Approfondies, Université Pierre et Marie Curie.

Lemasle, B. 1998. Propriétés optiques des eaux côtières: Bi-directionalité de la réflectance. Diplôme d'Etudes Approfondies, Université Pierre et Marie Curie.

0.9. CONCLUSIONS

It can be said that COAST/ OOC is a small revolution in the field of coastal ocean colour remote sensing. Although it did not fix every problems in this field, it will for sure allow to explore all of its possibilities.

1. INTRODUCTION

1.1. OBJECTIVES (*as initially stated*)

The general COAST/ OOC 's objective was to develop the necessary tools for exploiting the new potential of the ocean colour technique brought by the launching of improved sensors, over European coasts. The specific objectives were:

Objective #1: *To produce a large data set of the inherent optical properties of the main classes of optically significant substances in European coastal waters.* Relatively to already existing data sets, the one developed in this study would provide the following improvements:

- homogeneous data collection for the whole covered area in terms of the techniques used, operators performing measurements and sampling strategy;
- uses the state-of-the-art instruments and techniques;
- the most extensive sampling grid;
- measurements of inherent optical properties individually for the 3 main classes of sea water optically significant substances.

The target was a data set covering the Mediterranean Sea, the Atlantic Ocean (French and English coasts), the North Sea, The Baltic Sea (including Danish waters), and the Adriatic Sea, and including ca. 150 sampling points per site (total 750 sampling points).

Objective #2: *To determine quantitatively the effect of red tides on ocean colour.* The improvements brought by this study were the following:

- quantitative determination of liposoluble and hydrosoluble phytoplankton pigments using newly developed HPLC protocols;
- simultaneous measurements of all sea water inherent optical properties;
- use of an *in situ* profiler that emulates measurements by ocean colour sensors;
- assessment of the possibility to discriminate the major phytoplankton groups from optical signals, in the frame of an exhaustive chemical and optical analysis.

The target was algorithms allowing to discriminate toxic from non-toxic algal blooms.

*ACRI - LPCM - SAI - U. Ol denburg
NIOZ - U. Trondheim - FUB - PML - GKSS*

Objective #3: To produce new and optimised algorithms using the newly acquired optical data set, which will allow to produce maps of the main optically active sea water components (including red tides) using the future ocean colour sensors (new spectral bands). No proven algorithms presently exist for all European coastal waters. This study will provide a complete set of algorithms allowing to use ocean colour data over all European coasts.

The target was a set of algorithms allowing to derived in coastal waters, the content of chlorophyll, organic matter (dissolved and particulate) and mineral particles.

Objective #4: To provide operational ocean colour algorithms for specific ocean colour sensors. No standard currently exists among the different sensors expected to be launched in the next few years, concerning the way to process ocean colour data over coastal waters. This study will provide such a standard adapted to each of the sensors (SeaWiFS, OCTS, MERIS, MODIS).

The target was a set of coastal water algorithms adapted to each of these sensors.

Objective # 5: To implement ocean colour analysis into a video server frame, allowing a wide field of users to exploit this information for economically and socially important applications.

The target was a video server accessible to all Internet users, that provides day-to-day information on the state of the sea in terms of what can be derived from ocean colour data and related complementary techniques.

1.2. CONTEXT

Radiative transfer in oceanic waters has been approximated successfully by marine opticians during the last decade. These advancements in marine optics allowed the development of reliable ocean colour algorithms for oceanic waters. The lack being common to all attempts to model ocean colour in coastal waters is that of a very good knowledge on all inherent optical properties of coastal water constituents. COAST/OOC aimed at filling the gap in this field by setting a large and complete data set, combining all new technologies in marine optics for the measurement of inherent optical properties, and visiting various sites along European coasts. For the first time, a true concerted effort was proposed in the field of coastal marine optics. The interest of conducting this study at the European level was firstly motivated by the composition of a complete ocean colour remote sensing team. The different expertises necessary in such a team can be found only at the level of Europe. Secondly, the scope of the technique proposed here is obviously of European interest.

Coastal zones support many different economical activities such as vessel traffic, fisheries, fish farming, primary resources exploitation, tourism, etc. These activities induce needs for environmental controls. These controls support the management of coastal resources. Ocean colour remote sensing potentially represents an important link in this ideal retroactive management process.

1.3. PRESENTATION OF THE CONSORTIUM

The COAST/OOC consortium was made of 9 partners: a private company (the co-ordinator), and 8 laboratories from universities or state institutes:

1- ACRI , ACRI S. A., France

ACRI was COAST/OOC 's co-ordinator. ACRI has been strongly involved in Ocean Colour remote sensing and exploitation since its incorporation, mainly through its continuous involvement with the ESA MERIS mission. ACRI is currently leading a scientific group (Expert Support Laboratory) in charge of defining the MERIS data processing algorithms and developing a ground segment prototype. Other areas of research at ACRI involve wave propagation modelling, measurement and remote sensing; diffusion and transport in fluids; data processing for the GOMOS ozone monitoring mission (ESA), etc.

During COAST/OOC 's first year of completion, ACRI has designed the helicopter sampling system (winch specifications, instrument package assembling, configuration of the instrument package communication interface, system installation within the helicopter), supervised field activities and developed the data archiving support. During the second year, ACRI has been involved in all the technical improvements of the sampling platform and in supervising field campaigns. Then ACRI has managed the development and dissemination of the data base. They ultimately proposed a reflectance model and exploited COAST/OOC data for improving the MERIS ground segment simulator.

The main persons involved were Marcel BABIN (the co-ordinator), Grigor Obolensky, Vincent Fournier-Sicre and François Montagner.

2- LPCM, Laboratoire de Physique et Chimie Marines (LPCM), Université Pierre et Marie Curie et Unité Associée CNRS, France

During the past 35 years, LPCM has acquired an international notoriety in the field of marine optics and ocean colour remote sensing. Laboratory and *in situ* measurements of seawater inherent and apparent optical properties have given rise to several publications, which became references in the marine optics community. Simple parameterisation of inherent optical properties were proposed and included into ocean colour models.

During COAST/OOC, LPCM was deeply involved in *in situ* measurements (nearly all field campaigns), laboratory analyses and data interpretation. The two major achievements were IOPs parameterisations and the development of a ground segment prototype adapted to the data delivered by the airborne ocean colour sensor CASI.

The main persons involved were Frank Fell, David, Antoine, Hervé Claustre, Annick Bricaud and André Morel.

3- JRC, Space Application Institute, Joint Research Centre (JRC), Italy

*ACRI - LPCM - SAI - U. Oldenburg
NIOZ - U. Trondheim - FUB - PML - GKSS*

The general scientific programme of the SAI/JRC (Marine Environment division) concerns the application of remote sensing techniques, possibly integrated into wider assessment strategies, for the characterisation and understanding of ecological processes and relationships in the marine environment. This goal is pursued by means of: 1) scientific support activities, including data collections and the development of tools (algorithms and models) for their exploitation; 2) original research activities, either process- or site-oriented, combining remote sensing data and the relevant ancillary information, for the characterisation of the European Seas in terms of their surface optical properties, and of other derived parameters (biomass, primary production); 3) technological activities, including the development of software, of protocols, and of instruments.

During COAST/OOC, JRC was highly involved in field activities as they were responsible of several of laboratory measurements and analyses. Concerning data interpretation, they focused on the relationship between the concentration of dissolved organic carbon (DOC) and CDOM. They also explored the possibility to train a neural network directly on measured Chl, Y, SPM and reflectances, and on this basis proposed a prototype algorithm.

The main persons involved were Massimo Ferrari, Nicolas Hoepffner and Mark Dowell.

4- U. OLDENBURG, University of Oldenburg, Germany

During the last decade, U. Oldenburg has been involved in the development of custom-made in-water optical instruments (spectral radiometer, attenuation meter and fluorometer). These instruments were thoroughly tested and exploited during numerous field campaigns in different regions of the World ocean.

U. Oldenburg used their own “prototype” instrument package, simultaneously with the use of the COAST/OOC “core” instrument package, during four of the COAST/OOC ship campaigns. They highly contributed to the preparation and planning of ship campaigns (COAST/OOC-1, 5 and 6). Their data interpretation focused on the inversion of attenuation to derive IOPs. They were responsible for the local organisation (definition of the sampling grid, laboratory space, logistics, ...) of helicopter measurements performed in the German Bight and in the Baltic Sea.

The main persons involved were Hans Barth and Rainer Reuter.

5- NIOZ, Netherlands Institute for Sea Research, Netherlands

In the past, most of NIOZ activity in marine optics was around development of instruments for in-water measurement of IOPs and apparent optical properties (AOPs), and around interpretation of these measurements. During the last decade, they were involved in the optimisation of band-ratio algorithms dedicated to coastal waters.

During COAST/OOC, NIOZ was in charge on one laboratory analysis (bacteria counting) and involved in band-ratio algorithm development. They were responsible for the local organisation (definition of the sampling grid, laboratory space, logistics, ...) of helicopter measurements performed in Dutch waters.

*ACRJ - LPCM - SAI - U. Oldenburg
NIOZ - U. Trondheim - FUB - PML - GKSS*

The main person involved was Marcel Wernand.

6- GKSS, GKSS-Forschungszentrum Geesthacht GmbH, Institute of Hydrophysics, Germany

GKSS has been for the last decade one of the leaders in the use of inverse modelling techniques for deriving geochemical products from the ocean colour signal in coastal waters. They also introduced the use of neural networks for inversion in this field.

During COAST/OOC, GKSS mostly contributed to design and optimise algorithms based on the inverse modelling and neural network.

The main persons involved were Roland Doerffer and Hans Hakvoort.

7- FUB, Free University of Berlin , Germany

FUB is specialised in atmospheric and ocean radiative transfer. They developed their own radiative transfer code based on the matrix operator method (MOM). They also operated airborne sensors for atmospheric and ocean measurements in the visible range.

In the frame of COAST/OOC, FUB operated their airborne ocean colour imager CASI during three *in situ* measurement campaigns. They then performed the level 0 to level 1 processing of the CASI data (calibration, geo-localisation, ...).

The main persons involved were Carsten Olbert and Jürgen Fischer.

8- U. TRONDHEIM, University of Trondheim, Norway

The U. Trondheim partner is expert in the field of phytoplankton physiology, community ecology, and optical properties (including fluorescence).

During COAST/OOC, they performed the phytoplankton taxonomic analyses on all samples. They conducted a fluorescence analysis to attempt identification of taxonomic groups based on spectral signatures.

The main persons involved were Geir Johnsen, Mathilde Chauton and Egil Sakshaug.

9- PML, Plymouth Marine Laboratory, United Kingdom

PML is known for its expertise on coastal water ocean colour algorithms and atmospheric corrections. In COAST/ OOC, they improved their band ratio algorithm and tested an inversion method that allows to estimate IOPs (especially those that were not measured).

The main persons involved were Gerald Moore, Matthew Pinkerton and Jim Aiken.

*ACRJ - LPCM - SAI - U. Oldenburg
NIOZ - U. Trondheim - FUB - PML - GKSS*

2. WORK ACHIEVED AND RESULTS

2.1. OVERVIEW

The flow chart shown in Figure 0 summarises the scheme followed during COAST/OOC. **The first step** consisted of developing a “reflectance model” that allows to predict the water-leaving reflectance spectrum starting from values of the chlorophyll *a* concentration (Chl), coloured dissolved organic matter concentration (Y, also denoted CDOM and sometime called yellow substance or gelbstoff) and suspended particulate matter concentration (SPM) as input. Note that Chl, Y and SPM are the quantities we ultimately want to derive from the reflectance (ocean colour) signal in coastal waters. An ocean reflectance model essentially consists of the inherent optical properties (IOPs¹) of pure seawater, and of a set of statistical relationships between Chl, Y and SPM, and their respective IOPs. To derive such relationships, we performed measurements at sea of Chl, Y and SPM, and respective IOPs at 424 different locations along European coasts. Additional analyses (phytoplankton species composition, pigment composition, organic carbon concentration, ...) allowed to interpret these relationships.

The second step consisted of validating this reflectance model by comparing reflectances predicted at each COAST/OOC sampling stations (using measured Chl, Y and SPM as input) with those measured *in situ* at the same stations. Reflectance was predicted by using the IOPs provided by the reflectance model into radiative transfer calculations². This exercise was also conducted using reflectances measurement performed quasi-simultaneously using the airborne ocean colour sensor CASI.

The third step consisted of using the reflectance model to develop algorithms for the quantitative interpretation of the ocean reflectance signal in terms of Chl, Y and SPM. Band-ratio and inverse modelling techniques were examined. In both cases, a large set of simulated reflectances was exploited to optimise the algorithms. In the case of inverse modelling, a neural network was trained, while for band ratio algorithms, lookup tables were created. Measured reflectances were then used to validate these algorithms. This activity is still ongoing.

The fourth step consisted of incorporating new algorithms into processing chain prototypes (often called “ground segment”). This was done for the ESA sensor MERIS and the FUB airborne sensor CASI. These “simulators” of the operational processing chains include all steps that go from level 1 (calibrated top-of-atmosphere radiances) to level 2 products (including Chl, Y and SPM), including atmospheric corrections. Such simulators allowed to assess the performances of algorithms when operated in realistic conditions.

¹ IOPs are the spectral values of absorption and scattering coefficients, and the volume scattering function. The latter includes elastic scattering and, eventually, inelastic scattering (essentially Raman scattering and fluorescence).

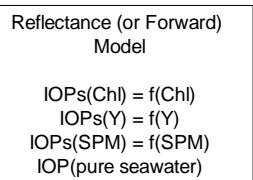
² The consortium runs its own set of radiative transfer codes based on the Monte Carlo and matrix operator methods.



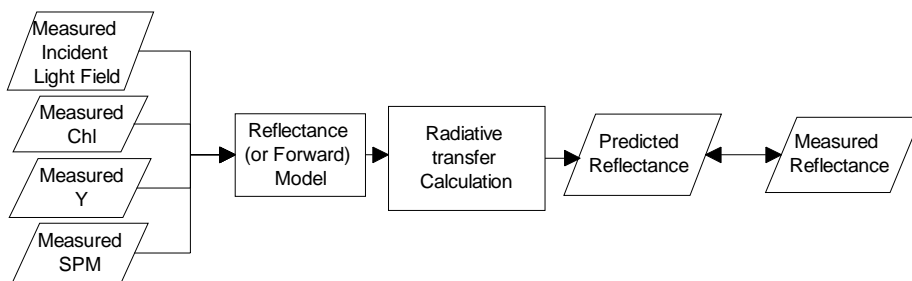
Final Report
ENV4-CT96-0310
03 January 2000

Page: 11

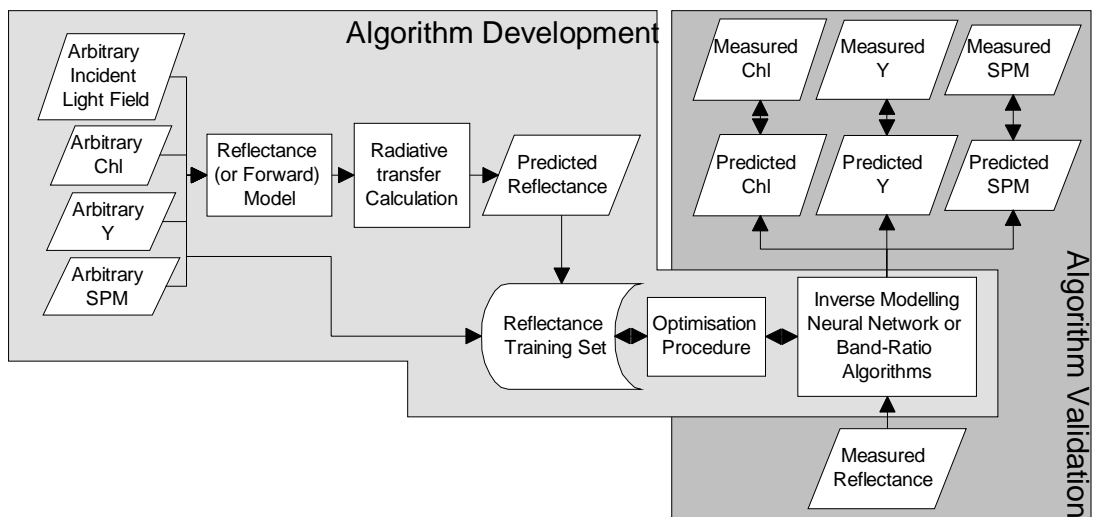
Step 1



Step 2



Step 3



Step 4

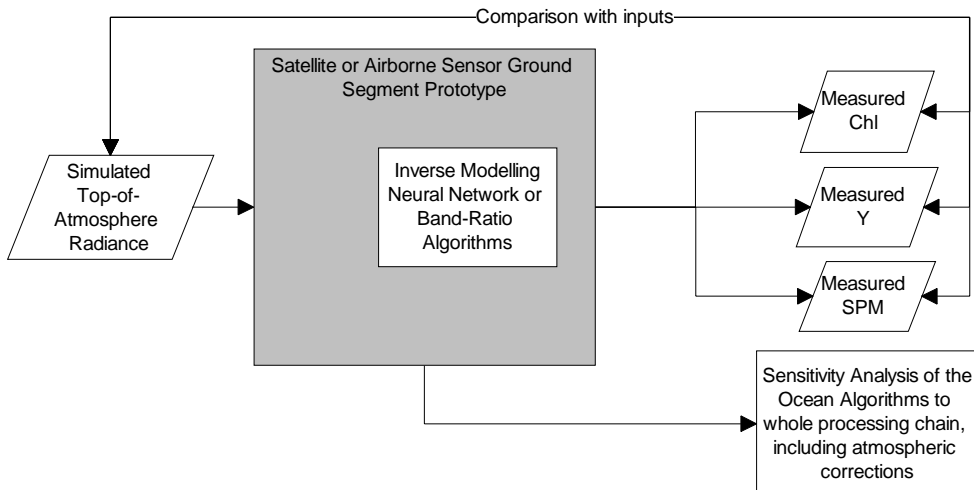


Figure 0. Flowchart illustrating the general approach adopted during COAST/OOC.

2.2. FIELD WORK

2.2.1. Sampling platforms and Field Campaigns

For *in situ* measurements of IOPs, AOPs and related variables, two different platforms were used: ship and helicopter.

The use of helicopter as sampling platform was one of COAST/OOC's main challenge. This challenge has been taken up and the proof-of-concept has been achieved. It led, during COAST/OOC's first year of completion, to a near-operational integrated system. The use of helicopter came up to our expectations: (1) the biasing shade generally produced by ships is avoided, (2) movements often occurring onboard ships is avoided, (3) it allows excellent optical measurement in the water layer very close to surface, which is the most relevant for coastal remote sensing, (4) it allows many stations to be visited within a single day, (5) it allows to conduct sampling only during good weather conditions, *i.e.* to adopt an opportunistic strategy (the use of ship always involves a long term planning and fixed reservations), (6) helicopter surveys allow real-time localisation of fronts which are especially apparent around river plumes following intensive rainfalls; samples can be collected on both sides of fronts to provide the high variability sought for by COAST/OOC, and (7) helicopters are easily available at all sampling sites. It can be stated that the cost of an helicopter sample is lower than a ship sample by 30 to 50%.

Briefly, the helicopter system consisted of the following components (see pictures in Figure 1):

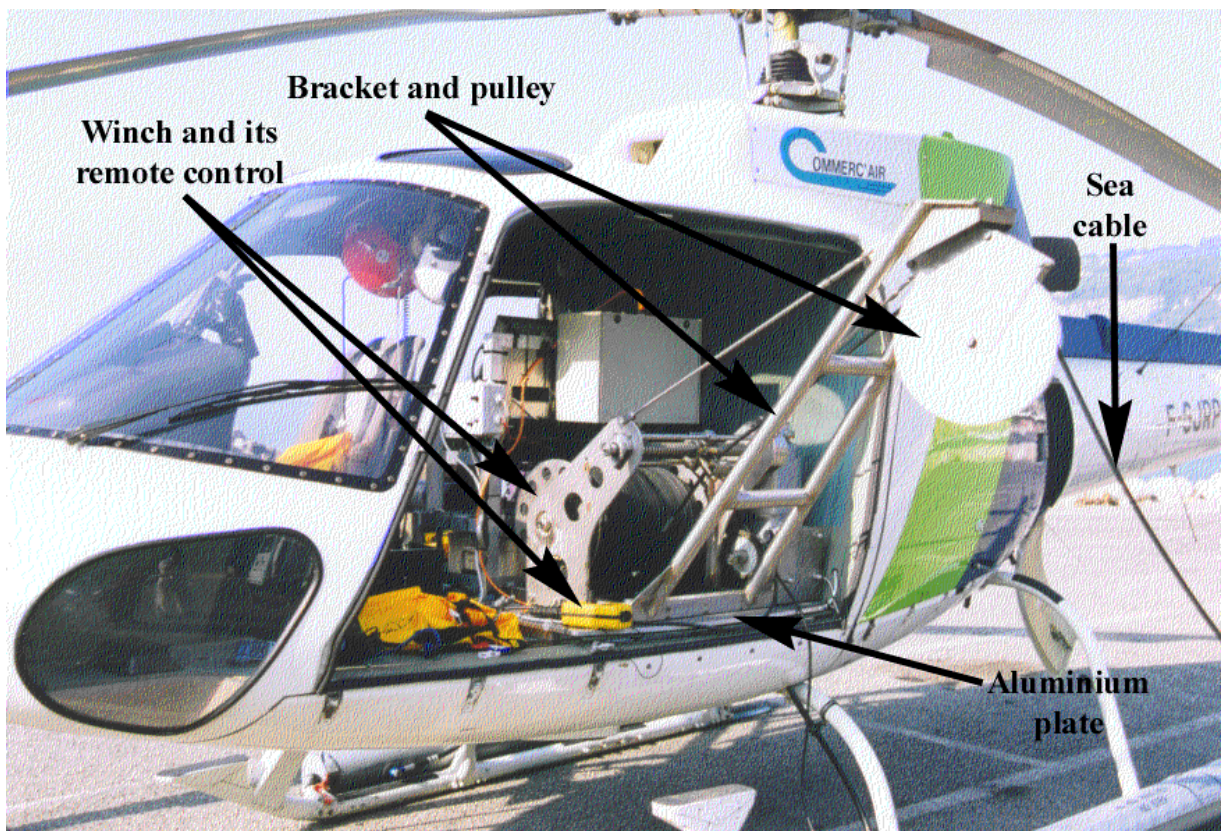
- An aluminium plate especially designed to fit the floor fastenings normally used for attaching backseats (which were removed) of the Ecureuil AS 350-B2 (helicopter built by Eurocopter). All material introduced into the helicopter was attached onto this plate. Thereby, the system could be installed into the helicopter as a whole very quickly (less than 30 minutes). Moreover, no modification of the helicopter was necessary.
- A winch especially designed to fit within available space. This electrical winch (24-28 DCV) was equipped with a 200-m kevlar sea cable (7 to 13 conductors, 600 kg breaking point) that power supplied submersible instruments, recovered data and grounded the helicopter. The winch, which has a variable and reversible speed between 0 and 0.5 m/s, had a torque limit (becomes null above 200 kg load), and an electrical security break (always on, except during operations), a bracket with a pulley at its end, and a safety steel cable to attach the instrument package during all transits.
- A desk especially designed to contain all deck units and computers. A high quality converter transforms 28 VDC to 220 VAC.
- A system for remotely triggering the Niskin water-sampling bottle.

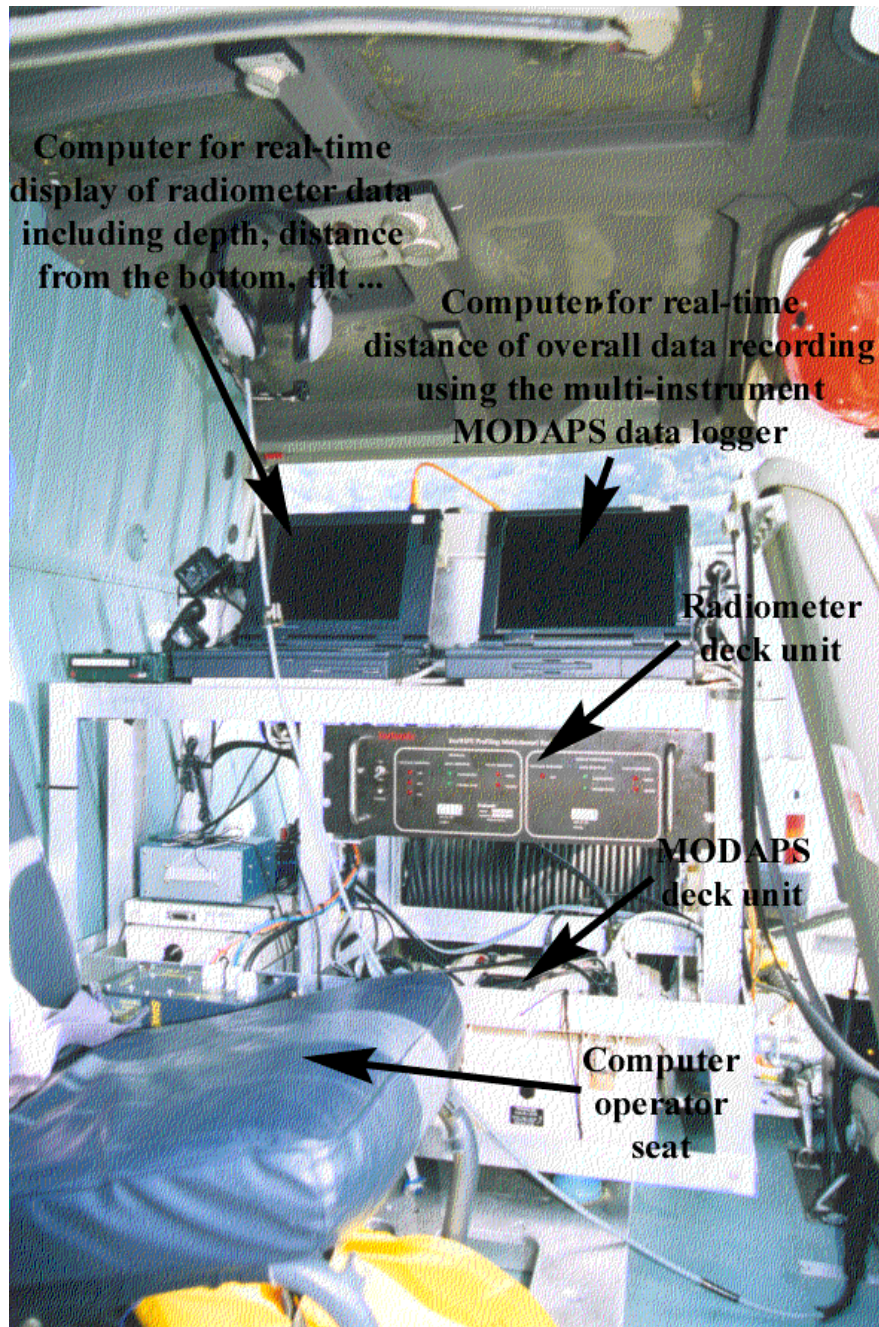
*ACRJ - LPCM - SAI - U. Oldenburg
NIOZ - U. Trondheim - FUB - PML - GKSS*

- A seat for the computer operator.
- A video camera looking at the instrument package during lowering operations. A small LCD monitor allows the pilot to watch at lowering operations and to maintain the sea cable as vertical as possible.
- A PAR (photosynthetically available radiation) reference sensor attached on the tail of the helicopter.

All tests (power consumption, load, weight equilibrium, ...), on helicopter were done by Commerc'Air to ensure that flights were done within the specifications of Eurocopter.

Four of the field campaigns were conducted onboard ships and three using the helicopter platform (see Table 1 below). A total of 191 and 233 stations were visited with the ship and helicopter platforms, respectively. On average, 2.7 and 7 stations per day were visited, respectively. Note that whether conditions were extremely bad (rain century record in Netherlands) during COAST/OOC-6, so that the helicopter sampling rate could easily be around 15 during normal weather conditions. Figure 2 to Figure 13 show the geographical locations of the different stations visited during COAST/OOC.

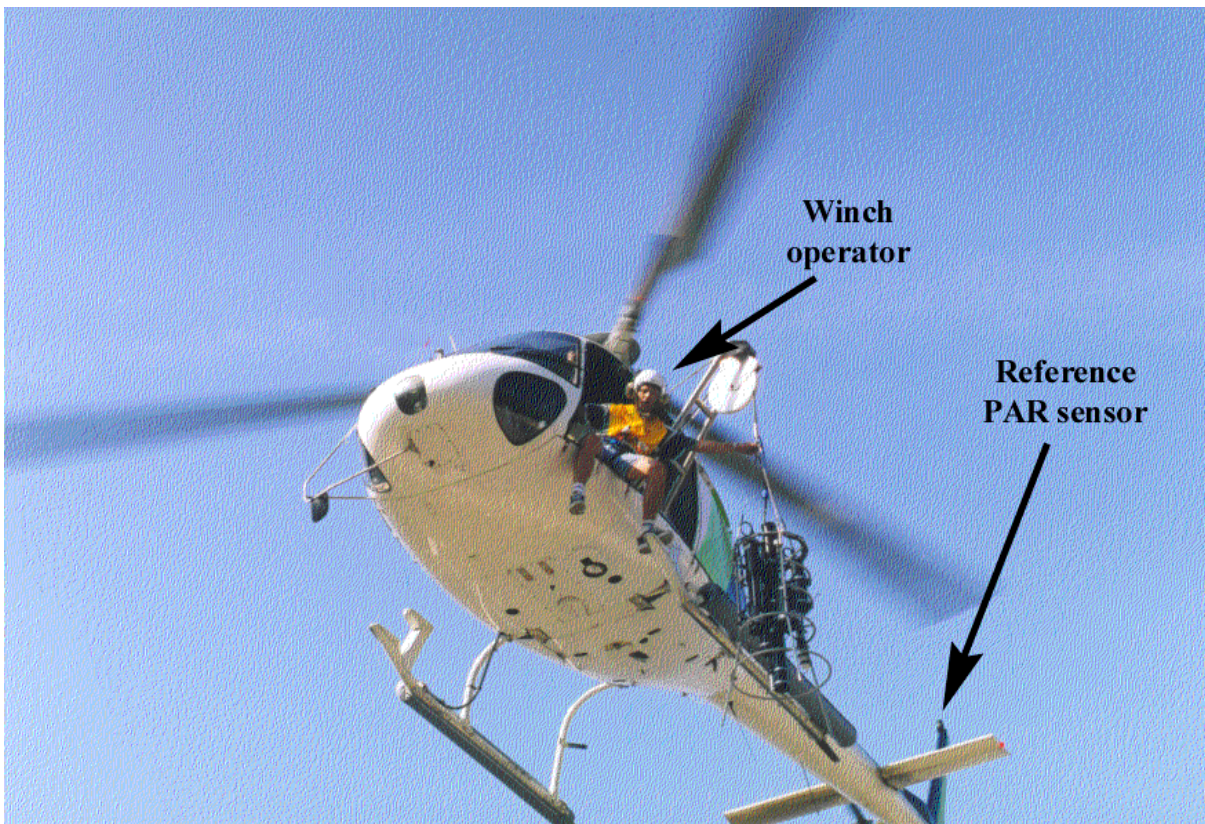




*ACRJ - LPCM - SAI - U. Oldenburg
NIOZ - U. Trondheim - FUB - PML - GKSS*



*ACRJ - LPCM - SAI - U. Oldenburg
NIOZ - U. Trondheim - FUB - PML - GKSS*

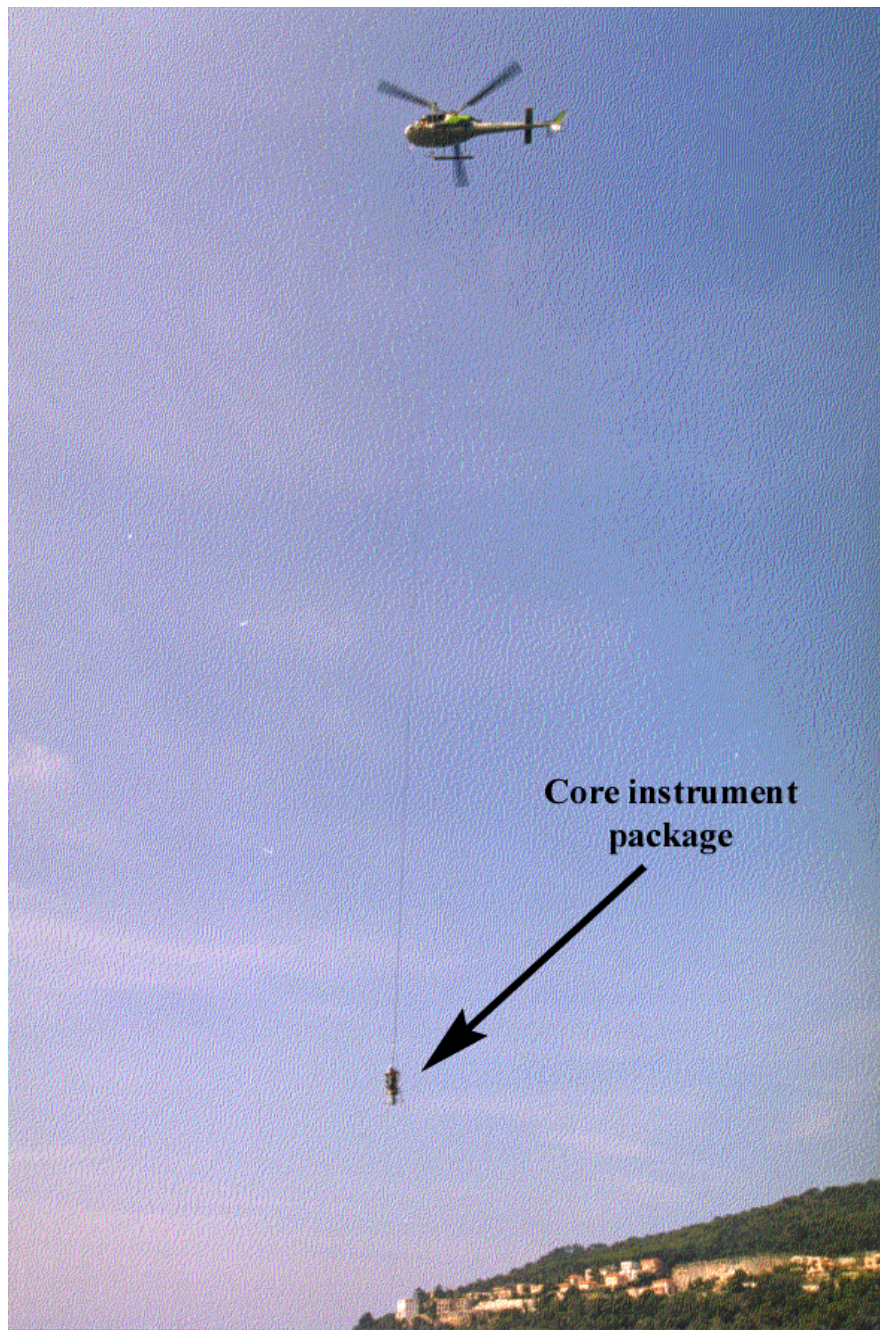


*ACRJ - LPCM - SAI - U. Oldenburg
NIOZ - U. Trondheim - FUB - PML - GKSS*



Final Report
ENV4-CT96-0310
03 January 2000

Page: 17



*ACRJ - LPCM - SAI - U. Oldenburg
NIOZ - U. Trondheim - FUB - PML - GKSS*

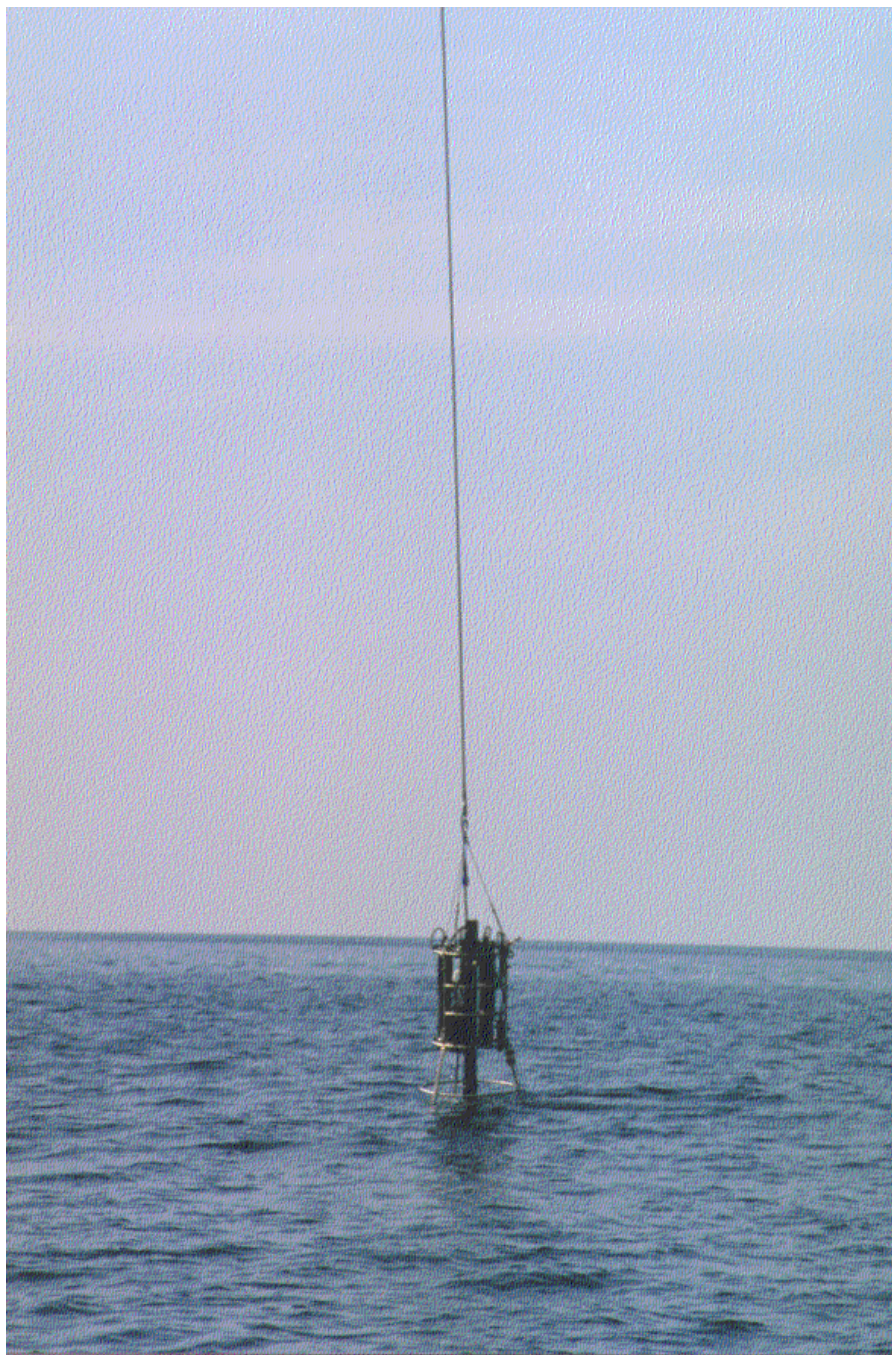


Figure 1. Pictures showing the different components of the helicopter system.

*ACRJ - LPCM - SAI - U. Oldenburg
NIOZ - U. Trondheim - FUB - PML - GKSS*



Final Report
ENV4-CT96-0310
03 January 2000

Page: 19

Table 1. List of field campaigns conducted during COAST/OOC.

Campaign ID	Platform	Area	N° of stations visited	Local Org.	Participants
COAST/OOC-1	R/V "Victor Hensen"	Atlantic Ocean - North Sea	46	Univ. Oldenburg	U. Olbenburg, ACRI, LPCM, JRC
COAST/OOC-2	Helicopter	Med. Sea (Gulf of Lions)	15	ACRI - LPCM	ACRI, LPCM, JRC
COAST/OOC-3	Helicopter	Northern Adriatic Sea	40	JRC	ACRI, LPCM, FUB, JRC, NIOZ
COAST/OOC-4	R/V "Tethys"	Med. Sea (Golfe du Lion, France)	48	ACRI - LPCM	ACRI, LPCM, JRC, U. Old., FUB, U. Trondheim
Almofront-2	R/V "Atalante"	Med. Sea (Alboran Sea)	47	LPCM	LPCM
COAST/OOC-5	R/V "Poseidon"	Atlantic Oc., English Ch., North Sea	56	Univ. Oldenburg	U. Oldenburg, ACRI, GKSS
COAST/OOC-6	Helicopter R/V "Heincke"*	English Channel, North and Baltic Sea	178	PML, NIOZ, Univ. Old.	ACRI, LPCM, PML, NIOZ, U. Oldenburg

* The R/V Heincke campaign was accompanying the Helicopter survey in the German Bight and the Baltic Sea. The stations visited then are not accounted for here because the core instrument package was not onboard R/V Heincke. Nevertheless, they are included into the U. Oldenburg data base (data from the U. Oldenburg prototype instrument package) which is available on COAST/OOC CDs.

ACRI - LPCM - SAI - U. Oldenburg
NIOZ - U. Trondheim - FUB - PML - GKSS

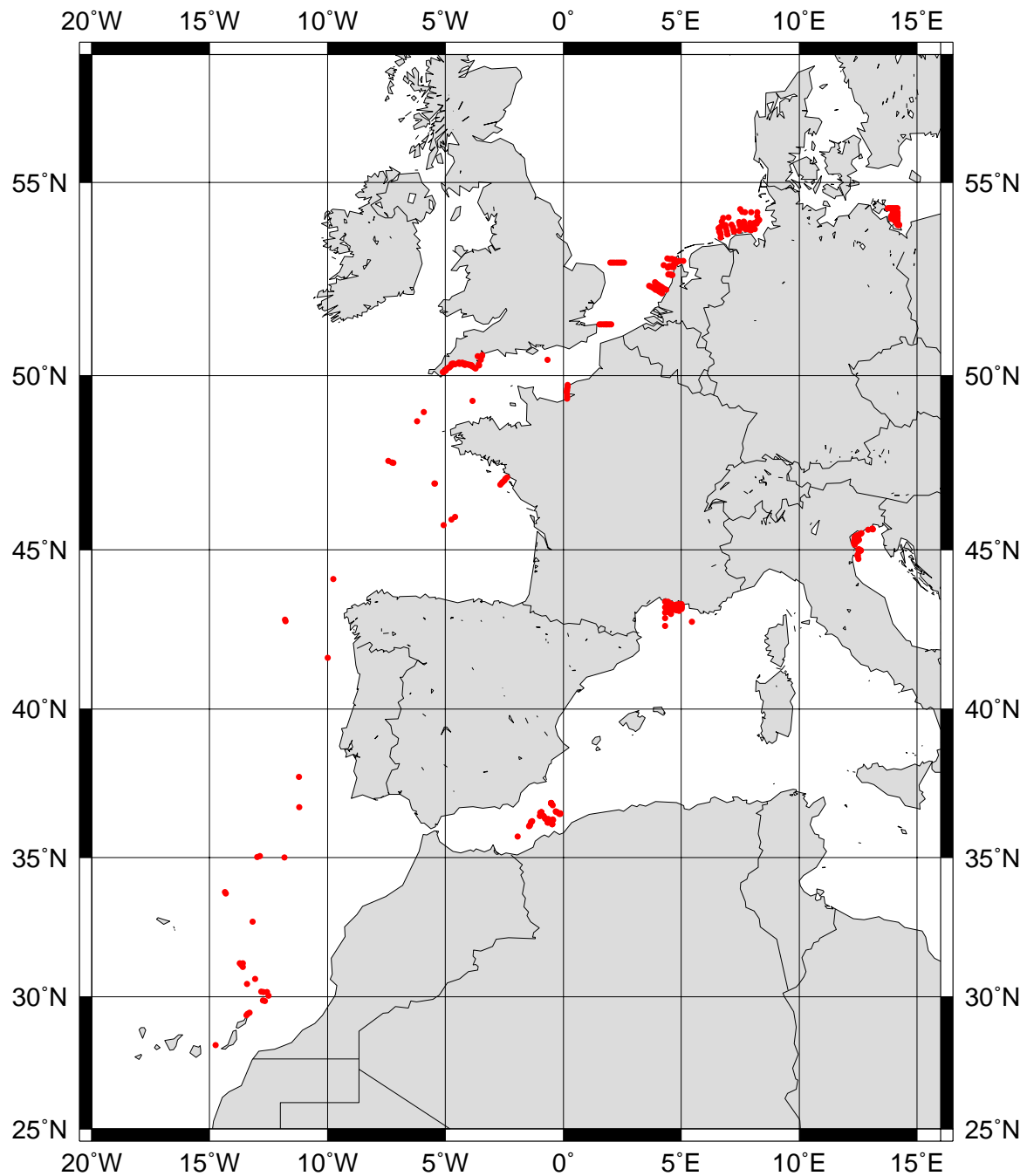


Figure 2. Map showing the location of stations visited during all COAST/OOC sampling campaigns.
Each point represents one surface station.

*ACRJ - LPCM - SAI - U. Oldenburg
NIOZ - U. Trondheim - FUB - PML - GKSS*

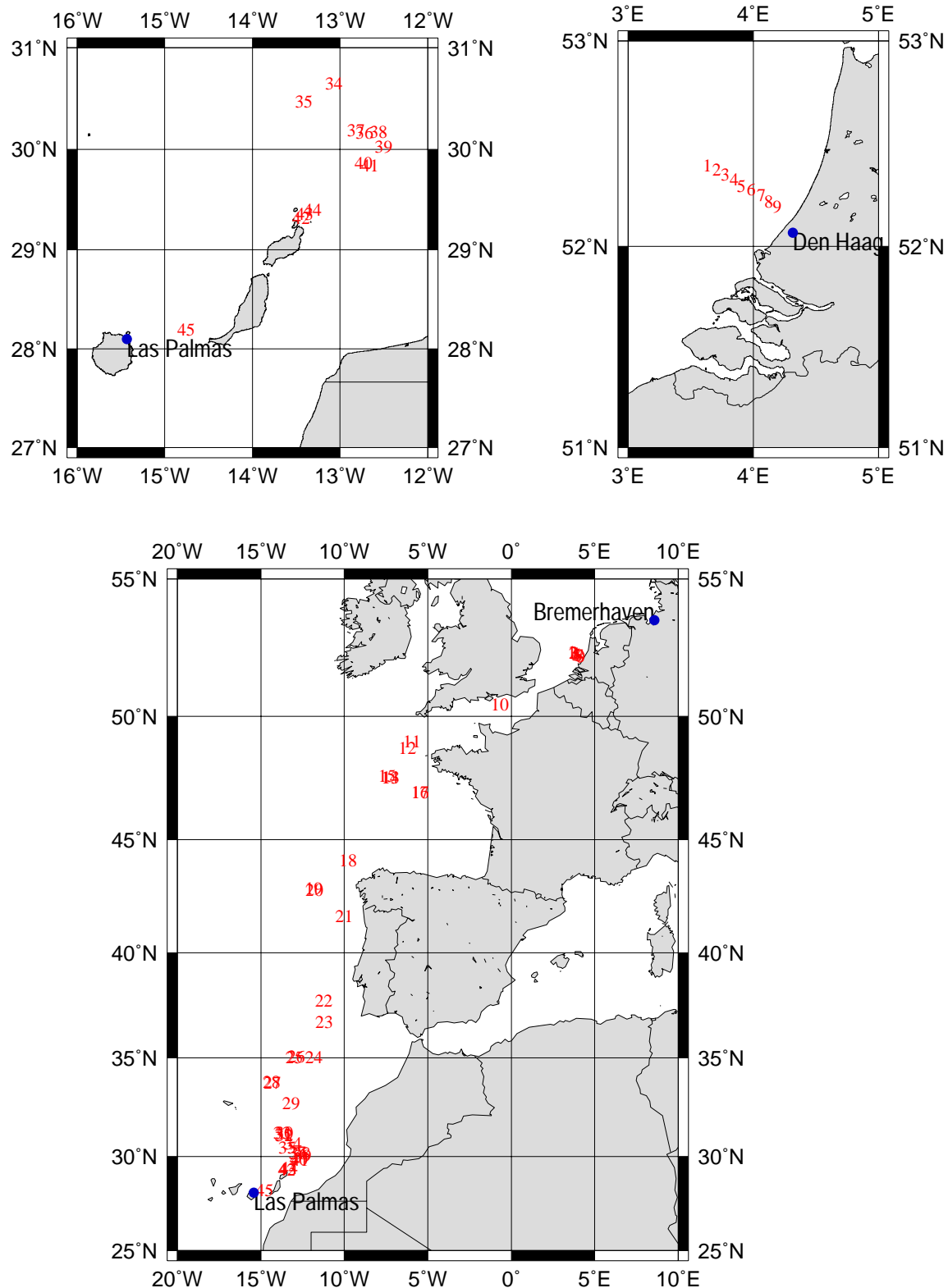


Figure 3. Maps showing the location of stations visited during COAST/OOC's campaign N°1.

ACRJ - LPCM - SAI - U. OI denburg
NIOZ - U. Trondheim - FUB - PML - GKSS

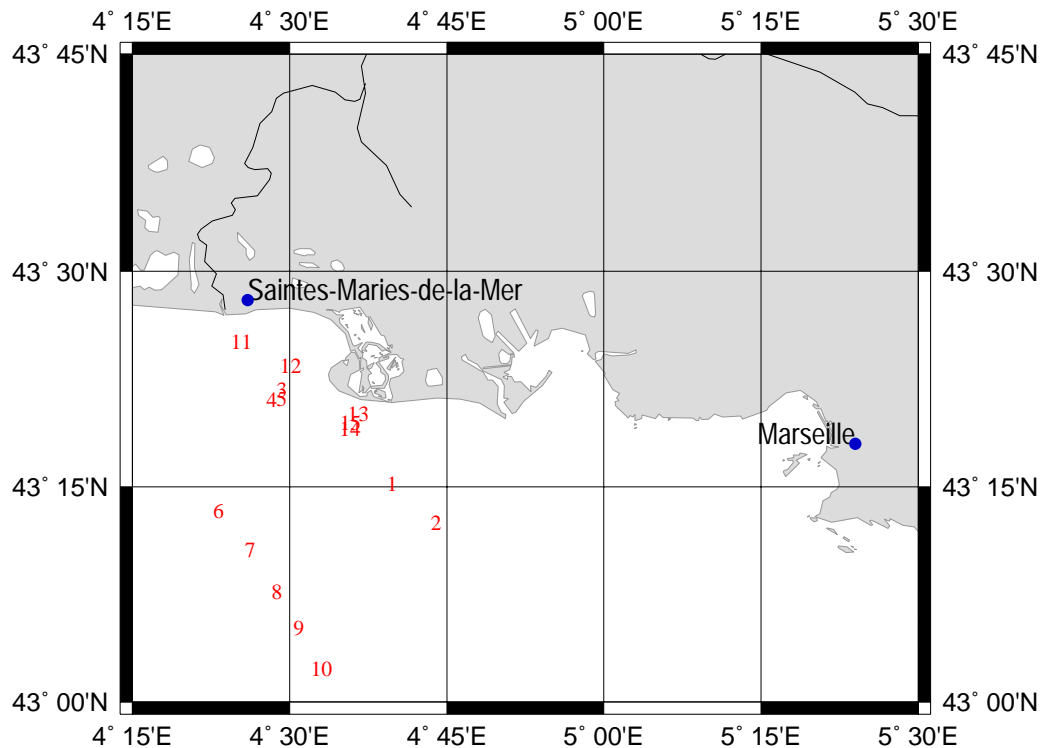


Figure 4. Map showing the location of stations visited during COAST/OOC 's campaign N°2.

ACRJ - LPCM - SAI - U. Oldenburg
NIOZ - U. Trondheim - FUB - PML - GKSS

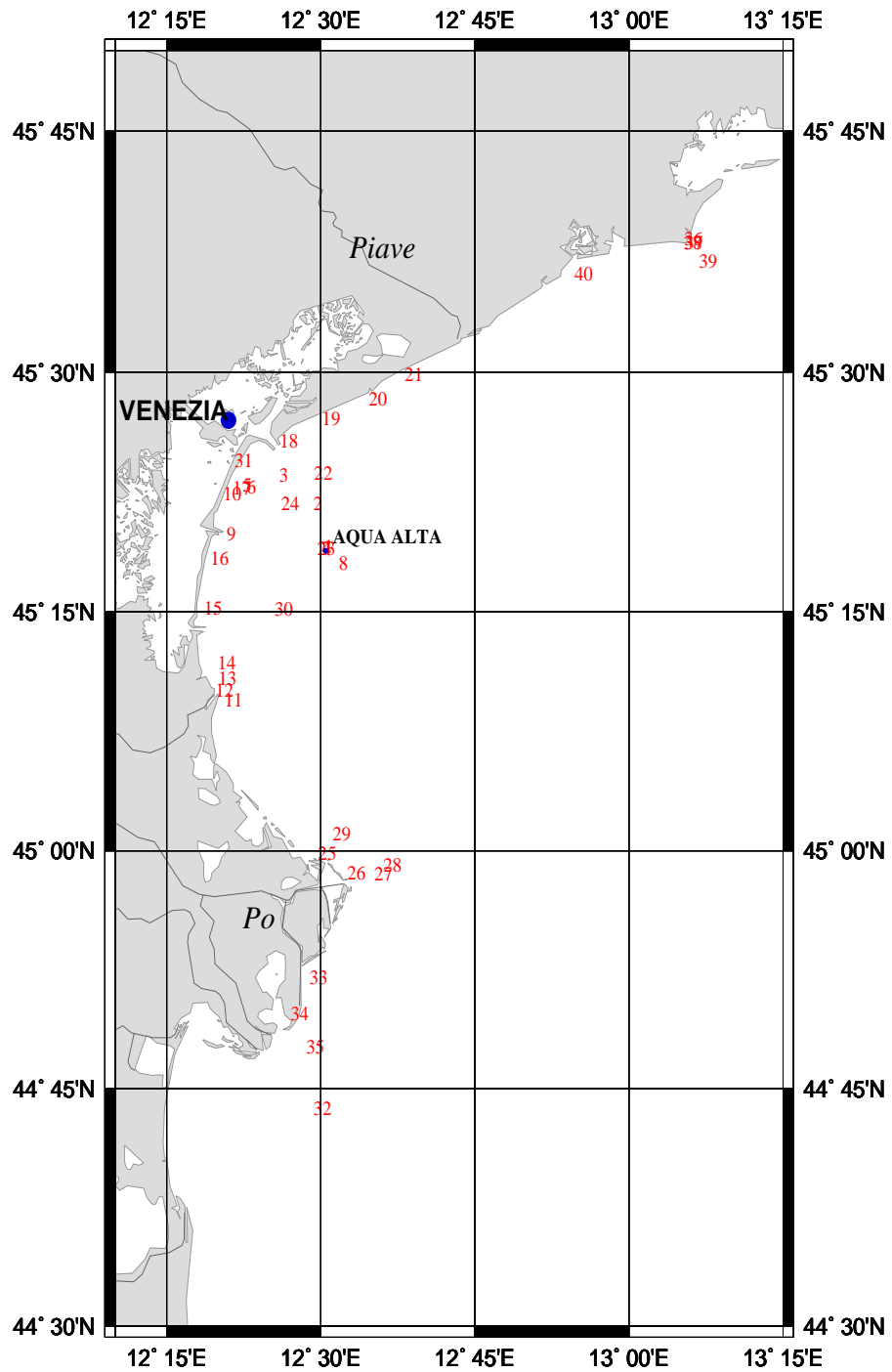


Figure 5. Map showing the location of stations visited during COAST/OOC 's campaign N°3.

ACRJ - LPCM - SAI - U. OI denburg
NIOZ - U. Trondheim - FUB - PML - GKSS



Final Report
ENV4-CT96-0310
03 January 2000

Page: 24

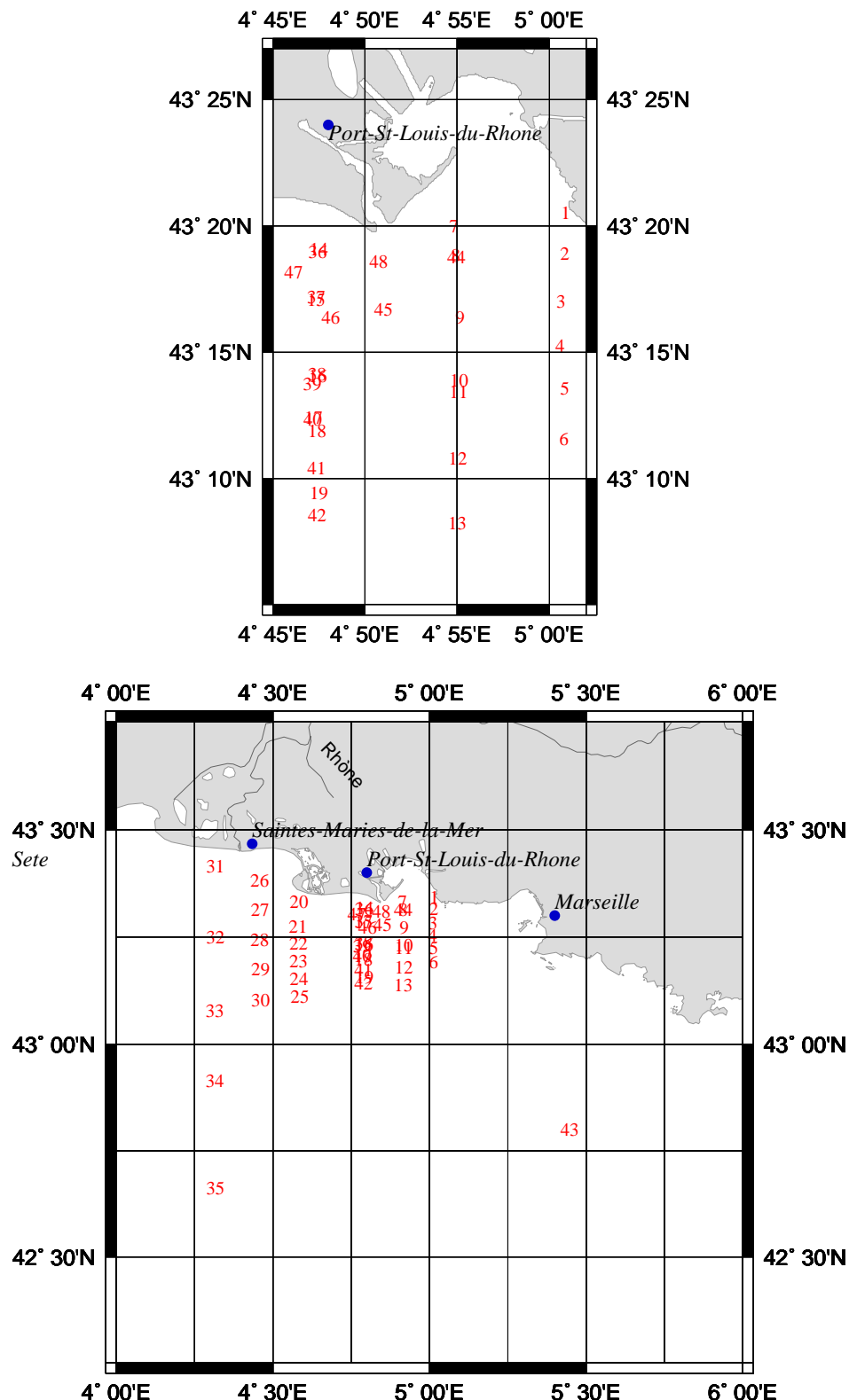


Figure 6. Maps showing the location of stations visited during COAST/OOC's campaign N°4.

ACRJ - LPCM - SAI - U. Oldenburg
NIOZ - U. Trondheim - FUB - PML - GKSS

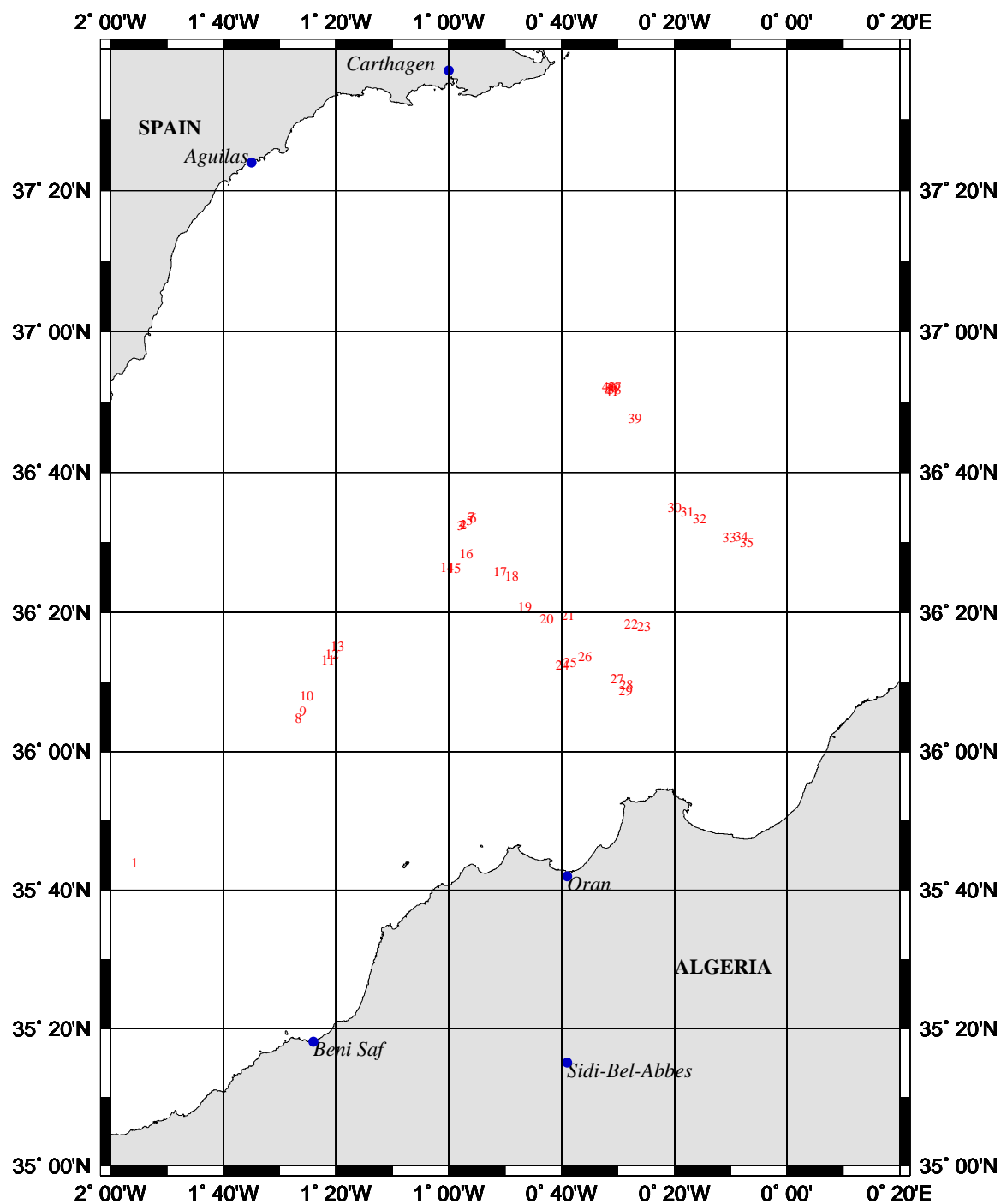


Figure 7. Map showing the location of stations visited during COAST/OOC's campaign N° 4b (ALMOFRONT).

ACR - LPCM - SAI - U. Oldenburg
NIOZ - U. Trondheim - FUB - PML - GKSS

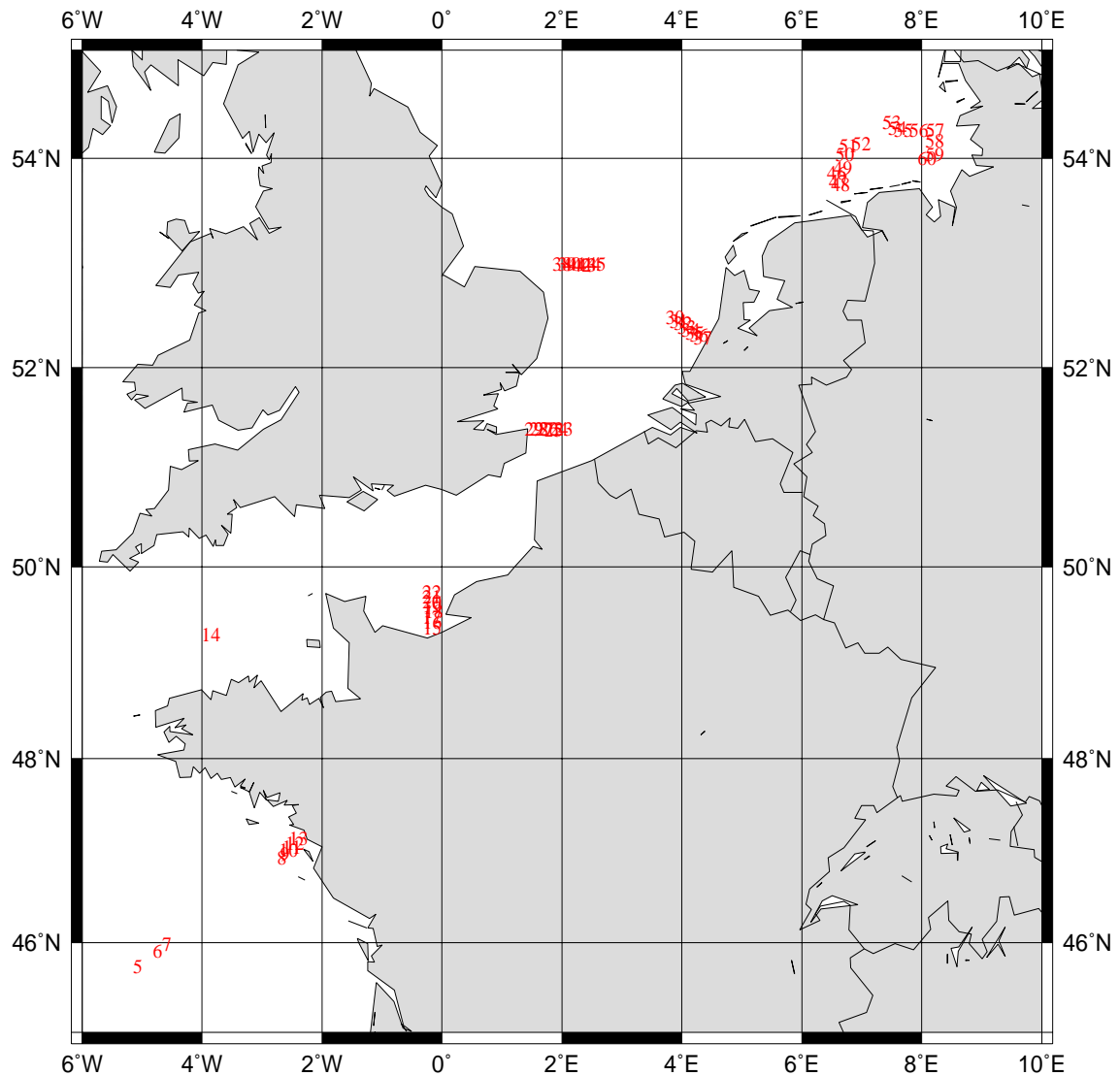


Figure 8. Map showing the location of stations visited during COAST/OOC's campaign N°5.

*ACRI - LPCM - SAI - U. Oldenburg
NIOZ - U. Trondheim - FUB - PML - GKSS*

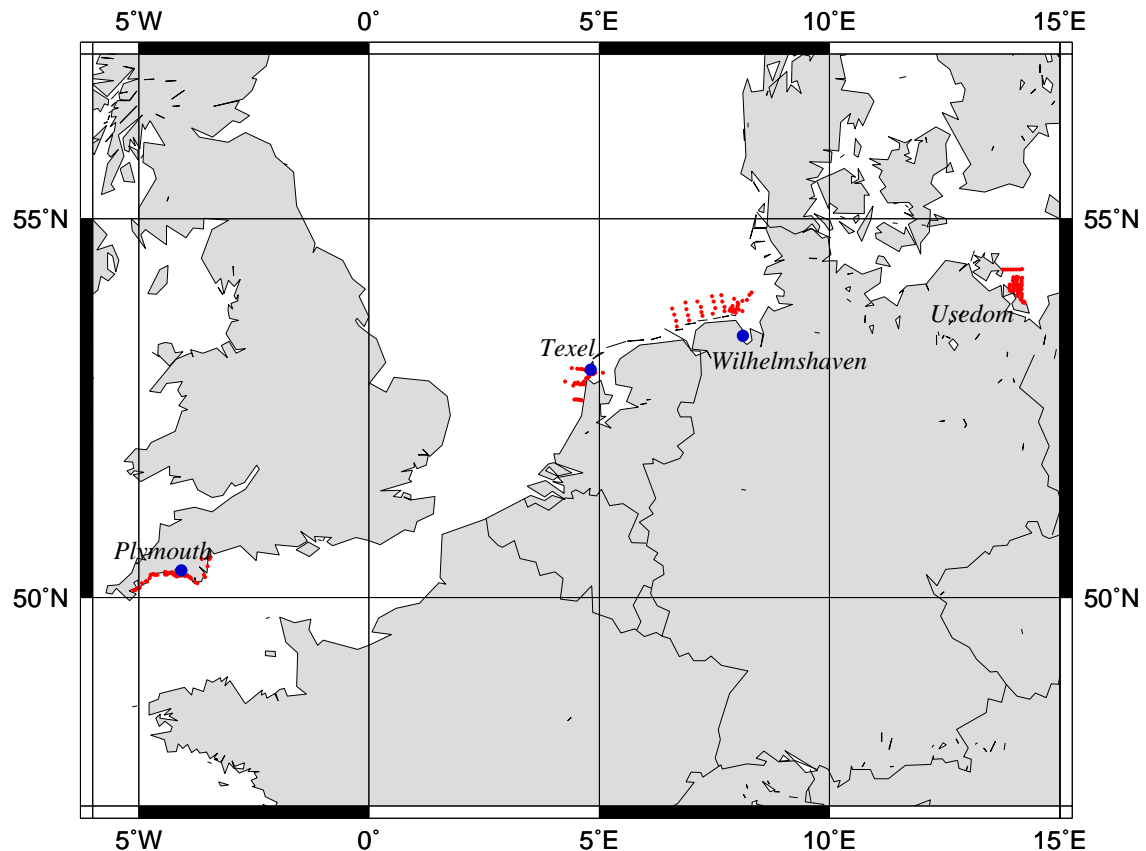


Figure 9. Map showing the location of stations visited during COAST/OOC 's campaign N°6.

*ACRJ - LPCM - SAI - U. Oldenburg
NIOZ - U. Trondheim - FUB - PML - GKSS*



Final Report
ENV4-CT96-0310
03 January 2000

Page: 28

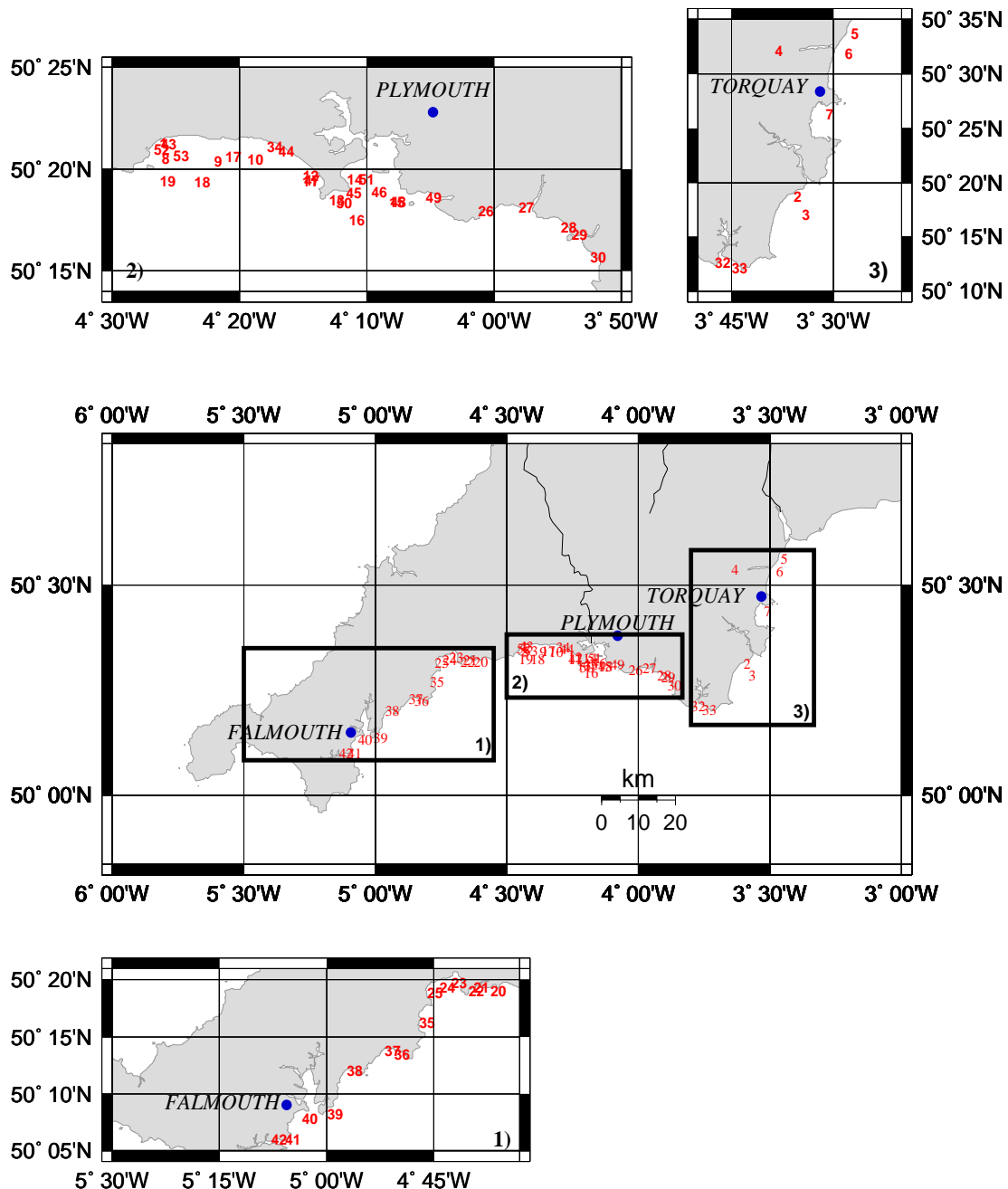


Figure 10. Maps showing the location of stations visited during COAST/OOC's campaign N°6. Details for the Plymouth Area.

ACRJ - LPCM - SAI - U. Oldenburg
NIOZ - U. Trondheim - FUB - PML - GKSS

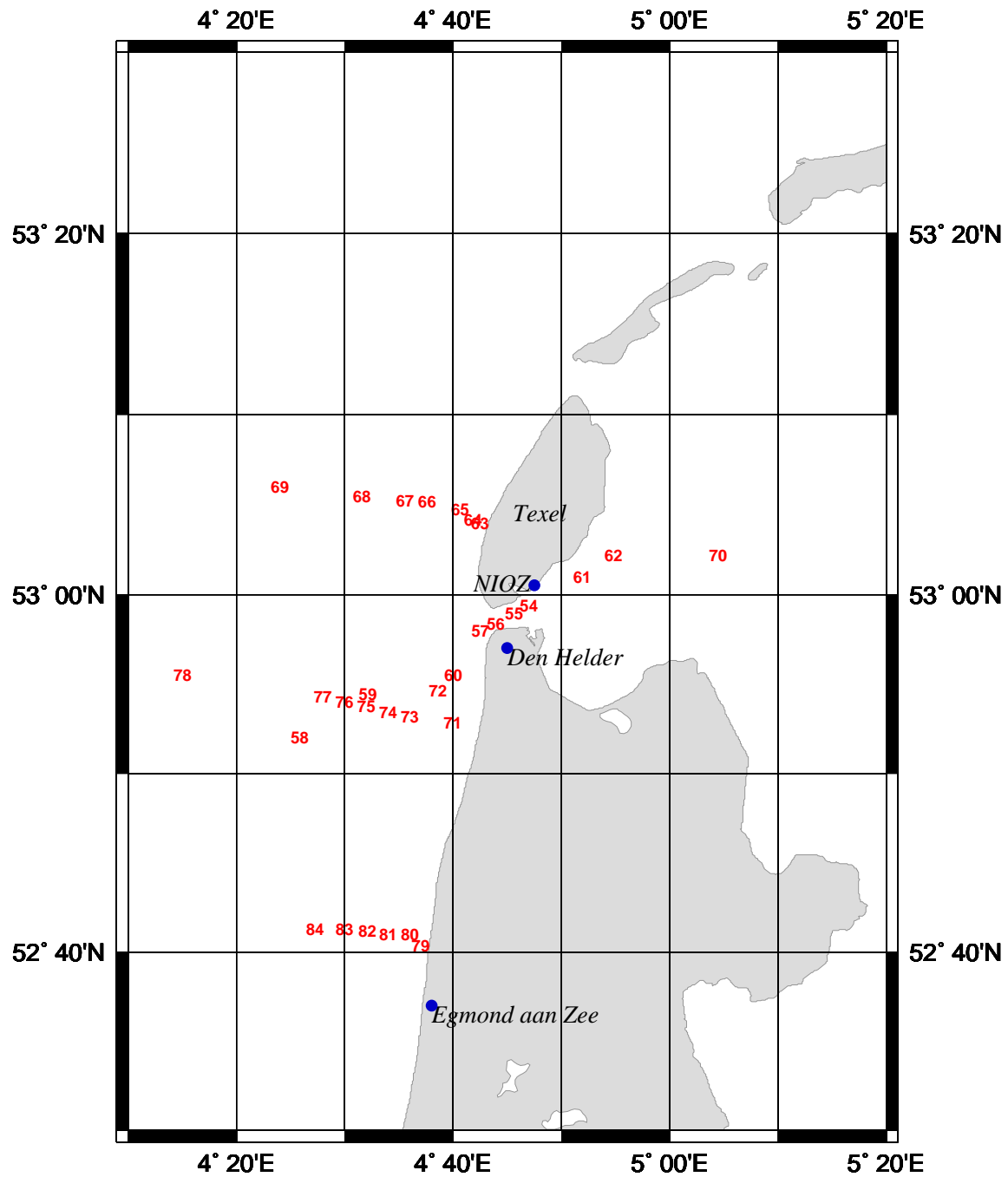


Figure 11. Map showing the location of stations visited during COAST/OOC's campaigns N°6.
Details for the Texel Island Area.

ACRJ - LPCM - SAI - U. Oldenburg
NIOZ - U. Trondheim - FUB - PML - GKSS

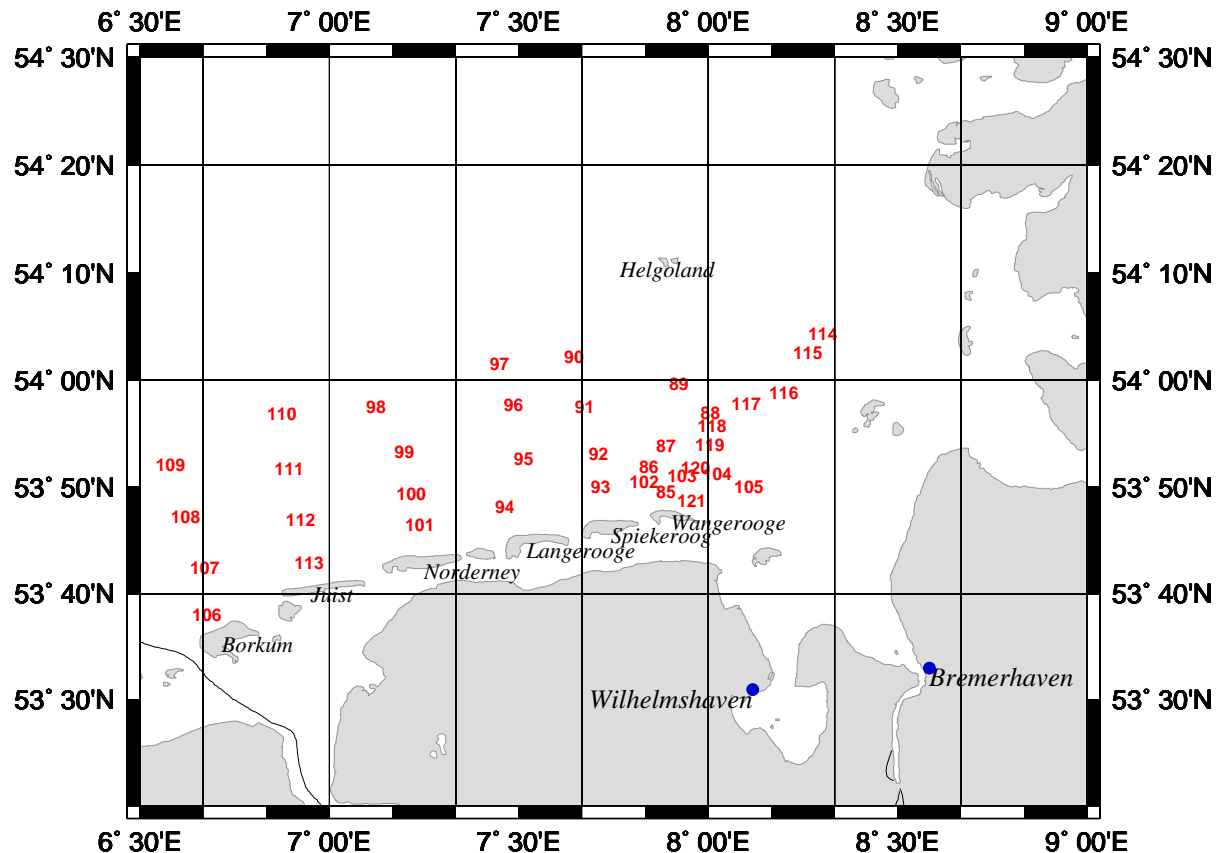


Figure 12. Map showing the location of stations visited during COAST/OOC's campaign N°6. Details for the Wilhelmshaven Area.

ACRJ - LPCM - SAI - U. Oldenburg
NIOZ - U. Trondheim - FUB - PML - GKSS

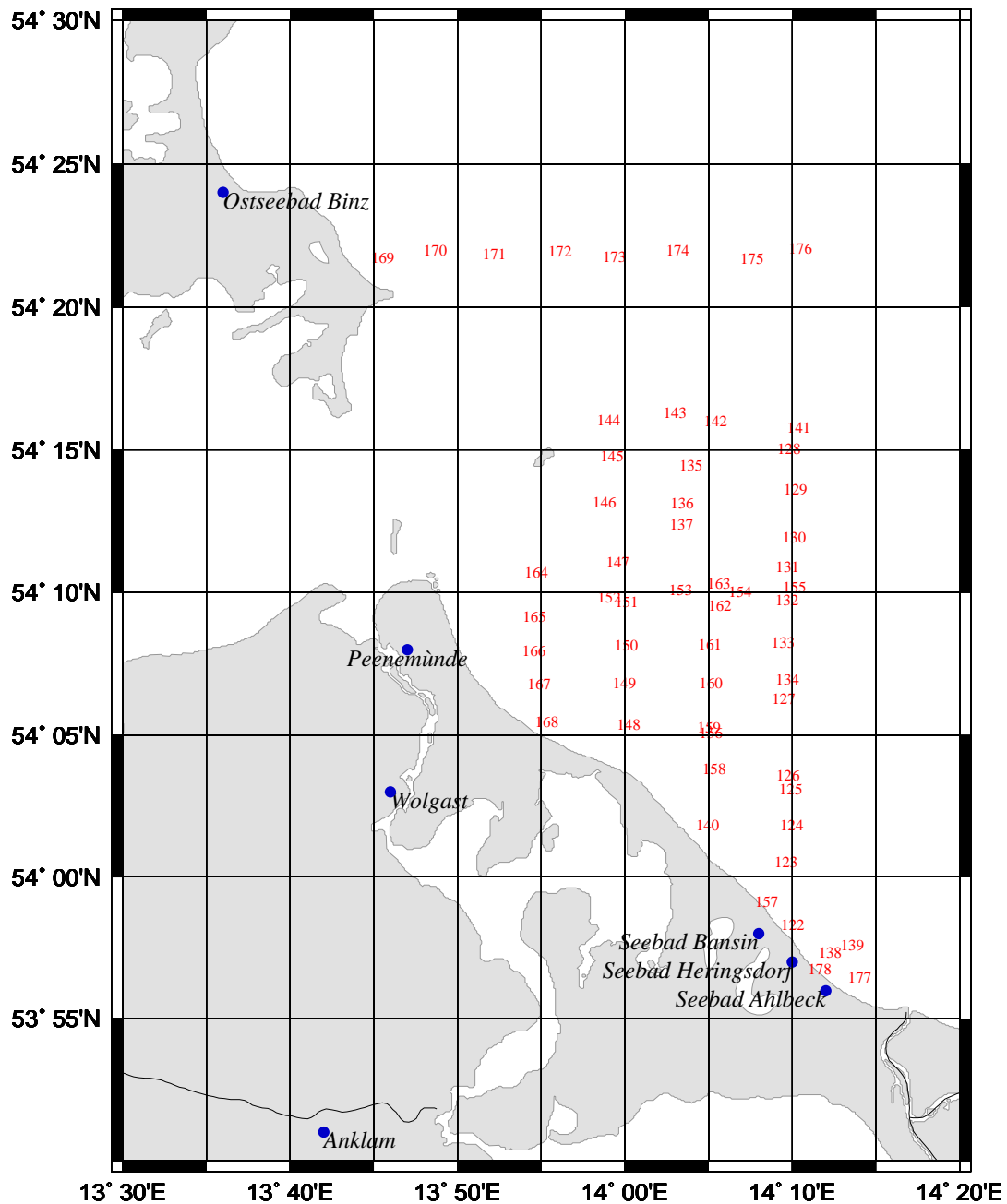


Figure 13. Map showing the location of stations visited during COAST/ OOC 's campaign N°6.
Details for the Usedom Island Area.

ACRJ - LPCM - SAI - U. Oldenburg
NIOZ - U. Trondheim - FUB - PML - GKSS

2.2.2. Measurements

Another important COAST/OOC challenge was to bring instruments, laboratory analyses and people on an unique platform:

- Instruments have been provided and made available by different partners for all sampling campaigns. A data acquisition and archiving system has been used and computer tools were developed.
- Most have contributed with their specific expertise to perform all necessary laboratory analyses.
- A core team involving different partners has been set up. This team was present in all field activities. It insured continuity and consistency in measurements.
- All partners took part to the sampling campaigns, both for the scientific work (collection and analysis of the samples), and for the field organisation (flight plans and logistics for helicopter, laboratory space and accommodation for the moving team, etc.)

Figure 14 shows the core instrument package and its different components. Note that, for the COAST/OOC-6 campaign, a Niskin water sampling bottle was added together with a triggering system that was remote controlled from the helicopter. Three kinds of optical profiler were used:

- The AC-9 absorption-attenuation meter (made by Wetlabs Inc., USA) measures the absorption and attenuation coefficients at 9 wavelengths (412, 440, 488, 510, 555, 630, 650 or 532, 665 and 715 nm). Some of the instruments we used also measures depth and temperature.
- The BB-4 backscattering meter (made by Hobilabs, USA) measures the backscattering coefficient at 4 wavelengths (415, 440, 510 and 675 nm)
- The SPMR radiometer (made by Satlantic Inc., Canada) measures downward and upward irradiance at 13 wavelengths (412, 443, 456, 490, 510, 532, 560, 620, 665, 683, 705, 780 and 865 nm). It also measures the instrument tilt, depth at high resolution, temperature, salinity and distance to the bottom.

When sampling from helicopter, the series of even was the following (during COAST/OOC-6):

- Takeoff with the instrument package lifted few centimetres above the ground and attached using the safety steel cable.
- Once on site, lowering of the instrument package above sea surface.
- Position recording using the DGPS and measurement of $E_d(\lambda)$ in air.
- Immersion of the instrument package and about 1 minute of measurements with all instruments just below surface (AC-9 pumps on).

*ACRJ - LPCM - SAI - U. Oldenburg
NIOZ - U. Trondheim - FUB - PML - GKSS*



Final Report
ENV4-CT96-0310
03 January 2000

Page: 33

- Few (up to 6) profiles at about 0.5 m/s down to about 50 m (when allowed by water column thickness).
- Collection of the water sample just below surface.
- Stop of AC-9 pumps.
- Slow emersion of the instrument package.
- E_d measurements in air just above surface.
- Measurement, from the helicopter, of $L_w(\lambda)$ using the PR-650 camera.
- Stopping of all instruments.
- Lifting of the instrument package to the helicopter and decanting of the water sampling into a container.

The instrument deployment from ship was much similar.

*ACRJ - LPCM - SAI - U. Oldenburg
NIOZ - U. Trondheim - FUB - PML - GKSS*

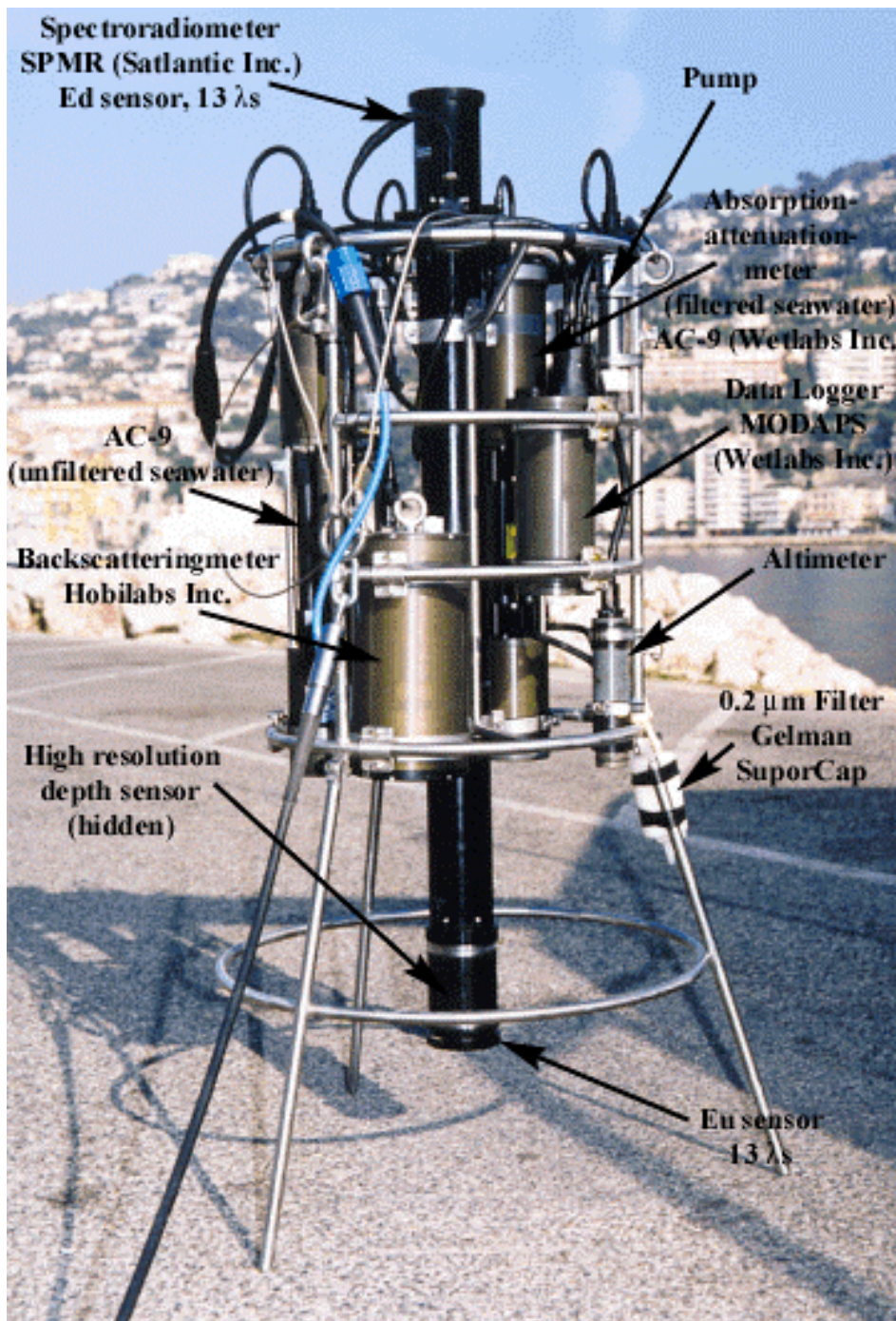


Figure 14. Picture showing the core instrument package and its different components.

The different variables measured *in situ* and on water samples are listed in Table 2 and Table 3.

*ACRJ - LPCM - SAI - U. Oldenburg
NIOZ - U. Trondheim - FUB - PML - GKSS*

Table 2. List of core measurements and analyses performed during COAST/OOC's campaigns.

Analysis	Responsible	Performed During Campaign N°						
		1	2	3	4	4b	5	6
Liposoluble Pigment Composition (HPLC)	H. Claustre (LPCM)	X	X	X	X	X	X	X
Particulate Matter Dry Weight	G. Obolensky (LPCM)	X	X	X	X	X	X	X
Particle Size Spectrum (Coulter Counter and YAC)	G. Obolensky (LPCM)	X	X	X	X			X
Particulate Matter Absorption Spectrum (discrimination between phytoplankton and other particles after bleaching) (T + R Filter Technique using laboratory spectrophotometer)	M. Ferrari (JRC)	X	X	X	X		X	X
Coloured Dissolved Organic Matter Absorption Spectrum (laboratory spectrophotometer)	M. Ferrari (JRC)	X	X	X	X		X	X
Dissolved Organic Carbon (TOC analyser)	M. Ferrari (JRC)	X	X	X	X		X	X
Particulate Organic Carbon (CHN analyser)	M. Ferrari (JRC)	X	X	X	X		X	X
Phytoplankton Species Composition (microscopic identification)	G. Johnsen (U. Trondheim)	X	X	X	X		X	X
Bacteria Counting (flow cytometry)	M. Wernand (NIOZ)	X	X	X	X		X	X

ACRJ - LPCM - SAI - U. Oldenburg
NIOZ - U. Trondheim - FUB - PML - GKSS



Final Report
ENV4-CT96-0310
03 January 2000

Page: 36

<i>In situ</i> Total Absorption and Attenuation Spectra (AC9 profiler)	F. Fell (LPCM) V. Fournier-Sicre (ACRI)	X	X*	X*	X	X**	X**	X
<i>In situ</i> Total Absorption by Coloured Dissolved Organic Matter (AC9 profiler)	F. Fell (LPCM) V. Fournier-Sicre (ACRI)	X	X*	X*	X			X
<i>In situ</i> Backscattering Spectrum (BB4 profiler)	F. Fell (LPCM) V. Fournier-Sicre (ACRI)		X*	X*	X		X**	X
Downward and Upward Irradiance Spectra, Salinity and Temperature (SPMR - Satlantic profiler)	F. Fell (LPCM) V. Fournier-Sicre (ACRI)	X	X	X	X	X	X	X
Water Leaving Radiance Spectrum (Hand Camera PR-650)	M. Wernand (NIOZ)			X				X
Near TOA Radiance Spectrum (CASI airborne sensor)	J. Fischer (FUB)			X	X			X
Atmosphere optical thickness (CIMEL)	G. Obolensky (LPCM)	X*	X*	X*	X*	X*	X*	

* because of technical difficulties, only few measurements were performed

** During COAST/OOC 5 campaign, these measurements were made by H. Hackvoort, NIOZ

ACRJ - LPCM - SAI - U. Oldenburg
NIOZ - U. Trondheim - FUB - PML - GKSS



Final Report
ENV4-CT96-0310
03 January 2000

Page: 37

Table 3. List of additional measurements and analyses performed during COAST/OOC's campaigns.

Analysis	Responsible	Performed During Campaign N°						
		1	2	3	4	4b	5	6
<i>In situ</i> Attenuation Detailed Spectrum (U. Oldenburg prototype profiler)	H. Barth (U. Oldenburg)	X			X		X	X**
<i>In situ</i> Fluorescence Spectrum (U. Oldenburg prototype profiler)	H. Barth (U. Oldenburg)	X			X		X	X**
Downward and Upward Irradiance Detailed Spectra (U. Oldenburg prototype profiler)	H. Barth (U. Oldenburg)	X			X		X	X**
X-Ray Analysis of Mineral Particles Composition	M. Ferrari (JRC)	X	X	X	X		X	X
Fluorescence Spectrum of Coloured Dissolved Organic Matter (laboratory spectrofluorometer)	M. Ferrari (JRC)		X	X	X		X	X
Fluorescence Spectrum of Coloured Dissolved Organic Matter (laboratory spectrofluorometer)	H. Barth (U. Oldenburg)	X						X**
Fluorescence Spectrum of Coloured Particulate Organic Matter	F. Fell (LPCM)				X			

ACRJ - LPCM - SAI - U. Oldenburg
NIOZ - U. Trondheim - FUB - PML - GKSS

(laboratory spectrofluorometer)								
Fluorescence Spectrum of Phytoplankton (laboratory spectrofluorometer)	G. Johnsen (U. Trondheim)				X			
Hydrosoluble Pigment Composition (HPLC or spectrofluorometry)	H. Claustre (LPCM)	X*						
Particulate Matter Absorption Spectrum (discrimination between phytoplankton and other particles using a numerical decomposition) (FTF Technique using laboratory spectrophotometer)	A. Bricaud (LPCM)			X				X

* Analyses will be performed on selected sampling according to occurrence of hydrosoluble-pigment-containing phytoplankton species

** Analysis performed on board R/V "Heincke" simultaneously with helicopter samplings

2.2.3. Data processing

2.2.3.1. Processing chain for multiple instruments system: Methodology and tool description

This tool was developed for processing bio-optical data of the COAST/OOC. Very few ocean colour coastal data are available, and none of the databases existing at the early stages of the project were consistent with one another, either the database did not hold all the necessary parameters, or the resolution on which they had been measured was not small enough. Therefore it was decided, for the COAST/OOC project, to develop a data acquisition system and use it to provide an ocean colour database dedicated to coastal waters.

The instruments that were used measure inherent (absorption, attenuation) and apparent optical water properties (irradiance, backscattering) together with non-optical auxiliary parameters used to develop the algorithm (Conductivity, Temperature, Depth) and to qualify the data (tilt, optical thickness, sky downwelling irradiance, distance to bottom). Instruments were not developed for this project but off the shelf available instruments were used from different companies (©WetLabs, ©Satlantic, ©SeaBird, ©Sequoia). The MODAPS data gathering system from WetLabs was used to merge the data from the different instruments. This document describes the methodology and tools that were used. This tool was developed in the objective of being able to add, remove or replace any

*ACRJ - LPCM - SAI - U. Oldenburg
NIOZ - U. Trondheim - FUB - PML - GKSS*

component (instrument or gathering system) of the system, and to produce a final data matrix with a common depth field.

Other tools used for processing bio-optical data exist and are readily available on the WWW (BBOP processing software), the tool that was developed for the COAST/OOC project cannot replace such a tool. Their goals are different, BBOP is used for quality controlling, binning and deriving auxiliary parameters from bio-optical data and the primary goal of the COAST/OOC processing software is to merge data collected from different instruments. It could be used as a pre-processor to any type of bio-optical processing tool similar to the BBOP software.

2.2.3.1.1. Methodology

2.2.3.1.1.1. *Packet validation*

The data extraction routines are improved versions of the routines delivered by the different instruments manufacturers. Most of the source code supplied by the different instruments manufacturers were kept and only a fraction of them was added to meet the requirements of the tool that was developed (standardise the output format and add a time field). This tool was developed in ANSI C and only the code that was written in another language (PASCAL) had to be rewritten. Packet validation is thus not standard between extraction tools and each one has its own methodology for defining and finding valid packets within a data flow. Packets may be accepted/rejected depending on its size, its header, its checksum, or the values that it contains.

2.2.3.1.1.2. *Time stamping*

Time stamping is essential since it is the only way to relate any packet to a common pressure value. That allows the merging to be performed with the best depth gauge installed on the system and therefore to have a coherent database throughout the project. Depending on the type of instrument that is used different cases have to be considered :

Data of one instrument is logged on two different data gathering systems

Using a parallel cable Satlantic profiler data is logged at the same time on two units, Satlantic and MODAPS. With this method in the Satlantic raw data file reference, data packets are interleaved with profiler data packets allowing, knowing the time stamp for each profiler packet, to time stamp each reference data packet with the closest profiler time stamp. Also, logging Satlantic data through its deck unit was essential for retrieving, when post-processing, header data that was only contained in the Satlantic raw data file header (location of each station entered by the operator, pressure tare, name of operator,...).

Packet does not hold time stamp

Then the datastream of that instrument goes through the MODAPS system and all packets are interleaved with MODAPS time stamps.

Packet holds time stamp

ACRI - LPCM - SAI - U. Oldenburg
NIOZ - U. Trondheim - FUB - PML - GKSS



Since a global synchronisation on all instruments is performed the first packet is given the closest MODAPS time stamp and times of packets logged by the instrument are shifted in time accordingly.

Packet holds several sub packets with time stamps

In that case the first sub packet of each packet is adjusted using the closest MODAPS time stamp. Following sub-packets in the same main packet are shifted in time accordingly.

Packet holds several sub packets without time stamps

The first packet is given the closest MODAPS time stamp, and the sub packets are stamped assuming a theoretical data acquisition rate.

2.2.3.1.1.3. Depth stamping

Since all packets are given a time stamp (using the clock of the instrument itself or the clock of MODAPS -see above) and since the instrument that logs the depth is also given a time stamp, the closest (in time) depth stamp is given (interpolated depths could also be considered but it was decided, considering the rate of the instruments and the descending/ascending rate of the instruments that a closest neighbour match was sufficient).

2.2.3.1.1.4. Depth merging

The main objective of the processing was to produce one single data matrix per profile with the best depth merging possible and at the meantime preserving the down/up cast organisation within the same profile. Therefore considering only the depth was not sufficient, to make sure that the different casts would not be shuffled a time window had to be taken into account. Within that time window the closest packets (with reference to depth and considering only the frames that were within a same depth window) were given the same depth. The pressure height that was used for the entire processing was 25 cm ; and the time window that was used to make sure that only frames of the same cast were considered was set to 2 seconds.

2.2.3.1.1.5. Global processing flow

Throughout the project, several configurations were used for different reasons. The reasons could be that one of the two systems was not working (either MODAPS or Satlantic), or that one of the instrument of one of the system was not working or was not present ; or one of the instrument was not properly configured and therefore its data was not useable etc. Also, it happened that the data of one of the instrument was not good enough to be used (filter clogged on one of the AC9, data too noisy etc.) Therefore, the data processing chain had to be as much flexible as possible and had to be able to identify which instrument was working.

Basically, two different modes had to be considered : either the two systems were working at the same time and were connected to each other (which was the ideal case and the data could be merged in one single database) ; either the two systems could not be connected and two independent

*ACRJ - LPCM - SAI - U. Oldenburg
NIOZ - U. Trondheim - FUB - PML - GKSS*



databases had to be constructed from one another with depth values measured with two completely independent gauges. Two different sets of data files were produced as follows :

Table 4. Files produced depending on the configuration.

CONFIGURATION			DATABASE		
Merging requested (MODAPS & SATLANTIC were connected)	SATLANTIC produced data file	MODAPS produced data file	*.MER file	*.SAT file	*.MOD file
Yes	Yes	Yes	Yes	No	No
	Yes	No	Yes	No	No
	No	Yes	No	No	Yes
No	Yes	Yes	No	Yes	Yes
	Yes	No	No	Yes	No
	No	Yes	No	No	Yes

Also, within the two main modes in which the systems were used several configurations were possible depending on availability and/or proper usage of each instrument. Therefore a processing chain capable of deciding which branch of the processing had to be considered was necessary. This was performed using a main shell script. In addition to deciding which processing branch had to be executed (the list of utilities - or filters - that were used and triggered by this script are described in the following chapter), the purpose of the main shell script was also to read the processing parameters from configuration files, to set up where the calibration files were located and to build up filenames (intermediate or final).

2.2.3.1.2. Filters

All filters accept various options ; these are listed in the tables below. In addition to these options there is also a help option (using **-h**) that provides a brief on line manual, and a verbose mode (using **-v**) that provides additional information to keep track of the processing that is performed..

They may all be used on data logged through MODAPS or logged directly through each specific instrument's data acquisition software.



Table 5. Filters used for converting binary data to ASCII data.

Filter	Input files	Miscellaneous	Options	Description
extmod	MODAPS *.ARC file MODAPS *.INI file	Display : '.' For each packet found 'm' if bad packet 'f' if bad routing	-a {MODAPS archive file} -i {MODAPS INI file}	evaluates time offsets between two MODAPS clocks and adjusts time scales accordingly retrieves raw data for all instruments logging data through MODAPS system creates a time scale table for each instrument one file is created for each instrument
aasci_ac9	*.DEV calibration file AC9 binary raw data file	data in wetview file cannot agree with acquisition time	-c {calibration file - Wetview *.dev file} -i {input raw data file} -o {output file} -w{wetview file} -m{time scale file}	converts AC9 binary data to ASCII tab delimited file with column headers (no temperature correction is performed)
asci_bb4	*.CFG calibration file BB4 binary raw data file	1 sensor is damaged (reference field) and the field is duplicated would need changes to use it with other BB4	-c {calibration file} -i {input raw data file} -o {output file} -m{time scale file}	converts BB4 binary data to ASCII tab delimited file with column headers
asci_pnf	PNF binary raw data file	No calibration file is required	-c {calibration file} -i {input raw data file} -o {output file} -m{time scale file}	converts PNF (helicopter reference) binary data to ASCII tab delimited file with column headers
asci_sat	*.calibration file Satlantic binary raw data file	works with any Satlantic instrument frame counter jumps are tracked down serial number is checked	-c {calibration file} -i {input raw data file} -o {output file} -m{time scale file} [-f{frame counter file}]	converts Satlantic binary data to ASCII tab delimited file with column headers

Table 6. Filters used for merging Satlantic data with MODAPS data.

Filter	Input files	Miscellaneous	Options	Description
comp_sat	*.calibration file for instrument logged in both data file Satlantic binary raw data file logged through MODAPS Satlantic binary raw data file logged through PROVIEW time scale file for data logged through MODAPS	the time scale (time versus byte offsets) is relative to file/acquisition mode - the time scale that is computed is found for the instrument logged in both data files and is latter applied to the that is only logged in the PROVIEW file Display : '.' when packet found in MODAPS extracted file 'p' when packet found in MODAPS extracted file 'y' when MODAPS and PROVIEW packet agree 'n' when MODAPS and PROVIEW packet donut agree 'r' when rewinding of PROVIEW file is needed	-m {file logged through MODAPS } -p { file logged through PROVIEW } -t{input time scale file} -o{output time scale file} [-f{frame counter file}] -c {calibration file}	compares raw Satlantic packets from 2 Satlantic binary data files creates a time scale file for the instrument bypassing MODAPS

ACRJ - LPCM - SAI - U. Oldenburg
NIOZ - U. Trondheim - FUB - PML - GKSS



Table 7. Filters used for merging data together wrt a common clock and/or depth.

Filter	Required Input files	Miscellaneous	Options	Description
dpth_adj	input COAST/OOC file output COAST/OOC file raw data file logged through PROVIEW	depth is counted positive going down	-i{input COAST/OOC file} -o{output COAST/OOC file} -p {raw data file logged through PROVIEW} -d{old depth field} -f {new depth field}	subtract pressure tare value retrieved from Satlantic raw file header from a specified depth field COAST/OOC data file
time_adj	input COAST/OOC file output COAST/OOC file	only used for WetLabs instruments	-i{input COAST/OOC file} -o{output COAST/OOC file}	adjusts time for instruments having packets with several data frames and different times
mergeall	input file 1 input file 2	when no matching is possible -999999 values are put for missing frame	input file 1 time field for input file 1 depth field for input file 1 input file 2 time field for input file 2 instrument depth offset output file name time offset threshold depth offset threshold	synchronizes data wrt depth (using the closest neighbour depth)

Table 8. Filters used to manipulate files produced by the COAST/OOC processing chain.

Filter	Required Input files	Miscellaneous	Options	Description
renamfld	input file file holding field names	when field is not found no changes are made, a file is still created and a WARNING is displayed	infile outfile -c f {string1} [{string2}] Note : string1 may be a filename	renames fields from file
fieldext	input file file holding field names		infile outfile -c f[p] {string1} [{string2}] Note : string1 may be a filename p file is plain without header	extracts fields from data file

Notes :

- 1) Depth offset for AC9 instrument is not using the instrument's dead volume ; since this procedure has not yet been validated this is left to the end user ;
- 2) CTD extrapolated fields (salinity, density,...) are not computed with these filters ;
- 3) All filters have been tested on Sun/HP workstations.

*ACRJ - LPCM - SAI - U. Oldenburg
NIOZ - U. Trondheim - FUB - PML - GKSS*

4) Once data has been extracted from a MODAPS archive file (with the extmod filter), any other filter may be applied to it as if the data had been directly stored in its native format (the format provided by the instrument).

2.2.3.1.3. Recommendations

2.2.3.1.3.1. *Data collection protocol*

As the main objective of the COAST/OOC database was to provide data useful for remote-sensing, providing the best possible surface database was the final goal. Since surface data may only be provided with data extrapolated to the surface from a profile, the procedure that is used by the operator on board a ship or a helicopter when performing in-situ measurements is essential.

This procedure should be as conservative and robust as possible and be as consistent as possible during the life of the project. A lot of emphasis should be set concerning the notes that are written by the operator during the data-acquisition process ; these notes are essential for the person that does the final processing. In addition to the configuration that was used for each station, the date and time of the acquisition, any change in sky or sea conditions should be logged. As these notes may be very subjective and may be very different between operators, a lot of effort should be undertaken in trying to standardise the comments that need to be written : it is not only necessary to write a comment that may be useful for the final processing but it is also essential to provide the comment in a manner that is sufficiently clear and complete for a useful scientific usage. Some time should be reserved for training the operators.

2.2.3.1.3.2. *Surface data computation*

Surface data were computed from data provided with this processing chain but using another set of functions developed under IDL. For adjusting some processing parameters and improving the processing of some data fields it is sometimes useful to have the knowledge of certain quantities specifying the first attenuation depth , as these values are usually estimated from surface data it would be useful to integrate to the main processing chain the tools that were developed for estimating surface data. This would also allow the entire processing to be performed at the same location and make it more operational.

2.2.3.1.3.3. *Self sufficient instruments*

The robustness of a data acquisition system with several very different instruments is very much dependent on the robustness of the instruments themselves ; and relying the processing of one instrument on the availability of a parameter that is measured with another instrument is very much unpredictable and very risky. Therefore, whenever possible and when thriving to have an operational data-acquisition system, self sufficient instruments (with their own depth and temperature gauges for example) should be used ; the availability of a sensor on another instrument should only be considered in view of improving an existing measurement and should not be considered when this measurement can not be done otherwise.

2.2.3.1.3.4. A User Interface to provide easy quality control

A number of IDL functions were developed to quality control the data. The main task of these functions were to provide visualisation capabilities for the person in charge of the data processing to identify very rapidly any flaws in the processing chain or any instrument failure. It was agreed by everyone involved in the processing that this was essential, these functions should be eventually integrated to the global processing chain.

But multiplying the functionalities and the different sorts of tools (C-program, shell scripts, IDL functions in addition to the softwares provided by the different companies that build the various instruments) of such a processing chain may be unrealistic as eventually the person in charge of the processing may be overwhelmed by the number of files and by the number of fields that he eventually has to face. Therefore, some effort should be put in trying to integrate the various functionalities and tools within one single user interface ; this would make the processing chain more operational and more user friendly, and therefore more productive and robust.

This user interface should not only be reserved to the final processing, it should also be provided to the operator that performs the in-situ measurements. It should help him to trouble-shoot the system and find the right diagnosis in the case of a failure ; it should also allow him to verify that the system works sufficiently well for the aims of the project ; and it should improve the communication between the in-situ operator and the data processor leading finally to improvements of the overall system.

2.2.3.1.3.5. Reminder of the different hurdles to pass

A number of hurdles had to be passed to perform the final data processing ; some of them were known before the project, some others were discovered during the project ; they should be kept in mind and are listed below :

- merge the entire data set into a comprehensive and consistent database;
- keep track of the configuration that was used during the data-acquisition ;
- keep track of the configuration that was used during data-processing to be in a position to reprocess the entire data set without too much trouble if needed ;
- chose the best profile when several profiles were performed during the same station ;
- chose the proper and best cast to estimate surface data for each profile ;
- take into account distances between sensors, measure them at the beginning of each campaign ;
- define criteria to identify suspicious data from good data ;
- when several gauges (for example depth or temperature) provide the same measurements in a multi-instruments system, make sure that they are all equivalent before merging the data, if not then try to estimate any relation between those gauges ;

- perform as many calibrations as possible for all instruments and keep properly track of the history of the different calibrations, this is just as essential as the data-acquisition and the data processing ;
- log all error and warning messages when performing the data processing, this will help in the post-analysis when discovering any flaws or artefacts of the data ;
- keep the number of data fields and data files reasonably low ;
- if the data that you are collecting are to be compared eventually with some other measurements performed at the same time, be very much co-ordinated with the group that performs that second set of measurements and agree on a common data naming convention before doing any measurement ;
- once you have collected the measurements, start the data processing as soon as possible ;
- produce self-sufficient data files.

2.2.3.2. Interpretation of the vertical profiles and outputs for a surface data base

2.2.3.2.1. SADAM – The SATLANTIC Data Manager

The radiometric data obtained during the oceanographic campaigns COAST/ OOC 1-6 and ALMOFRONT 2 were processed using an IDL-based software, the Satlantic Data Manager (SADAM), which was specifically designed for this purpose. The main reason for the development of SADAM lies in the fact that certain aspects of the helicopter-based data acquisition and a number of scientific approaches (e.g. extrapolation towards the sea surface) were not sufficiently covered by the existing software package ProSoft provided by the radiometer manufacturer.

In its actual state (Dec. 1999), SADAM comprises 5 major components:

- post-processing of raw data
- depth merging
- surface extrapolation
- graphical output
- numerical output

SADAM can be run in an interactive mode in order to visualise data from a single station or to determine the parameters required for a later automatic processing using the batch mode. One of the main advantages of SADAM is its flexibility with respect to the treatment and visualisation of data gathered in extremely different water types such as encountered during COAST/ OOC. The visualisation of radiometric data as offered by SADAM is very helpful for data inspection and quality

*ACRJ - LPCM - SAI - U. Oldenburg
 NIIOZ - U. Trondheim - FUB - PML - GKSS*

assessment purposes. In the following, the main functionality of SADAM is shortly outlined and illustrated by the graphical output for data gathered in July 1997 during COAST/OOC-3 in the Adriatic Sea.

2.2.3.2.1.1. Requirements

SADAM uses the output of ASCIICON.EXE (code provided by the manufacturer of the radiometer) for applying the manufacturers calibration coefficients and transforming the binary raw data into irradiance values. ASCIICON.EXE can be called directly from the SADAM main menu. Alternatively, the ASCII output of the operational raw data processing developed for the COAST/OOC (see section 2.2.3.1) campaigns can be read into SADAM.

2.2.3.2.1.2. Post-processing of raw data

2.2.3.2.1.2.1. Basic conversions

As first step of the data treatment, a number of physical parameters are derived from the ASCIICON output. These parameters comprise: time since the beginning of the measurements, vertical speed of the profiler in water, tilt of both profiler and reference instruments, salinity and density excess from the CTD data. The irradiance values are transformed into SI-units

2.2.3.2.1.2.2. Dark current subtraction

A proper correction for the dark current is essential, especially if the ambient light level is low as is the case in great depths or heavily absorbing waters. SADAM allows for three different methods of dark current correction: First, a dark correction file may be produced in the lab which is then used for subtracting the dark current. Second, measurements taken at great depths at a given station may be taken as dark signal and subsequently be subtracted. However, the depths required for this approach are often not reached, especially in case I waters where considerable light levels are observed even in the NIR due to Raman scattering from the shorter wavelengths. Therefore, SADAM disposes of an interactive tool to determine the dark current in the red and near infrared. It is based on the fact that the diffuse attenuation coefficient at the longer wavelengths in greater depths asymptotically approaches that of the corresponding Raman excitation wavelength. The user can interactively modify the dark current at a certain wavelength in the red or NIR until the K_d is similar to that of the Raman excitation wavelength. The such determined dark current correction values are stored and automatically reloaded when the raw data is newly processed.

2.2.3.2.1.2.3. Basic quality checks

Single spikes are removed from the data using a three element median filter, bad values are trapped and flagged using consistency checks based on threshold values.

2.2.3.2.1.2.4. Automatic cast detection

A specific aspect of the radiometric measurements using a helicopter as sampling platform is due to the fact that the helicopter is difficult to keep at a constant height, especially at low or varying

*ACRI - LPCM - SAT - U. Oldenburg
NIOZ - U. Trondheim - FUB - PML - GKSS*

wind speeds. These vertical movements, if amplified by the speed of the winch, may lead to fast vertical movements of the instrument in water on the order of 1-2 m/s. In order to ensure data of sufficient quality close to the surface for stations using the helicopter as sampling platform, several up- and down-casts were performed for each station. In order to assist the selection of the best measurements, SADAM disposes of a tool for the automatic identification of the different casts and to subsequently visualise data of the different casts one by one. A graphical representation of the “history” of each station, that is profiler depth, profiler tilt and E_d at 550 nm vs. time, is produced for each station (Figure 15).

2.2.3.2.1.2.4.1. Downward irradiance on the sea surface

A specific aspect of the helicopter-based campaigns is caused by the fact that the reference instrument used to measure the downward irradiance on the sea surface could not be installed on the helicopter. For these campaigns, measurements of E_d taken by the profiler while in air (before and after the in-water measurements) were used to assess E_d on the sea surface. In order to minimise the time lag between the in-water measurements and the E_d values on the sea surface, SADAM automatically chooses the air measurements closest in time.

2.2.3.2.1.2.5. Visualisation of the raw data

All radiometric raw data from the profiler and reference instruments are plotted as function of the profiler depth on a single graph. This allows for a first visual inspection of data quality and also for a first characterisation of the water type. Additionally shown are temperature and density excess profiles as well as vertical speed and profiler tilt (Figure 16).

2.2.3.2.1.3. Depth merging and binning

Depth merging and binning is performed for all casts independently. An independent depth scale is established for each instrument, according from its vertical distance to the pressure sensor. Inclination of the instrument is taken into account. Binning intervals of different vertical extensions may be selected by the user, according to the prevailing vertical stratification. Within each depth window, a regression is used to estimate the value of the parameter of interest: linear regression is used for physical parameters such as temperature or density excess, a logarithmic regression is used for irradiance or radiance measurements. Results of merging and binning are stored for all casts; the user may additionally interactively select single casts for visualisation on the screen or corresponding generation of a PostScript file (Figure 17).

2.2.3.2.1.4. Surface extrapolation

One of the main motivations for the development of SADAM was the motivation to calculate the water leaving light field as accurate as possible from measurements in the top-most water layer. In order to obtain proper results, it is of utmost importance to carefully select the data used for extrapolation. SADAM is supporting the selection of data used for surface extrapolation by a channel-wise graphic representation of the selected measurements and the resulting extrapolation towards the sea surface. The user may interactively select the cast and modify the depth interval used for the

*ACRJ - LPCM - SAI - U. Oldenburg
NIOZ - U. Trondheim - FUB - PML - GKSS*

extrapolation. In order to account for the effects of Raman scattering in the red and near-infrared parts of the upward light spectrum, the user can select a sum of two exponential functions for the extrapolation fit. This is of importance, if the topmost water layer may not be used for the extrapolation due to ship shadowing effects. Additionally, PAR is calculated just above the sea surface and also for a depth of $z=[K_d(685)]^{-1}$. The upward directed sun-induced chlorophyll fluorescence is calculated in Quanta $m^{-1} s^{-1}$. Statistical quality parameters of the surface extrapolation are calculated for a wavelength of $\lambda=560$ nm. The values of the extrapolated irradiances at $z=0^-$ for the selected cast are written on a file. Additionally, a graphical representation of the extrapolation is produced that comprises all spectral channels, as well as the resulting spectra of E_u , K_U and the sub-surface albedo (Figure 18).

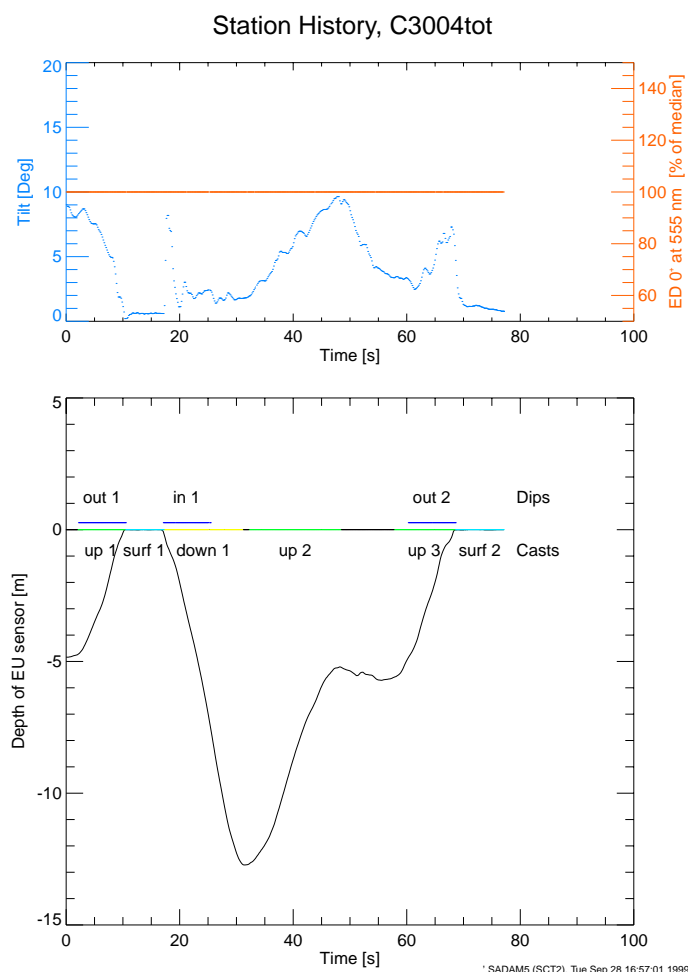
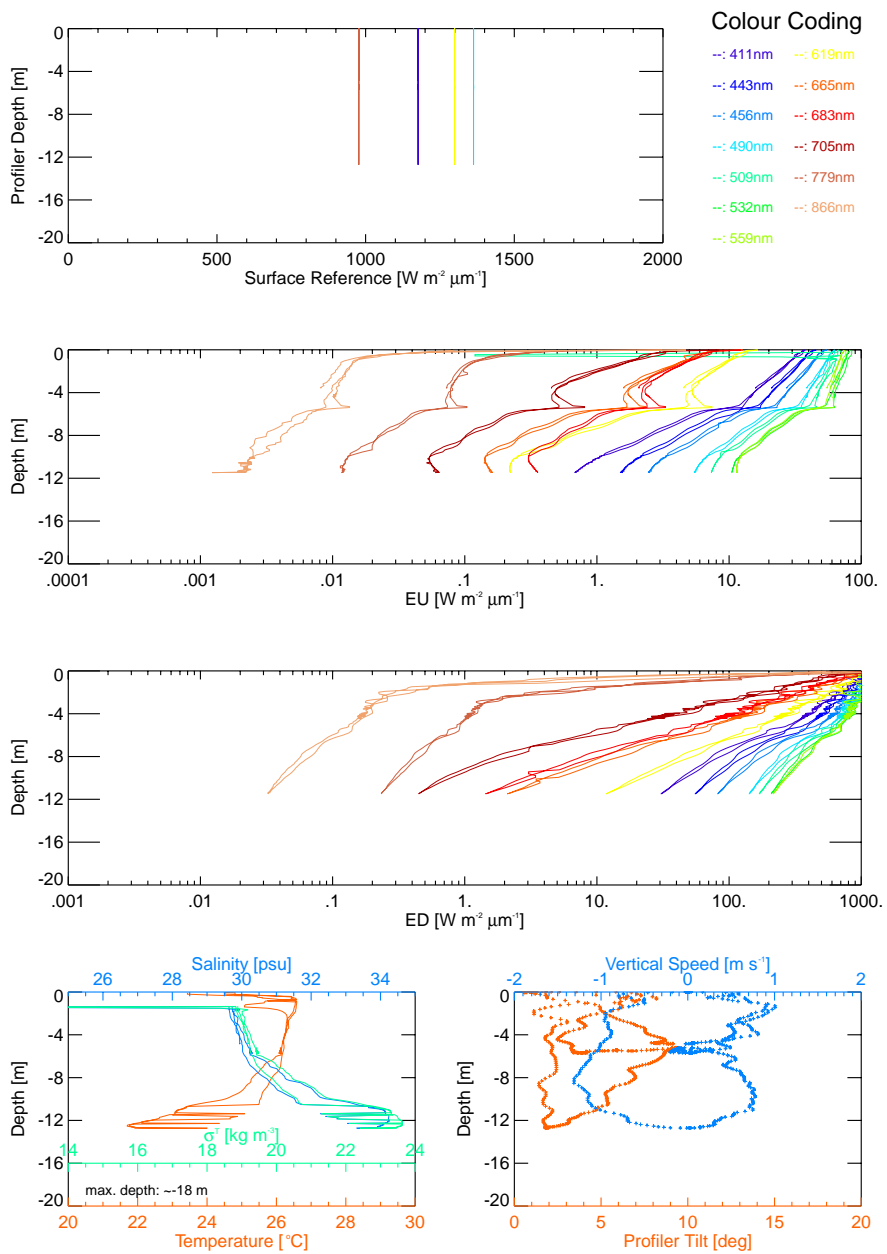


Figure 15. Station history plot. Upper image: Profiler tilt and downwelling irradiance on the sea surface at 555 nm. Lower image: Profiler depth vs. time and cast identifications.

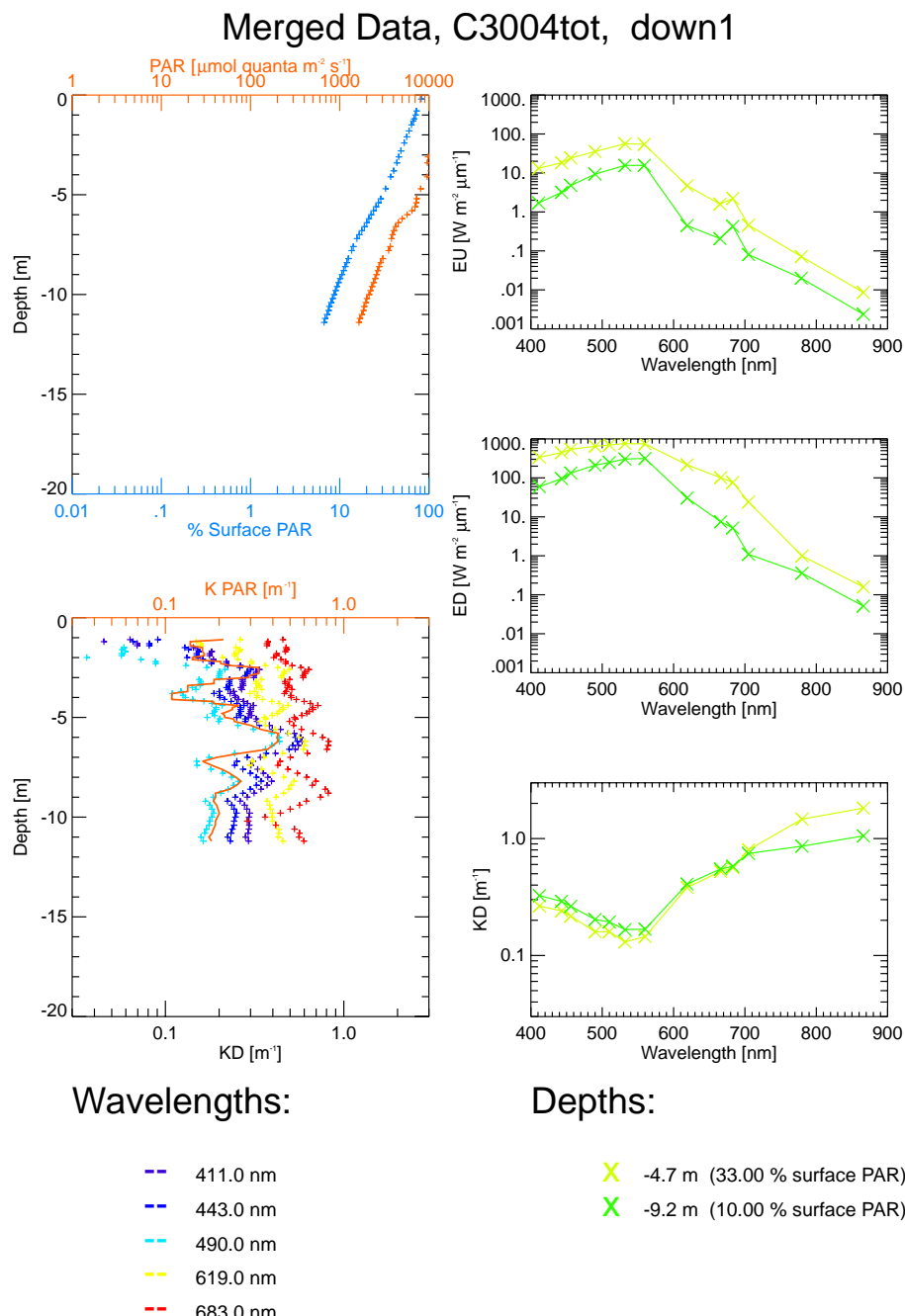
Raw Data: C3004tot



* SADAM5 (PLR4). Tue Sep 28 16:57:01 1999

Figure 16. Graphical representation of irradiances. From top: Irradiance incident on the sea surface at four selected channels, vertical profiles of upward irradiance for all channels, vertical profiles of the downward irradiance for all channels. Bottom left: vertical profiles of temperature, salinity and density excess, bottom right: vertical speed and profiler tilt during the measurements.

ACRJ - LPCM - SAI - U. Oldenburg
NIOZ - U. Trondheim - FUB - PML - GKSS

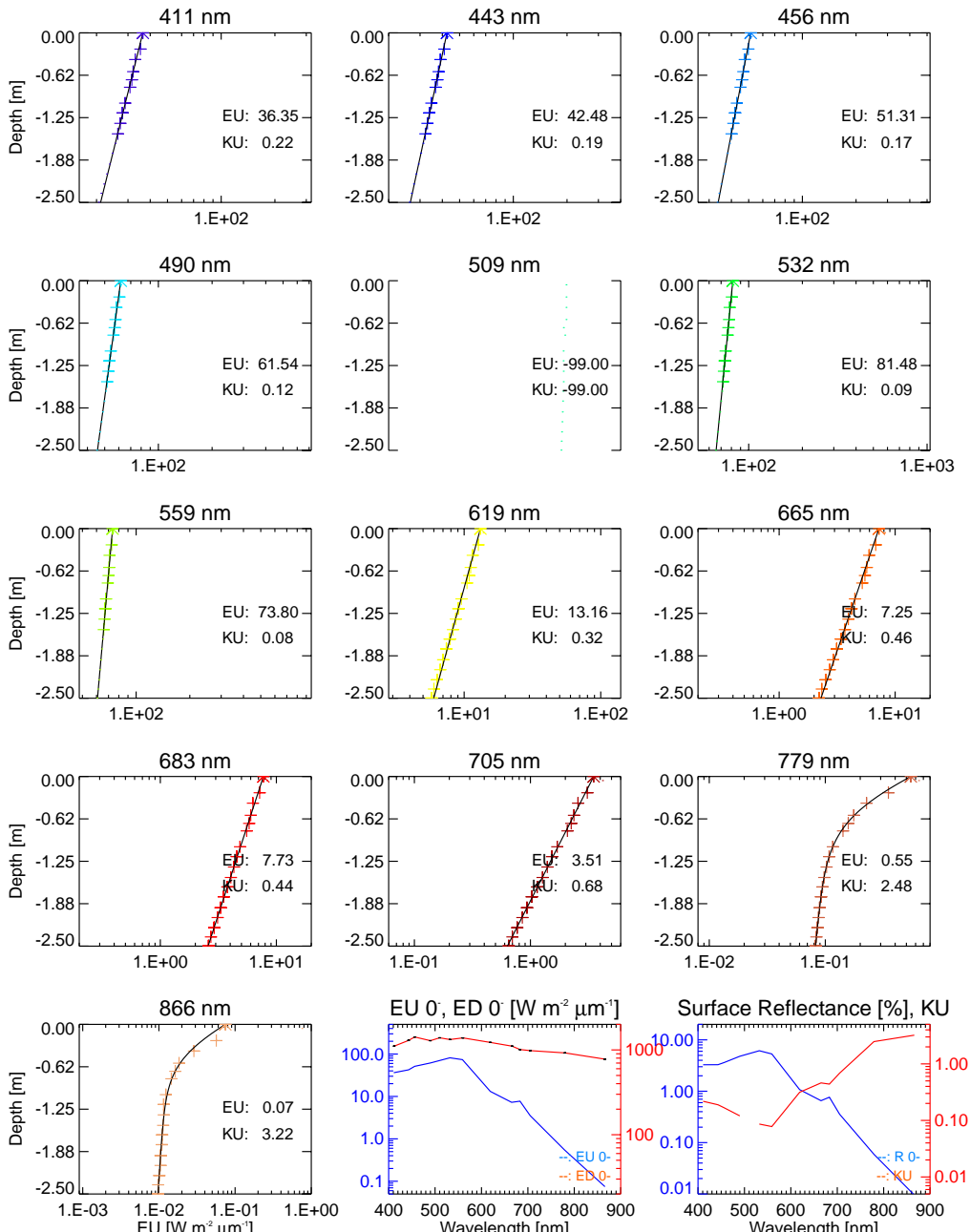


'SADAM5 (PLM3). Tue Sep 28 16:57:03 1999

Figure 17. Graphical representation of depth merged and binned irradiances and other parameters. Left column, top: PAR profile in absolute values and relative to the PAR incident on the sea surface. Left column, bottom: diffuse attenuation coefficients at selected channels and for PAR. Left column, from top: upwelling and downwelling irradiances at the depth level 33% and 10% surface PAR, diffuse attenuation coefficients at the same depth levels.

ACRJ - LPCM - SAI - U. Oldenburg
NIOZ - U. Trondheim - FUB - PML - GKSS

Surface Extrapolation, C3004tot, up1



ERROR CODES:

¹ SADAM5 (SRF6), Tue Sep 28 16:57:04 1999

Figure 18. Graphical representation of the surface extrapolation. Shown are the upward irradiances measured at all spectral channels and the surface extrapolations derived from these measurements. Values that have not been used for the fit are shown as dots. The Raman contribution was considered in the channels at 779 nm and 865 nm by fitting the measurements to a sum of two exponential functions. Additionally shown are upward and downward irradiance spectra just below the sea surface as well as spectra of the reflectance and diffuse attenuation coefficient.

ACRJ - LPCM - SAI - U. Oldenburg
NIOZ - U. Trondheim - FUB - PML - GKSS

2.2.3.2.2. IDL tool for interpretation of absorption, attenuation and backscattering coefficients profiles

As for radiometric data, an IDL tool was developed to perform final processing of and interpret profiles of the absorption and attenuation coefficients (obtained using the AC-9), as well as those of the backscattering coefficient (provided by the BB-4). The main functions of this tool are the following:

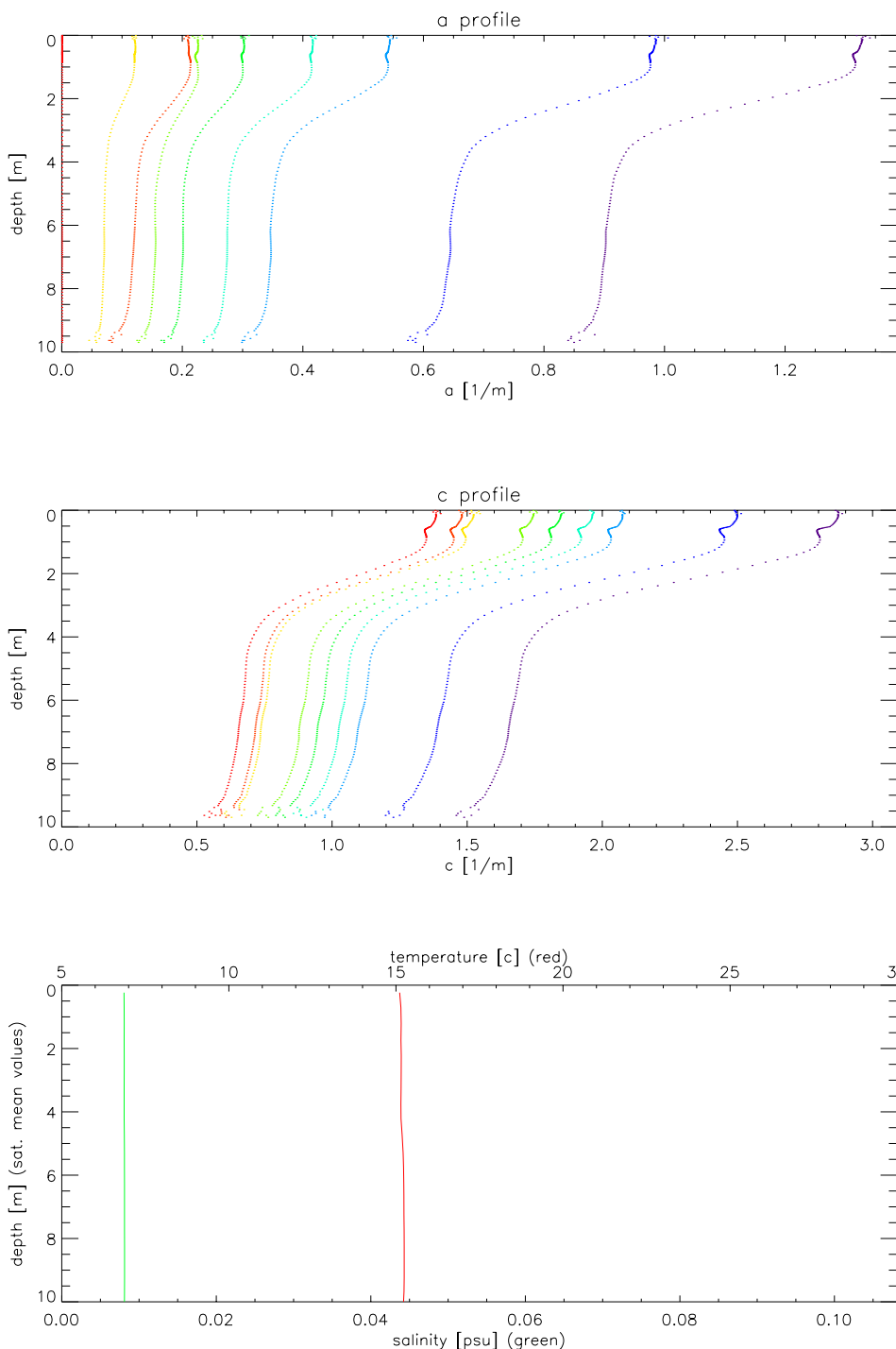
- Compensation of AC-9 data for variations in *in situ* temperature.
- Residual scattering correction of the absorption data.
- Correction of the backscattering coefficient data for attenuation by seawater.
- Depth adjustment when necessary.
- Visualisation of the profiles.
- Selection of the best casts.
- Calculation of mean surface values.
- Visualisation of the surface mean spectra.
- Output of the mean results into an ascii file.
- Output of corrected profiles into an ascii file.

The residual scattering correction applied to the absorption coefficient measured using the AC-9 is the so-called “constant correction”, which simply consists of subtracting $a(715)$ from $a(\lambda)$. Mean values (in fact a median) were generally calculated over one attenuation length (provided by SADAM).

AC9 182, file: C6158tot

lines: 177 to 319

version 1.0 (Nov 3 1999)



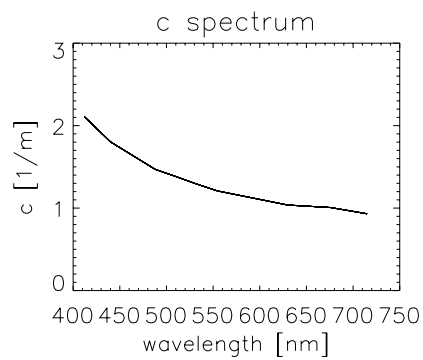
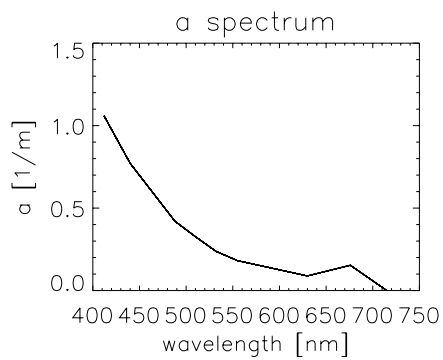
violet: 412nm, dark blue: 440nm, blue: 488nm, turquoise: 510nm, green: 532nm, bright green: 555nm, yellow: 630nm, orange: 676nm, red 715nm,
scattering correction for absorption tube: Zaneveld s method

Figure 19. Example of profiles of the of absorption and attenuation coefficients measured *in situ* using the AC-9.

*ACRJ - LPCM - SAI - U. OI denburg
NIOZ - U. Trondheim - FUB - PML - GKSS*

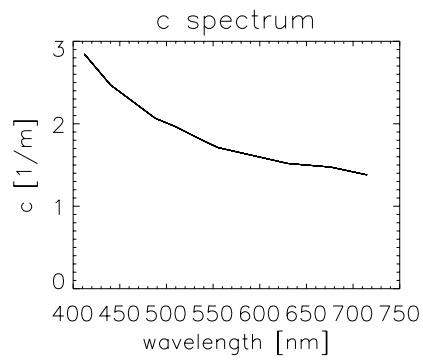
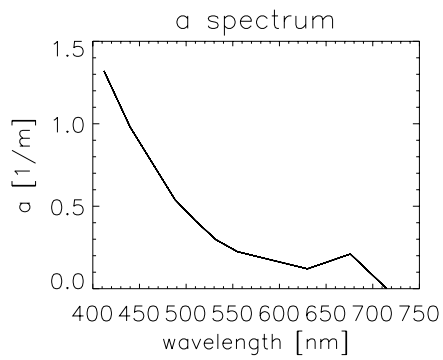
Between 0.00 and 10.00 m depth AC9 182 Total absorption and Total attenuation

Wavelength (nm)	a mean	SDEV	c mean	SDEV
412	1.060	0.198	2.109	0.563
440	0.772	0.161	1.803	0.513
488	0.420	0.094	1.470	0.459
510	0.327	0.069	1.383	0.454
532	0.238	0.050	1.293	0.439
555	0.182	0.036	1.207	0.407
630	0.088	0.025	1.037	0.372
676	0.153	0.046	1.007	0.362
715	0.000	0.000	0.931	0.344



Between 0.00 and first attenuation depth (m)

Wavelength (nm)	Depth (m)	a mean	SDEV	c mean	SDEV
412	0.627 1/E	1.320	0.013	2.846	0.043
440	0.819 1/E	0.980	0.013	2.471	0.047
488	1.279 1/E	0.541	0.014	2.067	0.079
510	1.578 1/E	0.412	0.024	1.965	0.169
532	1.966 1/E	0.297	0.022	1.836	0.177
555	2.114 1/E	0.224	0.010	1.712	0.113
630	1.532 1/E	0.120	0.004	1.518	0.100
676	1.162 1/E	0.210	0.005	1.475	0.097
715	0.881 1/E	0.000	0.000	1.380	0.086



file: C6158tot

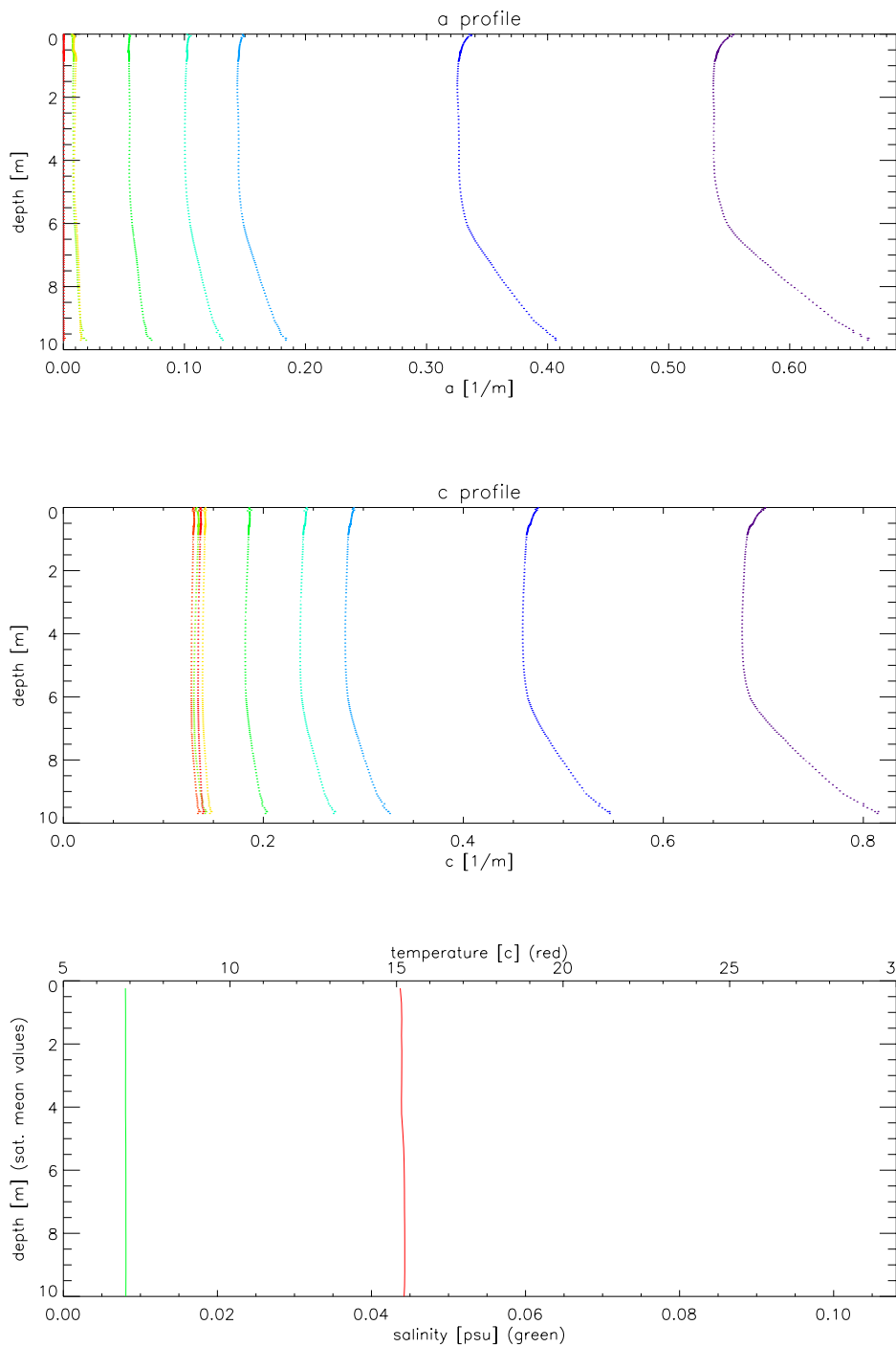
Figure 20. Example of mean surface values derived from the absorption and attenuation coefficients profiles measured *in situ* using the AC-9.

*ACRJ - LPCM - SAI - U. Oldenburg
NIOZ - U. Trondheim - FUB - PML - GKSS*

AC9 102, file: C6158tot

lines: 177 to 319

version 1.0 (Nov 3 1999)



violet: 412nm, dark blue: 440nm, blue: 488nm, turquoise: 510nm, green: 555nm, bright green: 630nm, yellow: 650nm, orange: 676nm, red 715nm,

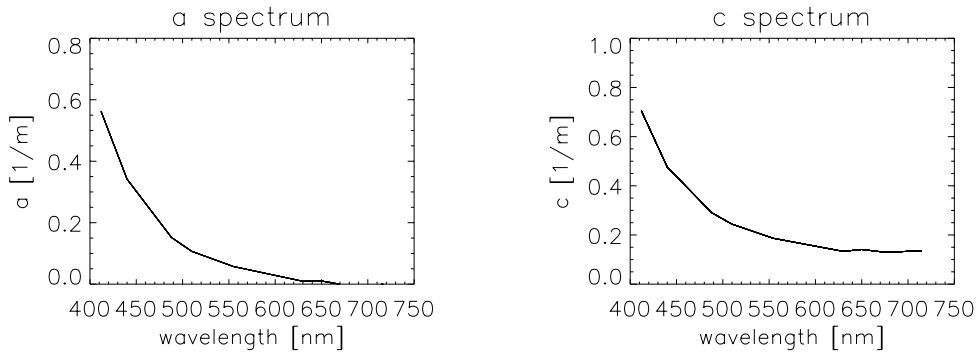
scattering correction for absorption tube: Zaneveld s method

Figure 21. Example of profiles of the of absorption and attenuation coefficients measured *in situ* using the AC-9 equipped with a 0.2 μm filter.

*ACRJ - LPCM - SAI - U. Oldenburg
NIOZ - U. Trondheim - FUB - PML - GKSS*

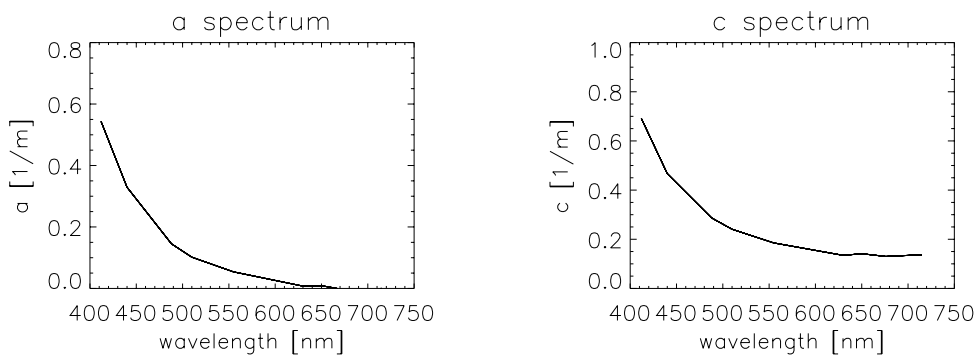
Between 0.00 and 10.00 m depth AC9 102 absorption by DOM and attenuation by DOM

Wavelength (nm)	a mean	SDEV	c mean	SDEV
412	0.562	0.037	0.705	0.037
440	0.342	0.023	0.476	0.023
488	0.152	0.011	0.291	0.011
510	0.107	0.009	0.244	0.009
555	0.057	0.005	0.186	0.005
630	0.009	0.003	0.133	0.003
650	0.010	0.003	0.141	0.002
676	-0.003	0.002	0.129	0.002
715	-0.000	0.000	0.136	0.002



Between 0.00 and first attenuation depth (m)

Wavelength (nm)	Depth (m)	a mean	SDEV	c mean	SDEV
412	0.627 1/E	0.543	0.005	0.692	0.005
440	0.819 1/E	0.329	0.003	0.467	0.003
488	1.279 1/E	0.145	0.002	0.287	0.002
510	1.578 1/E	0.102	0.001	0.241	0.002
555	2.114 1/E	0.054	0.001	0.185	0.001
630	1.532 1/E	0.008	0.001	0.134	0.001
650	1.337 1/E	0.009	0.001	0.141	0.001
676	1.162 1/E	-0.005	0.001	0.130	0.001
715	0.881 1/E	-0.000	0.000	0.137	0.001



file: C6158tot

Figure 22. Example of mean surface values derived from the absorption and attenuation coefficients profiles measured *in situ* using the AC-9 equipped with a 0.2 μm filter.

ACRJ - LPCM - SAI - U. Oldenburg
NIOZ - U. Trondheim - FUB - PML - GKSS

BB4_profiles file: C6158tot

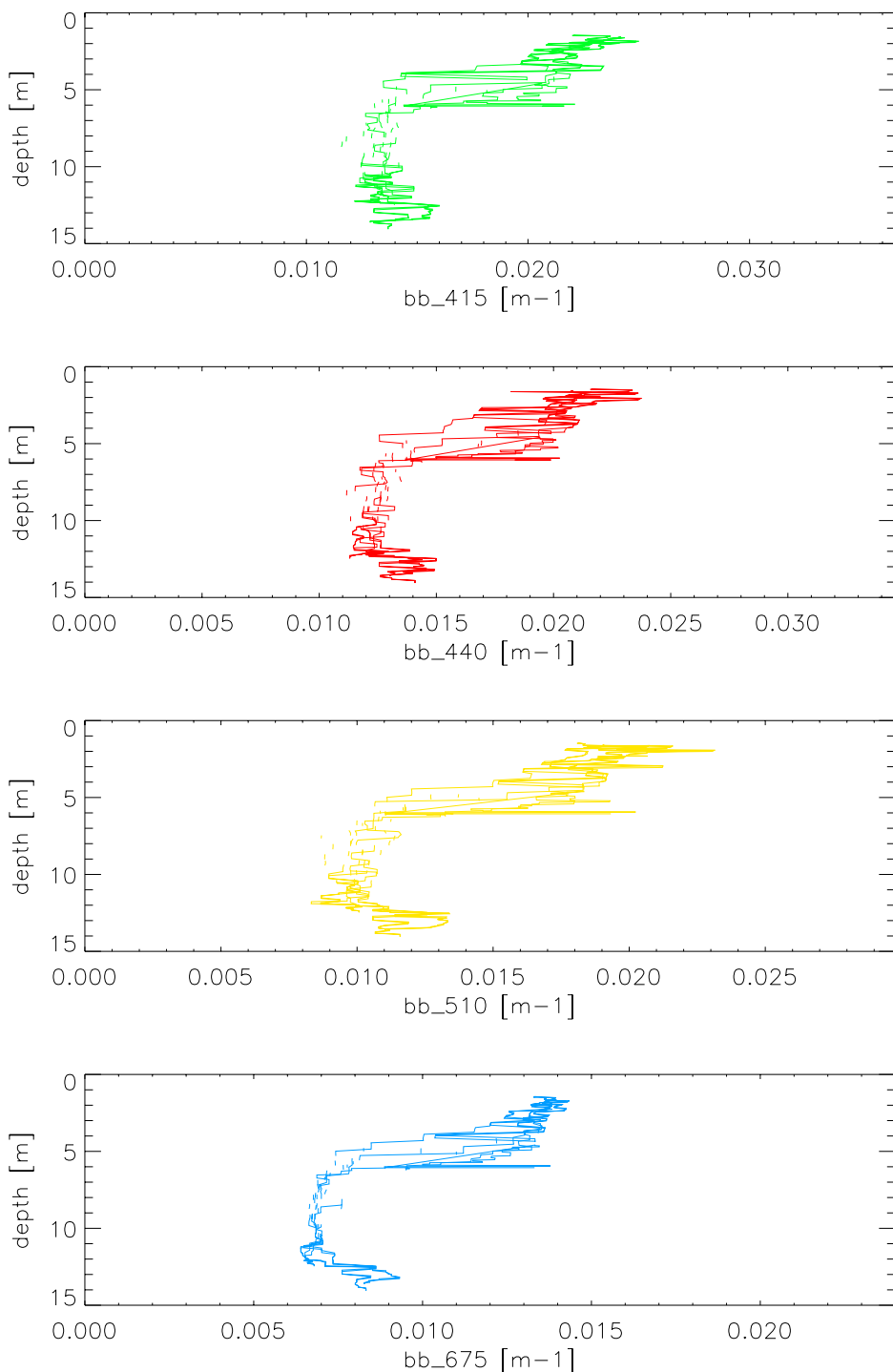
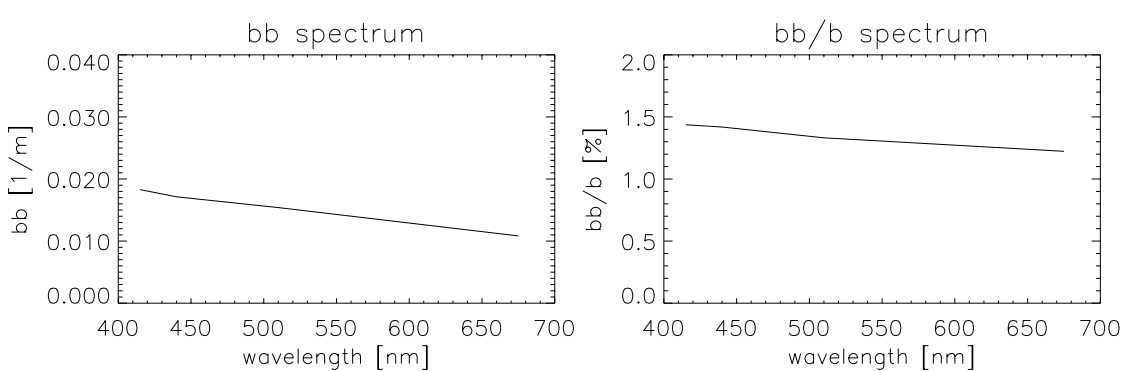


Figure 23. Example of profiles of the of backscattering coefficient measured *in situ* using the BB-4 backscattering-meter.

*ACRJ - LPCM - SAI - U. Oldenburg
NIOZ - U. Trondheim - FUB - PML - GKSS*

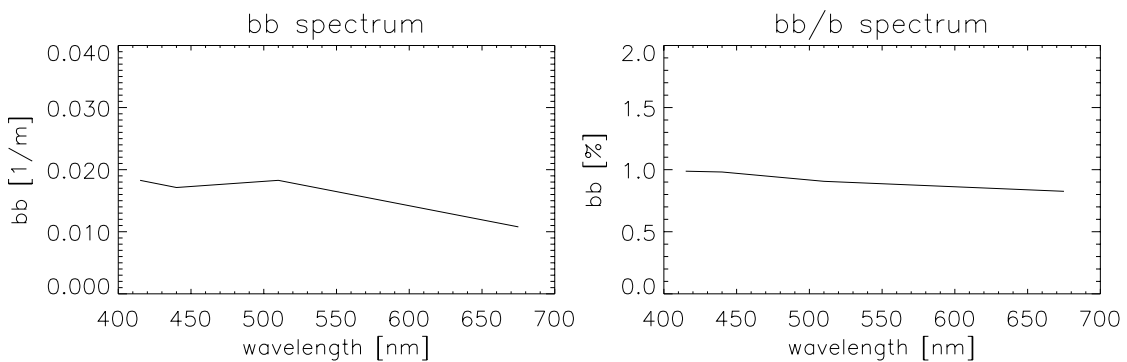
Between 0.00 and 10.00 m depth (BB4 measurements)

Wavelength (nm)	bb mean (m ⁻¹)	SDEV (m ⁻¹)	bb/b mean (%)
415.0	1.8293E-02	3.9847E-03	1.4371
440.0	1.7133E-02	3.7425E-03	1.4185
510.0	1.5394E-02	3.9017E-03	1.3319
675.0	1.0833E-02	2.7924E-03	1.2230



Between 0.00 and first attenuation depth (m)

Wavelength (nm)	Depth (m)	bb mean (m ⁻¹)	SDEV (m ⁻¹)	bb/b mean (%)
415.0	10.027	1.8284E-02	3.9865E-03	0.9879
440.0	10.019	1.7123E-02	3.7448E-03	0.9811
510.0	1.578	1.8282E-02	2.6457E-04	0.9064
675.0	10.162	1.0785E-02	2.8093E-03	0.8257



file: C6158tot

Figure 24. Example of mean surface values derived from the backscattering coefficient profiles measured *in situ* using the BB-4 backscattering-meter.

ACRJ - LPCM - SAI - U. Oldenburg
NIOZ - U. Trondheim - FUB - PML - GKSS

2.2.3.3. Data bases

Two objectives of the COAST/OOC project in relation with the development of a database and the implementation of a web server, as identified in the proposal submitted in 1995, were:

- "To produce a large data set of the inherent optical properties of the main classes of optically significant substances in the European coastal waters" (Workpackage 1, Objective #1)
- "To implement ocean colour analysis into a video server frame, allowing a wide field of users to exploit this information for economically and socially important applications" (Workpackage 4, Objective #5)

The successful flight of the CZCS ocean colour sensor during the 80's provided the scientific community with a large amount of data on the open ocean, and the knowledge about its chemical and biophysical properties was increased through the development of new bio-optical algorithms. Although they represent an important challenge in term of economic and social applications, the coastal zones where not considered by the first generation of ocean colour sensors, in particular because of a lack of reliable information about the *in situ* characteristics of the coastal waters; the first objective of the COAST/OOC project was devoted to improve this significant field of the knowledge. The latter objective was identified to make the information collected available for the largest possible panel of users. Approaching the new millennium, the exploitation of the ocean colour data was still a "specialists" problem, and it was important to products to the non-expert users, the simplest way being through the implementation of a video-server on the Internet platform.

2.2.3.3.1. The Database

At the end of the project 1.5 Gigabytes of data have been collected and a database has been built as shown in Table 9 and Table 10. It is composed of two main parts containing (a) the optical data characterising the in-water light field and (b) the so called "bottle data" which correspond to the analyses performed on the samples collected during the field campaigns. Some additional databases have been added to take in account the knowledge in some particular fields of the different partners involved in the COAST/OOC project. They are listed in the Table 10.

2.2.3.3.2. The www video server

During the first year of the COAST/OOC project, a draft version of a web server has been presented to the partners with a discussion about its future development and the needs of the scientific and public on the subject.

It appeared that since the writing of the proposal, a significant number of public web sites had appeared on the Internet providing for free, in near real-time, an information on ocean colour and its derived products. So the need identified in the Objective #5 was no more up-to-date, and the idea of the video-server was abandoned.

Description		approximate size (Mb)
OPTICS	Optics (Radiometry, Absorption, attenuation)	1000.0
BOTTLE DATA	Geolocalisation, meteorology	0.5
	Particulate absorption	5.0
	Coloured Dissolved Organic Matter absorption CDOM	5.0
	Pigments concentrations	0.7
	Phytoplankton counts	0.5
	Bacterii counts	0.4
	Total suspended particulate matter weight SPM	0.2
	Carbon/Hydrogen/nitrogen analysis CHN	0.6
	Dissolved Organic Carbon concentration DOC	0.4
	Atomic composition (X-ray fluorescence)	0.2
TOTAL		1013.5

Table 9. The general COAST/OOC database

Partner	Description	approximative size (Mb)
NIOZ	Radiometry	1.0
	Bottle data	0.3
PML	Radiometry	6.0
	Absorption/attenuation	6.0
	Bottle data	1.0
OLDENBURG	Radiometry	95.0
	Absorption/Fluorescence	16.5
	Bottle data	18.0
TOTAL		143.8

Table 10. The additional COAST/OOC databases

At the end of the project, the database is complete at 95%. Some additional data are still to be analysed, in particular some pigments concentrations from the last field campaign.

Concerning the www server, the initial objective #5 has been revised:

- The actual distribution of the data is on CD-rom, exclusively to the partners of the project
- The future public distribution will start at the end of the two years private use period. It will be done through an Internet site, on CD-rom support, and will only concern raw data.

*ACRI - LPCM - SAI - U. Oldenburg
NIOZ - U. Trondheim - FUB - PML - GKSS*

2.2.3.3.3. Perspectives for future

At the end of the two years private use period, the COAST/OOC database will be made available to the public community, and will be ready to be implemented in any existent marine optics database.

An effort will be done with the amelioration of the COAST/OOC web server to allow to the largest number of public users to gather information on marine optics, and to obtain the raw data collected during the field campaigns.

2.3. PARAMETERISATION OF IOPs

2.3.1. Bacteria

Water samples were collected for bacteria analyses all stations. After fixation the samples were kept under constant cooling and later analysed in the laboratory. Particles present in the samples are analysed using a research flow cytometer (Coulter-Elite-ESP) which has been adapted to analyse particle in the micron and sub-micron range and DNA values in the fg/cell range. The results of the bacteria analyses were split into 2 size fractions (Figure 25):

- Bacteria group I in counts/ml = cell number per ml; this group is characterised by relatively low DNA content expressed per cell.
- Bacteria group II counts/ml = cell number per ml; group is characterised by relatively high DNA content expressed per cell.

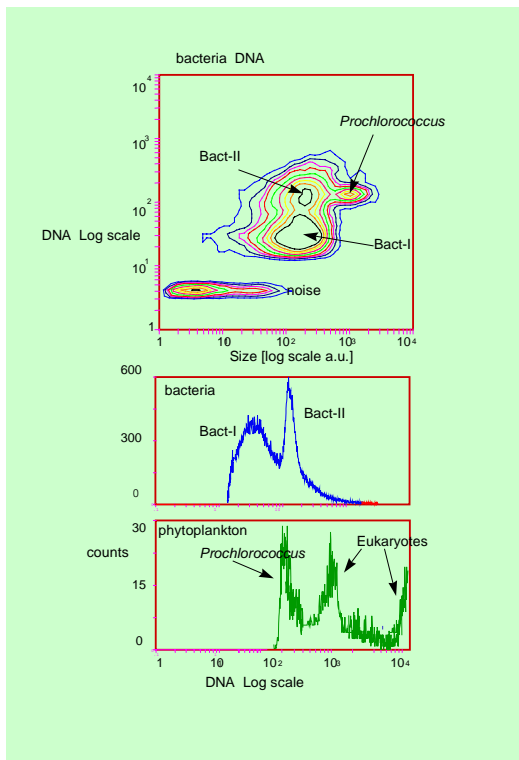


Figure 25. Typical bivariate contour plot and single parameter histograms of size versus DNA signal showing the presence of two subpopulations of bacteria. *Prochlorococcus* can be assigned based on their chlorophyll signal. Signal parameter plots show relative DNA signals of bacteria and phytoplankton component.

2.3.1.1. Instrument Description

This instrument is equipped with a 125 mW Ar-laser (488 nm). The dsDNA-dye complex is detected in the green PMT (FL1: emission 525 ± 20 nm). Since this dye hardly interferes with the fluorescence of the phytoplankton pigments this plankton group can be discriminated from the other particles. The chlorophylls signals of the phytoplankton are measured in the red PMT (FL3: emission > 610 nm). In addition the side scatter (SS) signals of each particle are collected as well. All signals are collected on a 4-decade log scale except for the DNA signal of *Prochlorococcus* which is also measured on a linear scale (peak and integral). A total of 0.5 tot 1 ml sample is screened and data is stored as list mode files (FSC 2.0.lmd type) for later analysis.

3. Instrument Calibration and Quality Assurance:

Alignment of the flow cytometer is examined on a daily base using $2.0 \mu\text{m}$ beads and settings are adjusted when needed. To minimise day to day variations DNA values of the different groups of bacteria and phytoplankton are also expressed relative to that of *Prochlorococcus*.

2.3.1.2. Methodology and Processing Description

Water sampling and treatment for bacteria: Sampled at surface. Brown glass bottles are filled with unfiltered seawater (100ml or 30 ml bottles). 0.8 ml pre-filtered Formaldehyde (37%) is added. The samples are stored in a (dark) refrigerator at 5 degrees Celsius until analysed.

For flow cytometry analysis:

- Samples are thawed shortly before use and the dsDNA of the particles are stained using PicoGreen (MP, P-7581) after Veldhuis et al (1997). 10 microliter PicoGreen (10 fold diluted) is added to 500 microliter of sample and incubated for 60 min in the dark prior analysis.
- DNA containing particles are discriminated from debris based on the fluorescent properties of the dsDNA-dye complex. Bacteria are abundantly present (Figure 25) but also phytoplankton can be distinguished based on their chlorophyll fluorescence. In particular *Prochlorococcus* shows a typical DNA signature (constant value with low CV). Considering the great abundance of this species its DNA signal was used may be used as an internal standard.

2.3.1.3. Data analysis and classification

Data files are analysed using ELITE software (version 4.3). The chlorophyll fluorescence signal (FL3) is used to discriminate phytoplankton from other particles. Different groups of bacteria-plankton can be assigned on their size versus DNA content (Figure 25). Essentially two groups of bacteria can be discriminated; Bact-I (group with relative low DNA content) and Bact-II (group of bacteria with 3 -4 fold higher DNA content) (cf. Li et al, 1995).

Cell abundance is estimated using a solution of beads with known density and corrected (when necessary) for counting coincidence when counting rate of particles exceeded 500 counts per second. In general cell numbers thus estimated for *Prochlorococcus* yield only slightly lower values (<10%) than those obtained in the analysis of the freshly analysed samples. The data set contains information on cell abundance of the two main groups of bacteria in relative numbers and normalised against DNA signal of *Prochlorococcus*.

2.3.1.4. Results

Results of all campaigns can be found as an Excel worksheet on the COAST/OOC CD-ROM. These campaigns are the Victor-Hensen cruise (C100), the area of Saint Marie de la Mer (C200), Venice (C300) shown in Figure 26, the Gulf de Lion (Thethys, C400), The Poseidon cruise (C500) and shown in Figure 27 for the Plymouth area, North Sea, German Bight and Baltic (C600).

The sampling and analyses were merely performed to monitor this parameter to give a more complete water quality impression of the visited stations and for eventually later interpretation.

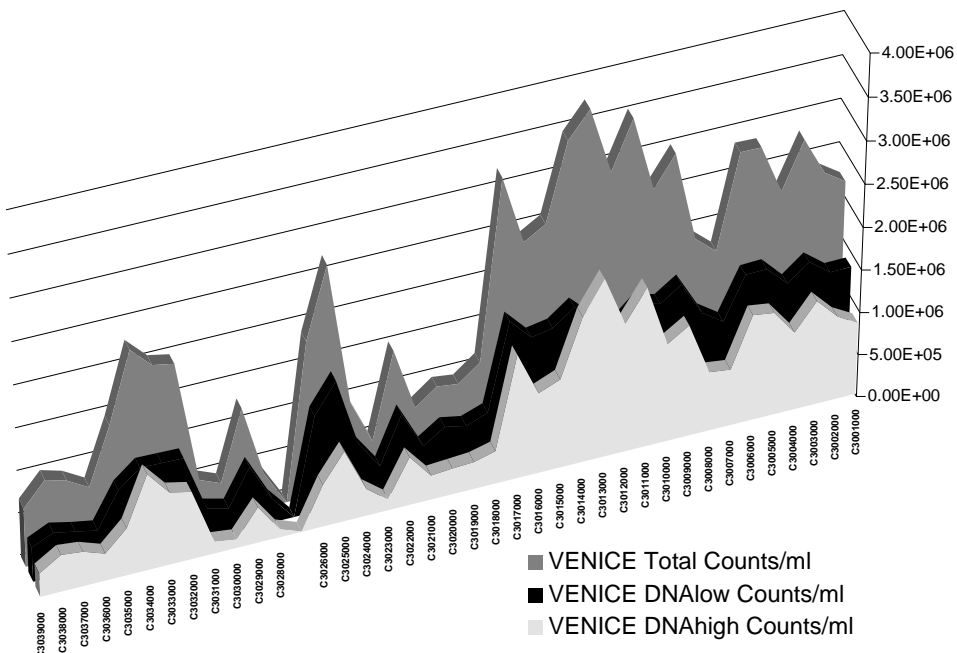


Figure 26. Bacteria concentration in cells/ml for all stations of campaign C300.

Variation in total bacteria concentrations range between an average of $1 \times 10^{+6}$ cells/ml for C200, 300 and 400 up to $3 \times 10^{+6}$ cells/ml for C600and C500. The bacteria concentration during C100 did not changed to much compared to the other campaigns and had an average concentration of $2 \times 10^{+6}$ cells/ml.

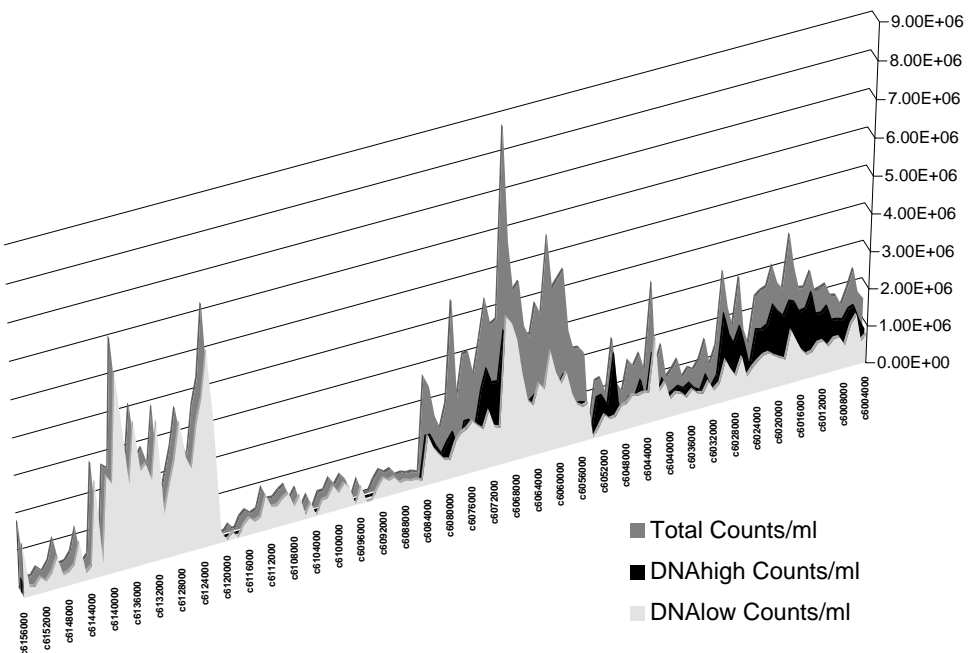


Figure 27. Bacteria concentration in cells/ml for all stations of campaign C600.

Acknowledgements:

Analysed with the help and instructions from Marcel Veldhuis and Gijs Kraay: Netherlands Institute for Sea Research.

References:

- Li, W.K.W., J.F. Jellett & P.M. Dickie, 1995. DNA distribution in planktonic bacteria stained with TOTO or TO-PRO. Limnol. Oceanogr. 40: 1485 - 1495.
- Vaulot, D., D. Marie, R.J. Olson & S.W. Chisholm. 1995 Growth of Prochlorococcus, a photosynthetic prokaryote, in the Equatorial Pacific Ocean. Science 286: 1480 - 1482
- Veldhuis, M.J.W., T.L. Cucci & M.E. Sieracki. 1997 Cellular DNA content of marine phytoplankton using two new fluorochromes: taxonomic and ecological implications. J. Phycol 33: 527 - 541.

2.3.2. Phytoplankton species composition

TBS (U. Trondheim) has been in charge of phytoplankton identification and enumeration of all COAST/ OOC campaigns. In addition, auxiliary measurements of *in vivo* fluorescence excitation spectra and pigment analysis (HPLC) have been carried out by TBS on two cruises.

During the COAST/ OOC project period it became clear that the project needed taxonomist identifying and enumerating the phytoplankton present in the surface samples/images. Because of this,

*ACRJ - LPCM - SAI - U. Oldenburg
NIOZ - U. Trondheim - FUB - PML - GKSS*

TBS major task has been to identify and enumerate the phytoplankton from water samples obtained from the COAST/OOC campaigns. Phytoplankton from surface water samples from all COAST/OOC stations have been counted and identified at TBS. All results are aligned in worksheets were sent to ACRI and included into the COAST/OOC data base.

The taxonomic data is currently used in combination with bio-optical characteristics, i.e. spectral total absorption, detrital absorption, absorption from phytoplankton, and light received by photosystem II by using fluorescence excitation spectra. This bio-optical information is then compared with chemotaxonomical information from pigment-specific pigment markers (HPLC). The different data sets are aligned together for comparison and may be an useful aid for optical characterisation of European waters. A compilation of this data set will be submitted for publication in an international scientific journal. The taxonomical information (species and cell numbers) will be a part of the COAST/OOC database, including data of toxic and potential bloom forming species found during the campaigns.

2.3.2.1. Notes on cell counts from COAST/OOC campaigns

2.3.2.1.1. Method

All samples were counted in sedimentation chambers. Because of the great variety in samples from the different COAST/ OOC cruises, sedimentation volume was determined after evaluation of population density. The smallest sedimentation volume was 2 ml, the largest 50 ml. Usually, the whole bottom area was examined, or several transects were counted when the sample was dense. Final numbers are the mean of two counts or more. Very dense samples were counted in 2 ml chambers, but some samples were still very dense. In such cases, only a small area of the chamber is counted, and cell contents in whole samples is calculated with a specific correction factor. In that case, more than two counts were made before calculating the mean. In the tables, all numbers are as they come after correction for area counted and sedimentation volume, and no rounding has been done. The numbers in the tables refer to cells per milliliter.

2.3.2.1.2. Discussion of error sources

Some groups are more difficult to identify than others when analysed with light microscopy and sedimentation techniques. The identity of the diatoms is usually quite clear, but in some cases they proved more difficult. I grouped some genera together because the identity was unclear (*Leptocylindrus* spp., *Guinardia delicatula* and *Dactyliosolen fragilisimus*) and in most cases it is of no big importance to separate them (e.g. the pigment composition is identical, the size distribution of the mentioned species in the actual samples were the same). The genus *Chaetoceros* has many different species and I made no effort to further identify them, as it seemed unnecessarily time-consuming considering the goal, namely to identify representatives of different pigmentation groups. The dinoflagellates are sometimes difficult to identify to species level, and when the samples are fixed with "Lugol's iodine", it is hard to separate autotrophs from heterotrophs. In the category 'Sum dinoflagellates', *Protoperidinium* has been omitted since most of the species are heterotrophs and do not contribute to pigment analysis. The group 'Flagellates' is hard to describe clearly, any small cell

ACRI - LPCM - SAI - U. Oldenburg
NIOZ - U. Trondheim - FUB - PML - GKSS

that looks like it was alive at the time of fixation and with no other distinguished feature (characteristic shape, coccoliths on the surface etc.) is included here. To my experience, even loose chloroplasts from large diatoms can in some cases be included here, since they sometimes look like a small, undistinguished cell when the silica wall is disrupted and chloroplasts are released in the sample. The smallest cells are not always recognised and counted, and some cells are destroyed by fixation and shaking of samples before sedimentation, so this group has a large error related to the cell counts. In some cases, e.g. when we came into waters with what seemed clearly like a bloom/post-bloom of the haptophyceae *Phaeocystis* (around the coast of Belgium/The Netherlands), the major part of the group 'Flagellates' will be of this species.

2.3.2.2. Results on a campaign basis

COAST/OOC # 1: Bremerhaven – Las Palmas (R/V Victor Hensen, April 1997).

Very few cells found in most samples from this cruise. In transect outside Rhine outlet (st. 01 – 09) some diatoms were registered, mainly *Chaetoceros* spp., *Guinardia* sp. and *Rhizosolenia* spp. Members of Cryptophyceae were found in the same transect, and the largest cell numbers belonged to the group often referred to as "Flagellates, indet." which consists of unidentified, small cells. A large error is related to these numbers.

Very few cells were found in the samples from the rest of the cruise. At st. 10 – 13, 17, 22 – 23, 26 – 30, 32 – 36, 40 and 43 no cells were found in samples.

COAST/OOC # 2: Golfe du Lion Sainte Maries de la Mer (July 1997).

Two transects from the coast and outwards, on two successive days. A main feature is higher numbers of diatoms at the station closest to the coast, st. 01 and 11. *Skeletonema* is the most prominent species, followed by *Chaetoceros*, *Leptocylindrus*³ and a pennate diatom. In some samples, dinoflagellates were found in numbers reaching 67×10^3 cells L⁻¹ (total number at st. 01), but in most of the samples the total number of cells were much less. On st. 01, 240×10^3 cells L⁻¹ of cryptophyceans were found. High numbers ($1-3.5 \times 10^6$ cells L⁻¹) of flagellates were found at some stations.

COAST/OOC # 3: Venise (Adriatic Sea, Helicopter, August 1997).

The populations are dominated by the large diatom *Cerataulina pelagica* during the whole cruise, reaching a density of approx. 11×10^6 cells L⁻¹ at st. 25. At most of the stations the diatoms *Thalassionema nitzschiooides* and *Pseudo-nitzschia* spp. were also found, but never in such high densities as *C. pelagica*. Stations 25-28 are localised near the outlet of the river Po, and this affects the plankton community in the area. High diatom density was registered, and also species of other groups mainly related to freshwater (the Cyanobacteria *Merismopedia* spp., the Chlorophyceans *Scenedesmus* spp. and *Pediastrum* spp., and Euglenophyceans). At st. 25, the diatoms *Cylindrotheca closterium* and

³ These numbers might include cells from *Leptocylindrus* spp., *Guinardia* spp., and *Dactyliosolen fragilisimus*

Chaetoceros spp. reached densities of 23 and 8.9×10^6 cells L⁻¹. Samples from st. 12 and 13 contained high numbers of Cryptophycean cells, 4.6 and 1.4×10^6 cells L⁻¹. Dinoflagellate numbers were usually not very high ($< 24 \times 10^3$ cells L⁻¹) but a small, unidentified dinoflagellate reached numbers as high as 372×10^3 cells L⁻¹ (st. 19).

COAST/OOC # 4: Golfe du LionSept- (Mediterranean Sea, Thethys II, Oct 97).

Several transects on different days, from land and outwards (crossing a front?). The transects st. 1 – 5, 7 – 13, 14 – 19 and 20 – 25 are characterised by dominance of the diatom *Skeletonema*. At stations 9, 10, 14, 15 and 16, *Skeletonema* was found in numbers from 37 to 64×10^6 cells L⁻¹. The largest cell numbers were found close to shore and outwards, but at the outermost station populations of *Skeletonema* were reduced to almost zero or very few cells. Another group of diatoms, *Chaetoceros* spp., occurred in quite big numbers in the same transects and again, populations seemed to diminish further away from the coast. *Pseudo-nitzschia* spp. was found in smaller numbers than *Chaetoceros* spp. but still in a primary position when it comes to cell numbers, and the distribution seemed similar to the other diatoms. Some dinoflagellates were found, and the highest counts were of an unidentified dinoflagellate. In these three transects Cryptophyceans were found in numbers from zero to 861×10^3 cells L⁻¹ (st. 16). Flagellates, indet. were found at all stations, in different amounts. In the next transect (st. 20 – 25) the diatom population was much the same as before, with dominance of *Skeletonema*, *Chaetoceros* spp. and *Pseudo-nitzschia* spp., and flagellates at all stations. The difference was the lack of registrations of dinoflagellates and Cryptophyceans. In the last three transects (st. 26 – 31, 32 – 35 and 36 – 42) The numbers of diatoms were radically lower than in the other transects ($< 91 \times 10^3$ cells L⁻¹ totally at st. 28, which had the highest count). Dinoflagellates and Cryptophyceans were scarce, and flagellates were sometimes not counted because of detrital material in the samples. The last transect was outside the Rhone outlet, and this probably explains the high detritus content.

COAST/OOC # 5: Las Palmas – Kiel (Poseidon, May 1998).

- St. 05 – 07 Biscaya: *Guinardia delicatula* was the most prominent diatom (highest record: 390×10^3 cells L⁻¹). Very few dinoflagellates were found ($< 5.5 \times 10^3$ cells L⁻¹) and some flagellates ($< 450 \times 10^3$ cells L⁻¹).
- St. 08 – 13 Outlet Loire: Several diatoms were found here, *Rhizosolenia* spp., *Chaetoceros* spp., *Cerataulina pelagica* being the most prominent (largest cell numbers 380 , 420 and 352×10^3 cells L⁻¹). No dinoflagellates registered in these samples. Cryptophyceae reached 330×10^3 cells L⁻¹ and flagellates 2.3×10^6 cells L⁻¹ at st. 08.
- St. 14 The English channel: Almost no cells found, only a few flagellates (16×10^3 cells L⁻¹).
- St. 15 – 22 Outlet Seine: *Guinardia delicatula* dominated the whole transect, maximum cell number 3.6×10^6 cells L⁻¹ at st. 16 and 17. A few dinoflagellates were seen in the samples. Quite a few Cryptophyceans were found, 600×10^3 cells L⁻¹ at st. 16. Flagellates reached a density of 4.1×10^6 cells L⁻¹ at st. 16.
- St. 23 – 29 Outlet Thames: A lot of detrital material (especially close to the shore) made the counting difficult and unreliable, and very few cells were found in the samples. At the outermost

stations 23 – 25, some Cryptophyceans (max. 270×10^3 cells L $^{-1}$) and flagellates (max. 5.8×10^6 cells L $^{-1}$) were found.

- St. 30 – 37 Outlet Schelde: Large numbers of flagellates were found, the highest count was at st. 34 (close to 40×10^6 cells L $^{-1}$). At one station some Cryptophyceans were registered and the diatom *Pseudo-nitzschia* spp. was found in all samples in this transect.
- St. 38 – 45 The Wash: High numbers of flagellates (max. 18×10^6 cells L $^{-1}$) were found, probably due to a bloom of the prymnesiophyte *Phaeocystis* sp. A few Cryptophyceans were found, and some individuals of diatoms (but too few to be counted).
- St. 46 – 52 Ems: A few diatoms were found in this transect, but never more than 11×10^3 cells L $^{-1}$ (st. 50). Some dinoflagellates of the species *Gyrodinium* were seen, the highest number being 150×10^3 cells L $^{-1}$ at st. 50. Flagellates spanned from 100×10^3 (st. 50) to 3.9×10^6 (st. 49) cells L $^{-1}$.
- St. 53 – 60 Helgoland: Some diatoms of the genera *Pseudo-nitzschia* and *Rhizosolenia* were found, and also some Cryptophyceans. The most prominent (in cell numbers) were the flagellates, highest number was found at st. 60 (6×10^6 cells L $^{-1}$).

COAST/OOC # 6: North Sea - Baltic, Sept 1998.

- About 60% of the COAST/OOC # 6 samples sent to Trondheim were destroyed (crushed) during transport, i.e. 84 water samples fixed formaldehyde were intact.
- Torquay region: The phytoplankton dominating in the Torquay region (UK) was the diatom genus *Chaetoceros* spp. With cell densities up to $110\,000$ cells L $^{-1}$. Only traces of dinoflagellates and other flagellates were found.
- Plymouth region: Sample stations from the Plymouth region were dominated the potential toxic diatom genus *Pseudo-nitzschia* ($10\text{--}85\,000$ cells L $^{-1}$) and the potential toxic dinoflagellate genus *Gymnodinium* ($100\text{--}300\,000$ cells L $^{-1}$). These two genera totally dominated the phytoplankton biomass in the area. $235\,000$ unknown flagellates were observed at station 47
- Falmouth region: Phytoplankton biomass was dominated by the diatoms *Chaetoceros* spp., *Leptocylindrus danicus*, and *Pseudo-nitzschia*, the latter with up to $150\,000$ cells L $^{-1}$. Very low concentrations of flagellates were observed. $61\,000$ cells L $^{-1}$ of the dinoflagellate *Prorocentrum cf. triestinum* was observed at station 41.
- Texel region: Generally low cell concentrations (< $72\,000$ cells L $^{-1}$) dominated by the diatoms *Chaetoceros* spp., *Leptocylindrus danicus* and *Paralia sulcata*. Bloom concentration of potential toxic dinoflagellate *Gymnodinium* sp. with $225\,000$ and $132\,000$ cells L $^{-1}$ were observed at stations 67 and 82, respectively. At the station 82 up to $450\,000$ cells L $^{-1}$ of unknown flagellates were observed.

- Helgoland region: Less than 35 000 cell L⁻¹ of diatoms, i.e. *Leptocylindrus danicus* and *Paralia sulcata* dominated the biomass present. At station 104, 110 000 cells L⁻¹ of the diatom *Guinardia delicatima* was observed.
- Baltic region: A significant brackish phytoplankton fraction detected. Typical for the region were the presence of 600 000 cells L⁻¹ of the toxic dinoflagellate *Prorocentrum minimum* and 1.1 x 10⁶ of the cyanobacteria *Merismopedia* sp (Station 124).

2.3.3. Phytoplankton pigments

Phytoplankton pigment were determined by HPLC using the protocol described by Vidussi *et al.* (1996; J. Plankton Res. **18**: 2377-2382). Few plots are shown in this section to illustrate the variability in pigment composition during COAST/OOC campaigns. But first, few useful definitions are provided for the interpretation in terms of phytoplankton classes.

Taxonomic pigments:

Size Class	Pigments summed within a class	Phytoplankton groups represented within a given size class
PICO < 0.2 µm	Chl <i>b</i>	"green" algae
	Zeaxanthin	prochlorophytes + cyanobacteria
NANO 2-20 µm	19'-HF	prymnesiophytes/some dinoflagellates
	19'-BF	pelagophytes/crysophytes
	Alloxanthin	cryptophytes
MICRO > 20 µm	Fucoxanthin	diatoms
	peridinin	dinoflagellates

Accessory pigments:

All pigments [carotenoids, Chl *b*, Chl *c(s)*], except phaeopigments

Photosynthetic pigments (PP):

Chl *b*, Chl *c*, fucoxanthin, peridinin, 19'-HF, 19'-BF + some minors

Non-Photosynthetic pigments (NPP):

Zeaxanthin, diadinoxanthin, diatoxanthin, alloxanthin, β-carotene

*ACRJ - LPCM - SAI - U. Oldenburg
NIOZ - U. Trondheim - FUB - PML - GKSS*

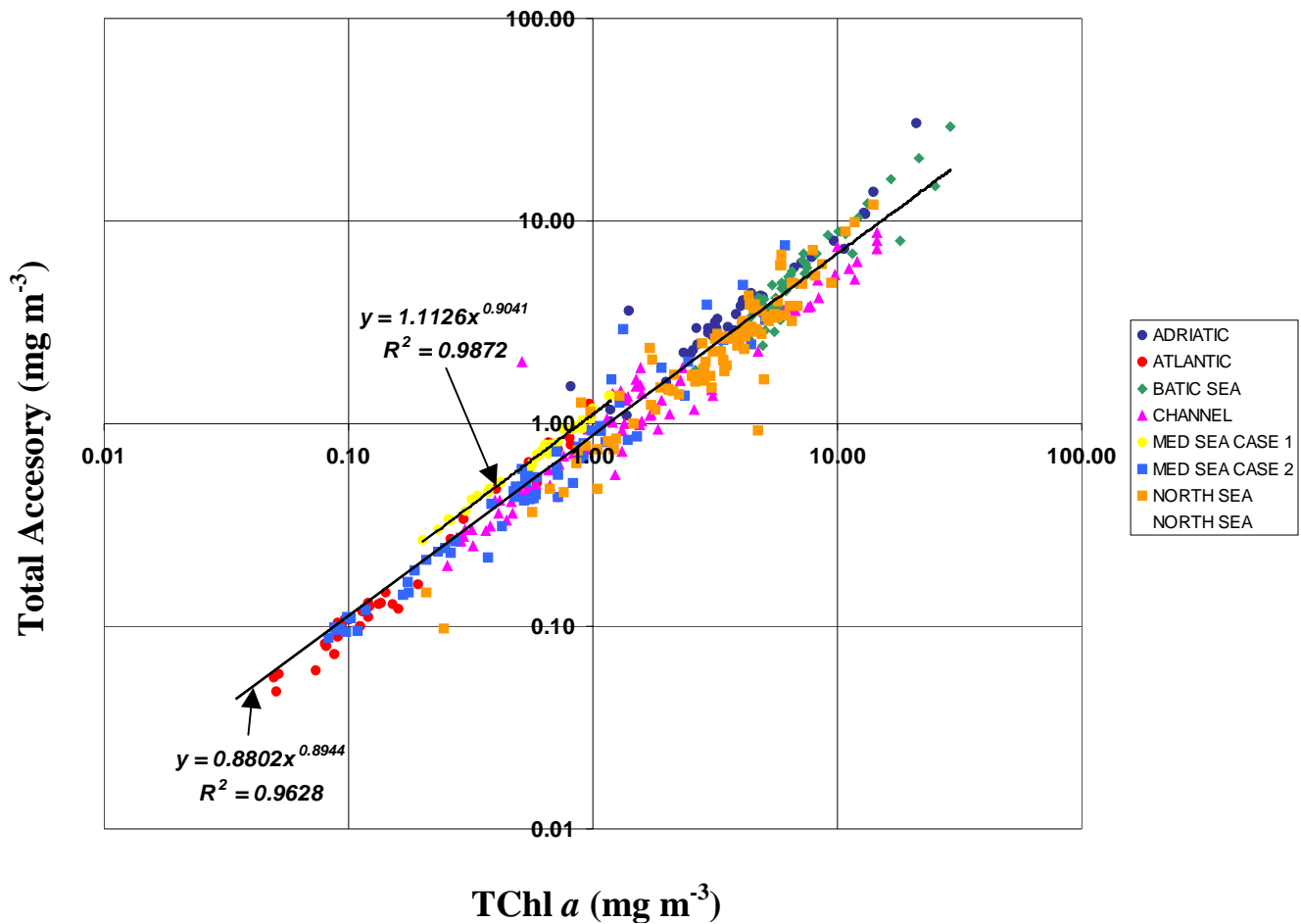


Figure 28. Plot showing that the amount of accessory pigments per unit Chl a slightly decreases with increasing Chl a concentrations, and that the amount of accessory pigment per unit Chl a is higher in case 1 waters.

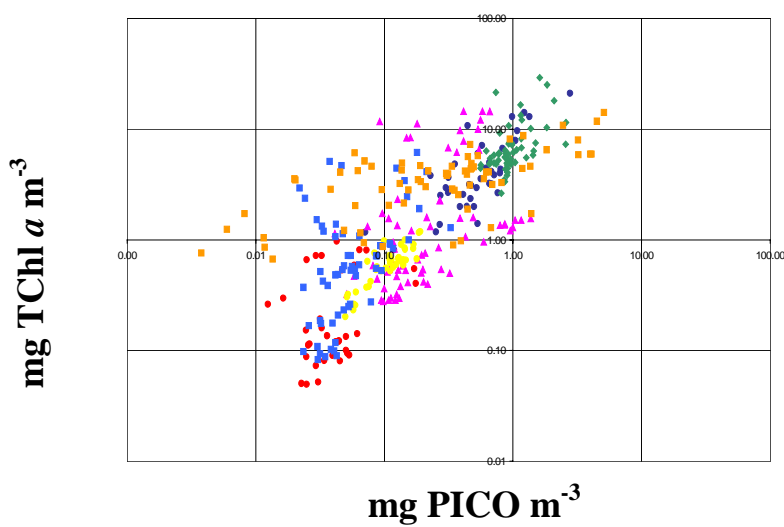
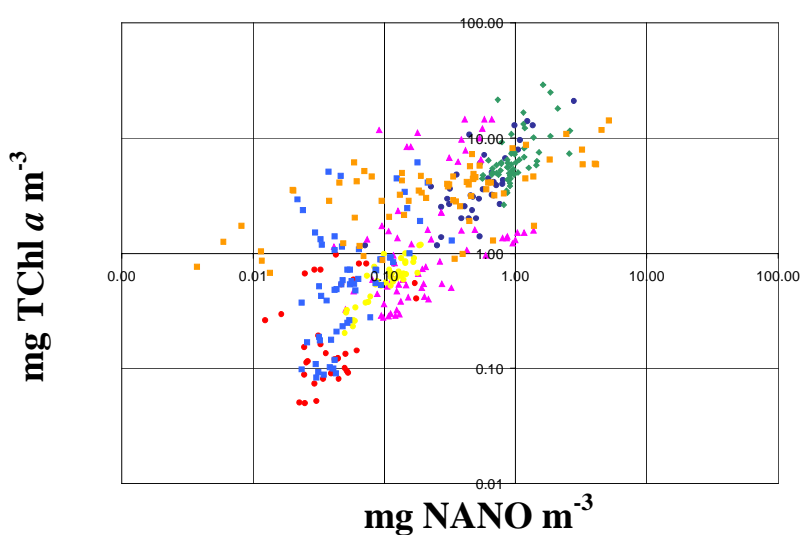
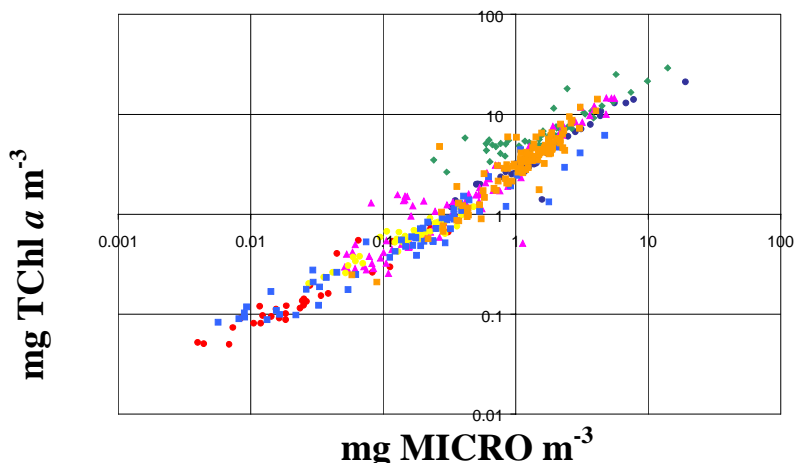


Figure 29. Plots showing that the increase in $\langle \text{TChl } a \rangle$ are essentially driven by increase in phytoplankton populations in the micro ($\sim 20 \mu\text{m}$) size range (diatoms + dinoflagellates).

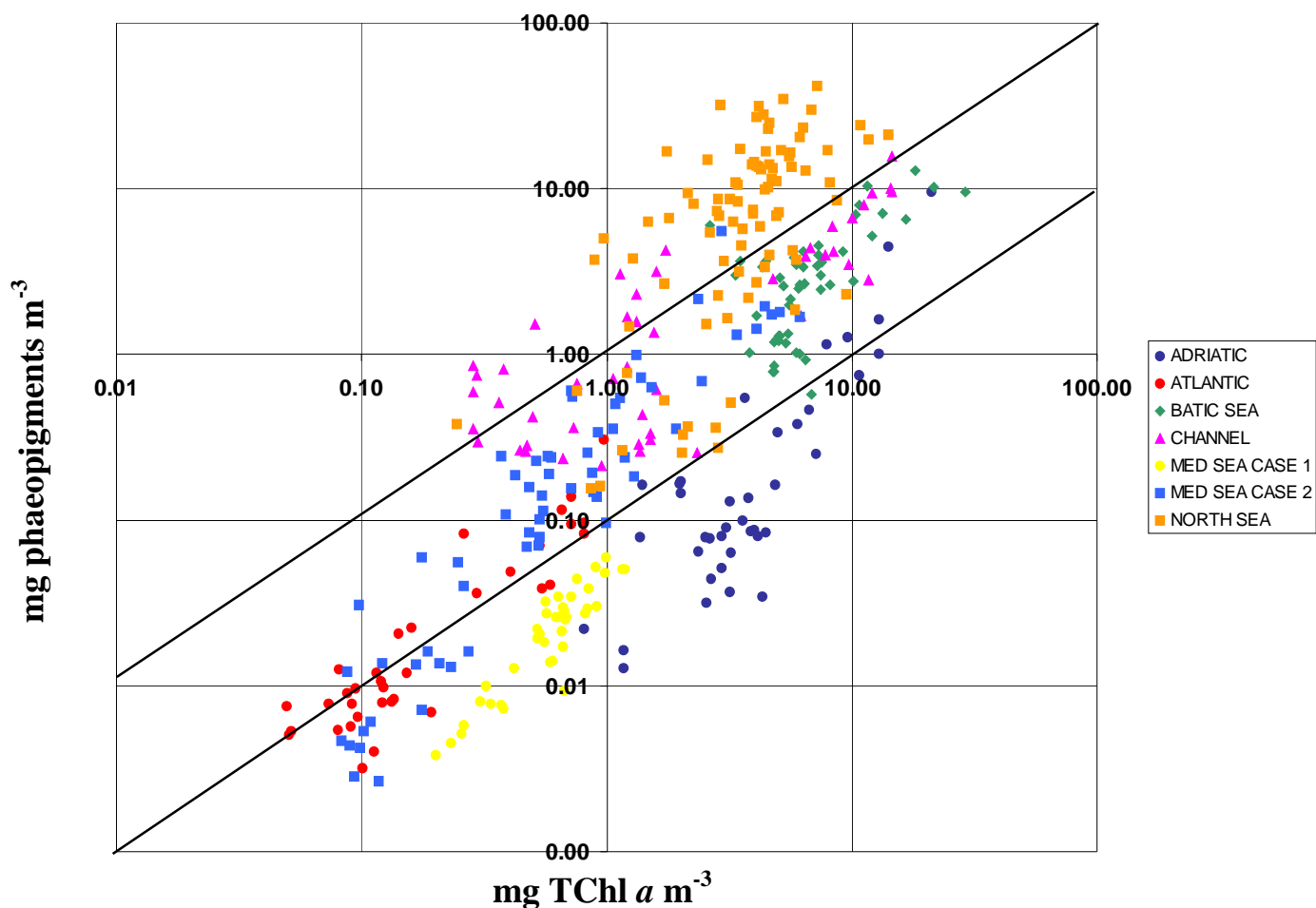


Figure 30. Plot showing that, in the North Sea, phaeopigments generally $>$ TChl a . In the Adriatic Sea (as in Med Sea case1), phaeopigments $<$ 10% TChl a (see Figure 32 below).

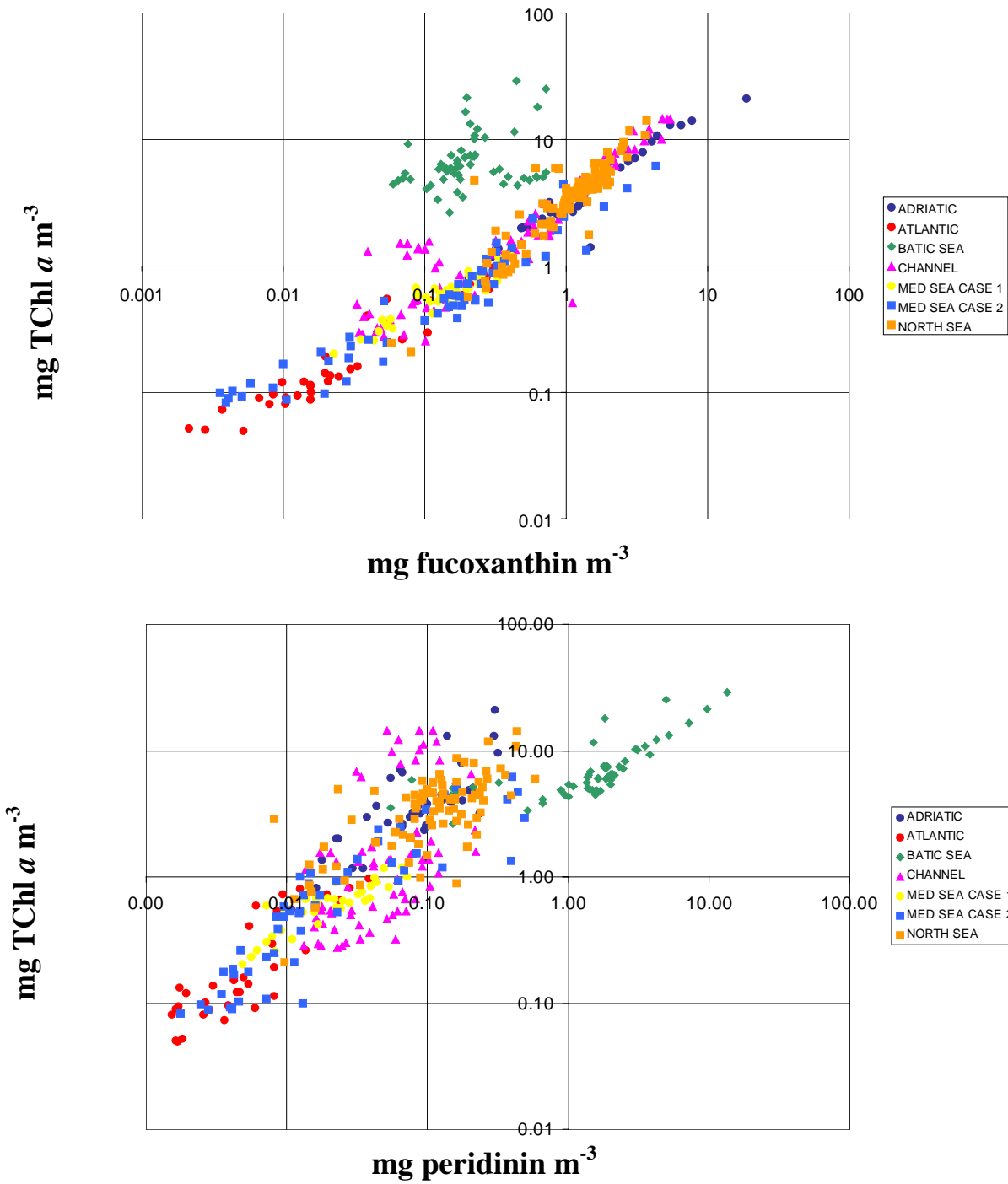


Figure 31. Plot showing that the blooms are generally diatom-dominated, except in the Baltic Sea where dinoflagellate is the dominant phytoplankton.

ACRJ - LPCM - SAI - U. Oldenburg
NIOZ - U. Trondheim - FUB - PML - GKSS

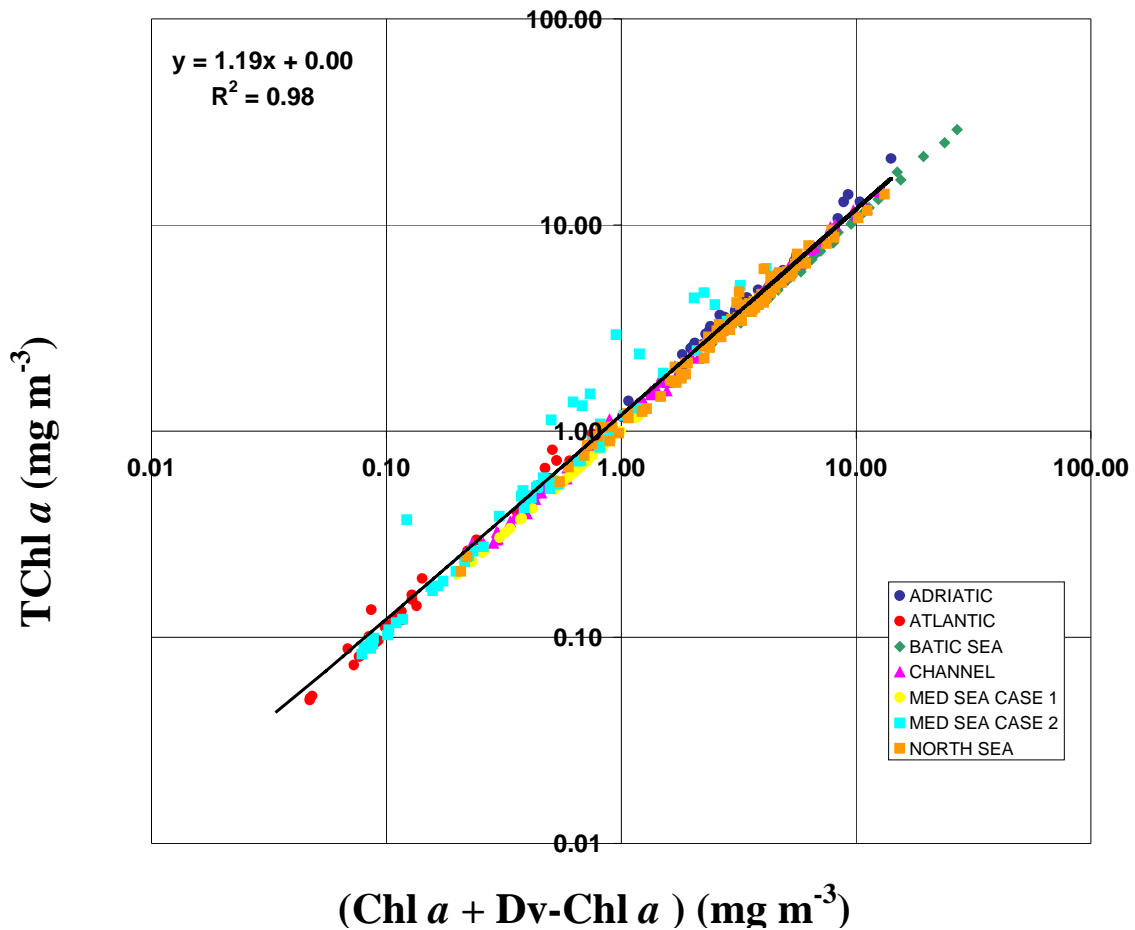


Figure 32. Tchla = Chla + Dv-Chla + allomer Chla + epimer Chla + chlorophyllids *a*. "Non active" Chl *a* (allomer, epimer and chlorophyllids) represent 20 % of the "active" Chla + Dv-Chla stock.

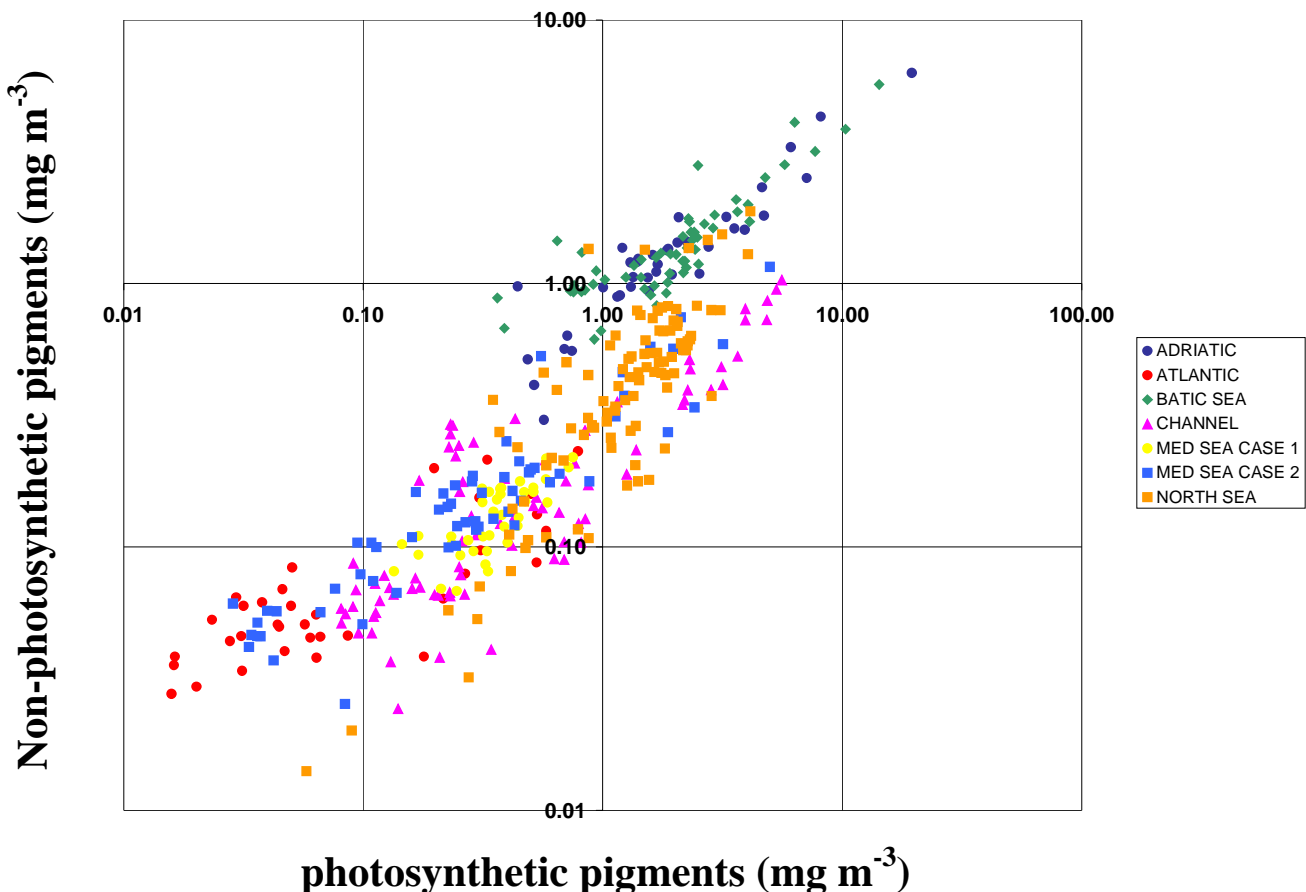


Figure 33. The Adriatic and Baltic Seas have a higher ratio of non-photosynthetic / photosynthetic pigments than other areas.

2.3.4. DOC vs. CDOM relationship, POC

DOC vs. CDOM relationship. Seawater particles were collected onto a GF/F glass fibre filter for measurements of their absorption properties. The water filtrates of the samples were used to determine the absorption spectra of the coloured fraction of the dissolved organic matter. For the same stations, measurements of dissolved organic carbon were conducted using an HTCO technique and a CE480 Carbon Analyser. All samples have been analysed to verify any existing relationship between both parameters and the possibility to retrieve DOC, playing an important role in the carbon cycle of coastal waters, from the optical properties of CDOM.

Empirical expressions relating the absorption due to CDOM and DOC were derived at various COAST/OOC sites :

*ACRJ - LPCM - SAI - U. Oldenburg
NIOZ - U. Trondheim - FUB - PML - GKSS*

Rhine plume (campaign C1)

$$aCDOM(355) = -1.07(\pm 0.78) + 0.003(\pm 0.01) DOC \quad r = 0.62$$

North Sea and Atlantic (campaign C1)

$$aCDOM(355) = -0.028(\pm 0.0007) + 0.00036(\pm 6.10^{-5}) DOC \quad r = 0.66$$

Rhone Plume (campaign C4)

$$St.FU(355) = -2.09(\pm 1.45) + 0.023(\pm 0.007) DOC \quad r = 0.65$$

Gulf of Lion (at depth of chl.max., campaign C4)

$$St.FU(355) = 0.15 (\pm 0.021) + 0.0047 (\pm 0.0015) DOC \quad r = 0.65$$

Plymouth, Texel, Wilhelmshaven (campaign C6)

$$aCDOM(355) = 0.0068 (\pm 2.7.10^{-4}) DOC \quad r = 0.81$$

CHN and particulate matter analyses. A Carbo Erba NCS 2500 Elemental Analyser was designed for simultaneous determination of carbon and nitrogen in the suspended material. Duplicate filters, pre-treated at 450°C for 2h., were used for this purpose. On one set of filters, total carbon and nitrogen were determined. The other filters were used to determine organic carbon and nitrogen after treatment with concentrated HCl. The inorganic carbon such as CaCO₃ can be derived from the difference between total and organic carbon. No significant differences were observed in the nitrogen concentration before and after HCl treatment.

Two homogeneity tests have been made on the samples:

- variability of the particle distribution within the surface of the GF/F filters
- variability between replicates

The averaged difference between two subsamples was 1.9% for POC measurements and 4% for PON using 10 observations. On the other hand, the standard deviations between replicates (14 couple of samples) were 3.7% for POC and 6.8% for PON. The results of these analyses are summarised in the table below.

Table 11. Averaged values for POC and DOC (in mg/l) for various areas within COAST/OOC.

Campaigns	av. POC (mg/l)	POC/PON	av. DOC (mg/l)
C1			
- Rhine pl.	0.15 (\pm 0.055)	5.12 (\pm 1.0)	6.27 (\pm 1.05)
- Atlantic	0.049 (\pm 0.019)	6.02 (\pm 1.56)	1.25 (\pm 0.84)
C2	0.052 (\pm 0.038)	-	3.5 (\pm 1.44)
C3	0.27 (\pm 0.19)	-	2.27 (\pm 1.5)
C4			
- surface	0.12 (\pm 0.1)	-	2.05 (\pm 0.83)
- euph. depth	0.04 (\pm 0.03)	-	1.88 (\pm 1.06)
C5			
- Open sea	0.216	5.36 (\pm 1.5)	1.75 (\pm 0.43)
- Loire plume	0.43	6.14 (\pm 1.9)	2.32 (\pm 0.72)
- Seine plume	0.65	4.77 (\pm 1.13)	1.3 (\pm 0.36)
- Thames pl.	0.24	6.57 (\pm 1.25)	1.11 (\pm 0.2)
- Rhine pl.	0.56	6.25 (\pm 0.73)	2.08 (\pm 0.66)
- Humber pl.	0.18	6.11 (\pm 1.1)	1.65 (\pm 0.32)
- Germ. bight	0.25	5.8 (\pm 0.5)	1.67 (\pm 0.45)
C6			
- Plymouth	0.12 (\pm 0.04)	6.16 (\pm 0.96)	1.02 (\pm 0.16)
- Texel	0.56 (\pm 0.42)	6.76 (\pm 0.86)	1.84 (\pm 0.92)

ACRJ - LPCM - SAI - U. Oldenburg
 NIÖZ - U. Trondheim - FUB - PML - GKSS

- Wilhelmsh.	0.54 (± 0.37)	7.06 (± 0.64)	1.84 (± 0.64)
- Heringsd.	0.8 (± 0.26)	9.9 (± 2.03)	5.12 (± 0.55)

Some POC versus PON relationships have been investigated for various sites:

campaign C1

$$PON = 0.179 (\pm 0.0746) POC$$

campaigns C2, C3, C4

$$PON = 0.4 (\pm 0.08) POC$$

campaign C5

$$PON = 0.17 (\pm 0.03) POC$$

campaign C6

$$\text{Plymouth } PON = 0.0043 (\pm 0.001) + 0.125 (\pm 0.009) POC \quad r = 0.901$$

$$\text{Texel } PON = 0.0082 (\pm 0.003) + 0.128 (\pm 0.004) POC \quad r = 0.986$$

$$\text{Wilhelms. } PON = 0.01 (\pm 0.003) + 0.116 (\pm 0.005) POC \quad r = 0.97$$

$$\text{Heringsd } PON = 0.013 (\pm 0.01) + 0.087 (\pm 0.005) POC \quad r = 0.82.$$

2.3.5. Particle absorption spectra measured in the laboratory

In vivo absorption of water particles. During the full period of the project, a total of 443 water samples (covering all campaigns) were filtered onto GF/F filters and analyzed for the absorption spectra of particulate matter using the Transmission-Reflection method (Tassan and Ferrari 1995) and a dual-beam spectrophotometer equipped with an integrating sphere. The samples were scanned from 370 to 750 nm before and after extraction of the pigmented material with sodium-hypochloride. As shown in Figure 34, the absorption by phytoplankton is retrieved from subtracting the spectra due to depigmented material from the total absorption spectra.

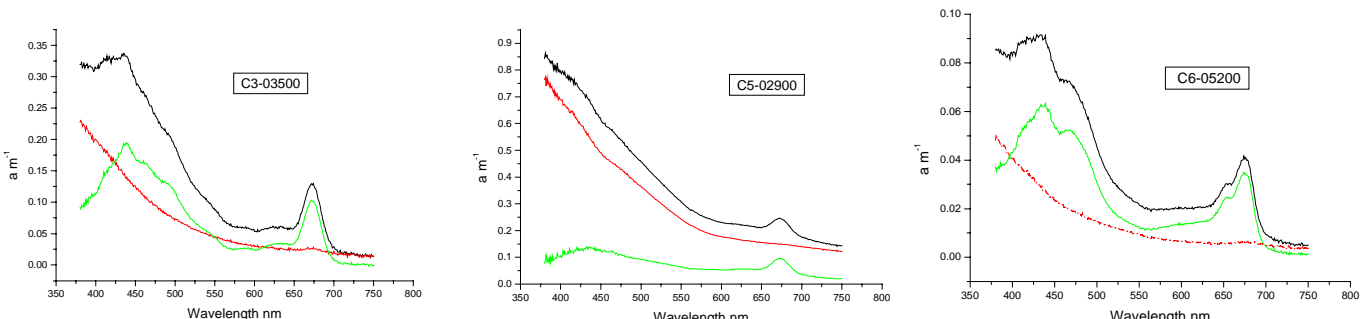


Figure 34. Examples of in vivo absorption spectra for particulate matter at various COAST/OOC sites (from right to left, campaigns C3, C5, and C6). Total particulate absorption spectra (black line), de-pigmented material, i.e. detrital absorption spectra (red lines), phytoplankton absorption spectra (green lines).

2.3.6. Chl, Y and SPM variability

Figure 35 to Figure 37 show the extent of variability and covariability in Chl (total chloropigments as defined in legend of Figure 32, denoted Chl + Pheo), Y [denoted $a_{CDOM}(443)$] and SPM. The main conclusions are the following:

- While Chl + Pheo and SPM varied over 3 orders of magnitude, Y varied over 2.
- Overall covariability is observed in Chl + Pheo, Y and SPM. Note that this covariability does not prevent discrimination as far as optical spectral signatures of these three components may be significantly different.
- It is highly relevant for algorithm development to observe that the 3-D space defined by Chl + Pheo, Y and SPM is not completely filled: e.g. turbid waters without CDOM do not exist. The actual 3-D domain is to be considered for defining the scope of algorithms.
- Some regional peculiarities appear. For instance, it seems that the Baltic Sea waters contain the highest proportion of CDOM relatively to SPM (Figure 36) and, to a lesser extent, to Chl + Pheo (Figure 37). Conversely, The Mediterranean Sea case 2 waters show the highest turbidity relatively to CDOM (Figure 36) and, to a lesser extent, to Chl + Pheo (Figure 35).

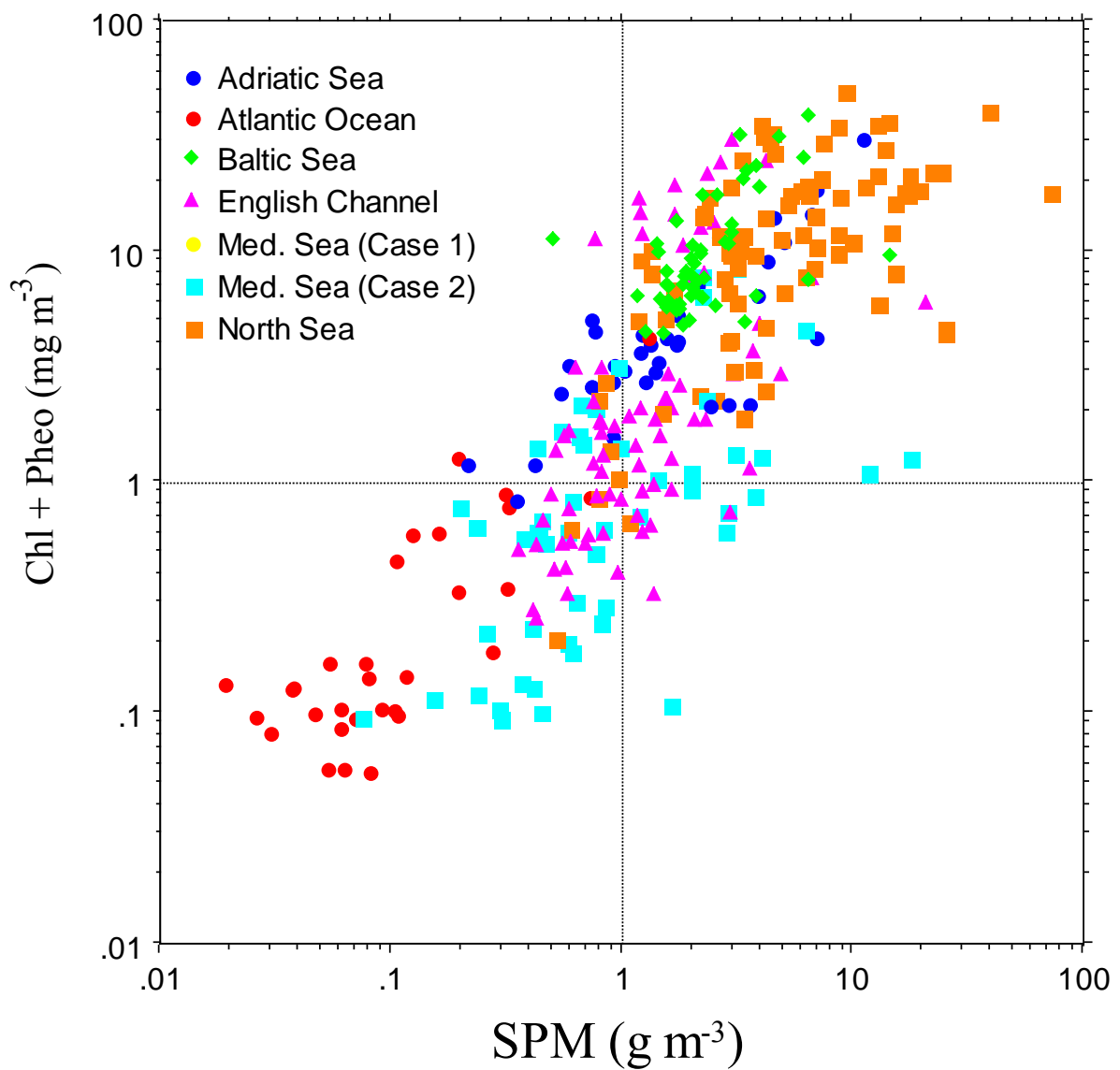


Figure 35. Relationship between Chl + Pheo and SPM.

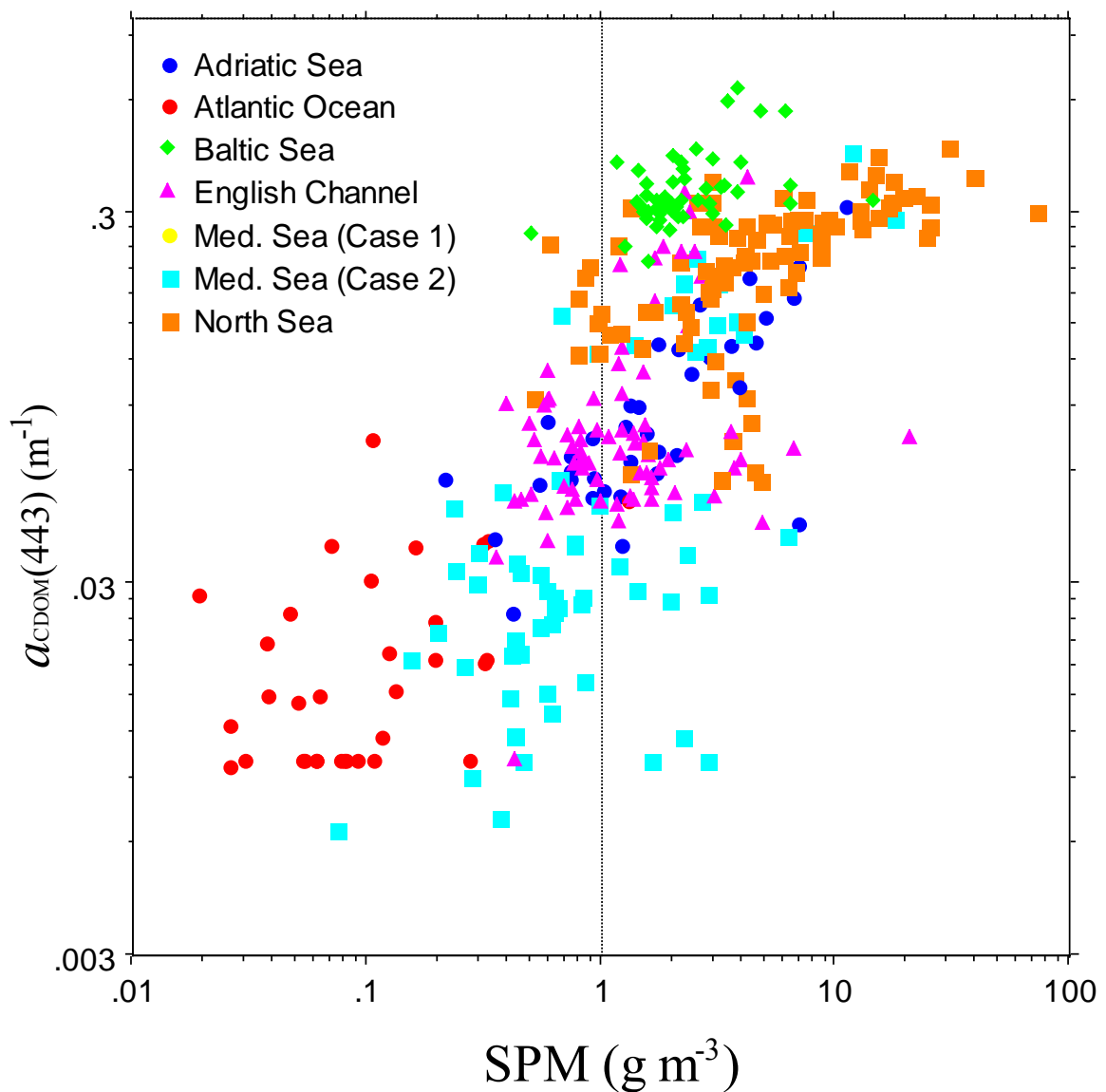


Figure 36. Relationship between Y [represented by $a_{CDOM}(443)$] and SPM.

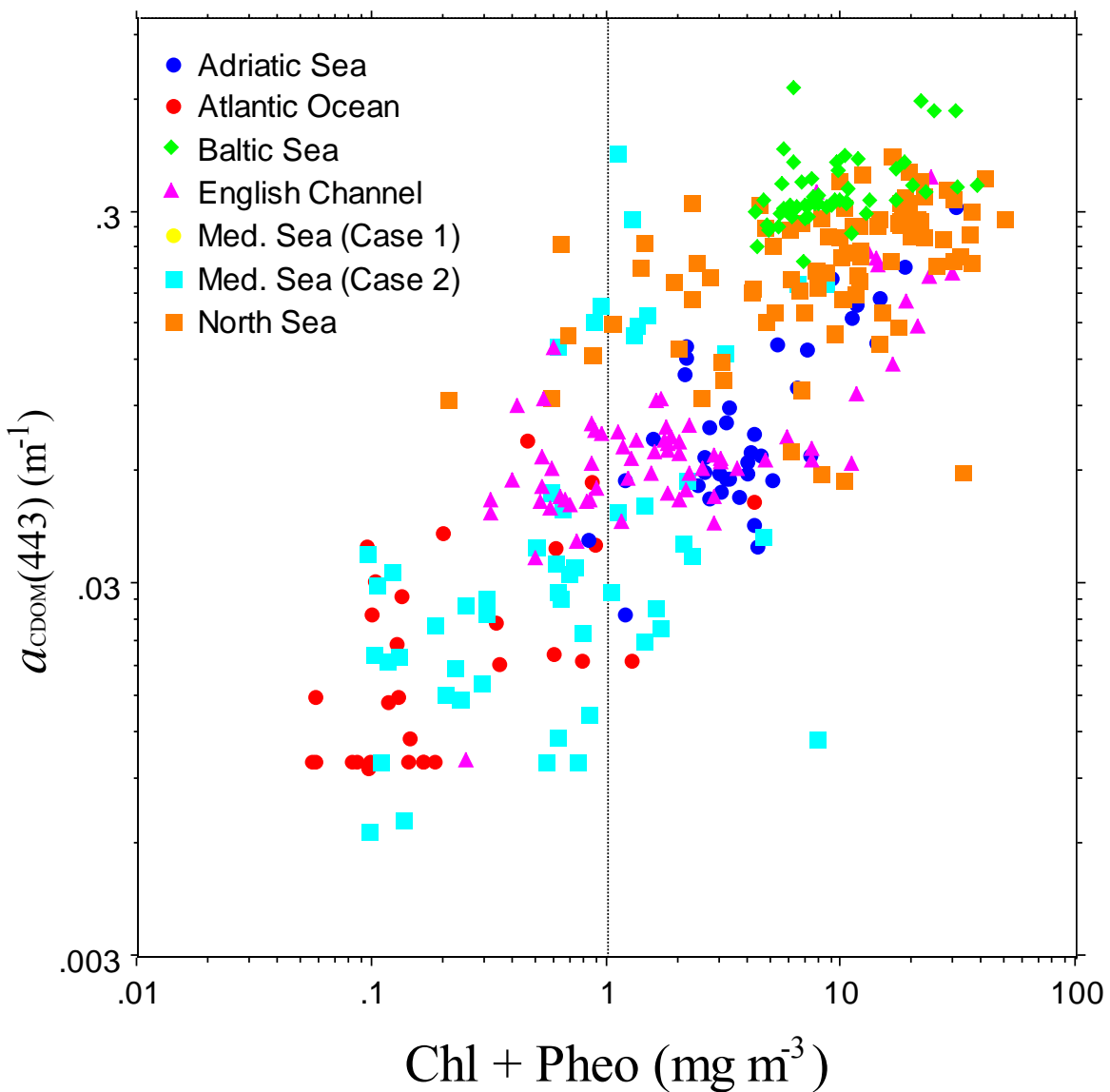


Figure 37. Relationship between Y [represented by $a_{\text{CDOM}}(443)$] and Chl + Pheo.

ACRJ - LPCM - SAI - U. Oldenburg
NIOZ - U. Trondheim - FUB - PML - GKSS

2.3.7. IOP variability

Figure 38 to Figure 47 show different relationships which will be used further for reflectance modelling. The main conclusions are the following:

- A relationship is observed between the *in vivo* phytoplankton absorption coefficient and Chl + Phéo (Figure 38). When fitting a power to this relationship, the coefficients obtained are not significantly different from those obtained by Bricaud *et al.* (1995; J. Geophys. Res. 100: 13 321-13 332) for Case 1 waters. This result suggest that the trends observed in Case 1 waters for phytoplankton and associated matter (endogenous CDOM and related particulate detritus) can be assumed to be valid in Case 2 waters.
- An exponential function has been successfully fitted (350-500 nm) to all COAST/OOC CDOM absorption spectra measured in the laboratory on fresh bottle samples. The resulting exponential slope varied within a narrow range ($0.0176 \text{ nm}^{-1} \pm 11.4\%$) (Figure 39).
- No relationship was found between the spectral slope of the CDOM absorption spectrum and its amplitude (Figure 40), although some weak trends (inverse relationship) appeared locally.
- The absorption spectra of non-algal particles, determined in laboratory on water samples, could be successfully fitted to an exponential function as those of CDOM. The average spectral slope was $0.0122 \text{ nm}^{-1} \pm 10.3\%$ (see Figure 41). In few cases, the non-algal particle spectrum differed from the exponential model, although not dramatically.
- A clear relationship between the amplitude of the non-algal particle absorption spectrum [represented by $a_{NAP}(443)$] and SPM was observed (Figure 42).
- Given the similarity between the shape of non-algal particle and CDOM absorption spectra, one could suspect that the former is depending on the latter because of adsorption of CDOM on marine particles. Nevertheless, although some covariability could be observed between $a_{NAP}(443)$ and $a_{CDOM}(443)$ (Figure 43), this hypothesis cannot be validated using the present data given the overall covariability between CDOM and SPM (see Figure 36). The difference in average spectral slopes of the non-algal particle and CDOM absorption spectra is to be considered.
- A linear relationship with a slope close to 1 and a negligible intercept was observed between the total particle scattering coefficient at different wavelengths in the visible range, and its value at 555 nm [*i.e.* $b_p(\lambda)$ vs. $b_p(555)$] (Figure 44 and Figure 45). This result suggest that the spectral shape of the $b(\lambda)$ spectrum is only slightly variable for marine particles in coastal waters (see Figure 46).
- A significant relationship was observed between $b_p(555)$ and SPM (Figure 47).
- Overall, several global trends were observed. Parameterisation of IOPs in coastal waters seems possible to a certain extent. More data (more specific) are still necessary.

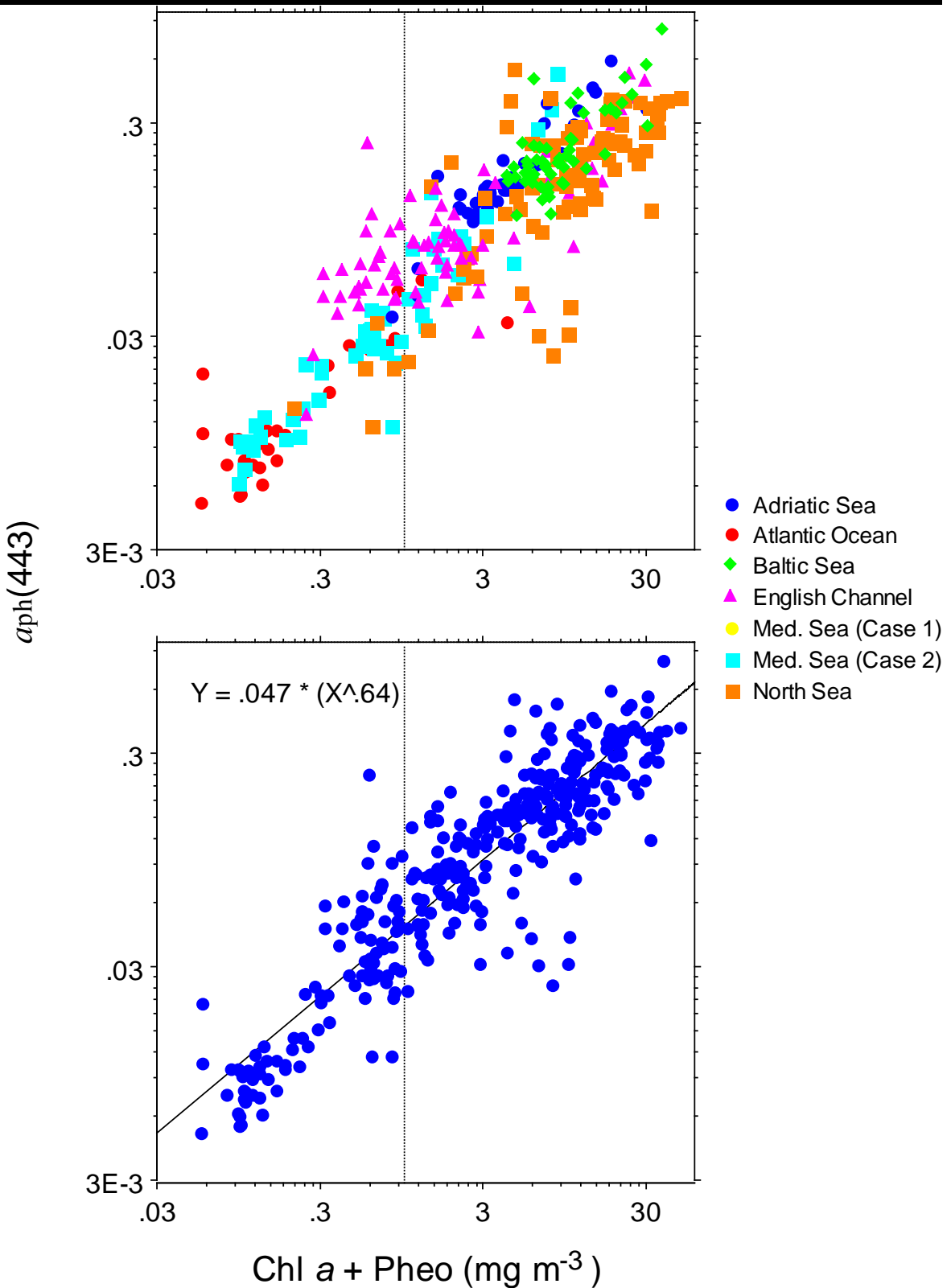
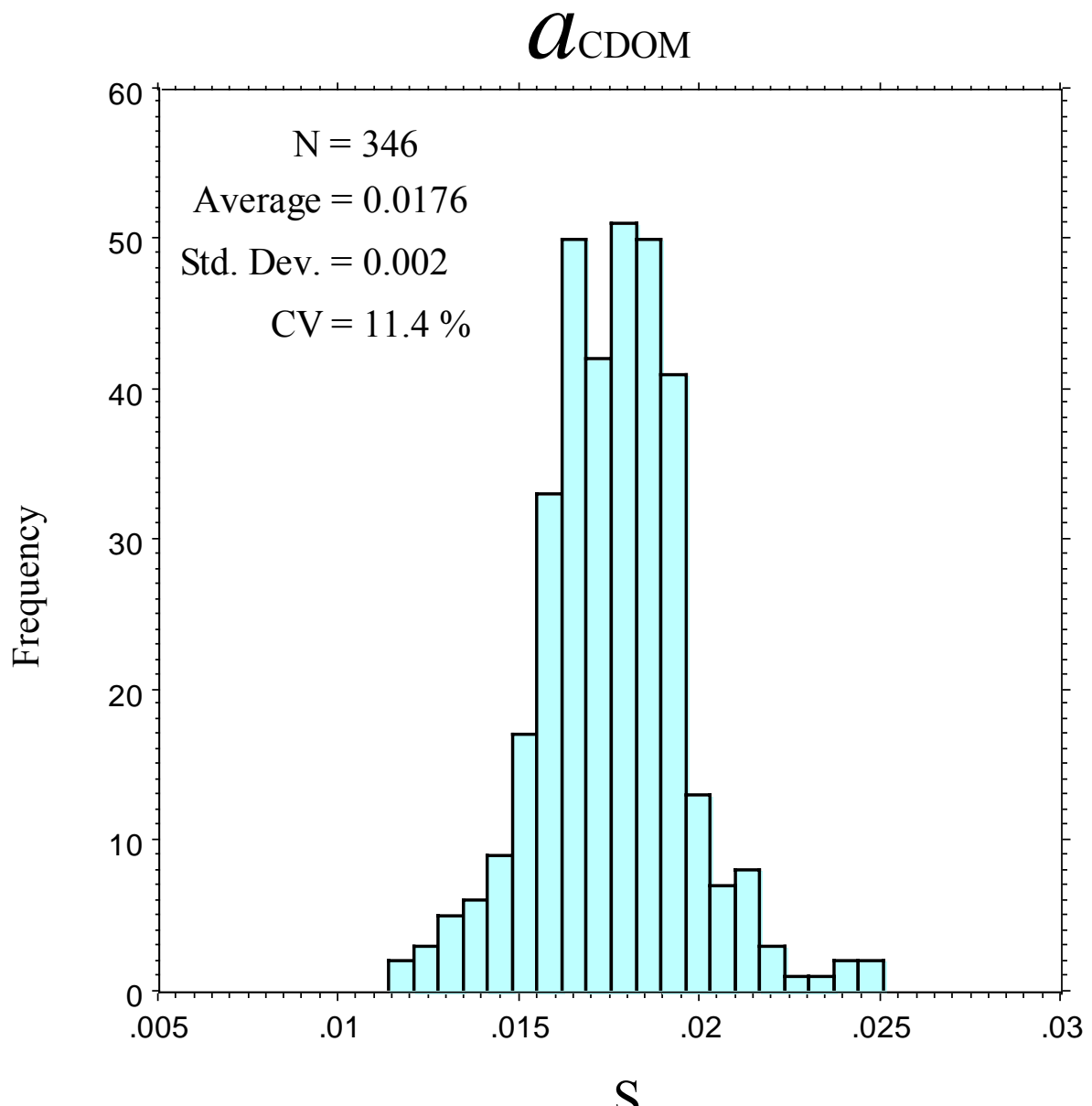


Figure 38. Relationship between the phytoplankton absorption coefficient at 443 nm and chl *a* + pheo concentration.

*ACRJ - LPCM - SAI - U. Oldenburg
 NIOZ - U. Trondheim - FUB - PML - GKSS*



$$a_{\text{CDOM}}(\lambda) = a_{\text{CDOM}}(443) \exp[-S(\lambda - 443)]$$

Interval: 350 - 500 nm

Figure 39. Histogram showing the frequency distribution of the spectral slope of the CDOM absorption coefficient.

*ACRJ - LPCM - SAI - U. Oldenburg
NIOZ - U. Trondheim - FUB - PML - GKSS*

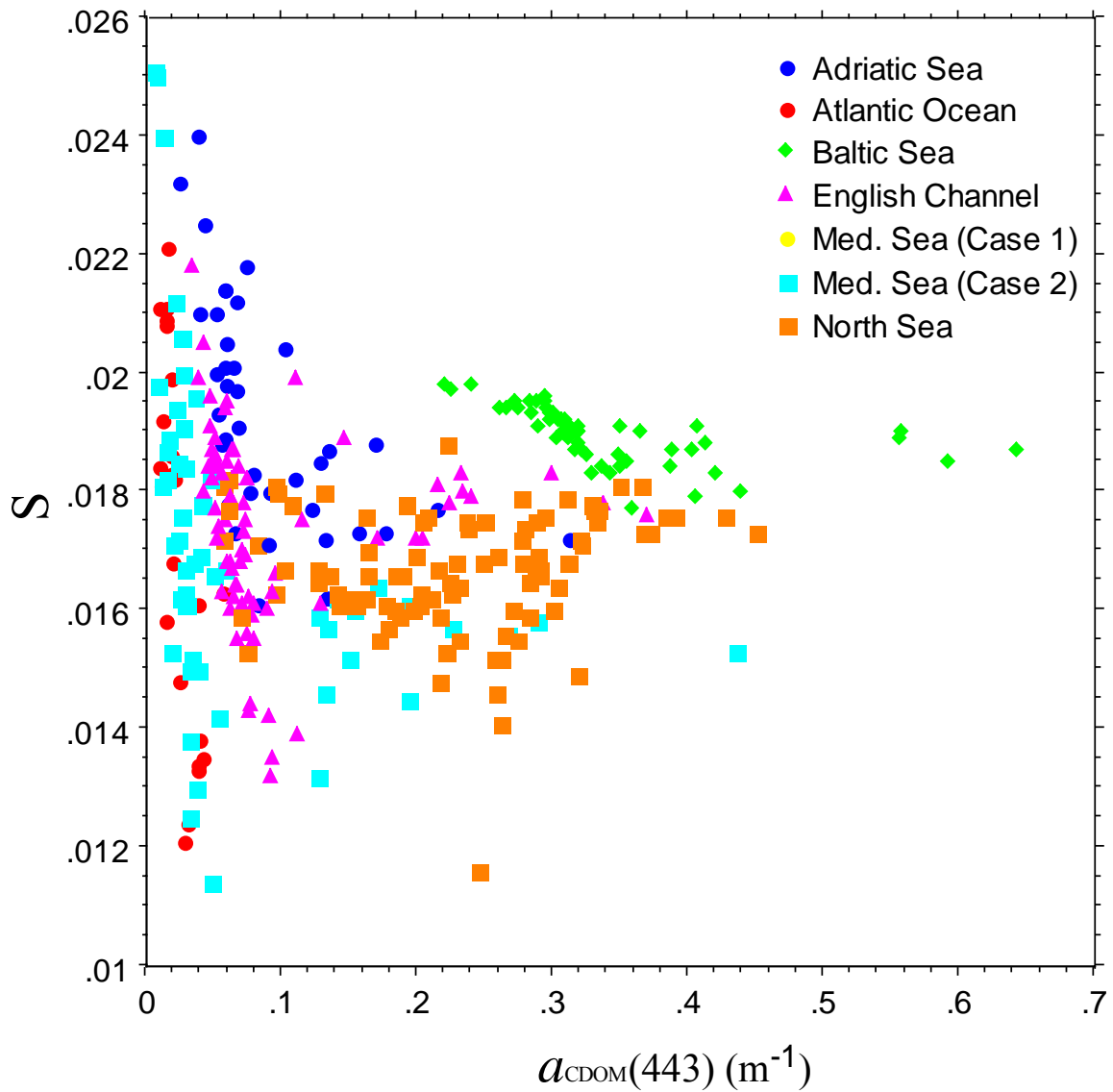
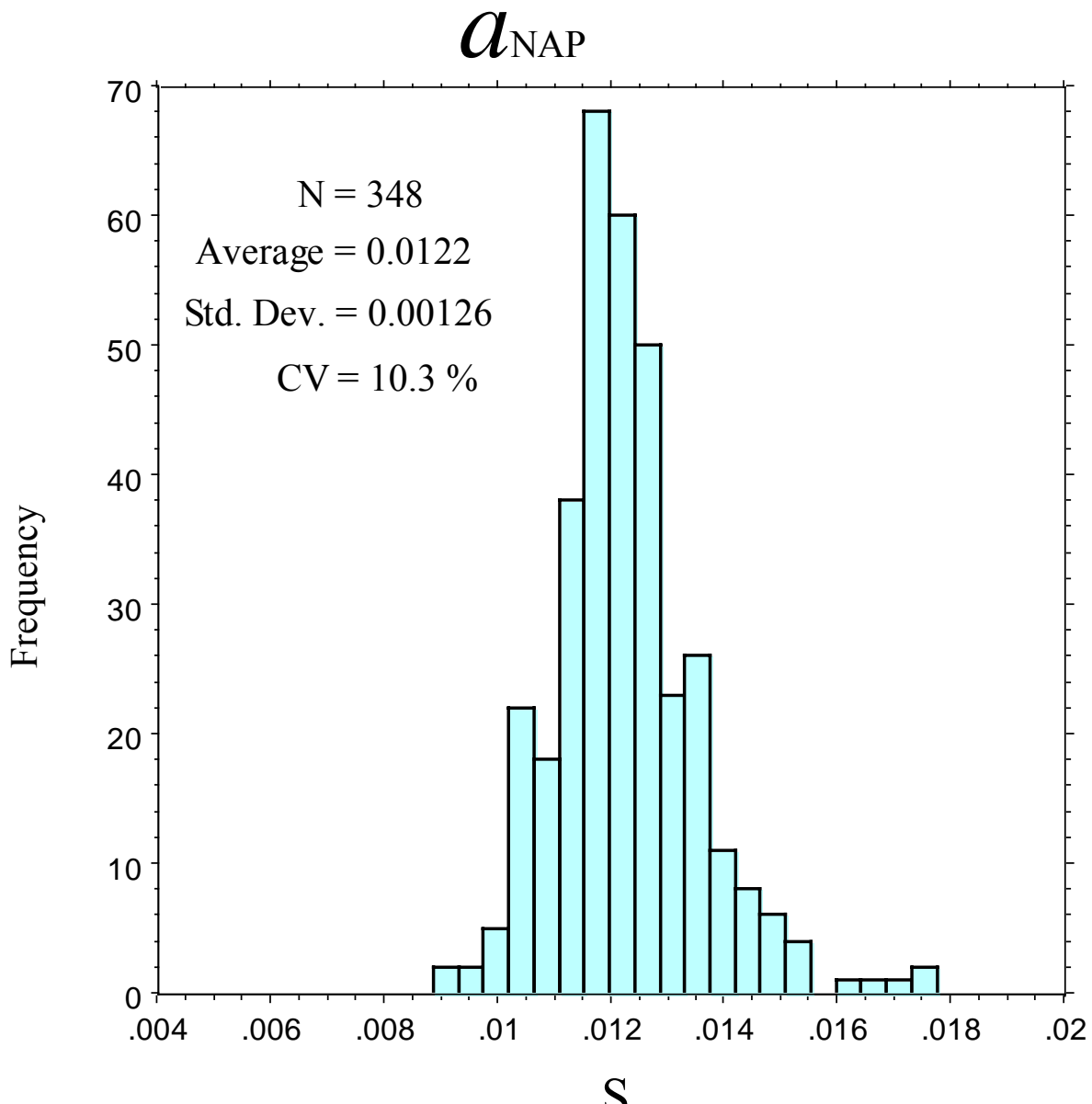


Figure 40. Relationship between the spectral slope of the CDOM absorption coefficient, and the CDOM absorption coefficient at 443 nm.

NIOZ - ACRJ - LPCM - SAI - U. Oldenburg
NIOZ - U. Trondheim - FUB - PML - GKSS



$$a_{NAP}(\lambda) = a_{NAP}(443) \exp[-S(\lambda - 443)]$$

Intervals: 380-400; 480-620; 710-730 nm

Figure 41. Histogram showing the frequency distribution of the spectral slope of the non-algal particle absorption coefficient.

*ACRJ - LPCM - SAI - U. Oldenburg
NIOZ - U. Trondheim - FUB - PML - GKSS*

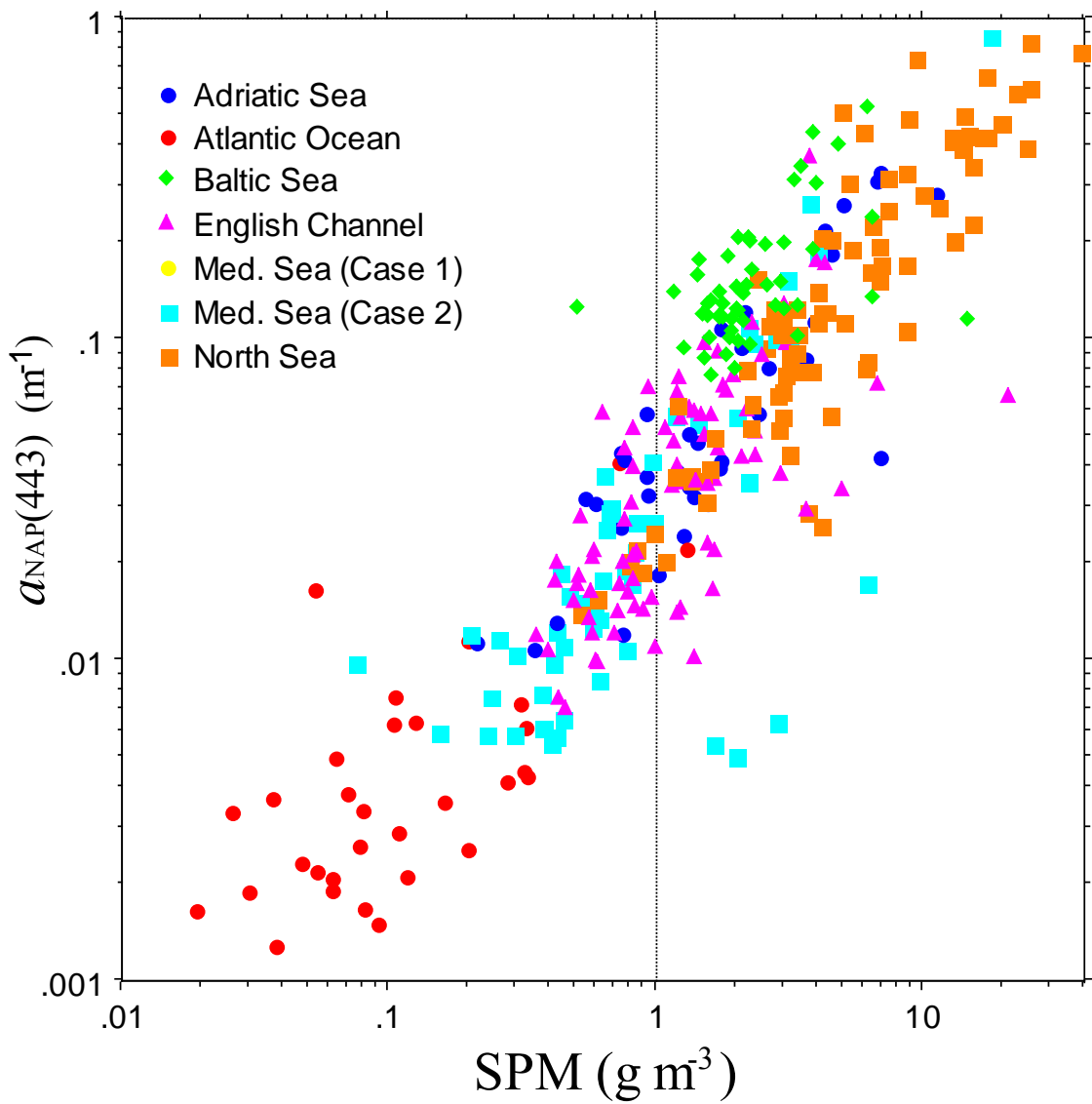


Figure 42. Relationship between the non-algal particle absorption coefficient at 443 nm and SPM.

ACRJ - LPCM - SAI - U. Oldenburg
NIOZ - U. Trondheim - FUB - PML - GKSS

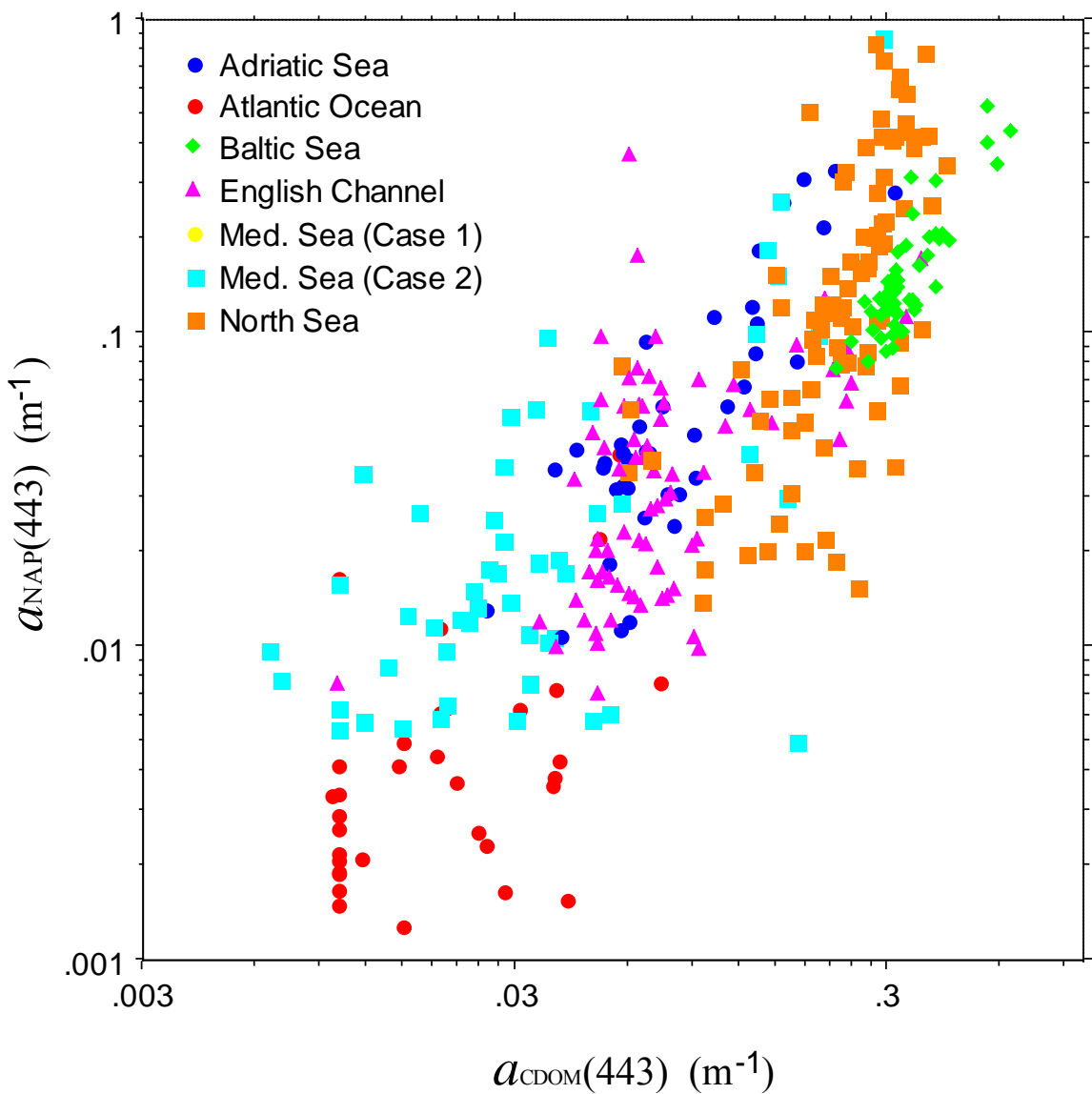


Figure 43. Relationship between the absorption coefficients at 443 nm of non-algal particles and CDOM.

*ACRI - LPCM - SAI - U. Oldenburg
NIOZ - U. Trondheim - FUB - PML - GKSS*

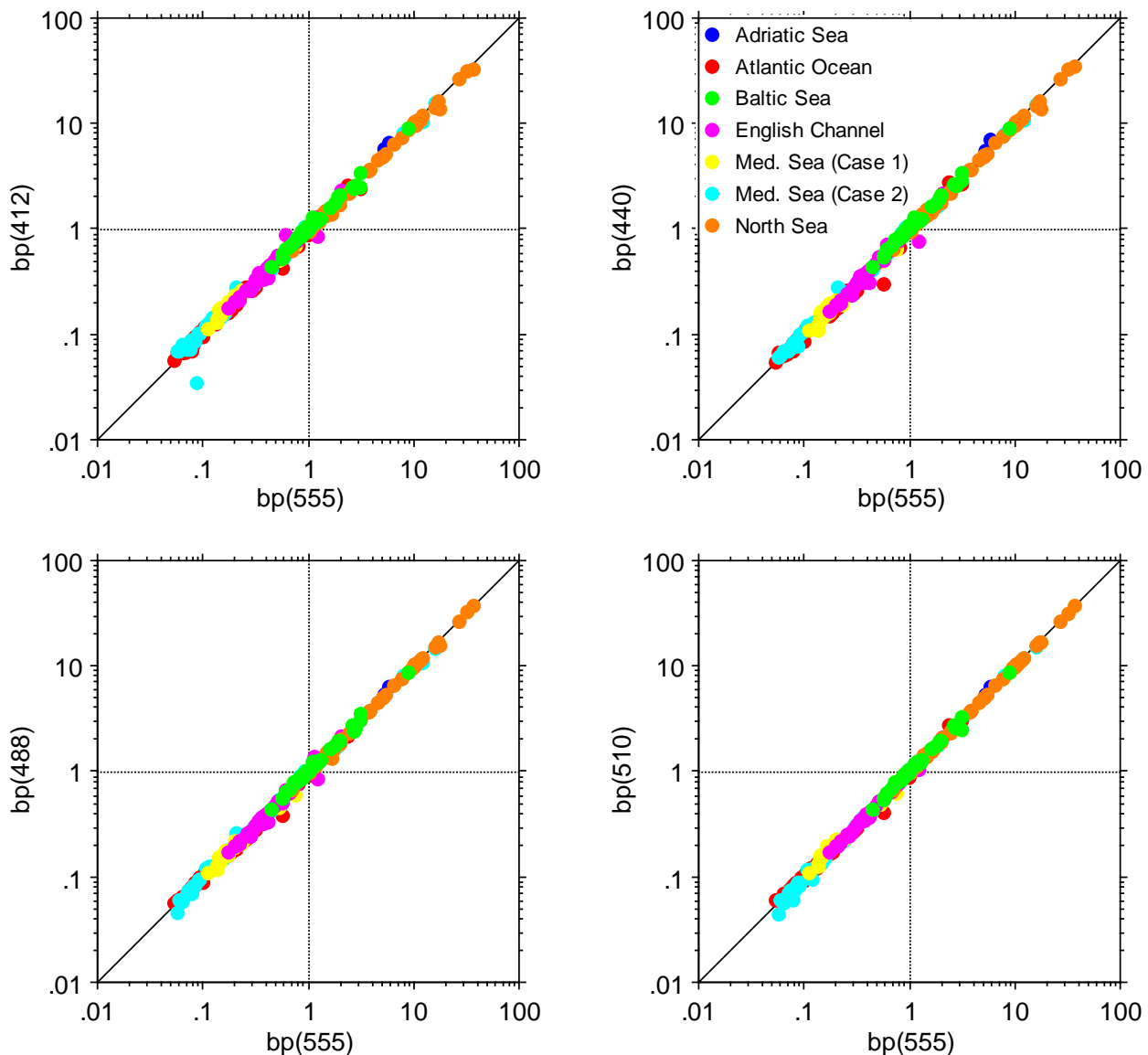


Figure 44. Relationship between the scattering coefficient at a given wavelength [$b(\lambda)$] and $b(555)$. Note that $b(\lambda)$ was determined by subtracting absorption from attenuation, as measured using the AC-9 absorption-attenuation-meter. Note also that, given that AC-9 measurements are made relatively to pure water, measured and determined IOPs exclude the water contribution.

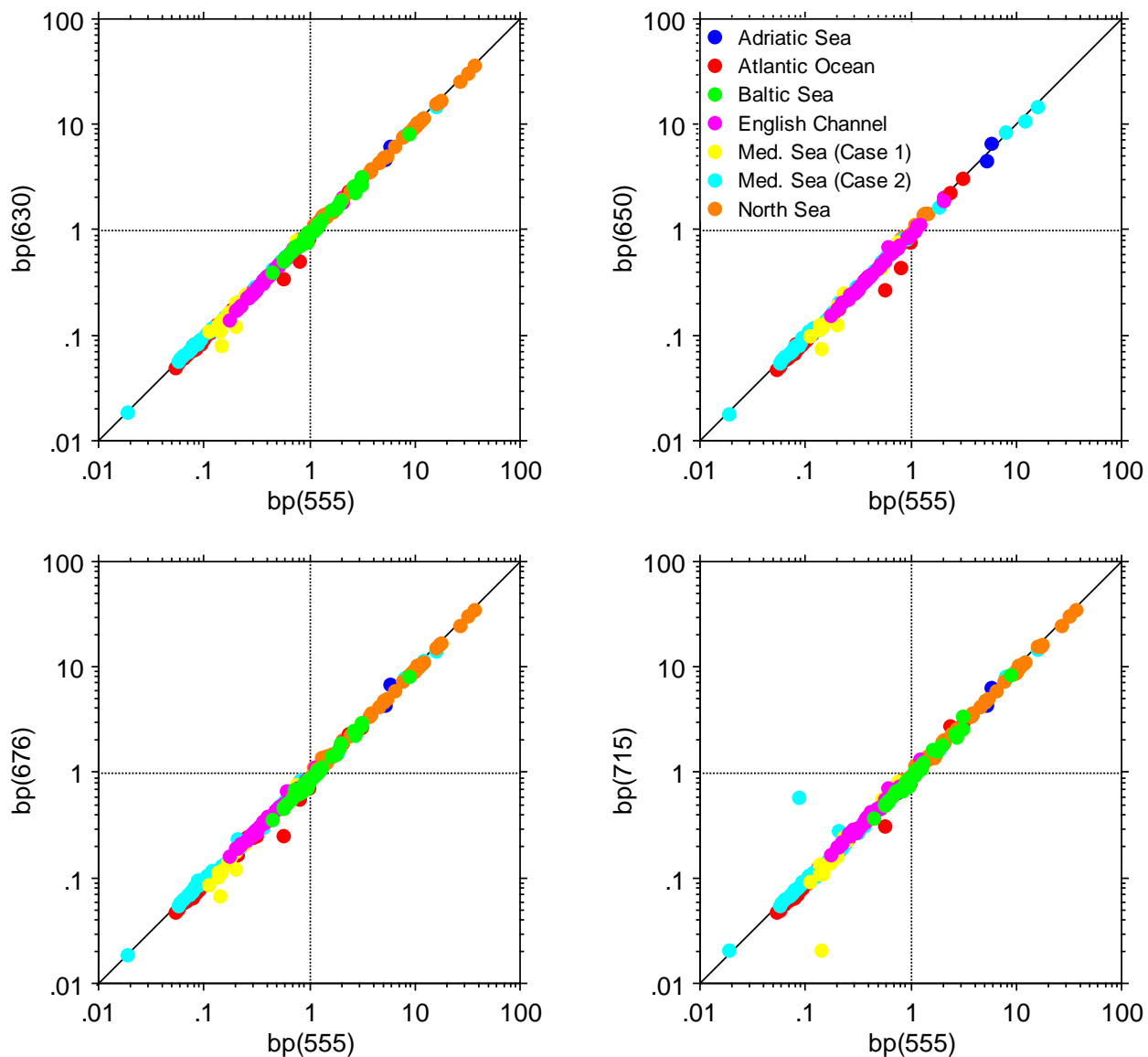


Figure 45. As in Figure 44.

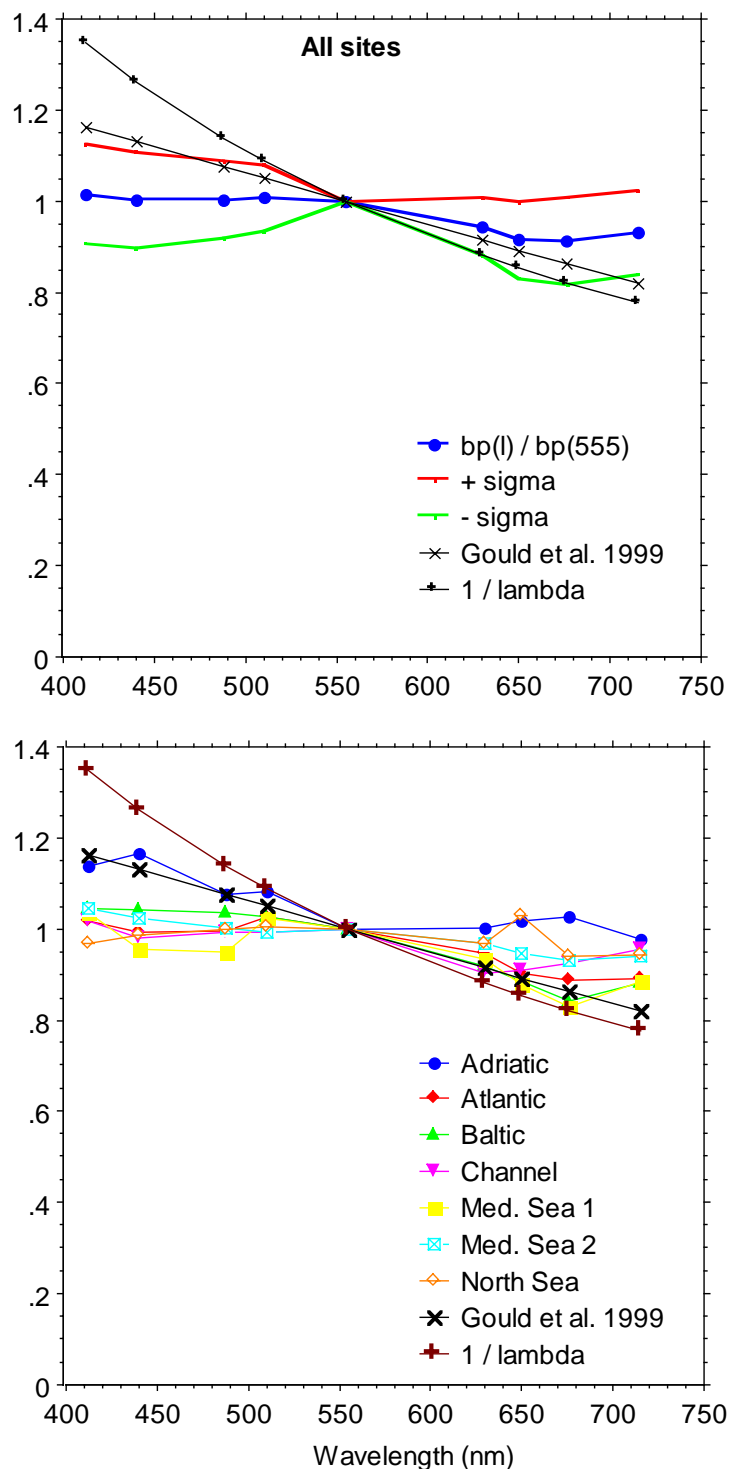


Figure 46. Average ratio between $b(\lambda)$ and $b(555)$ for all COAST/OOC stations (upper panel) and separately for each area (bottom panel). In the upper panel, the standard deviation is plotted. Other spectral dependencies of this ratio are also shown: that published by Gould *et al.* (1999, Appl. Opt. 38: 2377-2383) and the most classical one applied in models, *i.e.* the λ^{-1} dependency.

ACRJ - LPCM - SAI - U. Oldenburg
NIOZ - U. Trondheim - FUB - PML - GKSS

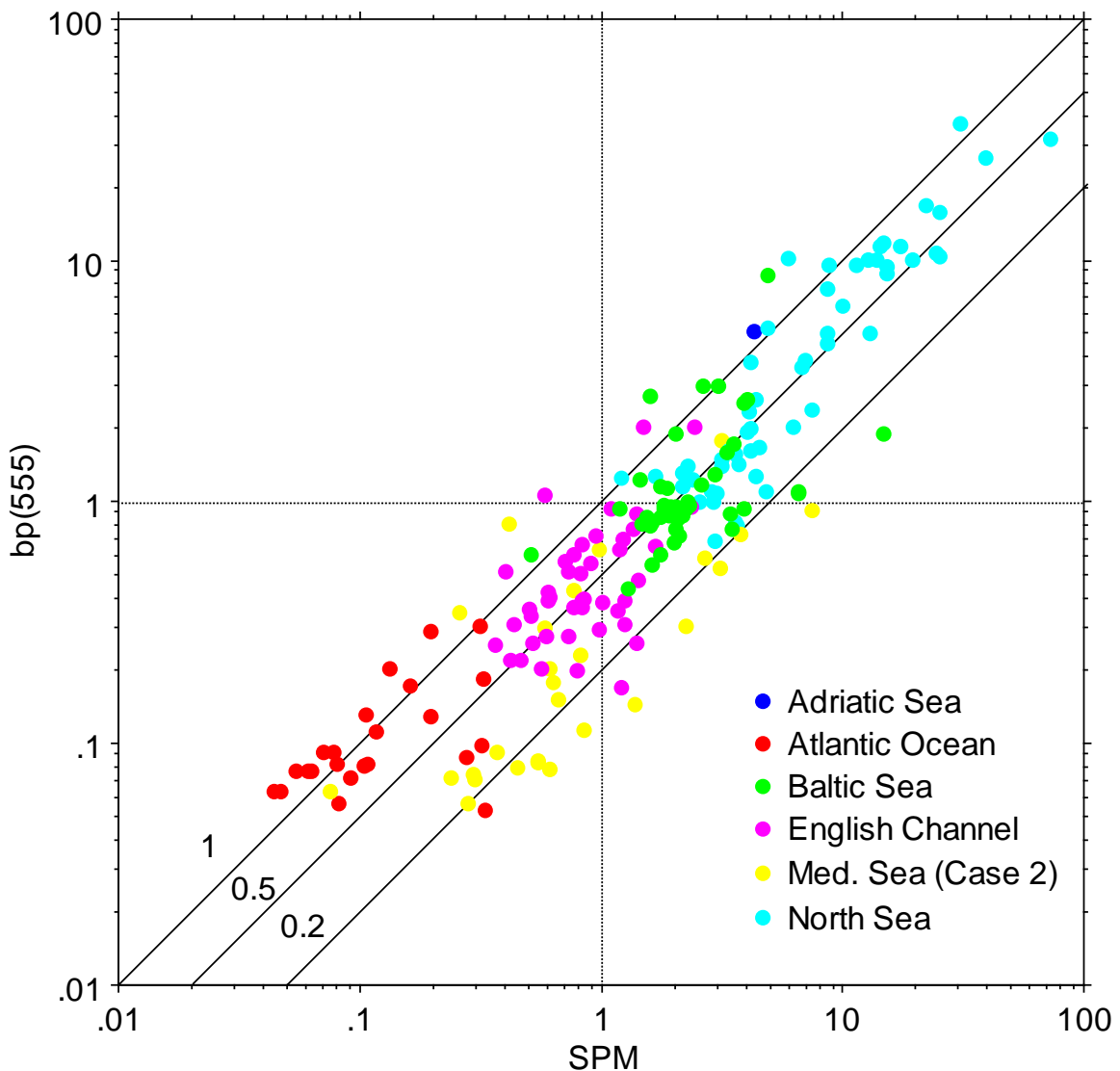


Figure 47. Relationship between $b(555)$ and SPM. The three straight lines indicate different $b(555)$: SPM ratios [or $b^*(555)$] (1, 0.5 and 0.2).

*ACRJ - LPCM - SAI - U. Oldenburg
NIOZ - U. Trondheim - FUB - PML - GKSS*

2.3.8. IOP variability as determined from the measurements performed using the Oldenburg instrument package

2.3.8.1. Material and Methods

Depth profiles were made with a sensor frame which includes different sensors.

2.3.8.1.1. Multi-channel fluorometer:

The instrument includes a 3-channel excitation that can be set at wavelengths in the UV and/or VIS, allowing a specific excitation of fluorescent substances and a modular set-up of up to ten detection channels at selectable wavelengths where the fluorescence emission of substances in seawater is high. During the cruises, these wavelengths were set to:

Excitation	Emission	detected substance
270	300	water Raman scattering
	350	tryptophan fluorescence
	450	yellow substance fluorescence
420	490	water Raman scattering
	685	chlorophyll fluorescence
530	680	fucoxanthin absorption chlorophyll fluorescence

2.3.8.1.2. Polychromatic daylight radiometer.

Measurements: The instrument measures scalar and net irradiance with two $\frac{1}{2}(E_0 + \vec{E})$ collector heads. The spectra are detected with two miniaturised polychromators, each in 134 channels from 340 to 760 nm wavelength. The data transmitted via telemetry unit on board the ship consists of two times 43 channels in this wavelength range of which the spectra are derived.

2.3.8.1.3. Transmissometer Polychromatic transmissometer PAAL

The instrument makes use of miniaturised Zeiss spectrometers to measure spectra of the beam attenuation coefficient c at 375-755 nm. The instrument is equipped with a movable retroreflector to fit the path length in water to a broad range of turbidity and to achieve a calibration *in situ*. The data interpretation includes algorithms to classify scattering and absorbing matter in terms of phytoplankton, transparent particles, and yellow substance.

2.3.8.1.4. CTD: Meerestechnik Elektronik, OTS 1500

Measurements: Pressure, conductivity, temperature, and O₂. From this data salinity is calculated (UNESCO 84).

Bio-optical *in situ* Probing System

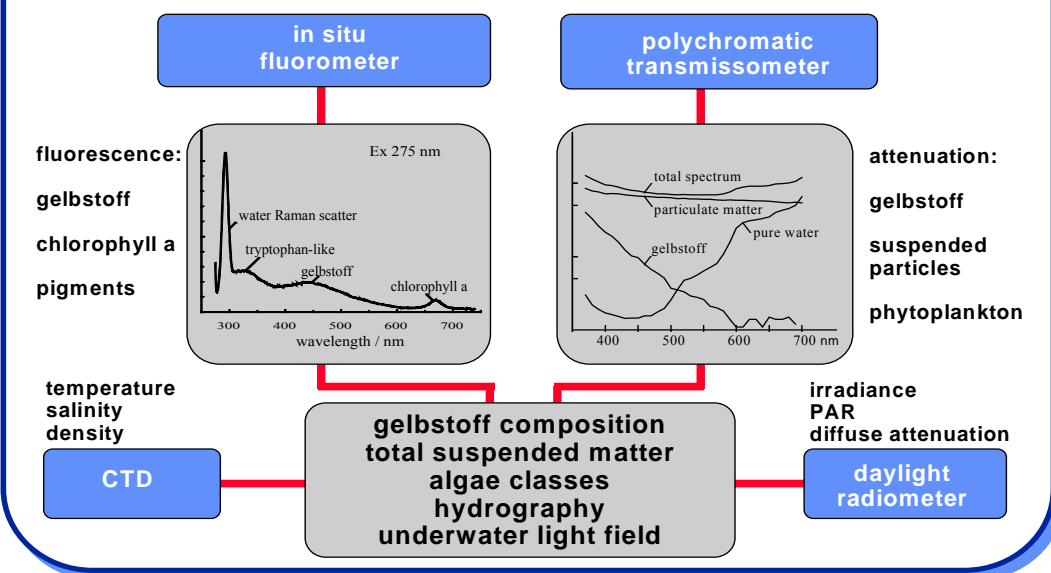


Figure 48. Information which can be obtained by simultaneous by measuring optical parameters.

Coupling of the Bio-optical Sensors

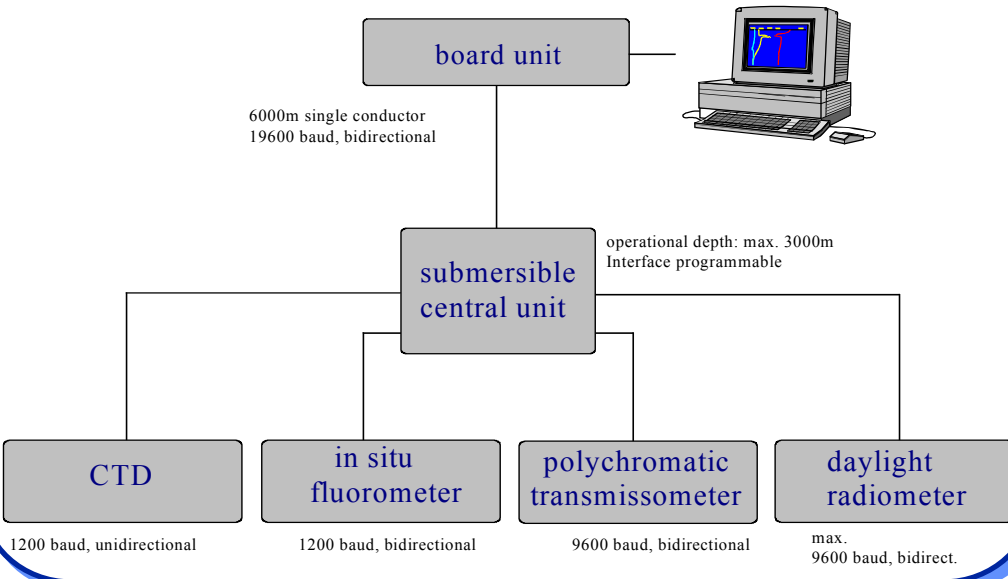


Figure 49. Principle of coupling of the optical sensors

ACRJ - LPCM - SAI - U. Oldenburg
NIOZ - U. Trondheim - FUB - PML - GKSS

Additional measurements were made using a spectrophotometer (Perking Elmer Lambda 18) and a spectrofluorometer (Perking Elmer LS 50). These data are used for the calibration and validation of the in situ profiles. The in situ profiles for chlorophyll are normalised to the *chl a* concentration of the hplc measurements from GKSS and LPCM.

2.3.8.2. Regions

The measurements performed by the group of Oldenburg University were carried out in the outflows of the rivers Loire, Seine, Thames, Rhine, Elbe, Oder, and Rhone. The measurements are completed by transects in the Region around Smith Knoll in the North Sea (see Figure 59), in the Gulf of Lion, and approx. 50 stations in oceanic (case I) waters. Examples of the inherent optical properties, the distributions of salinity, temperature, and chlorophyll concentration for the regions Seine, Humber, German Bight, and Rhone are presented in this report.

2.3.8.2.1. Seine

The location of the transect in the outflow of the river Seine is shown in Figure 50. Data from the in situ measurements are presented in Figure 51 to Figure 55. In the first two figures temperature and salinity are shown. The first station (15) is at 49°22.4' N. 000°09'7 W and the last station (22) is at 49°45.0' N, 000°10.2' W, the mean station distance is 2.5 miles. The influence of the river Seine is dominant at stations 15 - 17; at these stations down to a depth of 5 to 10 m warm water (13 - 14 °C) with low salinity (28 - 29) comes from the mouth of the river. In deeper waters and at stations 18 - 22 this influence vanishes gradually. In Figure 53 to Figure 55 data are shown which are calculated from the polychromatic transmissometer. The scattering coefficient for mineral particles depends on the wavelength and is shown for 400 nm in Figure 53. High scattering coefficients are measured near the mouth of the river, which is the main source for mineral particles in the Seine Bight. The absorption coefficient due to Gelbstoff is shown in Figure 54. The distribution of this absorption is nearly the same as the salinity distribution. The chlorophyll concentration in Figure 55 shows that the highest concentrations of phytoplankton are found in the regions between the influence of the Seine and the waters with higher salinity from the British Channel.

The influence of the waters from the river on the scattering coefficient due to mineral particles and the gelbstoff absorption coefficient is very high (Station 16 in Figure 53 and Figure 54). Around station 16 the gradient of the scattering coefficient is much higher than the gradient for the absorption coefficient and salinity. This may be caused by a sedimentation of the suspended particles in western regions of the transect.

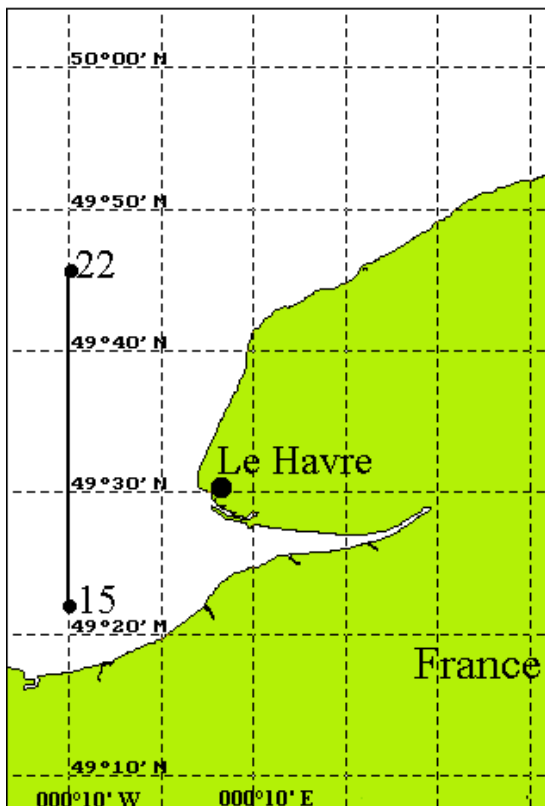


Figure 50. Location of the transect in the Seine Bight on May 8th 1998.

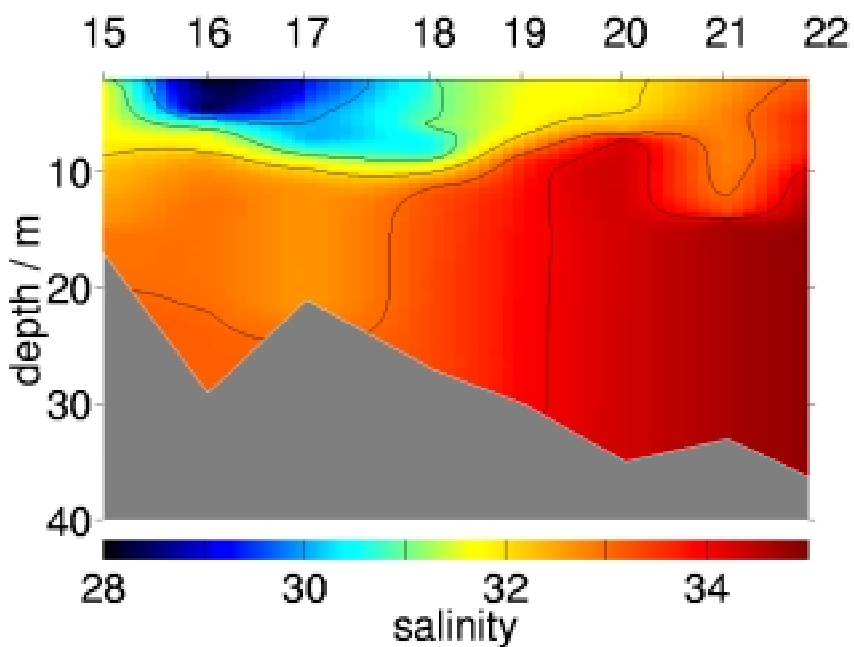


Figure 51. Salinity distribution in the Seine Bight measured on 08.05.98. The station numbers are the same as in Figure 50.

ACRJ - LPCM - SAI - U. Oldenburg
NIOZ - U. Trondheim - FUB - PML - GKSS

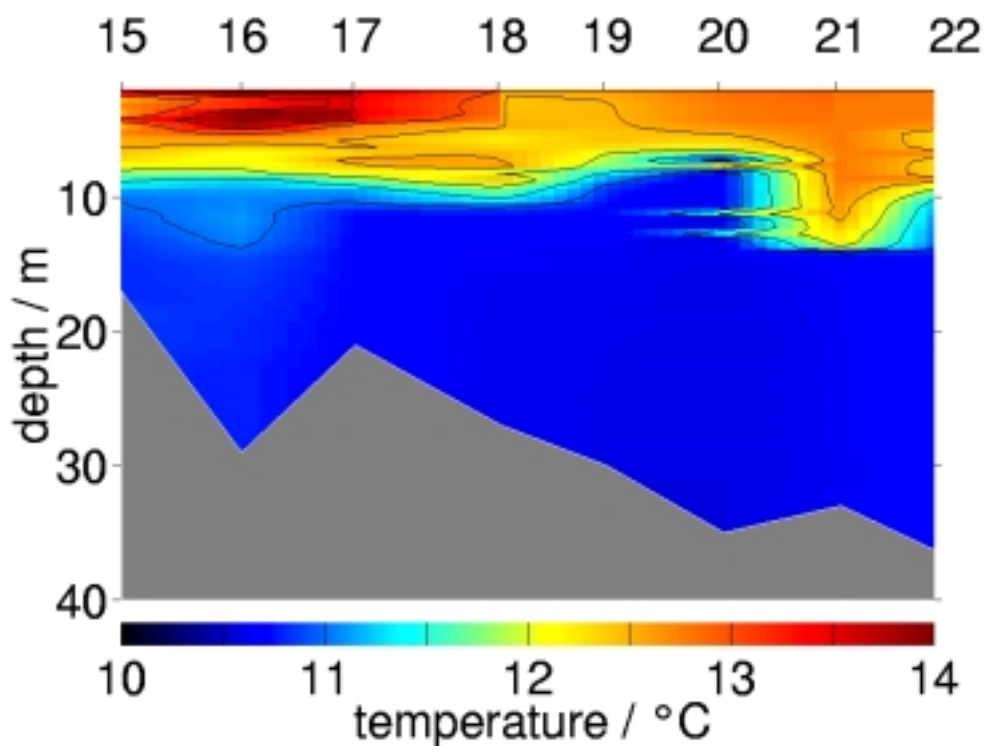


Figure 52. Temperature distribution in the Seine Bight. The station numbers are the same as in Figure 50.

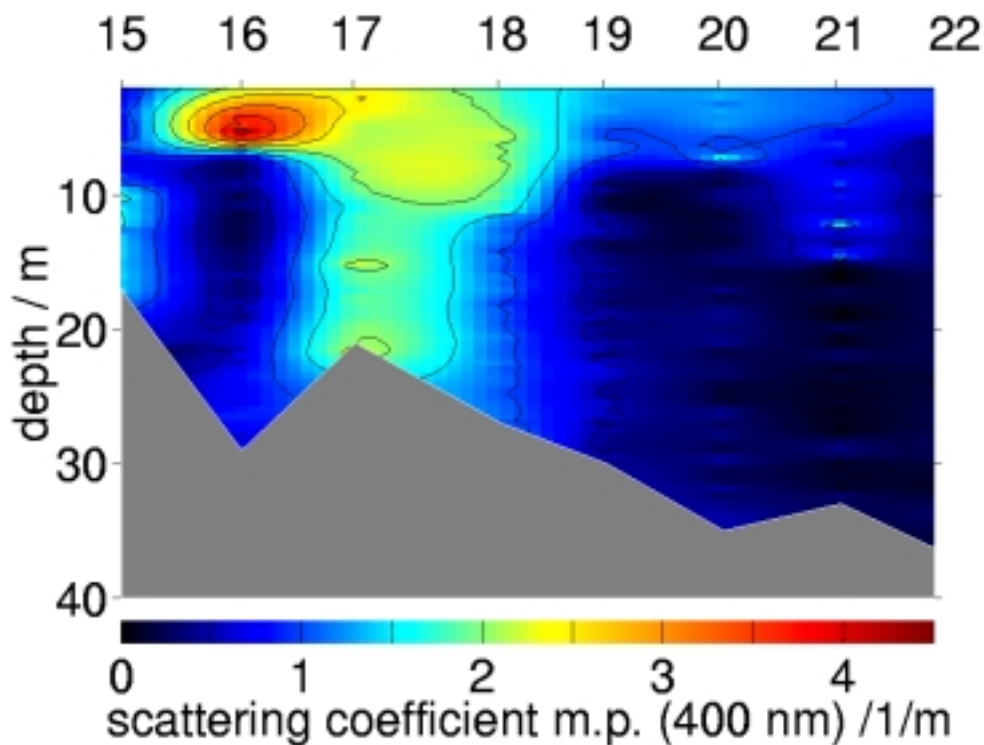


Figure 53. Distribution of the scattering coefficient for mineral particles in the Seine Bight. Data are calculated from beam attenuation spectra. The station numbers are the same as in Figure 50.

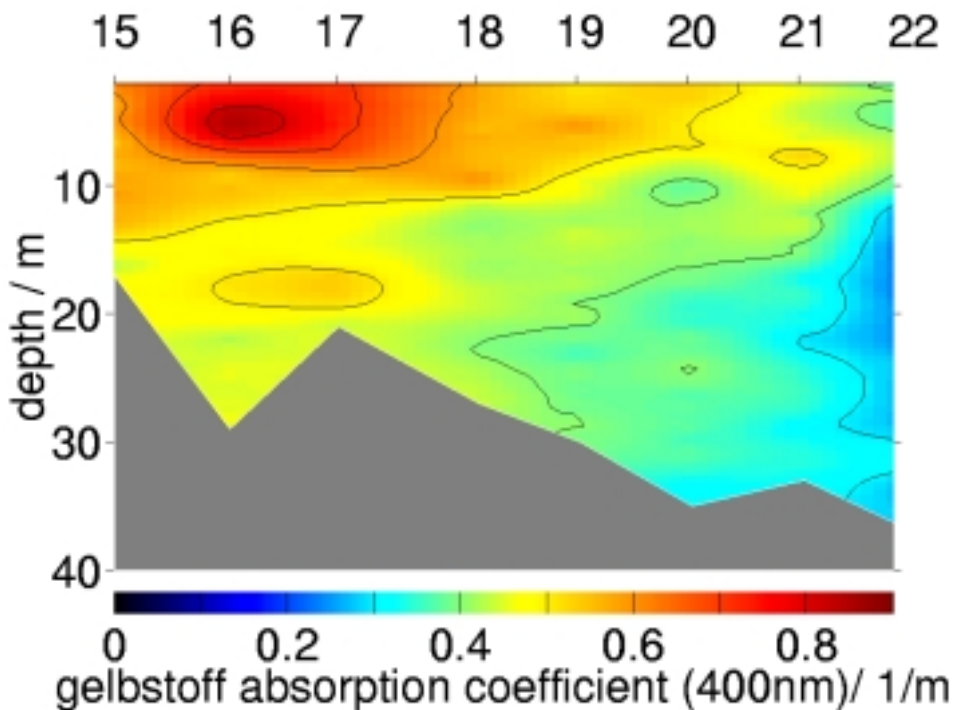
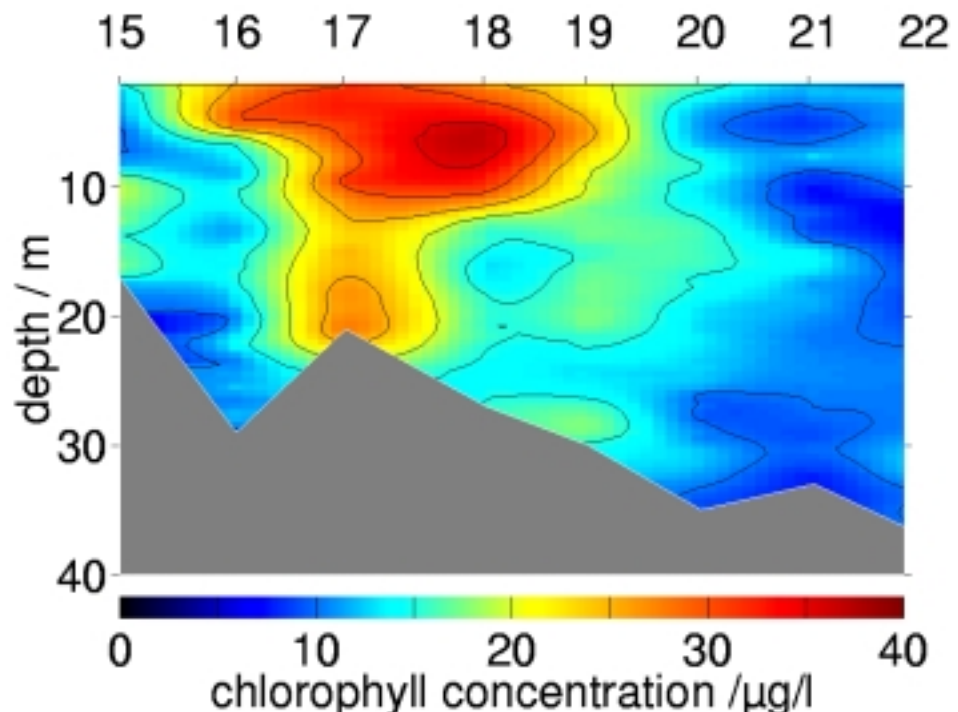


Figure 54. Gelbstoff absorption coefficient in the Seine Bight. Data are calculated from beam attenuation spectra. The station numbers are the same as in Figure 50.



ACRJ - LPCM - SAI - U. Oldenburg
NIOZ - U. Trondheim - FUB - PML - GKSS

Figure 55. Chlorophyll distribution in the Seine Bight. Data are calculated from beam attenuation spectra. The station numbers are the same as in Figure 50.

2.3.8.2.2. Humber

The location of the transect is shown in Figure 56. Data from the in situ measurements are presented in Figure 57 and Figure 58. Temperature, salinity, and the gelbstoff absorption coefficient (not shown) showed a low variation over the whole transect . The temperature was $10.0 \pm 0.1^\circ\text{C}$, the salinity, 34.45 ± 0.05 and the gelbstoff absorption coefficient at 400 nm was $0.31 \pm 0.01 \text{ l/m}$.

The scattering coefficient for mineral particles in Figure 57 shows a remarkable distribution. Due to calm weather conditions during and before the measurements, the mineral particles in the water column sank down to a layer of approximately 5-8 m above the seafloor. In this layer the scattering coefficient at 400 nm varies around 1.1 l/m , and in the upper layer around 0.75 l/m . The distribution for the phytoplankton concentration is characterised by a high ‘patchiness’, which makes it problematic to compare the data from the niskin bottles with the in situ data. The information of the fluorometer which is also connected to the sensor frame confirms the information of the attenuation data interpretation.

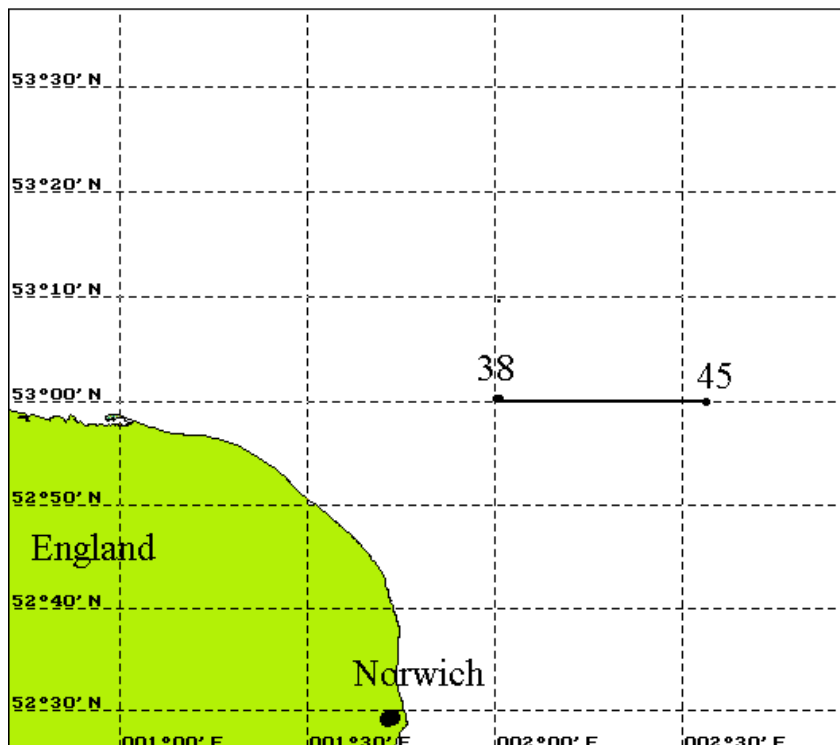


Figure 56. Location of the transect (Humber) around Smith Knoll near the south-east coast of England.

*ACRJ - LPCM - SAI - U. Oldenburg
 NIÖZ - U. Trondheim - FUB - PML - GKSS*

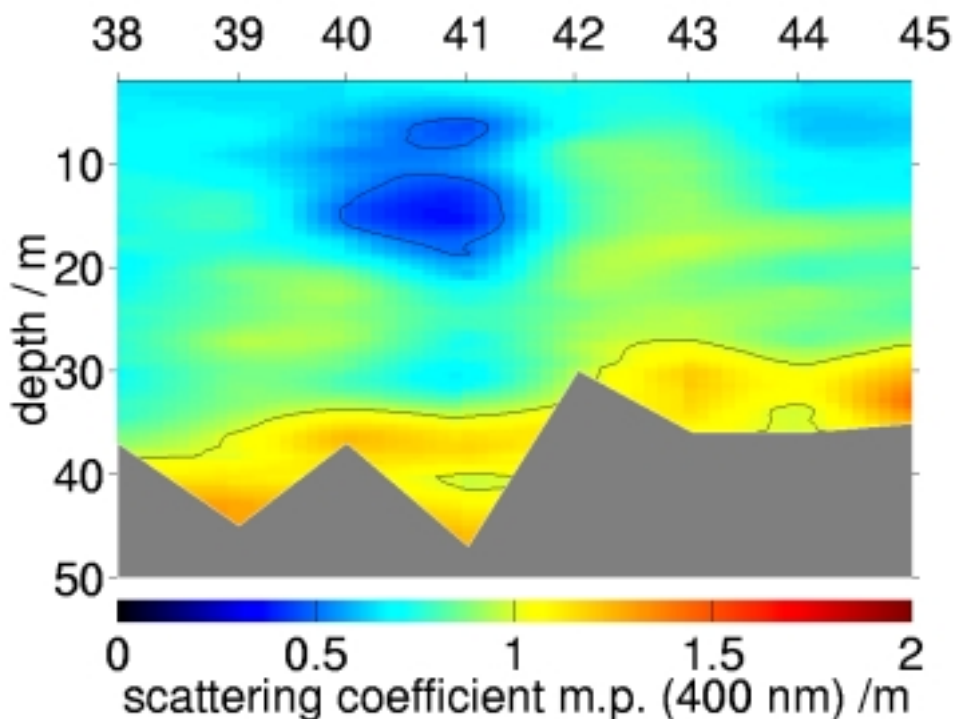


Figure 57. Distribution of the scattering coefficient for mineral particles in the region Humber. Data are calculated from beam attenuation spectra. The station numbers are the same as in Figure 56.

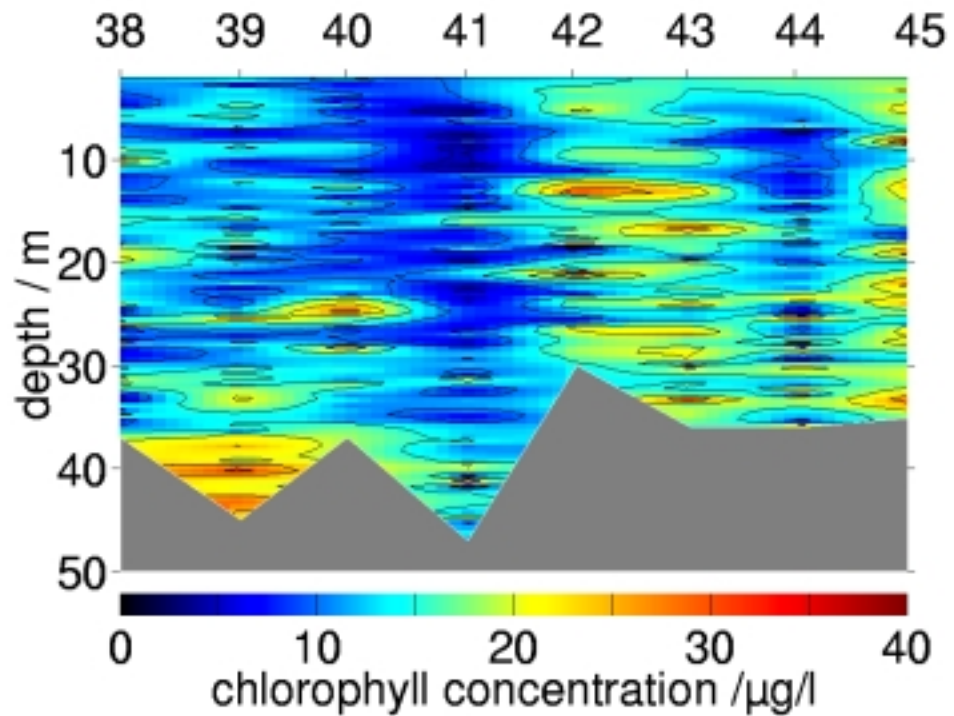


Figure 58. Chlorophyll distribution in the region Humber. Data are calculated from beam attenuation spectra. The station numbers are the same as in Figure 56.

ACRI - LPCM - SAI - U. Oldenburg
NIOZ - U. Trondheim - FUB - PML - GKSS

2.3.8.2.3. German Bight

The location of the transect is shown in Figure 59: It starts at station 46 and ends at station 48. Data from the in situ measurements are presented in Figure 60 to Figure 62. In Figure 60, the distribution of salinity shows a decrease towards the coast with increasing influence of the river Ems. Another water body is found below 10 m at station 46. The temperature dependence (not shown) is comparable with the salinity distribution, with high temperatures of around 12 °C at the coast and below 11 °C at station 46 below 10 m. The distribution of the scattering coefficient and the chlorophyll concentration in Figure 61 and Figure 62 is nearly the same. The water body with the high salinity at station 46 shows higher concentrations of chlorophyll ($\approx 8 \mu\text{g/l}$) and mineral particles ($\approx 1 \text{ l/m}$).

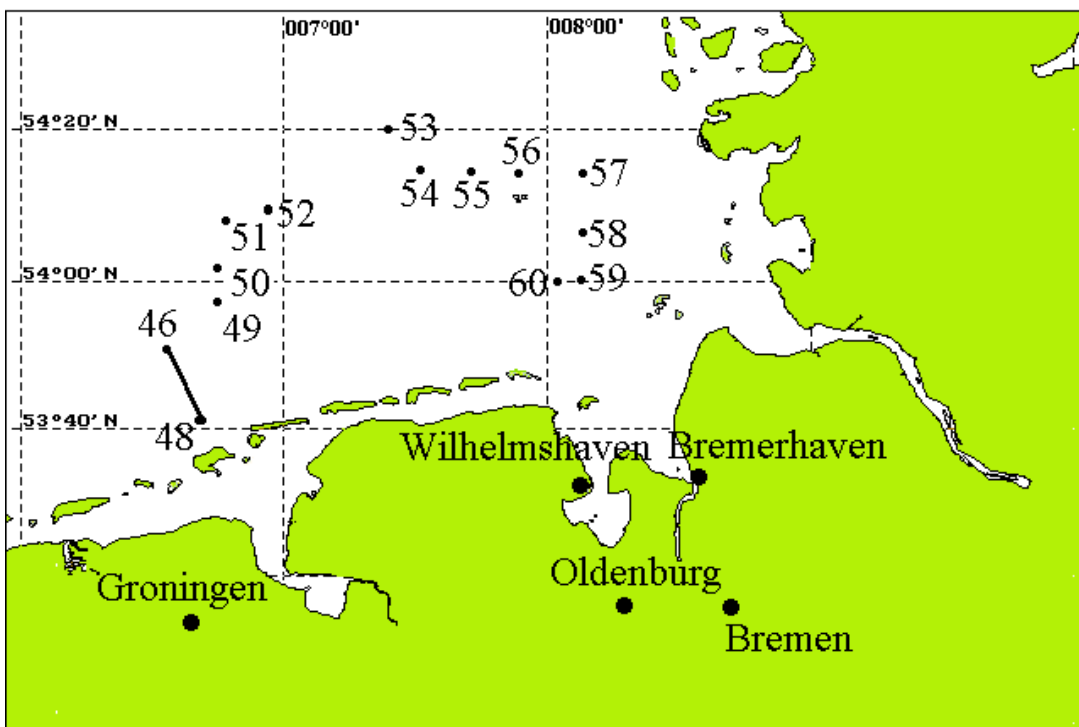


Figure 59. Transect and stations in the German Bight.

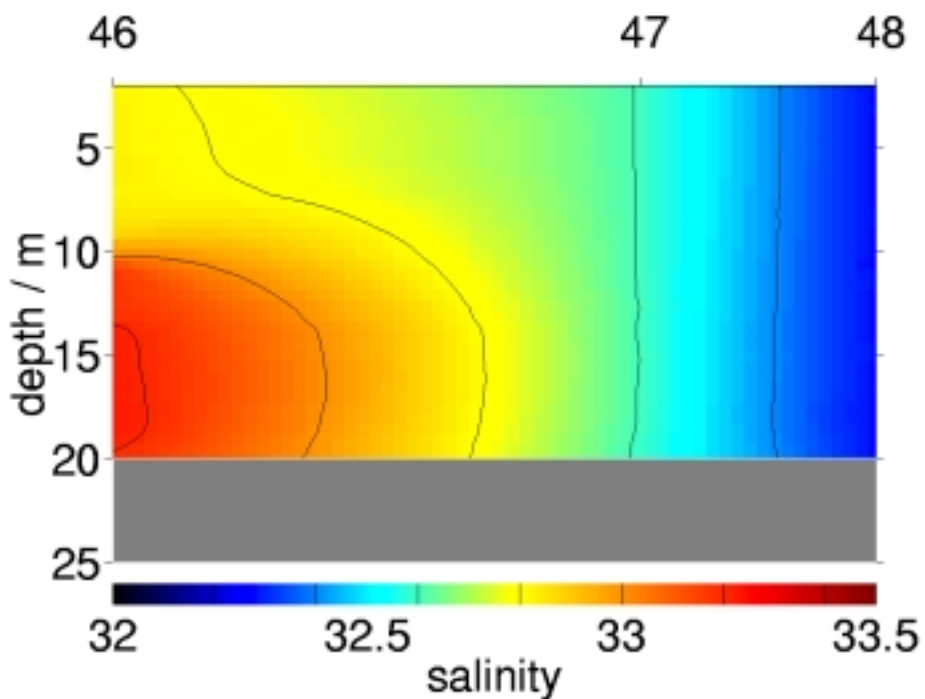


Figure 60. Salinity distribution on a transect in front of the island Borkum. The station numbers are the same as in Figure 59.

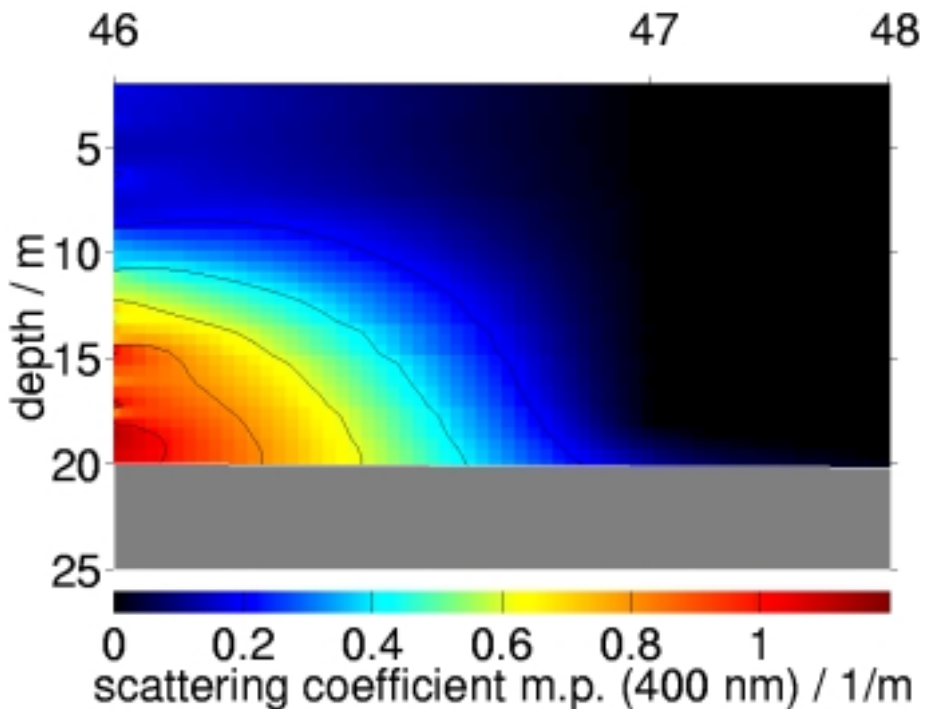


Figure 61. Scattering coefficient for mineral particles on a transect in front of the island Borkum. Data are calculated from beam attenuation spectra. The station numbers are the same as in Figure 59.

ACRJ - LPCM - SAI - U. Oldenburg
NIOZ - U. Trondheim - FUB - PML - GKSS

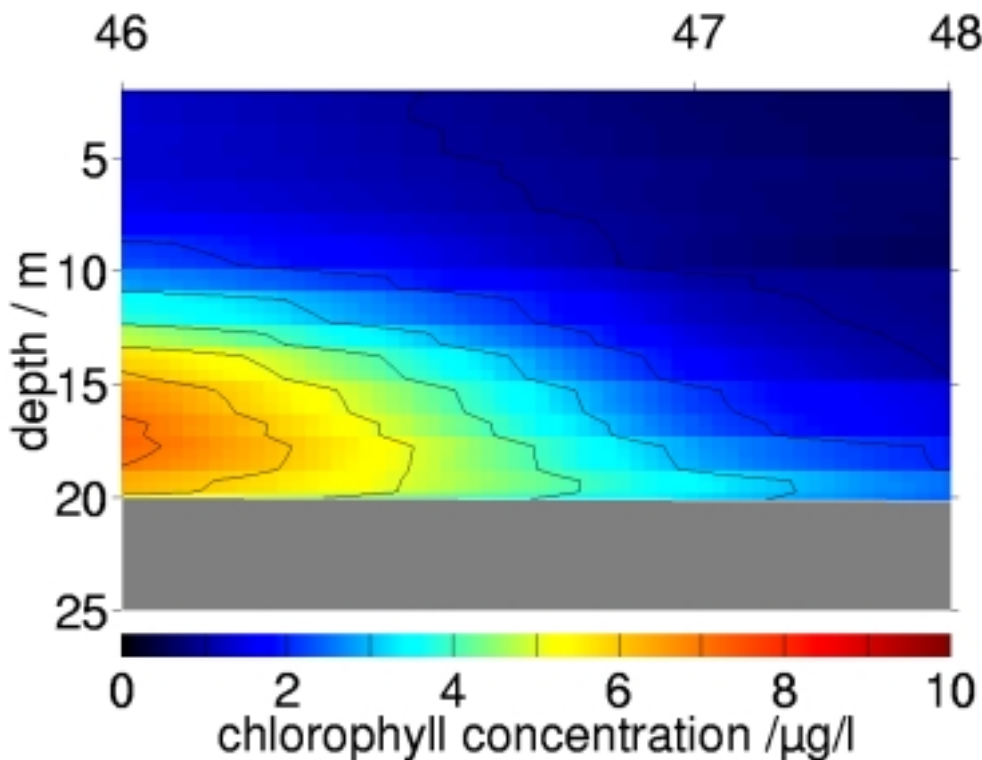


Figure 62. Chlorophyll distribution on a transect in front of the island Borkum. Data are calculated from beam attenuation spectra. The station numbers are the same as in Figure 59.

2.3.8.2.4. Rhone

The locations of two transects are shown in Figure 63. In this report data from the eastern transect (from station 7 to 13) are presented. The situation in the outflow of the river Rhone during the measurements was characterized by wind velocities of 1 m/s and a stable plume from the river Rhone with low salinity and amount of yellow substance and suspended matter in the first 5 m of the water column. This is documented in Figure 64 to Figure 68. The salinity and temperature distributions (Figure 64 and Figure 65) show this from station 7 to station 10. A hydrographical front with steep gradients in salinity and temperature was situated between station 10 and 11. The distributions for the scattering and absorption coefficients and the chlorophyll concentrations were nearly the same, with high coefficients in the region of the Rhone plume and a case I water situation behind station 11.

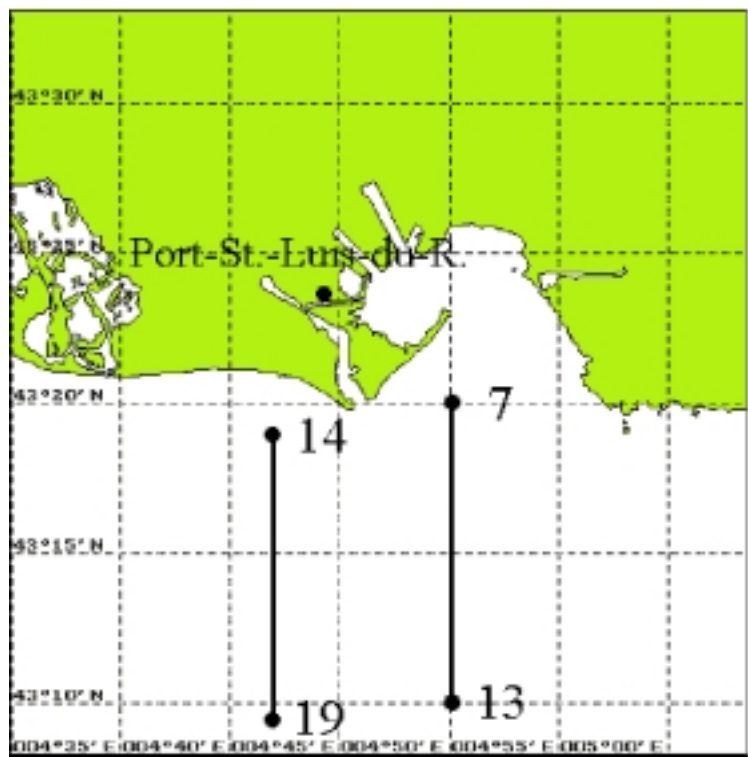


Figure 63. Location of two transects which were carried out during the Thethis II cruise in September 1997.

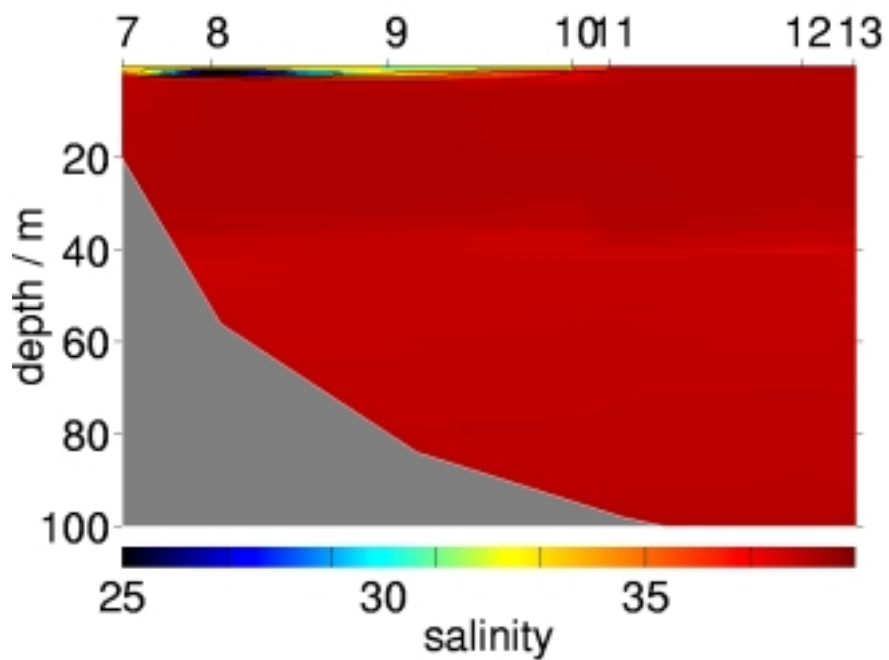


Figure 64. Salinity distribution on a transect from the plume of the river Rhone to case I water regions of the Mediterranean. The station numbers are the same as in Figure 63.

ACRJ - LPCM - SAI - U. OI denburg
NIOZ - U. Trondheim - FUB - PML - GKSS

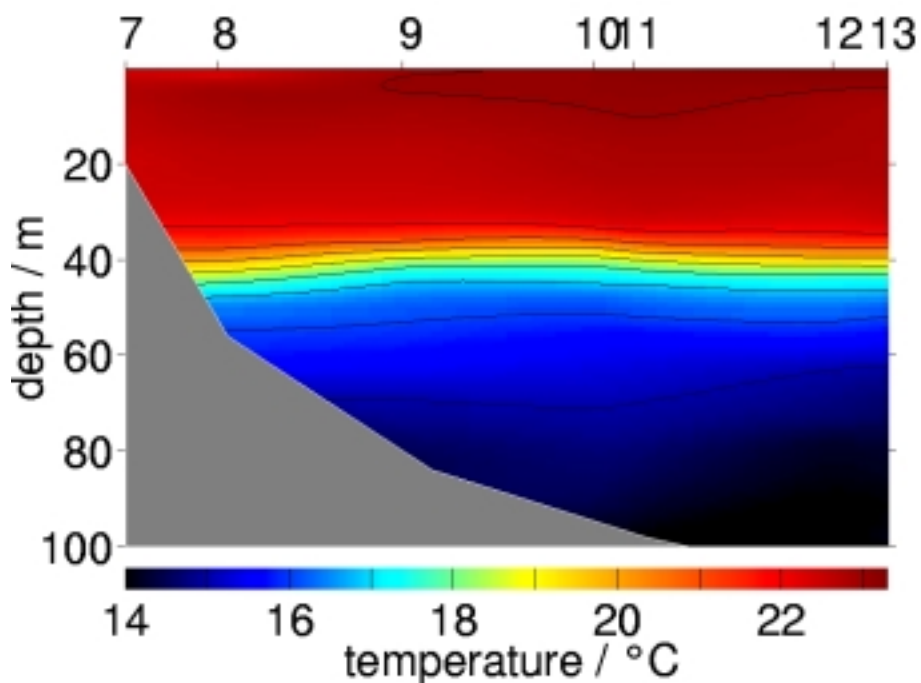


Figure 65. Temperature distribution on a transect from the plume of the river Rhone to case I water regions of the Mediterranean. The station numbers are the same as in Figure 63.

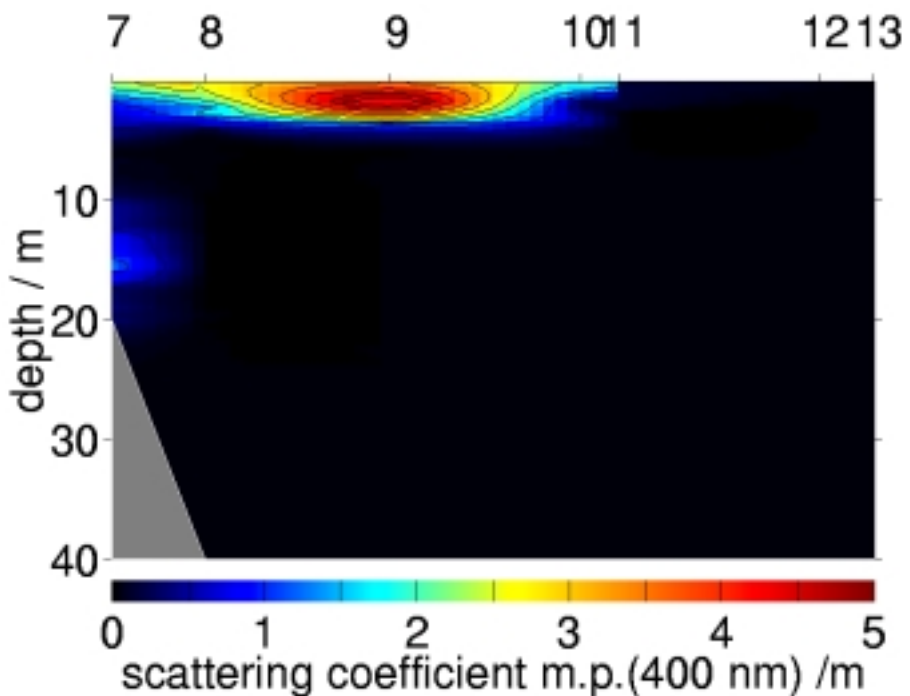


Figure 66. Distribution of the scattering coefficient due to mineral particles on a transect from the plume of the river Rhone to case I waters of the Mediterranean. Data are calculated from beam attenuation spectra. The station numbers are the same as in Figure 63.

*ACRJ - LPCM - SAI - U. Oldenburg
NIOZ - U. Trondheim - FUB - PML - GKSS*

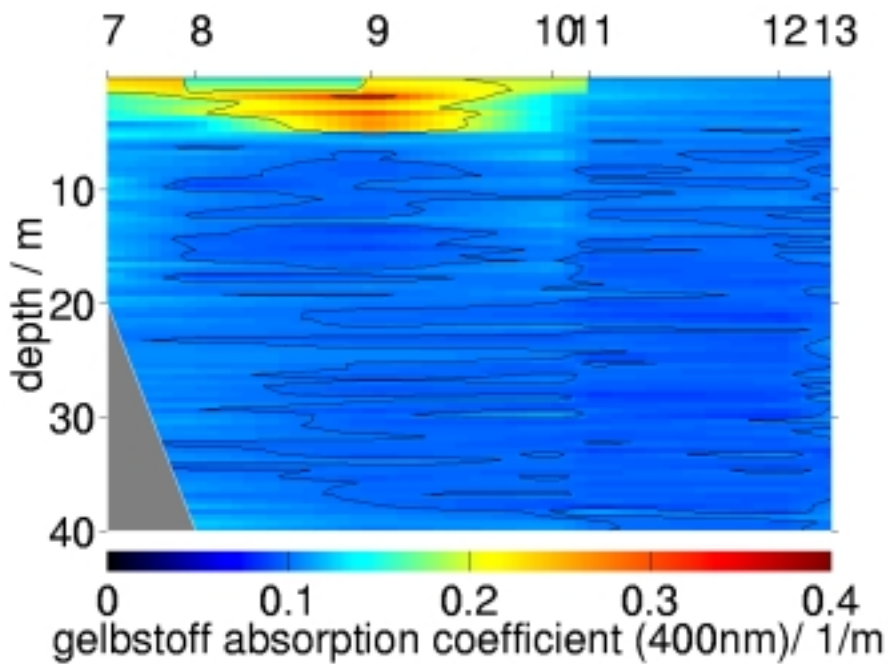


Figure 67. Distribution of the gelbstoff absorption coefficient on a transect from the plume of the river Rhone to case I water regions of the Mediterranean. Data are calculated from beam attenuation spectra. The station numbers are the same as in Figure 63.

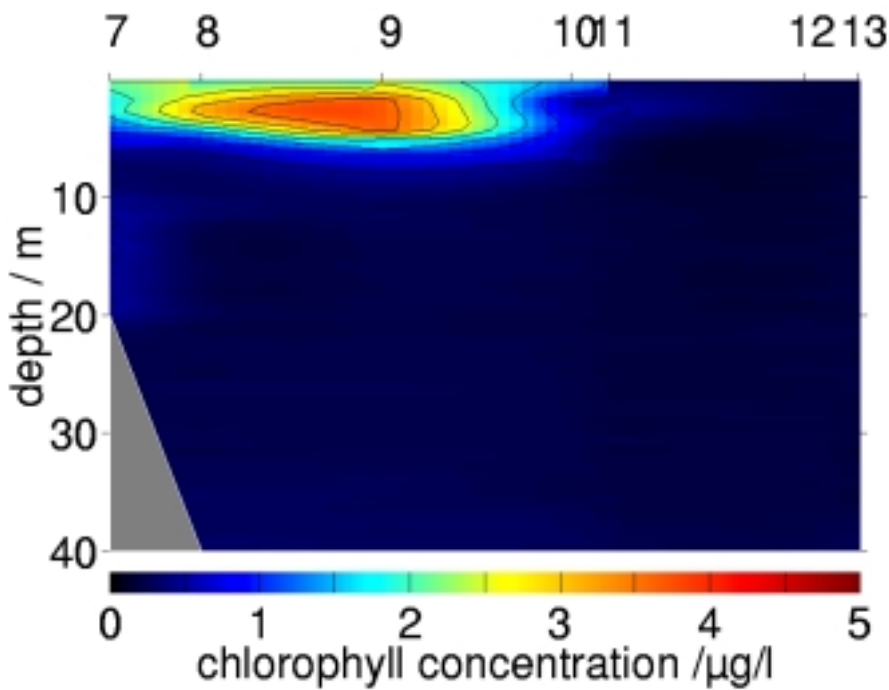


Figure 68. Distribution of the chlorophyll concentration on a transect from the plume of the river Rhone to case I water regions of the Mediterranean. Data are calculated from beam attenuation spectra. The station numbers are the same as in Figure 63.

ACRJ - LPCM - SAI - U. Oldenburg
NIOZ - U. Trondheim - FUB - PML - GKSS

2.4. REFLECTANCE MODELLING

2.4.1. Proposed Model

2.4.1.1. Remotely sensed layer

The geometrical thickness of the vertical water layer from which 90% of the remotely sensed ocean colour signal emerges [denoted $Z_{90}(\lambda)$; m] can be approximated by (Gordon and McCluney 1975):

$$Z_{90}(\lambda) = 1/K_d(\lambda) \quad (1a)$$

where $K_d(\lambda)$ (m^{-1}) is the vertical attenuation coefficient for downward irradiance. Here, we assumed that (whatever λ)

$$z \gg Z_{90}(\lambda) \quad (1b)$$

where z (m) is the geometrical thickness of the water column. In other words, bottom effect was not accounted for in the present model.

2.4.1.2. Water constituents

The apparent optical properties of sea waters were determined according to the inherent optical properties (absorption, a , and scattering, b) of 5 groups of substances (see Figure 69):

1. pure sea water, denoted "w"
2. phytoplankton and other associated particles (detritus, bacteria, ...), denoted "p1"
3. endogenous coloured dissolved organic matter (associated with biological activity), denoted "y1"
4. terrestrial (exogenous) particles (sediment resuspended from the bottom, brought by rivers, ...), denoted "p2"
5. exogenous coloured dissolved organic matter from land drainage (present in Case 2 waters only), denoted "y2".

While only groups 1, 2 and 3 are present in Case 1 (oceanic) waters, all of them co-exist in Case 2 (coastal) waters.

IOPs of groups 2, 3, 4 and 5 were related to the following "concentrations":

1. p1 and y1 IOPs as a function of Chl with units as $mg\ m^{-3}$
2. p2 IOPs were related to the sea water particles dry weight from which the contribution of p1 has been subtracted, denoted SPM and with units as $g\ m^{-3}$

*ACRJ - LPCM - SAI - U. Oldenburg
NIOZ - U. Trondheim - FUB - PML - GKSS*

3. y_2 IOPs as a function of the CDOM concentration as determined by its absorption coefficient at 443 nm, denoted " $a_{y2}(443)$ " and with units as m^{-1} (i.e. the total measured CDOM absorption from which a_{y1} has been subtracted)

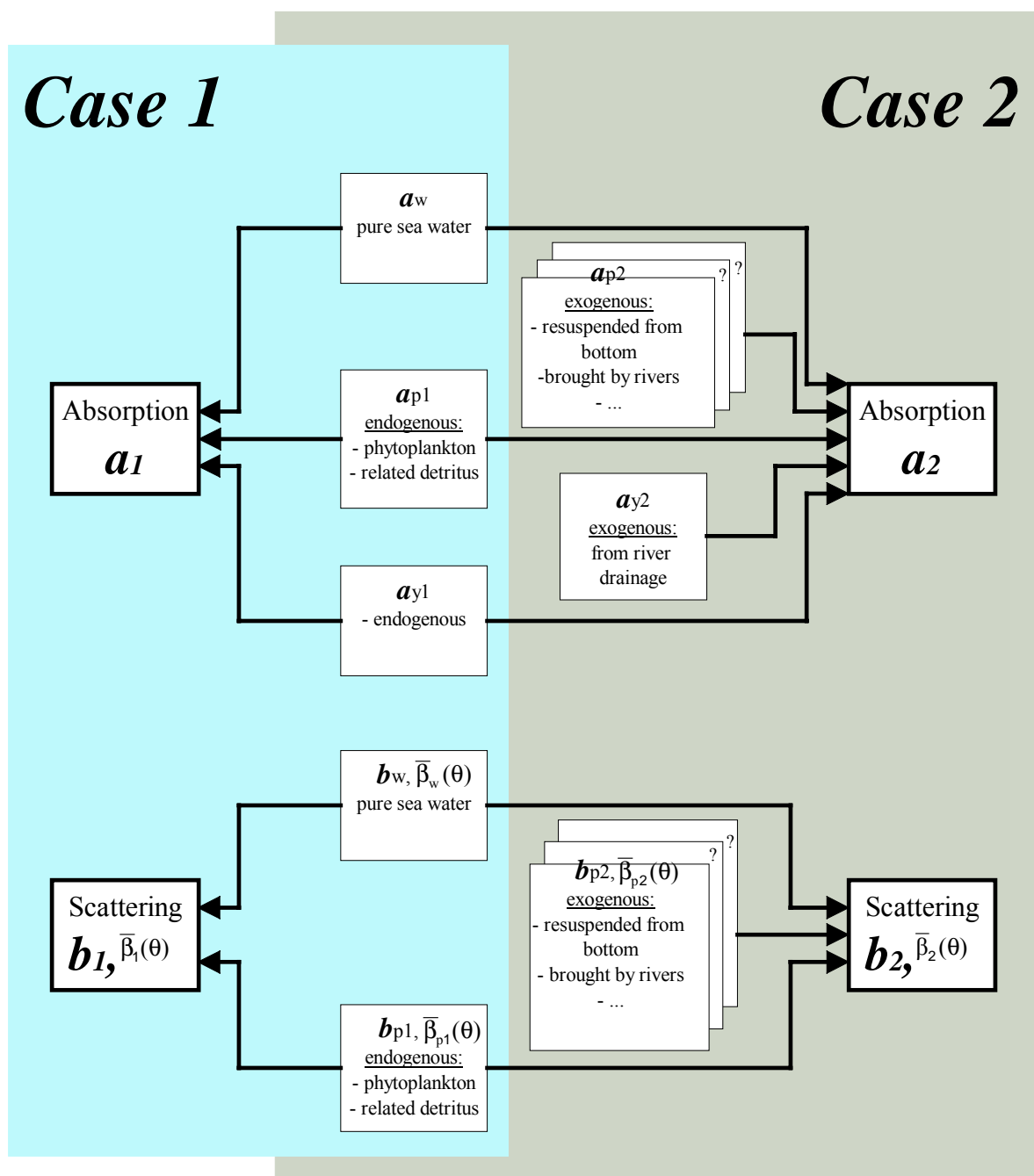


Figure 69. Schematic representation of IOP compartments.

*ACRJ - LPCM - SAI - U. Oldenburg
NIOZ - U. Trondheim - FUB - PML - GKSS*

Comments on Figure 69

Case 2 waters are seen as Case 1 waters to which other optically active substances are added. In other words, Case 1 waters can be seen as particular Case 2 waters when these additional substances are lacking.

Case waters 1 include 3 components:

- pure sea water for which 2 spectral IOPs must be specified: $a_w(\lambda)$ and $\beta_w(\lambda, \theta)$; this last term can be split into $\bar{\beta}_w(\theta)$ (independent from λ) and $b_w(\lambda)$
- all particulate matter found in open ocean, such as living algal cells, heterotrophic bacteria and organisms, various debris, ... Again, this compartment is described by its absorption and scattering properties: $a_{p1}(\lambda)$, $b_{p1}(\lambda)$ and $\bar{\beta}_{p1}(\theta)$
- coloured dissolved organic material presumably generated in open ocean (through processes like excretion, organism decay, ...), and likely related to the particulate matter abundance. This compartment comes into play through its absorption coefficient $a_{y1}(\lambda)$

In summary, there are 3 components in forming the absorption coefficient of Case 1 waters and 2 components in forming the scattering properties.

Case 2 waters include the two above components and in addition:

- exogenous particles, mainly sediment, either transported by rivers, or re-suspended from the bottom in shallow waters. The proportions between organic and mineral particles is varying according to the location and origin; the mineral particles are also geographically differing (clay, calcareous, ...). Therefore, several types of particles may be simultaneously present, and to each type corresponds a couple of properties like $a_{p2}(\lambda)$ and $\beta_{p2}(\lambda, \theta)$
- exogenous CDOM resulting from land drainage which acts only as absorber: $a_{y2}(\lambda)$. As for particles, it is likely that several types may be distinguished depending on the location.

2.4.1.3. Vertical distribution

It was assumed that all substances are homogeneously distributed in the water column. For many coastal waters, this is a realistic assumption, especially when considering the $Z_{90}(\lambda)$ layer (this is not true for river plumes, where very strong vertical gradients may be observed).

2.4.1.4. Inherent optical properties of water and its constituents

Using the present reflectance model, one should be able to calculate the reflectance just below surface, $R(\lambda)$ [defined as the ratio of upward to downward irradiance, $E_u(\lambda) / E_d(\lambda)$], using Chl, SPM and Y as input. The approach suggested here is based on the following set of equations:

$$R(\lambda) = f'(\lambda) \frac{b_b(\lambda)}{a(\lambda) + b_b(\lambda)} \quad (1)$$

*ACRJ - LPCM - SAI - U. Ol denburg
 NIÖZ - U. Trondheim - FUB - PML - GKSS*

where $b_b(\lambda)$ is the seawater backscattering coefficient, $a(\lambda)$ is the seawater absorption coefficient and $f(\lambda)$ is a proportionality factor. $a(\lambda)$ and $b_b(\lambda)$ can be broken into individual contributions by the different water constituents:

$$a(\lambda) = \sum_{n=1}^N a_n(\lambda) \quad (2)$$

$$b_b(\lambda) = \sum_{n=1}^N \tilde{b}_{bn}(\lambda) b_n(\lambda) \quad (3)$$

where the subscript n indicates a given optically significant seawater constituent, $b_n(\lambda)$ is the scattering coefficient of the nth substance and $\tilde{b}_{bn}(\lambda)$ is the ratio of backscattering to scattering of the nth substance.

In the following sections, we show how to derive $a_n(\lambda)$, $b_n(\lambda)$ and $\tilde{b}_{bn}(\lambda)$ from the inputs Chl, SPM and Y. The calculation of $f(\lambda)$ is described below in Section 2.4.1.4.3.

It must be mentioned that the proposed approach to calculate $R(\lambda)$ is different from the more classical one where $R(\lambda)$ is obtained from a full radiative transfer calculation using the fundamental IOPs, $a(\lambda)$ and $\beta(\theta)$ (the volume scattering function). The latter approach is in principle more rigorous. Nevertheless, it currently strongly suffers from our poor knowledge of the shape of $\beta(\theta)$ for particles. Generally, a single VSF for particles is used: most often the one determined three decades ago by Petzold (1972). In the proposed approach, we use Eq. 1, which is strictly valid, to derived $R(\lambda)$. On the one hand, the Petzold's VSF is used in the calculation of $f(\lambda)$. On the other hand, part of the VSF variability is accounted for by modulating particles $b_b(\lambda)$, based on actual measurements or on current knowledge. We believe that the error related to the use of the Petzold's VSF in the calculation of $f(\lambda)$ is small. A sensitivity analysis remains to be done to support this argument.

2.4.1.4.1. Pure sea water and phytoplankton

Case 1 waters absorption and backscattering coefficients, denoted $a_1(\lambda)$ and $b_{b1}(\lambda)$, respectively, can be expressed as:

$$a_1(\lambda) = a_w(\lambda) + a_{p1}(\lambda) + a_{y1}(\lambda) \quad (4)$$

$$b_{b1}(\lambda) = 0.5b_w(\lambda) + \tilde{b}_{bp1}(\lambda)b_{p1}(\lambda) \quad (5)$$

For wavelengths up to 700nm, $a_w(\lambda)$ is taken from Pope and Fry (1997), and above 700nm, from Hale and Querry (1973) (see Table 12 below).

λ (nm)	a_w (m^{-1})
412.5	.00452
442.5	.00696
490.0	.01500
510.0	.03250
560.0	.06190
620.0	.27550
665.0	.42900
705.0	.70400
775.0	2.4000
865.0	4.9000

Table 12. Water absorption $a_w(\lambda)$.

$a_{p1}(\lambda)$ is taken from Bricaud *et al.* (1998):

$$a_{p1}(\lambda) = A_{ap1}(\lambda) \text{Chl}^{B_{ap1}(\lambda)} \quad (6)$$

coefficients $A_{ap1}(\lambda)$ and $B_{ap1}(\lambda)$ are reproduced in Table 13 below.

λ (nm)	$A_{ap1}(\lambda)$	$B_{ap1}(\lambda)$
412.5	.0474995	.6840705
442.5	.0511810	.6266249
490.0	.0341240	.6200260
510.0	.0231810	.7060040
560.0	.0100310	.8412540
620.0	.0089570	.8438080
665.0	.0167630	.8207835
705.0	.0010000	1.0000000
775.0	.0000000	1.0000000
865.0	.0000000	1.0000000

Table 13. $A_{ap1}(\lambda)$ and $B_{ap1}(\lambda)$ coefficients.

$a_{y1}(\lambda)$ is given by:

$$a_{y1}(\lambda) = a_{y1}(443) e^{-S_{y1}(\lambda - 443)} \quad (7)$$

where S_{y1} equals 0.014 nm^{-1} (Bricaud *et al.* 1981), and

$$a_{y1}(443) = k(a_{y1}) [a_w(443) + a_{p1}(443)] \quad (8)$$

where $k(a_{y1})$ is assumed equal to 0.5. $b_w(\lambda)$ is determined from Morel (1974):

NIOZ - U. ACR] - LPCM - SAI - U. OI denburg
 Trondheim - FUB - PML - GKSS

$$b_w(\lambda) = 0.00288 \left(\frac{\lambda}{500} \right)^{-4.32} \quad (9)$$

$b_{p1}(\lambda)$ is taken from Loisel and Morel (1998):

$$b_{p1}(\lambda) = A_{bp1} \cdot \text{Chl}^{B_{bp1}} \left(\frac{\lambda}{550} \right)^{-1} \quad (10)$$

where A_{bp1} and B_{bp1} equal 0.416 and 0.766, respectively. The backscattering to scattering ratio for case 1 waters particles is expressed as (from Morel, *in preparation*):

$$\tilde{b}_{bp1}(\lambda) = .002 + .01 [.5 - .25 \log_{10} \text{Chl}] (550/\lambda)^v \quad (11)$$

with $v = 0.5 \left[0.3 - \log_{10} (\text{chl}) \right]$ when $\text{Chl} < 20 \text{ mg m}^{-3}$

and $v = 0$ when $\text{Chl} \geq 20 \text{ mg m}^{-3}$

2.4.1.4.2. Non-chlorophyllous suspended sediments and gelbstoff

The CDOM absorption coefficient in Case 2 waters is expressed as:

$$a_{y2}(\lambda) = a_{y2}(443) e^{-S_{y2}(\lambda-443)} \quad (12)$$

where S_{y2} equals 0.0176 nm^{-1} , as derived from COAST/OOC data.

The absorption coefficient of suspended sediments (exogenous particles), $a_{p2}(\lambda)$ is expressed as:

$$a_{p2}(\lambda) = a_{p2}(443) e^{-S_{p2}(\lambda-443)} \quad (13)$$

where S_{p2} equals 0.0122 nm^{-1} , and

$$a_{p2}(443) = A_{ap2} \text{ SPM}^{B_{ap2}} \quad (14)$$

where A_{ap2} and B_{ap2} equal 0.0216 and 1.0247, respectively. All of these values were derived from COAST/OOC data. Note here that Eq. 14 was obtained after subtracting phytoplankton and related particles contributions from both $a_{p2}(443)$ and SPM using the relationships (as a function of Chl) published by Bricaud *et al.* (1998) and Malone (1982), respectively.

The scattering coefficient of suspended sediments (exogenous particles), b_{p2} is expressed as (from COAST/OOC data):

ACR - *LPCM* - *SAI* - *U. Ol denburg*
NIOZ - *U. Trondheim* - *FUB* - *PML* - *GKSS*

$$b_{p2}(\lambda) = b_{p2}(550) \quad (15a)$$

$$b_{p2}(550) = A_{b_{p2}(550)} \text{ SPM} \quad (15b)$$

where $A_{b_{p2}(550)}$ equals $0.5 \text{ m}^2 \text{ g}^{-1}$. Equation 15b was derived from COAST/ OOC data. The backscattering to scattering ratio for case 2 water particles is expressed as:

$$\tilde{b}_{p2}(\lambda) = 0.01 \quad (16)$$

It is important to mention that although single parameterisations are presented for suspended sediments (exogenous particles) absorption and scattering properties, other relationships may be found for other particle types that were not encountered during COAST/OOC (illustrated in Figure 69 by box stacks).

Thus, the bulk absorption and scattering properties of Case 2 waters can be expressed as:

$$a_2(\lambda) = a_l(\lambda) + a_{p2}(\lambda) + a_{y2}(\lambda) \quad (17a)$$

$$b_{b2}(\lambda) = b_{b1}(\lambda) + \tilde{b}_{b_{p2}}(\lambda) b_{p2}(\lambda) \quad (17b)$$

2.4.1.4.3. $f'(\lambda)$ lookup table calculation

$f'(\lambda)$ is obtained through radiative transfer calculations using $a(\lambda)$ and $b(\lambda)$ as derived using the parameterisation presented above, and the normalised volume scattering function, which is defined as:

$$\tilde{\beta}(\theta, \lambda) = \frac{\beta(\theta, \lambda)}{b(\lambda)} \quad (18)$$

where

$$\beta(\theta, \lambda) = \frac{d\Phi(\theta, \lambda)}{\Phi_o(\lambda)} \frac{1}{d\omega dr} \quad (19)$$

$\Phi_o(\lambda)$ is the radiant flux onto a volume element of thickness dr , and $d\Phi(\theta, \lambda)/d\omega$ is the radiant intensity scattered from this volume in the direction θ with respect to the direction of the incident flux. Note that the wavelength dependency of $\tilde{\beta}(\theta)$ is neglected. $\tilde{\beta}(\theta)$ can be broken into molecular and particulate components through:

$$\tilde{\beta}(\theta) = \frac{b_w(\lambda)\tilde{\beta}_w(\theta) + b_p(\lambda)\tilde{\beta}_p(\theta)}{b_w(\lambda) + b_p(\lambda)} \quad (20)$$

The normalised volume scattering function of pure sea water we used is that published by Morel (1966), which can be expressed as:

ACR - LPCM - SAI - U. Oldenburg
NIOZ - U. Trondheim - FUB - PML - GKSS

$$\tilde{\beta}_w(\theta) = \frac{3}{4\pi(3+p)}(1+p\cos^2\theta) \quad (21)$$

where the parameter p (polarisation factor at 90°) equals 0.84.

For particles, $\tilde{\beta}_p(\theta)$, the normalised volume scattering function given for marine particles by Mobley (1994) (Table 3.10, last column) was applied. Mobley's $\tilde{\beta}_p(\theta)$ values are listed in Table 14 below.

θ	$\tilde{\beta}_{p1}(\theta)$	θ	$\tilde{\beta}_{p1}(\theta)$
1.00E-01	1.77E+03	5.00E+01	2.28E-02
1.26E-01	1.30E+03	5.50E+01	1.70E-02
1.58E-01	9.50E+02	6.00E+01	1.31E-02
2.00E-01	6.99E+02	6.50E+01	1.05E-02
2.51E-01	5.14E+02	7.00E+01	8.49E-03
3.16E-01	3.76E+02	7.50E+01	6.98E-03
3.98E-01	2.76E+02	8.00E+01	5.84E-03
5.01E-01	2.01E+02	8.50E+01	4.95E-03
6.31E-01	1.44E+02	9.00E+01	4.29E-03
7.94E-01	1.02E+02	9.50E+01	3.78E-03
1.00E+00	7.16E+01	1.00E+02	3.40E-03
1.26E+00	4.96E+01	1.05E+02	3.12E-03
1.58E+00	3.40E+01	1.10E+02	2.91E-03
2.00E+00	2.28E+01	1.15E+02	2.80E-03
2.51E+00	1.52E+01	1.20E+02	2.69E-03
3.16E+00	1.00E+01	1.25E+02	2.57E-03
3.98E+00	6.58E+00	1.30E+02	2.48E-03
5.01E+00	4.30E+00	1.35E+02	2.38E-03
6.31E+00	2.81E+00	1.40E+02	2.33E-03
7.94E+00	1.82E+00	1.45E+02	2.31E-03
1.00E+01	1.15E+00	1.50E+02	2.36E-03
1.50E+01	4.89E-01	1.55E+02	2.51E-03
2.00E+01	2.44E-01	1.60E+02	2.66E-03
2.50E+01	1.47E-01	1.65E+02	2.83E-03
3.00E+01	8.61E-02	1.70E+02	3.03E-03
3.50E+01	5.93E-02	1.75E+02	3.09E-03
4.00E+01	4.21E-02	1.80E+02	3.15E-03
4.50E+01	3.07E-02		

Table 14. Normalised volume scattering function for marine particles as derived by Mobley (1994) from Petzold's measurements.

The refractive index of sea water relative to air was taken from Table 15. Values are interpolated from Mobley (1994) at the MERIS wavelengths, for a pressure 1013 hPa, salinity 35‰, temperature 15°C.

ACRJ - LPCM - SAI - U. Oldenburg
 NIÖZ - U. Trondheim - FUB - PML - GKSS

λ (nm)	n
412.5	1.349
442.5	1.347
490.0	1.344
510.0	1.343
560.0	1.341
620.0	1.339
665.0	1.338
705.0	1.337
775.0	1.336
865.0	1.334

Table 15. Refractive index of sea water.

$f'(\lambda, \theta_s)$ is defined as:

$$f'(\lambda) = \frac{E_u(\lambda)}{E_d(\lambda)} \frac{b_b(\lambda) + a(\lambda)}{b_b(\lambda)} \quad (22)$$

We developed of a $f'(\lambda)$ lookup table with the following entries:

- The molecular to total scattering ratio as derived from the above parameterisation: $b_w / (b_w + b_p)$
- The single scattering albedo as derived from the above parameterisation: $b/(b+c)$
- Sun zenith angle; θ_s
- Atmospheric optical thickness; $\tau(550)$

2.4.1.5. Warning concerning the use of the model: State-of-the-Art and uncertainties

First, this model does **not** take into account other phenomena, in particular:

1. fluorescence of phytoplankton
2. fluorescence of CDOM
3. Raman scattering by water;

Second, this model takes into account all other following phenomena. There are, however, some uncertainties in their parameterisation or even some assumptions. These properties with their corresponding uncertainties are listed below in the same order as they appear above. The column "Expectation" indicates which scientific evolutions are foreseen.

*ACRJ - LPCM - SAI - U. Oldenburg
NIOZ - U. Trondheim - FUB - PML - GKSS*

IOP	Equation number or table	Comment	Expectation
$a_w(\lambda)$	Table 12	Known with sufficient accuracy	Will not evolve
$a_{p1}(\lambda)$	Eq. 6, Table 13	Well documented for World Ocean (but see the large variation factor). Seasonal variability under investigation †	Will not evolve significantly
$a_{y1}(\lambda)$	Eq. 7	Spectral dependency rather well documented	Will not evolve significantly
	Eq. 8	Problematic concerning $k(a_{y1})$ magnitude variability	May evolve
$b_w(\lambda)$	Eq. 9	Known with sufficient accuracy	Will not evolve
$\tilde{\beta}_w(\theta, \lambda)$	Eq. 21	Slight uncertainty on p ; very weak influence on the result	Will not evolve
$b_{p1}(\lambda)$	Eq. 10	Well documented for World Ocean (but see the large variation factor)	Will not evolve significantly
$\tilde{\beta}_p(\theta)$	Table 14	Arbitrary (questionable) choice of an unique VSF **	Will not evolve
$a_{y2}(\lambda)$	Eq. 12	Reasonably well documented for European coastal waters. Seasonal variability under investigation †	Will not evolve significantly
$a_{p2}(\lambda)$	Eq. 13	Spectral dependency reasonably well documented for European coastal waters	Will not evolve significantly
	Eq. 14	Magnitude reasonably well documented for European coastal waters but very large variation factor* †	
$b_{p2}(\lambda)$	Eq. 15a Eq. 15b	Poorly documented Poorly documented, $A_{bp2(550)}$ (theoretically expected to vary). Seasonal variability under investigation	Will evolve from the exploitation of COAST/OOC data

* May evolve based on a trial and error approach; no field data expected on short term for documenting $k(a_{y1})$ natural variability in Case 1 waters. At middle term, the relationship between the local CDOM content and the phytoplankton crop will be likely more documented.

** The unique volume scattering function used here is not optimal for representing Case 1 waters particles, in particular this function leads to a backscattering to total scattering ratio of 1.9%, which is not realistic. It is used because of the lack of data and by continuity with some other RT computations and exercises. The same holds true for Case 2 waters particles. Moreover, the variability in $\tilde{\beta}_{p2}(\theta)$ is expected to be larger than that of $\tilde{\beta}_{p1}(\theta)$ given the high diversity of particles (different proportions of organic and inorganic matter, different geological origins, different size spectra). The uncertainties about $\tilde{\beta}_{p1}(\theta)$ and $\tilde{\beta}_{p2}(\theta)$ are considered to be the largest source of error in the present model. It is likely that the adoption of several VSF would be necessary for organic debris, minerogenic sediments, ... to account for this variability.

As a general warning, the present model is based on statistical relationships that represent “average” situations. Therefore, its use as a predictive tool leads to various results when the large standard errors associated with each input parameters are taken into account; it may largely fail when, case by case, compared to actual data (as reflectance for instance).

2.4.1.6. References

- BRICAUD, A., A. MOREL and L. PRIEUR. 1981. Absorption by dissolved organic matter of the sea (yellow substance) in the UV and visible domains. *Limnol. Oceanogr.* **26**: 43-53.
- BRICAUD, A., A. MOREL, M. BABIN, K. ALLALI and H. CLAUSTRE, 1998, Variations of light absorption by suspended particles with Chlorophyll-a concentration in oceanic (case 1) waters: Analysis and implications for bio-optical models, *J. Geo. Res* **103**: 31033-31044
- GORDON, H. R. and W. R. McLUNEY. 1975. Estimation of the depth of sunlight penetration in the sea for remote sensing. *Appl. Opt.*, **14**:413-416.
- HALE, G.M. and M.R. QUERRY 1973: Optical constants of water in the 200nm to 200 μm wavelength region, *Appl. Opt.*, **12**: 555-563
- LOISEL, H. and A. MOREL,. 1998. Light scattering and chlorophyll concentration in Case 1 waters: A re-examination. *Limnol Oceanogr.* **43**(5): 847-858.
- MALONE, T.C. 1982. Phytoplankton photosynthesis and carbon-specific growth: Light saturated rates in a nutrient rich environment. *Limnol. Oceanogr.* **27**: 226-235.
- MOBLEY, C.D 1994 Light and water: Radiative transfer in natural waters, Academic Press
- MOREL, A. 1966. Etude expérimentale de la diffusion de la lumière par l'eau, les solutions de chlorure de sodium et l'eau de mer optiquement pure. *J. Chim. Phys.*, **10**: 1359-1366.
- MOREL, A. 1974. Optical properties of pure water and sea water. In : Optical aspects of Oceanography, N. G. Jerlov and E. Steemann-Nielsen, N. G. Jerlov and E. Steemann-Nielsen, Academic, pp. 1-24.
- PETZOLD, T. L. 1972. Volume scattering functions for selected ocean waters. San Diego: Scripps Inst. Oceanogr., Ref. 72-78, 79 pp.
- POPE R. M. and E. S. FRY. 1997. Absorption spectrum (380-700 nm) of pure water. II. integrating cavity measurements. *Appl. Opt.* **36**: 8710-8723.

2.4.2. Validation

The above reflectance model was applied to all COAST/OOC stations to calculate $R(\lambda)$ by using the measured Chl, SPM and CDOM as inputs. θ_s was assumed constant at 45° . For all campaigns except ALMOFRONT-2, the $a_y(\lambda)$ parameterisation was switched off because it was

ACRJ - LPCM - SAI - U. Ol denburg - NIÖZ - U. Trondheim - FUB - PML - GKSS

included into the $a_{y2}(\lambda)$. Indeed, the endogenous and exogenous CDOM cannot be experimentally distinguished. In the specific case of ALMOFRONT-2 (Mediterranean Case 1 waters) during which CDOM and SPM were not determined (exogenous matter was assumed to absent) the $a_{y1}(\lambda)$ parameterisation was applied.

Figure 70 to Figure 77 show the comparison between calculated and measured reflectances. The following conclusions can be drawn about this validation of the above Case-2 reflectance model:

- Overall, the range of calculated reflectances falls within that of the measured one.
- Deviation from the 1:1 line is observed for low reflectances. In the blue spectral range, this deviation is shown by Baltic Sea samples while, in the red spectral domain, it is shown by Case 1 water samples. This deviation may be due to instrumental self shading which was not accounted for in the processing the reflectance data. This is to be done.
- On one hand, the dispersion around the 1:1 line is about the same over the whole spectrum. On the other hand, the variation range is much large in the red than in the blue spectral domain. This suggests that, discrimination of optically significant constituents will be harder to achieve in the blue spectral domain.
- The performances of the present reflectance model are globally good. Nevertheless, the use of it for deriving operational algorithms is questionable. There is a need to reach validation results with much less dispersion.

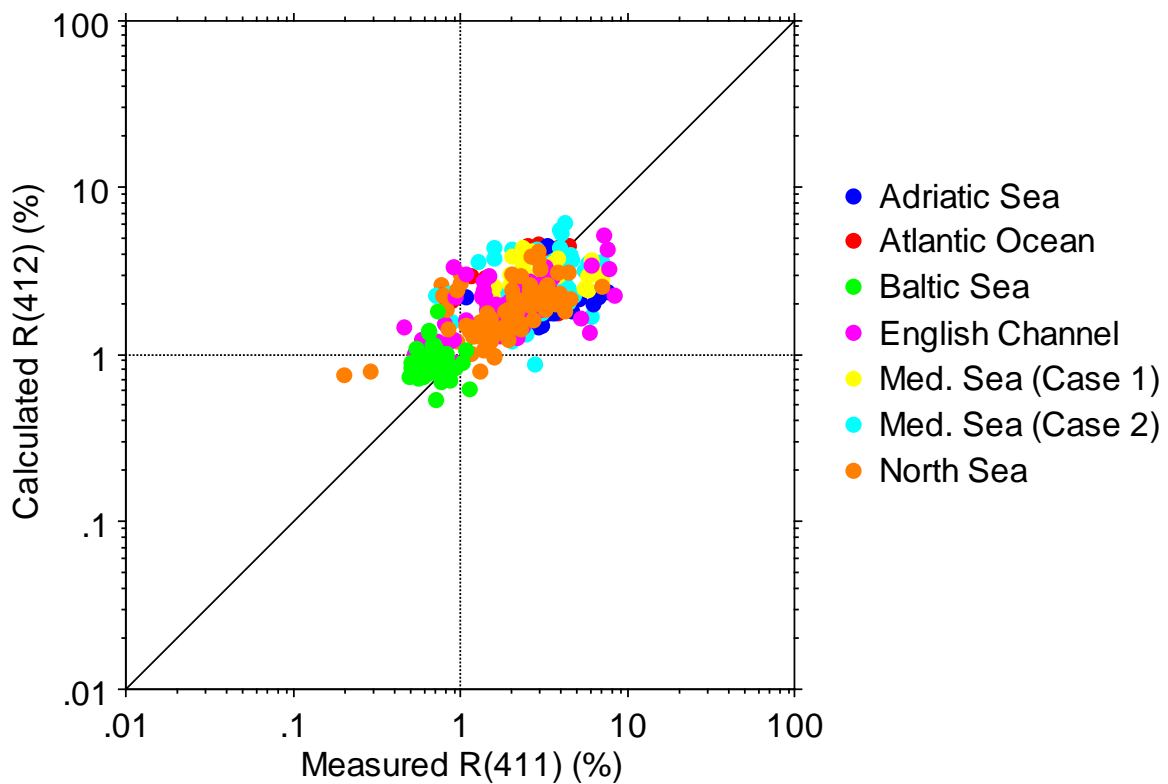


Figure 70. Relationship between calculated and measured reflectance at 412 nm.

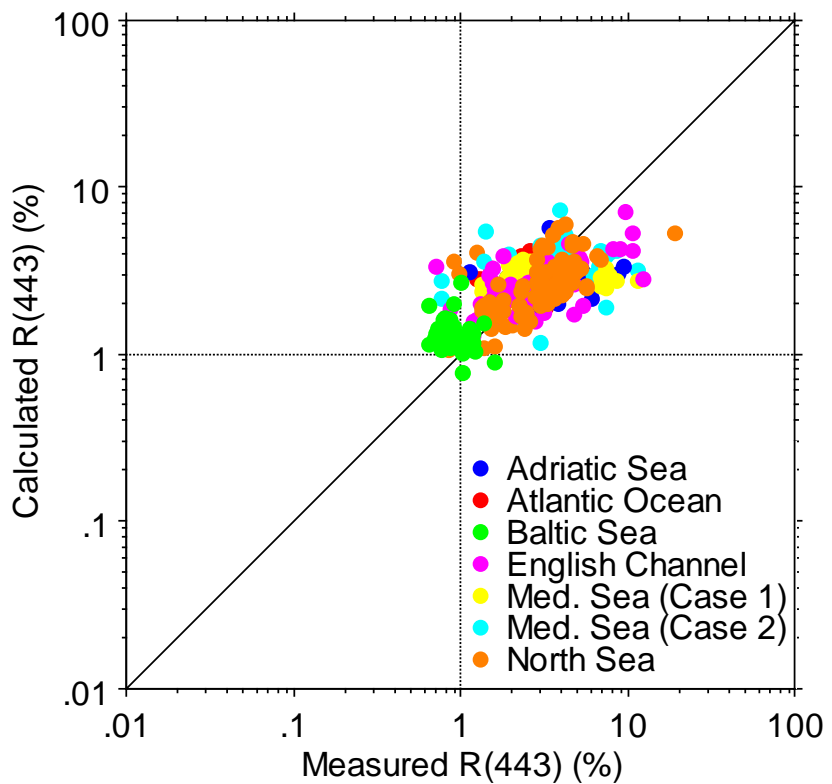


Figure 71. Relationship between calculated and measured reflectance at 443 nm.

*ACRJ - LPCM - SAI - U. Oldenburg
NIOZ - U. Trondheim - FUB - PML - GKSS*

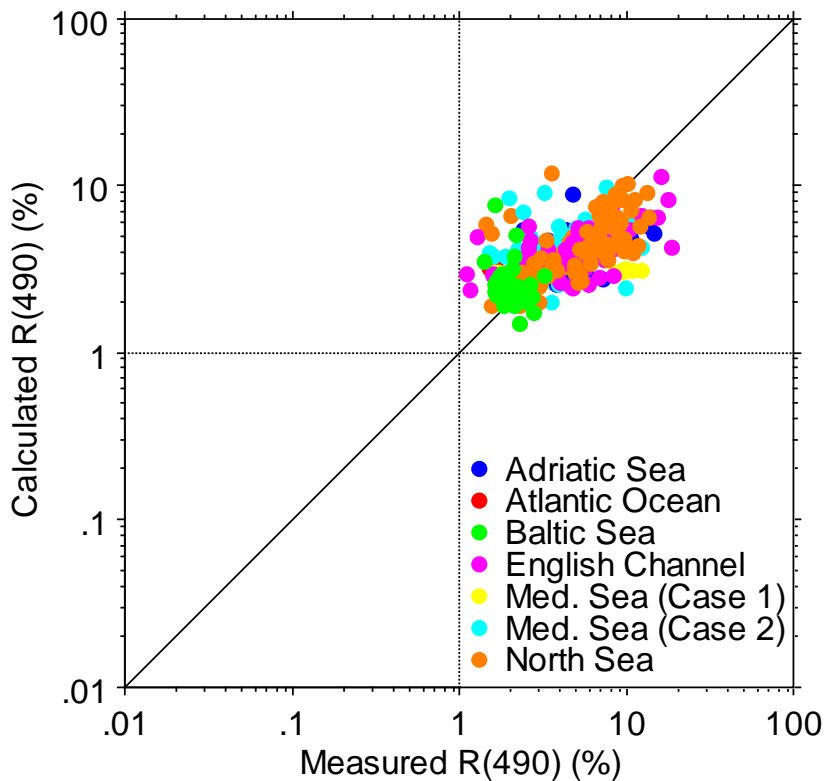


Figure 72. Relationship between calculated and measured reflectance at 490 nm.

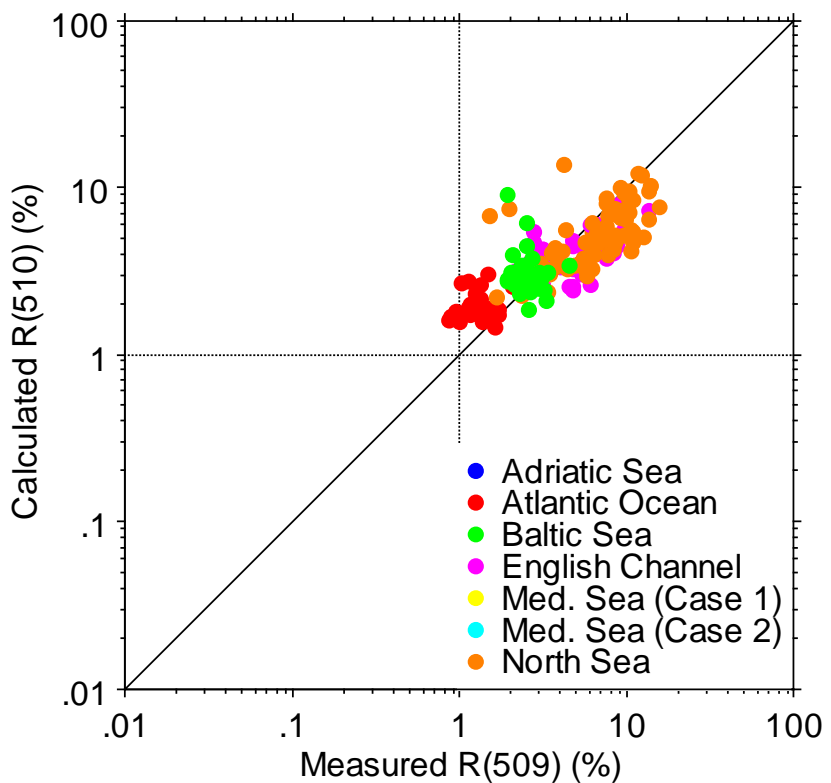


Figure 73. Relationship between calculated and measured reflectance at 510 nm.

*ACRJ - LPCM - SAI - U. Oldenburg
NIOZ - U. Trondheim - FUB - PML - GKSS*

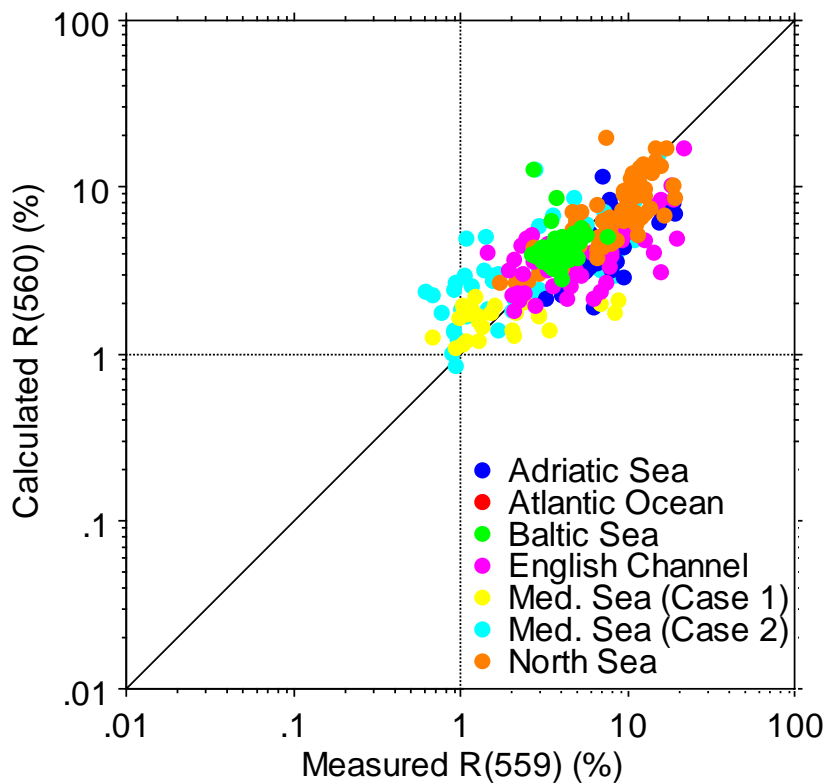


Figure 74. Relationship between calculated and measured reflectance at 560 nm.

*ACRJ - LPCM - SAI - U. Oldenburg
NIOZ - U. Trondheim - FUB - PML - GKSS*

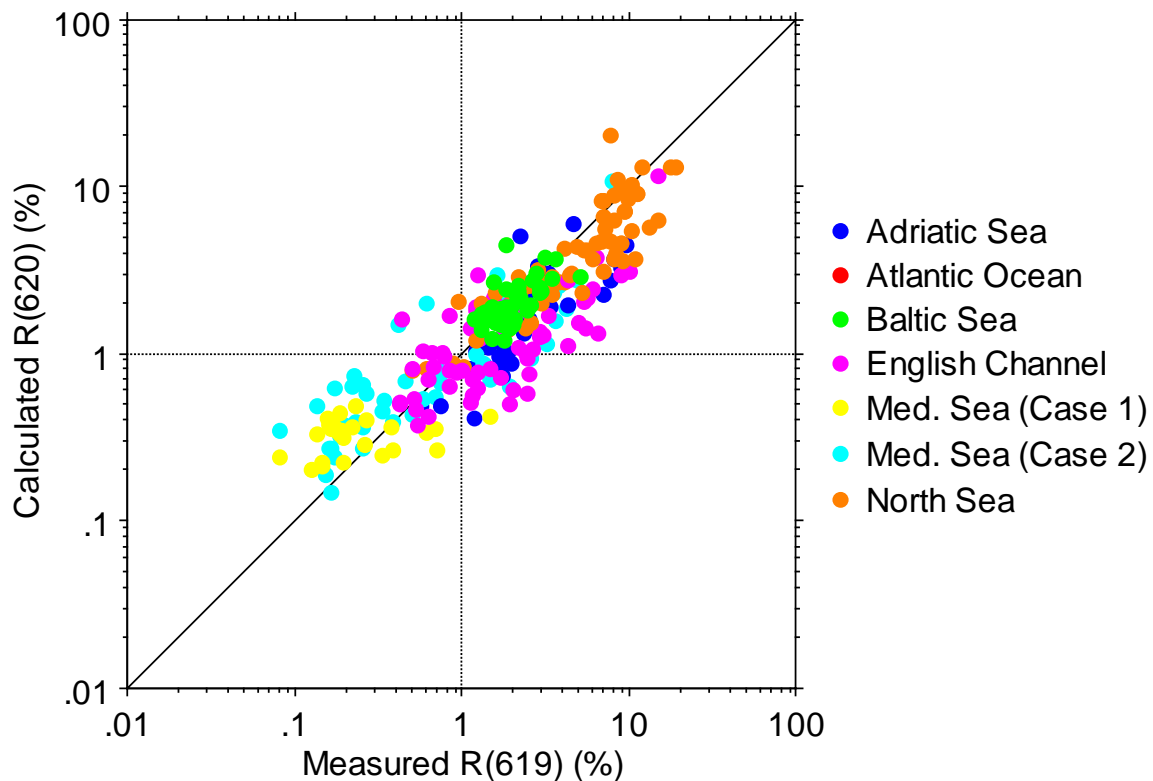


Figure 75. Relationship between calculated and measured reflectance at 620 nm.

*ACRJ - LPCM - SAI - U. Oldenburg
NIOZ - U. Trondheim - FUB - PML - GKSS*

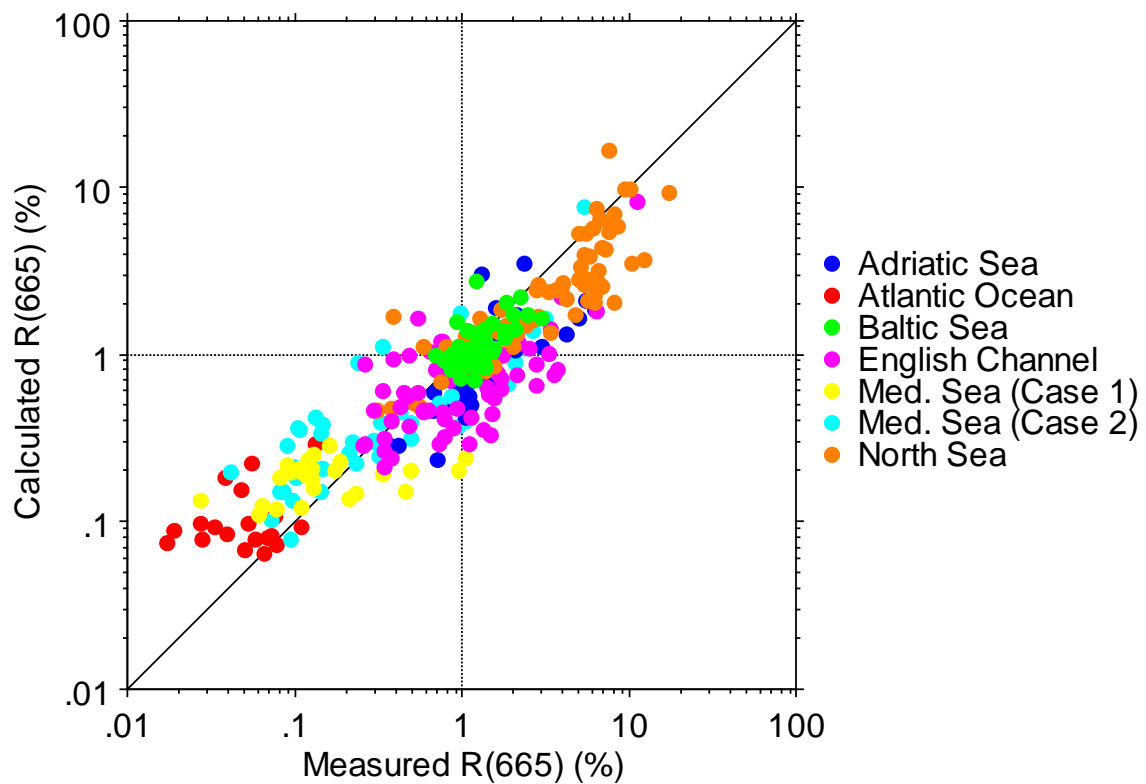


Figure 76. Relationship between calculated and measured reflectance at 665 nm.

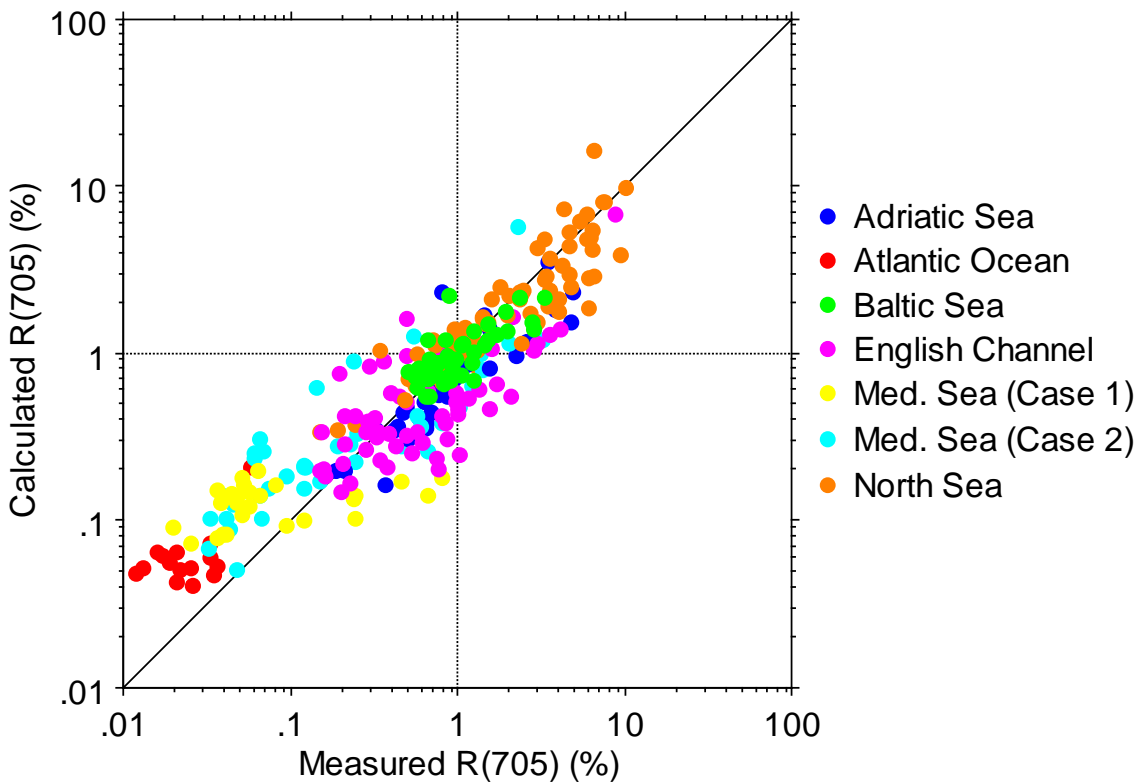


Figure 77. Relationship between calculated and measured reflectance at 705 nm.

2.5. ALGORITHM DEVELOPMENT

2.5.1. Algorithms

2.5.1.1. NIOZ band-ratio algorithm

2.5.1.1.1. Introduction

NIOZ - ACRJ - LPCM - SAI - U. Oldenburg -
U. Trondheim - FUB - PML - GKSS

The aim of this sub-study is to compare water quality parameters gained by using present coastal colour algorithms, compare the results with in-situ values and refine, if necessary, these algorithms.

At two helicopter campaigns the above water radiance and the incident spectral irradiance were measured together with in-situ water sampling.

During former fieldwork (Particulate Matter North Sea [PMNS] project) semi-empirical algorithms were established for North Sea and English Channel waters. The outcome of these algorithms is validated against the in-situ chlorophyll and total suspended matter values. The algorithms are based upon SeaWiFS and MERIS bands.

For semi-empirical algorithm development the spectral characteristics of the coastal waters, generally well known, are used to improve the algorithms by statistical analysis. The remote sensing reflectance $R_L(0^+, \lambda)$ is the most appropriate optical parameter to measure for use in remote sensing algorithms. In this case the upwelling and downwelling (ir)radiance from which the reflectance is derived were measured quasi-simultaneously, so the reflectance would be independent of the variations in the ambient light field.

2.5.1.1.2. Instrument description

2.5.1.1.2.1. PR650 Spectrascan Spectracolorimeter

The PR650 Spectrascan radiometer (Manufactured by Photo Research, California, USA) is a portable, fast scanning multi-spectral radiometer that acquires the spectrum of optical radiation from 380 - 780nm simultaneously. Each measurement cycle consists of two parts; first, the measurement of the optical radiation (light measurement), and second, a measurement of equal length while no radiation is permitted to strike the detector (dark measurement). The dark measurement is subtracted from the light measurement to give relative spectral data. The relative data are assigned to a wavelength band and corrected for wavelength accuracy and spectral intensity. The objective lens has a field-of-view of 7° for accurate focusing of the target but optical radiation being measured only passes through an aperture with a 1° field-of-view. After the radiation to be measured passes through the aperture, it reaches the measuring shutter, which closes automatically during the 'dark' measurement. From there the radiation passes to a concave holographic diffraction grating polychromator, which diffracts the radiation into its constituent colours from 380 - 780nm. The diffracted spectrum is then focused onto a photodiode array such that each end of the spectrum is permanently aligned with the detector array detector elements. The instrument has a spectral accuracy of 2nm with a FWHM of 8nm. The PR650 can be fitted with a cosine receptor, which is mounted on the front instead of the objective lens and measures the integrated irradiance from all sources in the forward hemisphere. The collector is cosine corrected so that the correct cosine reading will be obtained regardless of where in the forward hemisphere the light sources are located [not used in case of helicopter measurements].

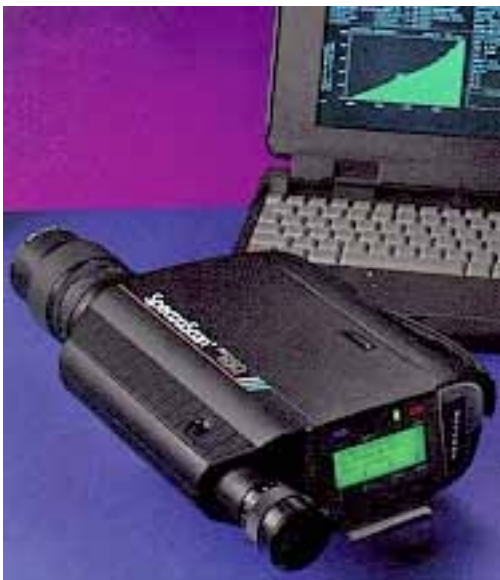


Figure 78. The PR650 multi-spectral radiometer.

2.5.1.1.2.2. Satlantic Radiometer

For the description of the Satlantic radiometer see Section 2.2.2.

2.5.1.1.3. Data collection and processing

During the helicopter field experiment at campaign C3 (Venice) on 30 July 1997 13 stations were sampled and at C6 between 1 Sept. to 23 Sept 1998, 131 stations were sampled. The PR650 radiometer was used to collect the above water radiance $L_w(\lambda)$ between 380 and 780 nm in 101 bands. The instrument was pointed towards the sea surface, between 30 and 40 degrees of nadir away from the sun at an altitude of 35 to 50 meters depending on the wave conditions. Two measurements were taken and later averaged. Quasi-simultaneously a Satlantic radiometer, mounted on a CTD frame, was used during lowering, to collect the incident spectral irradiance $E_s(\lambda)$ with a sampling frequency of 6 Hz. In Table 16 the spectral bands are given for both instruments.

From these two measurements the remote sensing reflectance can be calculated as follows:

$$R_L(0^+, \lambda) = L_w(\lambda) / E_s(\lambda) \quad (\text{Eq. 1})$$

An example of the measured radiance and irradiance collected during a helicopter flight including the calculated reflectance is given in Figure 79.

2.5.1.1.4. Incident spectral irradiance correction

Satlantic measurements between 5 and 200 seconds (total of 30 to 200) before hitting the water surface were used to calculate the median incident irradiance. Due to the unstable weather conditions at the C600 campaign changes in incident irradiance during the lowering of the Satlantic sensor

*ACRJ - LPCM - SAI - U. OI denburg
NIOZ - U. Trondheim - FUB - PML - GKSS*

variations within a single median irradiance spectrum occurred. Therefor corrections of the incident irradiance $E_S(\lambda)$ had to be made prior to the calculation of the remote sensing reflectance ($R_L(0^+, \lambda)$). This correction was done by comparing the form of the raw E_S Satlantic-spectra with a reference E_S PR650-spectra obtained elsewhere but under similar circumstances (overcast). Therefor these channels were multiplied by a channel specific factor. This factor was obtained using the form of the reference spectrum with the amplitude of the involved Satlantic median (averaged) spectrum and recalculate diverged data points.

Table 16. Wavebands (in nm) of the 2 radiometers used for above water measurements.

Wavebands	
PR650	Satlantic
Between 380 and 780 nm in 4 nm steps over 101 bands	411
	443
	456
	490
	509
	532
	559
	619
	665
	683
	705
	779

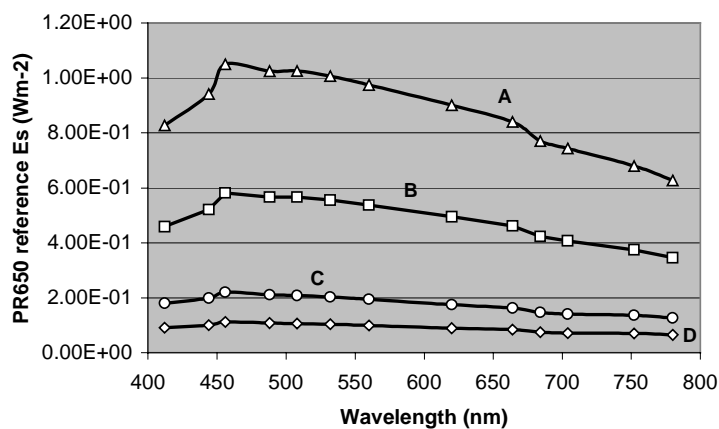


Figure 79. The incident spectral irradiance measured with the PR650, at Satlantic wavelengths, on a different location. The spectral form was used as a reference to correct for the unstable spectral shape of the Satlantic incident irradiance obtained during the C600 helicopter measurements. A: Sunny at 12 noon (Plymouth), B: Average clouds/sunny, C: clouds/raindrops, D: Heavy clouds.

During this exercise it occurred that the Satlantic channels 456, 490, 532 (only campaign C600), 665 and 779 nm differed slightly but constantly with the form of the reference PR650 spectra (between 2 to 7 percent). For these channels the multiplication factor is given in Table 17. An example of a raw and form corrected Satlantic irradiance spectrum including the reference spectrum B is shown in Figure 80.

Table 17. Multiplication factor used to correct the raw Satlantic incident spectral irradiance. The factors were obtained by comparing the form of the raw spectrum with a reference spectrum obtained elsewhere but under the same weather conditions.

Satlantic channel (nm)	Multiplication factor
456	1.03
490	1.05
532	1.07
665	0.98
779	0.93

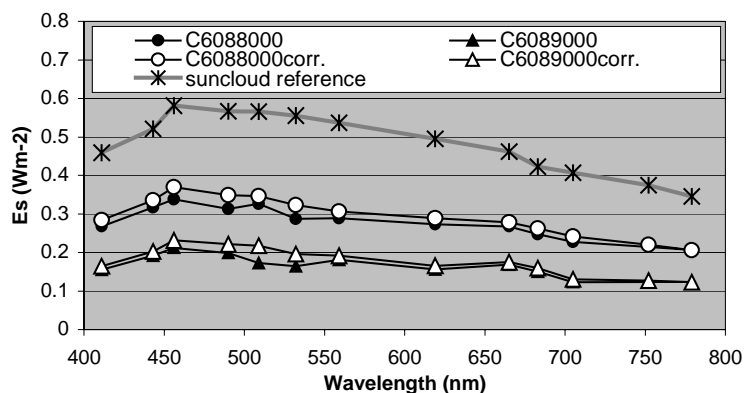


Figure 80. An example of two raw (white) and corrected (black) Satlantic incident irradiance spectra at stations C6088000 and C6089000. The reference spectrum B is shown as a bold grey line.

2.5.1.1.5. Sun/sky glint correction

Unfortunately the sky radiance was not measured during the helicopter exercise. But the type of the general PMNS algorithm indicates a form of sun/sky glint correction by subtracting the R_L at 752 nm from the used spectral band reflectances. As the Satlantic radiometer does not include this 752 nm

*ACRJ - LPCM - SAI - U. Oldenburg
NIOZ - U. Trondheim - FUB - PML - GKSS*

band for the sun/sky glint correction a reconstruction of the downwelling irradiance was established according to two different approaches.

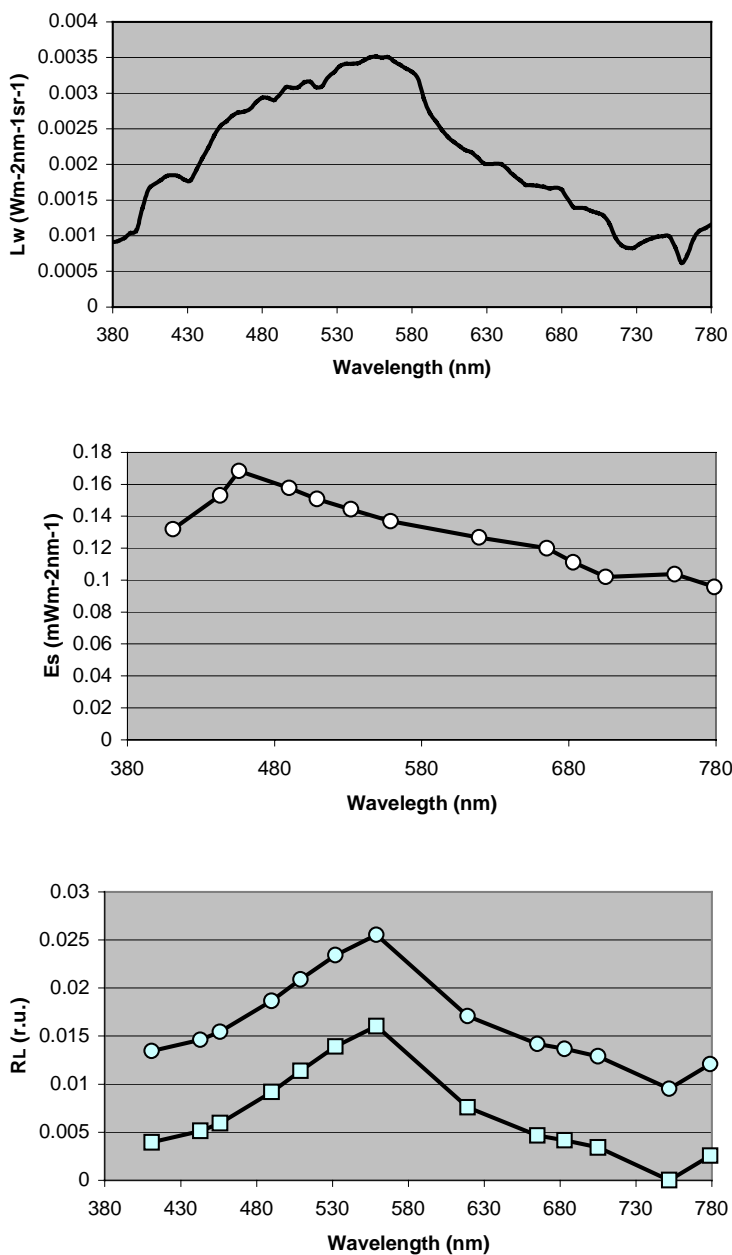


Figure 81. An example of the PR650 measured radiance (top) and, including the reconstructed 752 channel, the Satlantic corrected irradiance (middle) and the calculated remote sensing reflectances (bottom) of station C6064000. The latter uncorrected and corrected (approach 1) for sun/sky glint by subtracting the 752nm reflectance.

Approach 1: By using a historic PR650 data set containing 190 measurements (clear sky, cloudy) of incident spectral irradiance measurements. A determination coefficient r^2 of 0.998 was gained by linear regression of the 2 closest Satlantic bands, in this case 705 and 779 nm, with the 752 nm band according to

$$Es_{(752)} = 0.008 + 0.354 * Es_{(705)} + 0.615 * Es_{(779)} \quad (\text{Eq. 2})$$

This relation was used to reconstruct indirectly through the missing $Es_{(752)}$ of the Satlantic data set prior to the calculation of the remote sensing reflectance. Figure 81 shows an example of the $L_w(\lambda)$, $ES(\lambda)$ and $R_L(0^+, \lambda)$.

Approach 2: By using a historic PR650 data set containing 190 measurements (clear sky, cloudy) of calculated remote sensing reflectance $R_L(\lambda)$ containing the $R_L(752)$ nm. A linear relation was found for this channel with the $R_L(779)$ nm channel with a correlation coefficient r of 0.91 according to

$$R_{L(752)} = -0.000283 + 0.722 * R_{L(779)} \quad (\text{Eq. 3})$$

This relation was also used to reconstruct directly the missing $R_{L(752)}$ of the Satlantic data set prior to the application of the investigated algorithms. The method to reconstruct the missing $R_{L(752)}$ will be mentioned each time a result is presented and indicated simply as approach 1 or 2.

In case of very turbid waters this correction, subtracting $R_{L(752)}$ nm is not preferable but can be used until better methods are established. According to Equation 1 the remote sensing reflectance was calculated for all stations, sun/sky glint correction included.

2.5.1.1.6. Coastal Colour algorithms

The investigated coastal colour algorithms are all of the band ratio type according to:

$$C1 * (R_{Lc}(\lambda 1) / R_{Lc}(\lambda 2))^{C2} \quad (\text{Eq. 4})$$

Where C1 and C2 are constants and $R_{Lc}(\lambda 1)$ and $R_{Lc}(\lambda 2)$ are the sun/sky corrected reflectances. Stations with bad reflectance data or missing water quality parameters were thrown out prior to the calculations.

2.5.1.1.7. Suspended Particulate Matter

Depending on the water quality parameter (SPM, Chl) and the involved satellite sensor (SeaWiFS, MERIS) the applied algorithms are given in Table 18. Note that some of the wavelengths given in this table slightly differ from the Satlantic wavelengths. However at the maximum a shift of 5 nm in case of the 665 nm channel was used in case of the SPM SeaWiFS algorithm.

Table 18. The investigated coastal colour algorithm developed after the PMNS project. The reflectance at 752 nm has been subtracted from the involved band reflectance.

ACRJ - LPCM - SAI - U. Oldenburg
NIOZ - U. Trondheim - FUB - PML - GKSS

Sensor	Algo-Type	WQP	PMNS Coastal Colour Algorithm
SeaWiFS	Band ratio	SPM	$12.4 * (R_{Lc}(412)/R_{Lc}(670))^{-1}$
MERIS	Band ratio	SPM	$53.1 * (R_{Lc}(560)/R_{Lc}(620))^{-2.58}$
SeaWiFS	Band ratio	Chl	$3.4 * (R_{Lc}(510)/R_{Lc}(555))^{-3.65}$
MERIS	Band ratio	Chl	$22.3 * (R_{Lc}(665)/R_{Lc}(705))^{-2.85}$

With **approach 1** and using the algorithms according to Table 18 a good result, with a determination coefficient r^2 of 0.74, was obtained through the relation for SPM using the MERIS bands 560 and 620 nm as can be seen in Figure 82. A determination coefficient r^2 of 0.22 could only be seen in case the SPM SeaWiFS algorithm was applied.

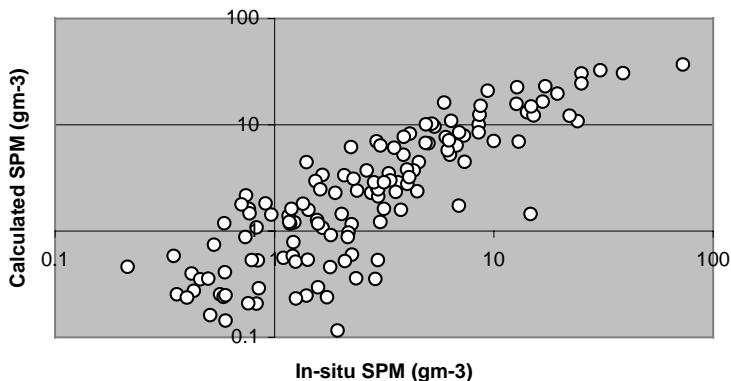


Figure 82. The log-log comparison of the calculated and the measured SPM concentration after applying the PMNS MERIS coastal colour algorithm. The R_L used is obtained by approach 1.

When ignoring the PMNS constants but keeping the same algorithm form, the model was optimised by means of the COAST/ OOC data set. The refined MERIS SPM model with a determination coefficient r^2 of 0.78 now reads as:

$$SPM = 77.1 * (R_{Lc}(560)/R_{Lc}(620))^{-3.51} \quad (\text{Eq. 5})$$

The small improvement of the r^2 can not be seen as a major breakthrough in refining a semi-empirical coastal colour algorithm and therefore it would be recommended to merge both the PMNS

*ACRJ - LPCM - SAI - U. Oldenburg
NIOZ - U. Trondheim - FUB - PML - GKSS*

and COAST/OOC data sets and redefine this particular algorithm. The results implicate similar optical characteristics for suspended matter present in different European coastal waters. According to PMNS recommendations and confirmed by the shown result remote sensing techniques and the application of a semi-empirical algorithm can be a good alternative for the monitoring of SPM.

With **approach 2** and using the algorithms according to Table 18 a good result, with a determination coefficient r^2 of 0.74, was obtained through the relation for SPM using the SeaWiFS bands 412 and 670 nm. This result is much better than in case approach 1 was used with only a r^2 of 0.22. Also a reasonable result, (as with approach 1), with a determination coefficient r^2 of 0.71, was obtained through the relation for SPM using the MERIS bands 560 and 620 nm. Figure 61 shows the relation of the in-situ SPM and the calculated SPM for both the SeaWiFS and MERIS algorithms.

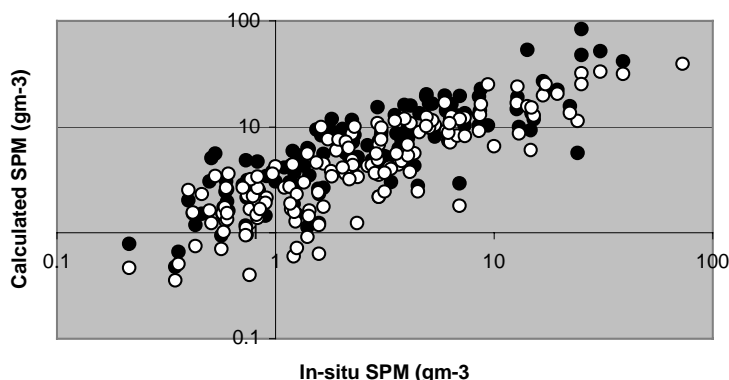


Figure 83. The log-log comparison of the calculated and the measured SPM concentration after applying the both PMNS MERIS and SeaWiFS coastal colour algorithm. The R_L used is obtained by approach 2. White dots represent the outcome with the MERIS, black dots with the SeaWiFS algorithm.

With both the approaches a reasonable result was gained to derive the SPM concentration from the MERIS channels 560 and 620 nm. However using approach 1 with the SPM SeaWiFS algorithm and comparing the result with the outcome using approach 2 complete different results were obtained. This needs further investigation. A possible reason could be the use of SeaWiFS band 1 in the blue. Small difference in R_L after subtraction of $R_{L(752)}$ can result in large differences using the specific algorithm ratio.

2.5.1.1.8. Chlorophyll

Using the PMNS Chlorophyll (+Pheo) algorithm nothing more than a trend (determination coefficients $r^2 < 0.16$) could be found for both the SeaWiFS and MERIS type and both the approaches 1 and 2. The result after the application of the SeaWiFS algorithm with approach 1 is presented in Figure 84.

*ACRJ - LPCM - SAI - U. Oldenburg
 NIOD - U. Trondheim - FUB - PML - GKSS*

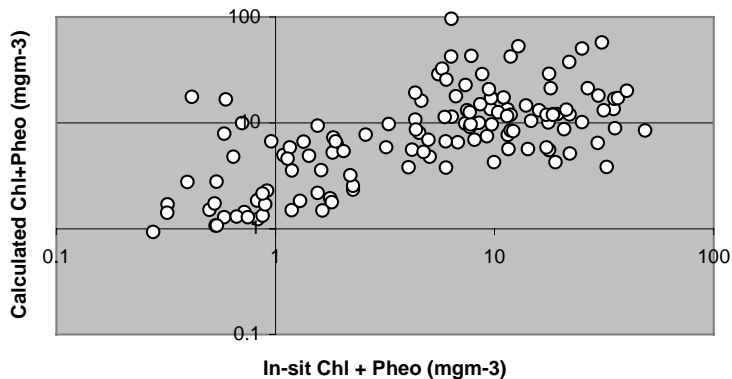


Figure 84. The log-log comparison of the calculated and the measured Chlorophyll (+ Pheo) concentration after applying the PMNS SeaWiFS coastal colour algorithm and according to approach 1. Nothing more than a trend can be seen.

At this stage (after 20 years) it is still not clear why the in-situ chlorophyll and the R_{Lc} ratio relation results in this bad correlation. In this case either applying the PMNS Chl-algorithm or developing a new COAST/OOC algorithm using the same type (Equation 4) seems not to make any difference.

Comparing for example the Venice station C300500 with a Baltic Sea station C612800 with a chlorophyll concentration of respectively 4.5 mg m^{-3} . Realising the small concentration difference and comparing the heights of the fluorescence peaks at 683 nm of both spectra (Figure 85) it seems that the Baltic spectrum was taken from an area unquestionably more rich of chlorophyll. At least the in-situ values are too near to each other to result in such different remote sensing reflectance spectra. The reason could be either or both the time difference between the water sampling and the PR650 measurement or a possible patchy chlorophyll pattern at the sampling site.

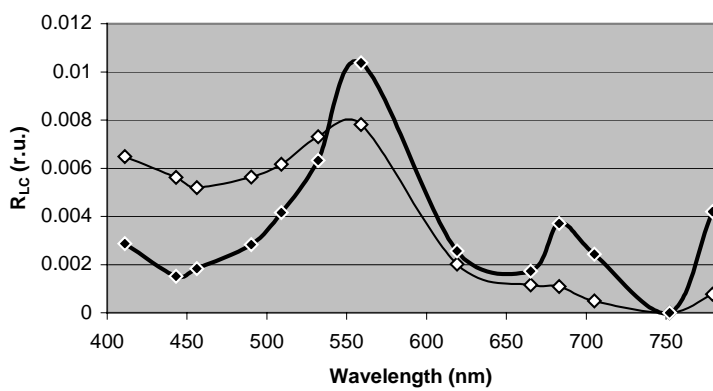


Figure 85. The sun/sky glint corrected remote sensing reflectance at the Venice station C300500 (thin line) with a chlorophyll concentration of 4.5 mg m^{-3} and the turbid station C612800 (bold line) with

$\begin{matrix} ACRJ - LPCM - SAI - U. OI \text{ denburg} \\ NIOZ - U. Trondheim - FUB - PML - GKSS \end{matrix}$

an in-situ value of 6.4 mgm^{-3} . The absorption of Yellow Substance at the turbid station as well as the chlorophyll fluorescence peak at 683nm can be seen clearly.

After the mentioned result the fluorescence baseline method was tried to fit the R_{Lc} at the fluorescence wavelength with the in-situ chlorophyll concentration according to:

$$\text{Chl} = C1 + C2 * (R_{Lc}(683)) - ((R_{Lc}(665) + R_{Lc}(705))/2)$$

Where $C1$ and $C2$ are the regression coefficients, $R_{Lc}(683)$ is the sun/sky glint corrected remote sensing reflectance at the fluorescence peak and $R_{Lc}(665)$ and $R_{Lc}(705)$ are the wavelength to define the baseline. With a determination coefficient $r^2 < 0.05$ the result was disappointing.

2.5.1.1.9. Conclusions and recommendations

From a helicopter platform, during part of this project, upwelling radiance measurements (PR650) above the water surface were quasi simultaneously measured with the incident spectral irradiance (Satlantic). Due to variable atmospheric conditions during the C600 campaign and the necessary averaging of the, during lowering but above water, collected incident irradiance could cause spectral variations within a single irradiance spectrum. Also the inevitable time difference between the PR650 and the Satlantic measurements could result in errors in the calculated remote sensing reflectance. It is recommended therefor that ocean colour measurements are coupled to a incident spectral irradiance sensor to assure simultaneous measurements.

The reconstruction of the missing Satlantic 752 nm irradiance channel (approach 1) can be done by reconstructing this irradiance channel prior to the calculation of the remote sensing reflectance. This is recommended because under stable atmospheric condition the incident spectral irradiance does not vary much in form. The approach 2, first calculation of the remote sensing reflectance, the reconstruction of $R_L(752)$ from $R_L(779)$ was tried because from former irradiance measurements a good correlation was found between these wavelengths.

In case of very turbid waters this correction, subtracting $R_L(752)$ nm is not preferable but can be used until better methods are established. Also this band is not available in SeaWiFS and MERIS but most hyper-spectral airborne scanners have.

A semi-empirical algorithm is recommended to derive the SPM concentration from coastal colour measurements until better analytical models are available. Either the PMNS or the COAST/OOC SPM algorithm generates reasonable results. It is still under discussion if traditional water sampling techniques, especially to derive the SPM concentration, results in a more representative SPM value for the investigated area than in the case a remote sensing technique is used to achieve this. With a remote sensing technique a more averaged water quality quantity of the subsurface water column can be obtained compared to a one litre (or a little bit more) sample. A great constraint is the validation of the water quality parameter. Especially in a short-term regime, concerning the water composition variations, as that of coastal waters.

For a water quality parameter like chlorophyll the semi-empirical algorithm approach does not give us more than trend.

*ACRJ - LPCM - SAI - U. Oldenburg
NIOZ - U. Trondheim - FUB - PML - GKSS*

However it can be concluded that the COAST/ OOC project established a unique bio-optical data set of European coastal waters. Also an innovative way of sampling coastal areas by helicopter could be a good cost effective alternative compared to traditional ship sampling. A day of helicopter sampling produces 20 bio-optical station, a day of ship measurements produces 5 bio-optical station considering identical areas. The data with statistical results will be available as an Excel workbook on CD-ROM.

A last recommendation is, if possible, wait for stable weather conditions to perform coastal colour measurements.

2.5.1.2. PML band-ratio algorithm

The principal role of PML was to develop both a reflectance model and appropriate band ratio algorithms for use in Case 2 waters. If possible, the band ratio algorithm was to be extended to the detection of red tides, when and if observations were made. The report of the work carried out during COAST/ OOC consists of two parts: the development of a forward reflectance model and the development and extension of band ratio algorithms for the retrieval of geophysical products.

2.5.1.2.1. Development of a Reflectance Model.

2.5.1.2.1.1. The Forward Model

A table driven model of reflectance was developed using multiple runs of Hydrolight (Mobley, 1995) to cover the range of turbidity expected in the COAST/ OOC fieldwork. Interpolation of these tables effectively solves the radiative transfer for any combination of scattering and absorption. The tables have been generated for both irradiance and directional radiance reflectance. The former is measured by the COAST/ OOC *in situ* sensor and the latter is measured by remote sensors such as SeaWiFS and MERIS. The use of this table driven approach has allowed us to validate models using the COAST/OOC observations and apply these directly to satellite observations. By appropriate inputs of the inherent optical properties (IOPs) of absorption and scattering, these tables can be used to simulate the reflectance observed and the potential performance of remotely sensed algorithms.

2.5.1.2.1.2. Application of The Forward Model to Band Ratio Algorithms.

Aiken *et. al.* (1995) demonstrated that the 490:555nm radiance reflectance ratio presented the optimal empirical band ratio pair for the retrieval of chlorophyll in Case I waters. O'Reilly *et. al.* (1998) extended this work to develop an optimal polynomial fit to the SeaBASS data set. Figure 86 shows the retrieval of this algorithm in both Case I and Case II gelbstoff and sediment dominated waters. The simulation was parameterised using the MERIS reference model (1999) that was partly based on the outcome of the COAST/ OOC fieldwork. Although the reference model does not at present represent a full quantitative ocean model, it shows the potential errors in algorithms. The retrievals shown show that both added sediment (Figure 86a) and added gelbstoff (Figure 86b) produce significant errors in the retrieval of chlorophyll: the worst errors resulting from the additional

*ACRI - LPCM - SAI - U. Oldenburg
NIOZ - U. Trondheim - FUB - PML - GKSS*

absorption by gelbstoff which, in a band ratio algorithm, cannot be distinguished from the absorption by phytoplankton.

2.5.1.2.1.3. Relationship of Band Ratios and IOPs

From theoretical considerations (Aiken *et. al.*, 1995) it has been shown that band ratio algorithms approximate to the retrieval of the absorption coefficient at a median point between the two bands of the ratio. Figure 87 shows, for the same cases above, the relationship of the OC2-V3 chlorophyll retrieval and the absorption coefficient and scattering coefficient. Figure 87a shows a good relationship between $a(510)$ and the OC2-V3 chlorophyll at low absorption (Case I waters). However, the relationship becomes considerably worse as the absorption increases. Figure 87b shows the relationship between OC2-V3 chlorophyll and scattering. This shows a set of slopes corresponding to different gelbstoff concentrations, there is, however, a linear relationship between scattering (i.e. backscatter from sediments) within a particular gelbstoff regime. This observation explains the success of band ratios in retrieving sediment for local areas, but shows that such ratio methods will not be successful over a range of water types.

2.5.1.2.2. Development of Novel Band Ratio Algorithms

2.5.1.2.2.1. Case I Parameterisation

The observation that band ratios are related to the IOPs of the water column in a consistent way in both Case I and Case II waters has led to the development on IOP retrieval models for the COAST/OOC project. These models have robust properties and applications, since their parameterisation is based on hydrological optics rather than empirical observations. As such that algorithms can be applied to both irradiance and radiance reflectance, and are able to accommodate new observations of IOPs when available and to incorporate local relationships between IOPs and physical parameters.

The ratio algorithms can retrieve absorption, since both the scattering and absorption are correlated in both Case I and Case II waters. In Case I waters the absorption between bands is correlated due to the relationships between pigments and their absorption slopes. Figure 88 shows the inter-relationships between the major groups of pigments, chlorophylls, carotenoids, both photosynthetic (PSC) and photoprotectant (PPC). Both the 490:555 band ratio (SeaWiFS) and the 442:555 band ratio (CZCS, MERIS) produce good Case I chlorophyll retrievals since carotenoids mainly PSCs absorb strongly at 490nm and weakly at 555nm, and the chlorophylls absorb at 443nm but are correlated with carotenoids. In fact the 490:555 ratio is a carotenoid rather than chlorophyll algorithm. These data show both the COAST/OOC data and data from the Atlantic Meridian Transect (AMT, Aiken *et al*, 2000) series of cruises, showing no difference in the relationship between the pigments in coastal waters and in Case I waters.

2.5.1.2.2.2. Case II Parameterisation and Retrieval

In Case II waters the total absorption is influenced by phytoplankton, gelbstoff and sediment, and the scattering is influenced by sediment and phytoplankton. Figure 89 shows the relationship between the absorption at each adjacent band pair for the absorption of phytoplankton, the sum of

*ACRJ - LPCM - SAI - U. Oldenburg
NIOZ - U. Trondheim - FUB - PML - GKSS*

gelbstoff and detritus, and the total absorption. There is a very significant relationship between the absorptions at all band pairs with R^2 being greater than 95%, except for the phytoplankton 412:442 relationship, where R^2 is 88%. The best relationship is for the 490:510 absorption relationship, where the slopes of gelbstoff and phytoplankton converge. This convergence allow the implementation of a simple two-band absorption retrieval. The absorption and scattering at the 490:510 wavelength pair can be solved given the reflectance and the spectral slope of scattering (ϵ_{bb}) for particles and absorption (ϵ_a) for phytoplankton and CDOM i.e.

$$a(\lambda_1) = f_a[\rho_w(\lambda_1, \theta_s, \theta_v, \Delta\phi), \rho_w(\lambda_2, \theta_s, \theta_v, \Delta\phi), \epsilon_{bb}, \epsilon_a, a, b_b] \quad (1)$$

$$b_b(\lambda_1) = f_{bb}[\rho_w(\lambda_1, \theta_s, \theta_v, \Delta\phi), \rho_w(\lambda_2, \theta_s, \theta_v, \Delta\phi), \epsilon_{bb}, \epsilon_a, a, b_b] \quad (2)$$

where f_a and f_{bb} are two analytical functions.

At present, the slope of scattering is assumed unity, but further work will be done when the b_b measurements for COAST/ OOC become available. Figure 90 shows the results of these retrievals using the reference modelling data for all cases of SPM and gelbstoff. The retrieval of backscatter compared to the model has a slope of 0.017 corresponding to the b/b_b ratio for the Petzold phase function used in the model. The absorption shows a 1:1 slope.

2.5.1.2.2.3. Implementation of the Model

Implementation of the model for retrieval of absorption at other wavebands and for determination of geochemical parameters requires a detailed processing chain. Figure 91 shows the overall structure of the model and the necessary inputs. The design is modular in that the parameters at each wave band are fed in by simple tables. The original parameterisation of the model was from the AMT series of cruises, which provided data on the characterisation of phytoplankton absorption. All inputs to the model are in terms of parameters that have known geophysical units. This has the advantage of permitting simple table changes when testing the model on differing sensors. For example, the COAST/ OOC data contained data from both the 555 channel (SeaWiFS) and the 560 channel (MERIS), the structure of the model permitted seamless processing of these data. Figure 92 shows the detailed structure of the iterative loop of the model. The model requires an initial guess of a and b , since both (1) and (2) require these IOPs in order to estimate the effects of sun angle and view angle. The estimate of a and b_b from the model enables an iterative solution of f and Q (Morel and Gentili, 1991), which converge in two to five iterations. At the same time the estimates of gelbstoff absorption at 412nm and phytoplankton absorption at 490nm allow for the small changes in ϵ_a that result from the difference in the relative proportion of gelbstoff and phytoplankton absorption at 490nm and 510nm. The variation in ϵ_a is small as is shown in Figure 89c, where the slope difference changes from 1.26 to 1.4.

2.5.1.2.2.4. Results

Figure 93 show the results of the model applied to both the AMT and the COAST/ OOC data. Figure 93a shows the retrieval of $b_b(490)$ with an R^2 of 56.8% and a slope of 0.00626. The slope corresponds to a $b^*(SPM)$ of 0.35 assuming the Petzold phase function or 0.62 assuming a b_b/b ratio of

*ACRF - LPCM - SAT - U. Oldenburg
NIOZ - U. Trondheim - FUB - PML - GKSS*

0.01. Figure 93b shows the retrieval of phytoplankton absorption at 442nm with an R^2 of 76.7 and a slope of 0.18. The algorithms works on both the AMT data (radiance reflectance) and on the COAST/OOC data (irradiance reflectance) with no stepwise changes discernible between band-sets or reflectance type. The slope is higher than is typical for the $a^*(chlorophyll)$ at 490 nm and indicates that some further parameterisation is necessary for the algorithms.

2.5.1.2.3. Applications

The performance of the new model has been assessed by the analysis of the SeaWiFS data of the NE Atlantic ocean and shelf seas adjacent to the UK for 18 May 1998, shown in Figure 94a, by compositing the R555, R510 and R443 bands (red, green, blue). The image shows a wide variety of bio-optical conditions: blue areas (B) of low chlorophyll; green areas (G) of moderate surface chlorophyll; white areas (C) of high reflectance from coccolithophores (detached liths) or other highly reflecting phytoplankton in high concentrations (D), small diatoms); sediments (brown or yellow) in the tidally mixed areas of the Irish Sea (IS), Bristol Channel (BC) or Western English Channel (WEC). These data have been atmospherically corrected for case II, high scattering waters, by a modification of the method developed for MERIS (Moore, *et. al.* 1999). The $b_b(490)$ image (Figure 94b) shows that the off-shelf patches and the shelf seas sediment patches are high scattering, due to the high abundance of particles. These areas generally have low absorption, though the patch off the west coast of Ireland (D), has both high scattering and high absorption. The $a490$ image (Figure 94c) is independent of the particle backscatter b_b , and both the coccolith areas (C) and the tidally mixed area (IS) show no erroneous effects from the SPM.

2.5.1.2.4. Conclusions

The objectives of COAST/OOC were:

- To produce a large data set of inherent optical properties of the main classes of optically active substances in European coastal waters.
- To determine quantitatively the effect of red tides on ocean colour
- To produce optimised algorithms using the newly acquired optical data set, which will allow to produce maps of the main optically active sea water components (including red tides) using future ocean colour sensors.
- To provide operational ocean colour algorithms for specific ocean colour sensors
- To implement ocean colour analysis into a video server frame, allowing a wide field of users to exploit this information for economically and socially important functions.

Plymouth Marine Laboratories role was in achieving objectives 1 to 4, within this we have provided support for field operations and taken concurrent measurements with the helicopter. The modelling activity was to produce a forward reflectance model to support objectives 2 and 3, which was achieved. During COAST/OOC, an algorithm was developed that could incorporate new data sets

*ACRJ - LPCM - SAI - U. Oldenburg
NIOZ - U. Trondheim - FUB - PML - GKSS*

– objective 3. Finally, the modelling from COAST/OOC has resulted in an operational Case II ocean colour algorithm that has been implemented with SeaDAS, the operational NASA processor for SeaWiFS images. The structure of the algorithm that has been developed, such that it can use data from both the MERIS and MODIS sensors. As a result of the COAST/OOC database, it is expected that images of the new optical properties will become widely available from Plymouth in the near future. At present, images such as those shown in Figure 94 are available for interested researchers.

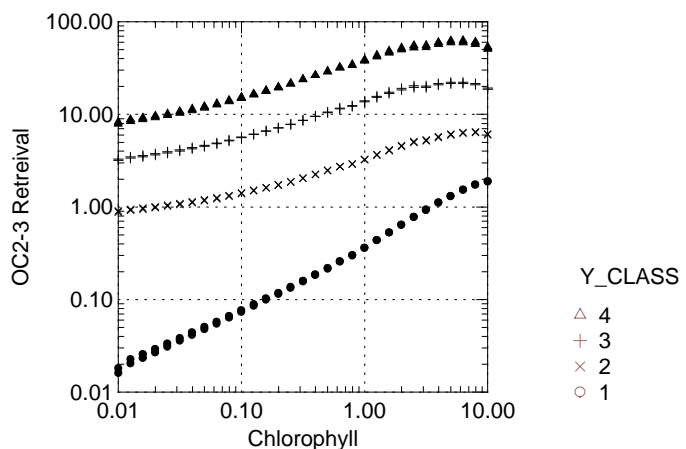
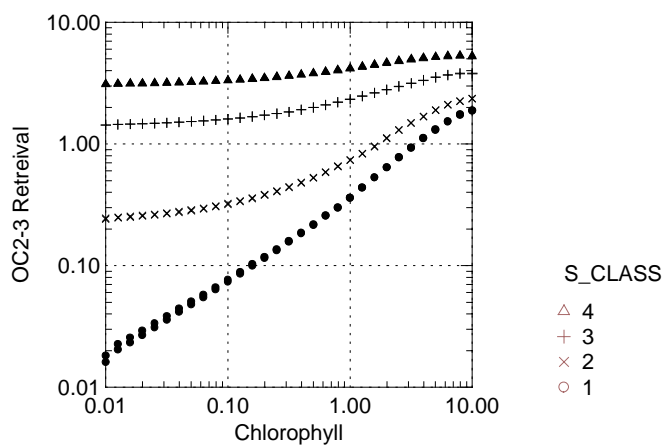


Figure 86. Retrievals of chlorophyll determined by OC2-V2 algorithm. a. The effect of increasing sediment. The classes are; **1**, no sediment, **2** 1.0 mg.l^{-1} , **3** 5 mg.l^{-1} , and **4** 10 mg.l^{-1} . b. The effect of increasing gelbstoff. The classes are; **1**, no gelbstoff, **2** $a(440) 0.2 \text{ m}^{-1}$, **3** $a(440) 0.5 \text{ m}^{-1}$, and **4** $a(440) 1.0 \text{ m}^{-1}$. Note the change in the y axis compared to 1.a

*ACRJ - LPCM - SAI - U. Oldenburg
 NIOZ - U. Trondheim - FUB - PML - GKSS*

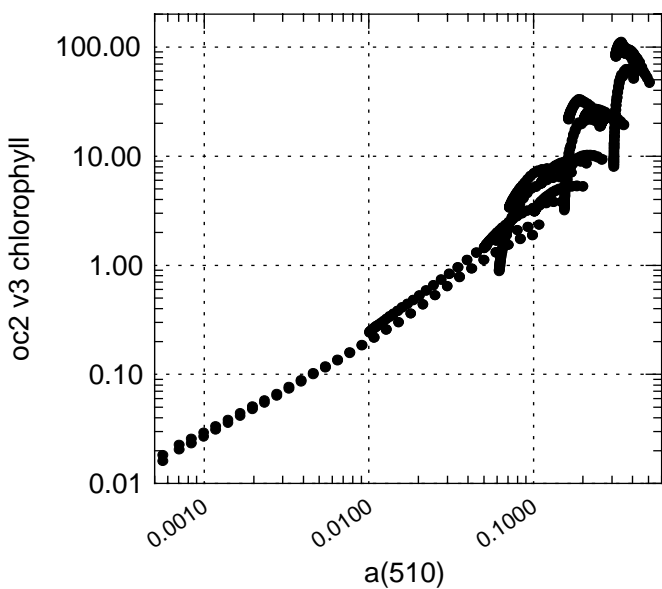
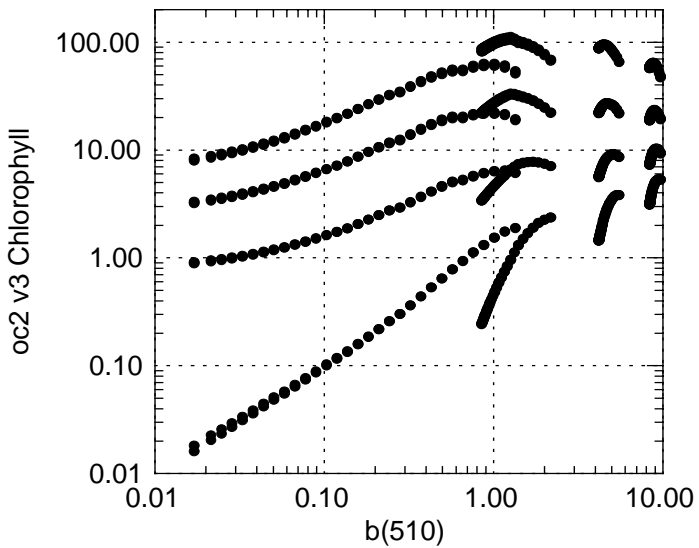
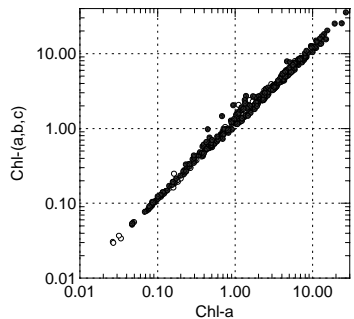


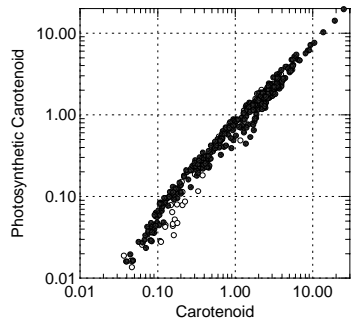
Figure 87. The relationship between apparent chlorophyll retrieved by the oc2 v3 algorithms. a) the absorption coefficient and b) the scattering coefficient. The variations in scattering and gelbstoff correspond to those in Figure 86.

*ACRJ - LPCM - SAI - U. Oldenburg
NIOZ - U. Trondheim - FUB - PML - GKSS*

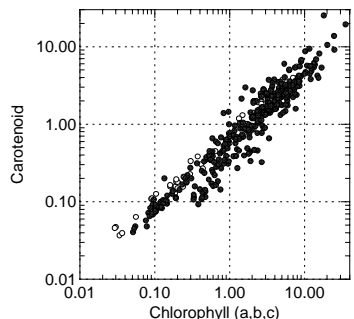
a



c



b



d

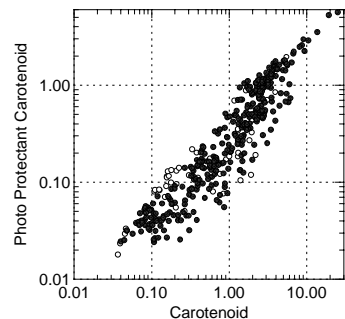
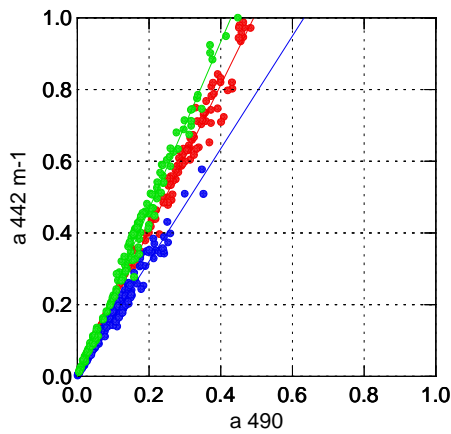
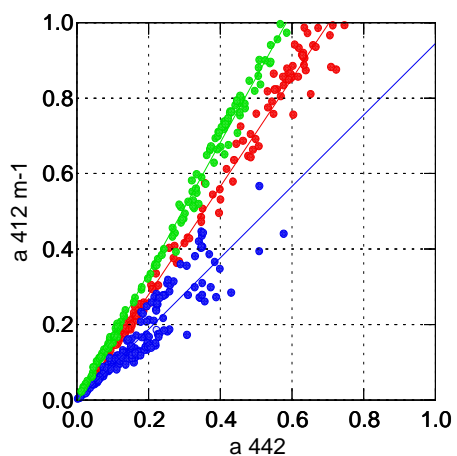


Figure 88. The relationships between pigments. a) the relationship between chlorophyll a and total chlorophyll, b) the relationship between total chlorophyll and carotenoids, c) the relationship between carotenoid and photosynthetic carotenoids, and d) the relationship between carotenoid and photoprotectant carotenoids. The solid circles are from the COAST/OOC data and the open circles are from the AMT (Case I) data.

a

b



c

d

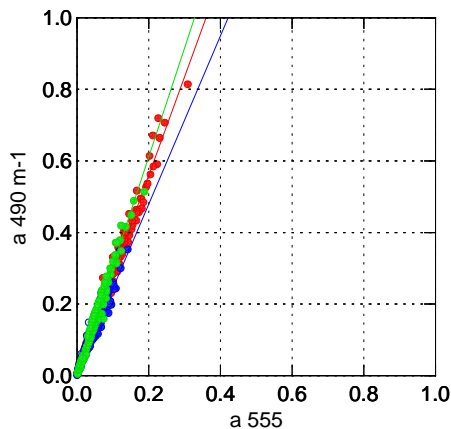
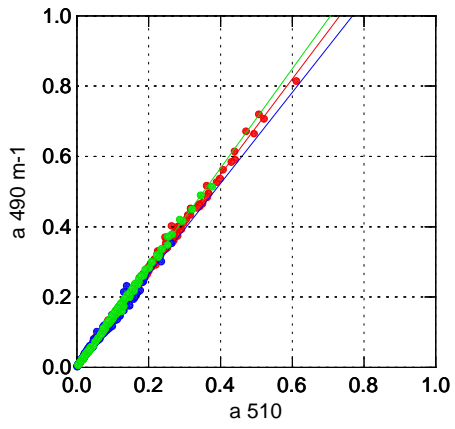


Figure 89. The relationship between the absorption coefficients for successive band pairs. a) 412:442, b) 442:490, c) 490:510 and d) 510:555. The green line (steeper) is the relationship between gelbstoff + detrital absorption, the blue line (lower) is the relationship between phytoplankton absorption, and the green line (centre) is the relationship between total absorption. AMT phytoplankton absorption is represented by open circles.

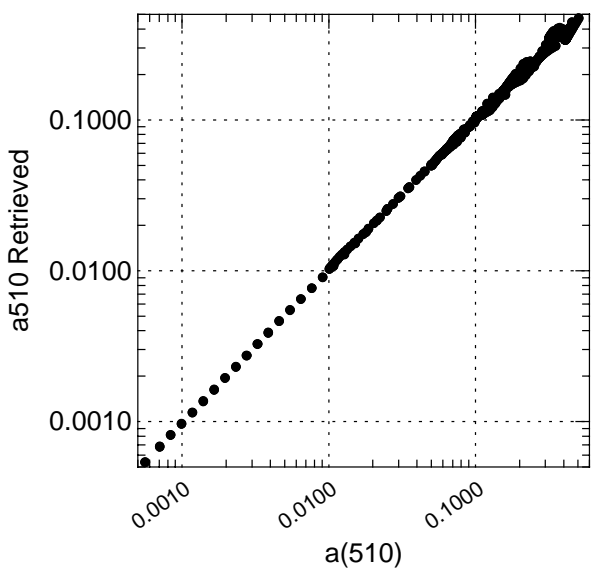
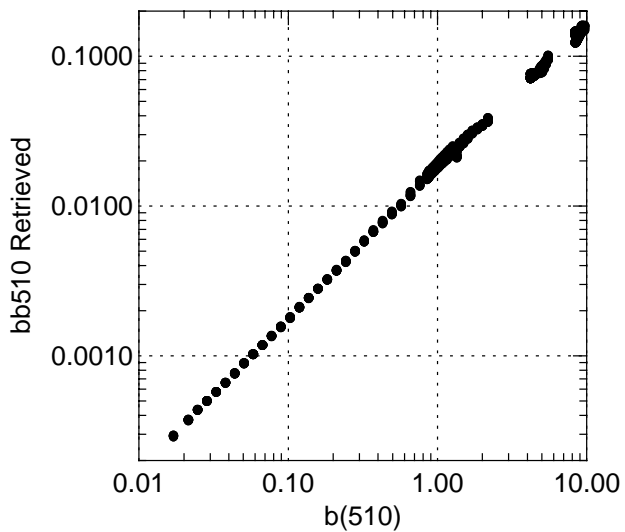


Figure 90. Retrievals of a), $b_b(510)$ vs $b(510)$ for all Cases of SPM and gelbstoff, b) retrievals of $a(510)$ for all cases of chlorophyll and gelbstoff.

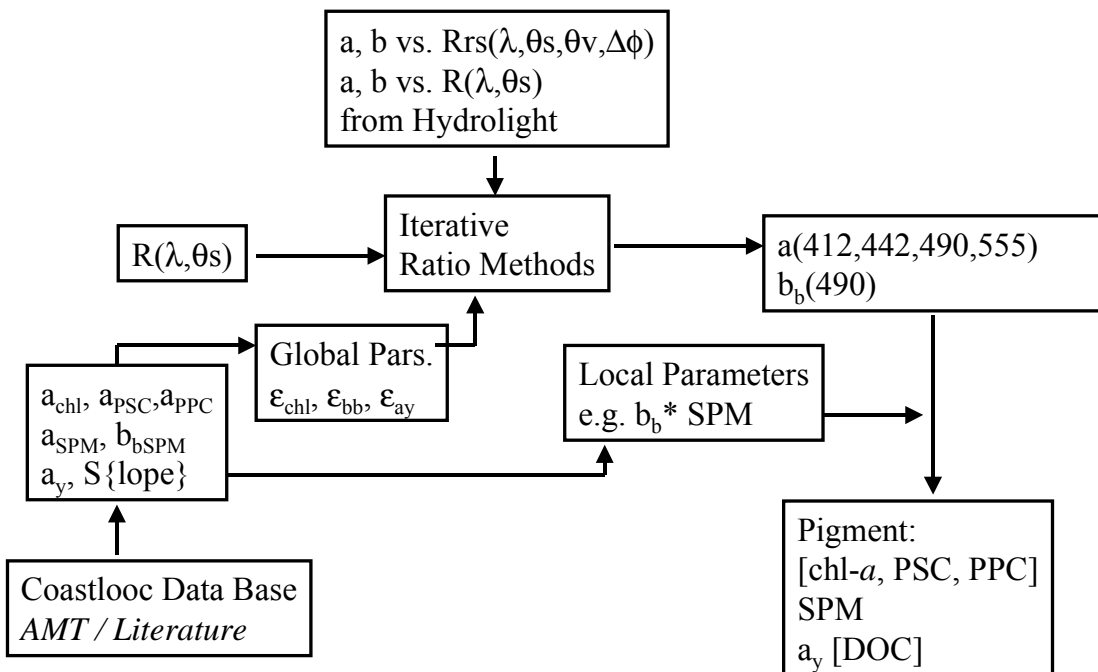


Figure 91. Overall structure of model

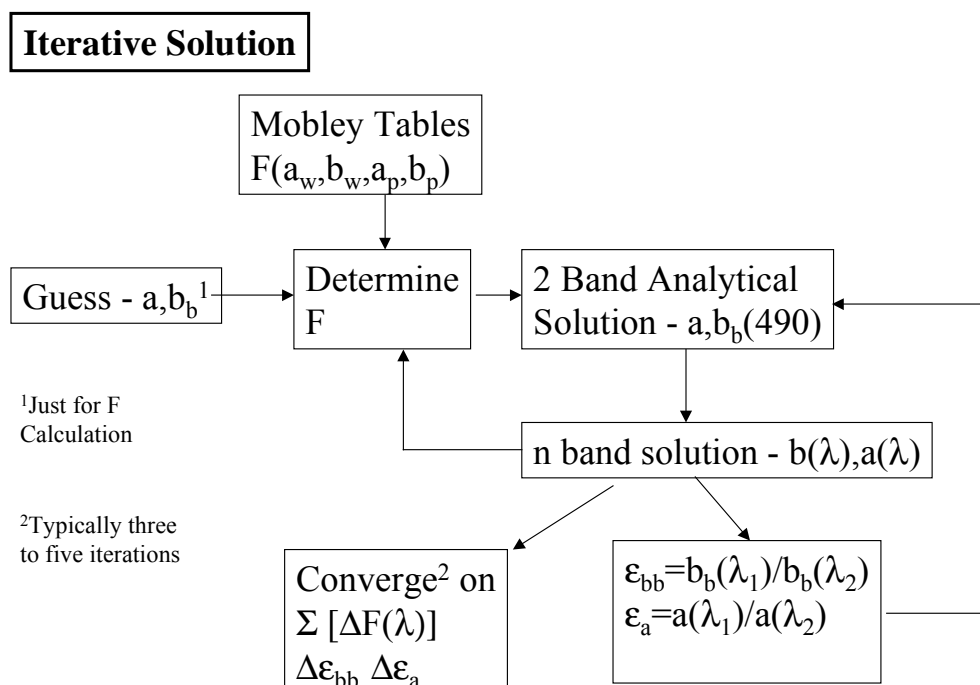


Figure 92. Model Iterative Solution

ACRJ - LPCM - SAI - U. Oldenburg
NIOZ - U. Trondheim - FUB - PML - GKSS

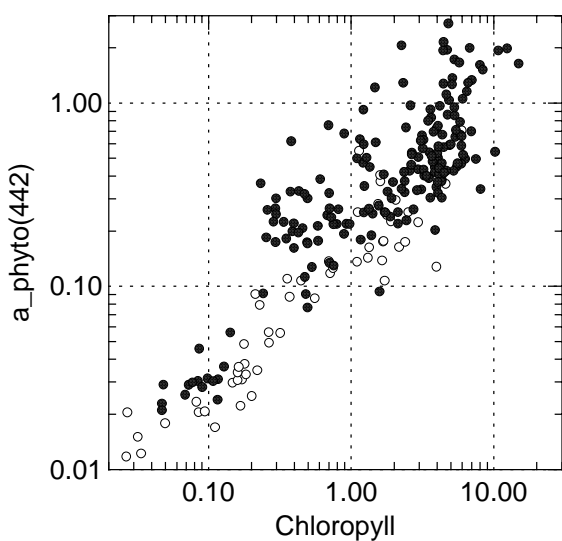
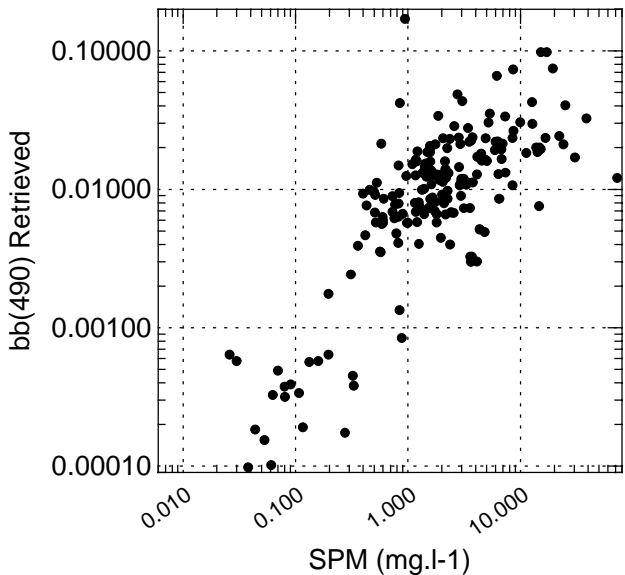
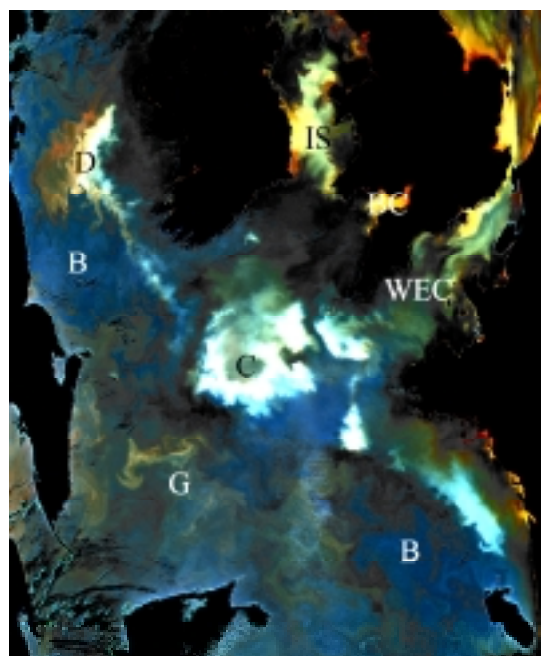


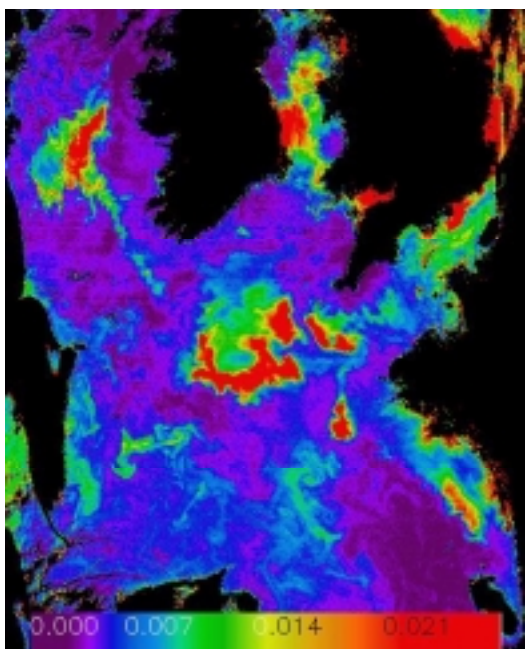
Figure 93. a) retrievals of $b_b(490)$ compared with SPM and b) retrievals of $a_{phyto}(442)$ compared with chlorophyll. The open circles are the AMT data and the filled circles are the COAST/OOC data.

*ACRJ - LPCM - SAI - U. Oldenburg
NIOZ - U. Trondheim - FUB - PML - GKSS*

a



b



c

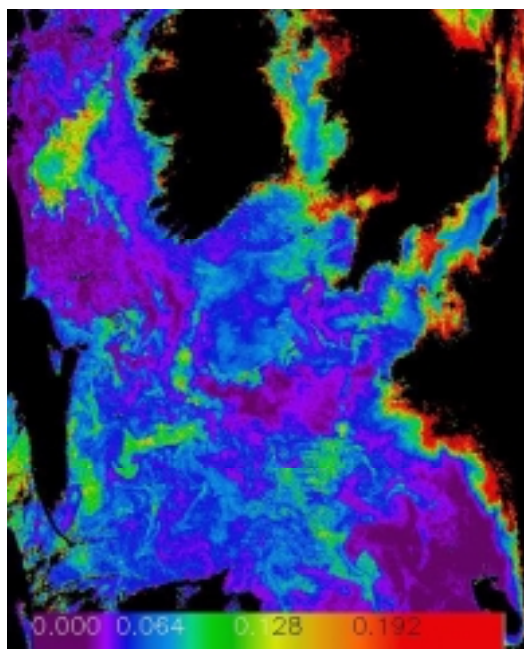


Figure 94. SeaWiFS data for the 18 May 1998: (a) Pseudo true colour composite (blue, green, red) of bands 443 nm, 510 nm & 555 nm; (b) b_b490 , IOP model; (c) $a490$, IOP model.

*ACRJ - LPCM - SAI - U. Oldenburg
NIOZ - U. Trondheim - FUB - PML - GKSS*

2.5.1.2.5. References

Aiken J., Rees N., Hooker S., Holligan P., Bale A., Robins D., Moore G., Harris R., & Pilgrim D. The Atlantic Meridional Transect: Overview and synthesis of data. In press, *Prog Ocean*, 2000

Aiken, J., Moore, G., Trees, C., Hooker, S. & Clark, D., The SeaWiFS CZCS-Type Pigment Algorithm. *NASA Tech. Memo.*, 104566, 29, 34 pp., 1995.

MERIS reference model: 'Reference Model for MERIS Level 2 Processing, Document reference PO-TN-MEL-GS-0026.

Mobley, C.D. ,1995, Hydrolight 3.0 Users Guide', SRI Project 5632.

Morel, A. and Gentili, B., 1991, Diffuse reflectance of oceanic waters. I. Its dependence on sun angle as influenced by the molecular scattering contribution. *Applied Optics*, **30**, 4, 427-4, 438.

Moore, G. F., Aiken, J. and Lavender, S. J., The atmospheric correction of water colour and the quantitative retrieval of suspended particulate matter in Case II waters: application to MERIS, *Int. J. Rem. Sens.*, 20, 1713-1733, 1999.

O'Reilly, J. E., Maritorena, S., Mitchell, G. B., Seigel, D. A., Carder, K. L., Garver, S. A., Kahru, M. & McClain, C., Ocean color algorithms for SeaWiFS, *J. Geophys. Res.*, 103, 24,937 – 24,953, 1998.

2.5.1.3. SAI neural network approach

In recent years various multi-component algorithms have been proposed to retrieve Chlorophyll "a", Total Suspended Matter (TSM – dry weight) and yellow substance absorption coefficient over coastal and enclosed marine regions. These have been based of different types of inversion methodologies including Principal Component Analysis (e.g. Neumann 1996) and Neural Networks (Schiller and Doerffer 1999). The application of these datasets to actual ocean colour imagery (i.e. MOS and SeaWiFS) have shown that two main aspect are critical in the performance of such algorithms which are:

- The parameterization of the implemented forward reflectance in describing the variability in magnitude and spectral shape of the individual components of the Inherent Optical Properties over large ranges of concentrations.
- The range of the concentrations for the individual components constituting the simulation dataset: which often does not reproduce the *true* natural variability found in the area of the imagery considered.

Of these two aspects determining the accuracy of the algorithm the first point has been extremely well investigated by the COAST/OOC project with various initiatives aiming at improving and consolidating the individual component of a *standard reflectance model* for coastal waters. The second point has received less attention although it is obvious that the COAST/OOC dataset itself provide a strong basis for information on the distribution functions and relationship between the

*ACRJ - LPCM - SAI - U. Oldenburg
 NIOD - U. Trondheim - FUB - PML - GKSS*

concentrations of the individual Optically Active Components (OACs) in European coastal waters. However to date most inversion algorithms have been based on all encompassing simulation datasets covering extremely large ranges of concentration and often many combinations of concentration which are not at all feasible in the natural environment. This therefore results in algorithms that performed extremely well over certain concentration ranges but poorly over others.

The aim of the investigation is to attempt a statistical exercise with the COAST/OOC surface parameter dataset used as the basis in the development of preliminary algorithm for the retrieval of the main OACs. This would therefore provide information on the distribution functions of the OACs in different European waters. Whilst being a rather empirical approach it is not intended to substitute the more complex semi-analytic inversion algorithms but merely to provide a first order estimate to enable the definition of more representative simulation datasets.

In the formulation of this baseline algorithms the following guidelines were adopted which clearly underline the motives of such an algorithm. It was decided that the algorithm should use standard Level 2 products as produced by operational processing chains (i.e. SEADAS, Terascan). The algorithm should be formulated in such a way to minimize possible errors due to an incorrect atmospheric correction or incorrect consideration of bi-directional effects (both of which are still known to be significant issues in the accuracy of Level 2 products – particularly over Case II waters). Also the algorithm should be a simple and fast algorithm both in the implementation phase and in the subsequent operational processing of satellite imagery.

The surface dataset of 423 sample was considered. In particular the current investigation uses the values for subsurface reflectance in the first six channels (412, 443, 490, 510, 555, 665), the concentrations of Chlorophyll "a" and dry weight and the yellow substance absorption coefficient at 440nm. The value of the subsurface reflectance at 412nm was correct with a factor of 3.2 resulting from post-fieldwork calibration and pre-processing analysis (M. Babin personal communication). The data from the subsurface reflectance at 532nm were converted to that at 510 using an empirical relationship resulting from samples in which both wavelengths were available. The resulting dataset considered after a minimum amount of quality control was 275 of the original 423 samples. In an attempt to minimize any subsequent sensitivity of the algorithm to errors in atmospheric correction the resulting dataset of subsurface reflectance were normalized to a specific wavelength thus eliminating the algorithm's dependence on the absolute magnitude of the subsurface reflectance. The wavelength of 555 was chosen as the normalization wavelength as this corresponds to the minimum value of absorption that is the key component in the determination of the spectral shape of reflectance.

For inversion of the measured reflectance a neural network approach was selected. As it is potentially the most adequate in reproducing the non-linear nature of the measured dataset in its relationship with the main OACs. Due to the *limited* size of the in-situ dataset (compared to simulated datasets) the objective was to keep the neural map as simple as possible. This implies that only 1 hidden layer was adopted and the number of neurons in this hidden layer was kept to a minimum. The 5 inputs (412, 443, 490, 510 and 665 all normalized to 555) and 3 outputs (Chlorophyll, TSM and a_{ys440}) were considered for the development of the algorithm. This dataset was split randomly into a 67% training dataset (184 samples) and 33% (91 samples) dataset for subsequent validation. An iteration threshold of 20000 epochs was set and a convergence criterion of 0.01, the logistic function was selected for the representation of the data in the net.

*ACRI - LPCM - SAI - U. Oldenburg
NOZ - U. Trondheim - FUB - PML - GKSS*

The results from this investigation are summarized in Table 19. It is seen that a neural map of log converted values (when compared to the linear and semi-log trials) for input and output values and ten neurons provides the best results for the 5 input 3 output version of the algorithm. In this case the retrieval accuracy of Chlorophyll, dry weight and ays440 are 0.623, 0.807 and 0.876 respectively based on the output from the validation dataset. Further tests were made to evaluate the sensitivity of the individual OACs (specifically TSM and ays440) to the omission of the certain of the input variables in the blue and the red. As expected the retrieval accuracy of dry weight diminishes when the red wavelength is removed. However, surprisingly, the retrieval accuracy of ays440 is not effected to such an extent through the removal of the blue wavelength as may be expected on the basis of knowledge of the optical properties in the blue region of the spectrum.

An image of the Adriatic (SeaWiFS data) showing the application of the log, 5 input 3 output, version of the algorithm is included in Figure 95. It is apparent that there is still some atmospheric contamination particularly in the dry weight product, undoubtedly due an inadequate removal of the aerosol signal from the satellite measured radiances. Nevertheless it is also apparent that there a good separation of the different contributions to the radiances of the individual in water constituent resulting in different patterns in the surface distributions of the OACs. These features are particularly apparent in features associated with the outflow of the Po river.

In conclusion it has been shown that the COAST/ OOC dataset is an adequate source of empirical data to formulate a representative preliminary multi-component algorithm for European coastal waters. The algorithm retrieval accuracy assessed on the basis of an independent validation dataset has shown that Chlorophyll "a" is retrieved to within 40% and dry weight and yellow substance absorption coefficient to within 25% error. This result is obtained using a parameterization based on 5 ratio inputs, and log converted input and output datasets for the training of the neural net. This algorithm was selected by considering the different retrieval accuracy of linear, log and semi-log version of the training datasets. Finally a sensitivity analysis considered the effect of the removal of the red and blue wavelength from the inputs data on the retrieval accuracy. This test showed that dry weight retrieval accuracy is greatly determined by the available of information on the red channel. The test however also showed that at least for concentrations found in the considered dataset, the removal of the first channel did not seriously compromise the retrieval accuracy of the yellow substance absorption (contrarily to what may be expected).

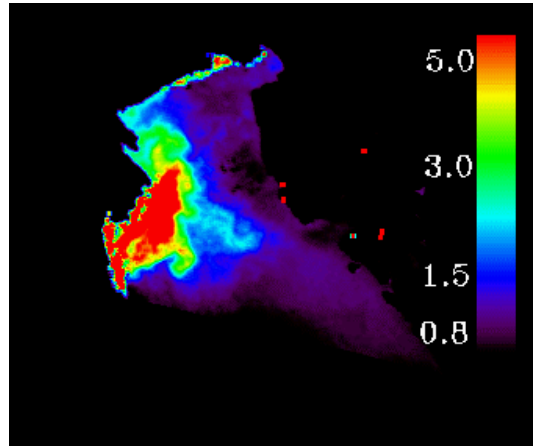


Final Report
ENV4-CT96-0310
03 January 2000

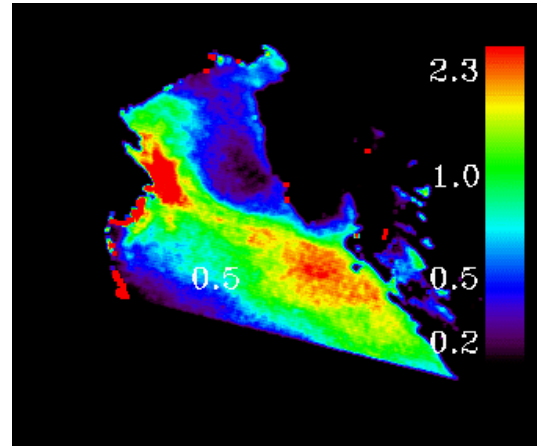
Page: 155

Table 19. Summary of the results from this investigation.

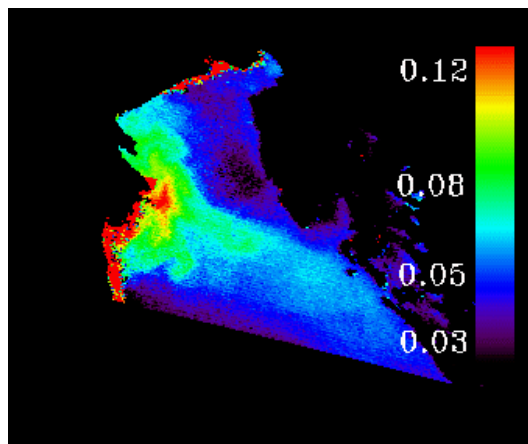
lin/log	no. of input wavelengths	no. of neurons	Training/ Validation	r ² Chlorophyll	r ² Dry Weight	r ² a _{ys440}
lin	5	10	Training	0.877	0.874	0.917
			Validation	0.523	0.939	0.761
log	5	10	Training	0.845	0.787	0.914
			Validation	0.623	0.807	0.876
slog	5	11	Training	0.847	0.868	0.901
			Validation	0.436	0.502	0.823
log	4(no 1)	10	Training	0.767	0.805	0.885
			Validation	0.527	0.867	0.858
log	4(no 5)	9	Training	0.806	0.735	0.892
			Validation	0.564	0.293	0.837
log	3	9	Training	0.728	0.653	0.839
			Validation	0.579	0.523	0.823



Chlorophyll (mg/m^3)



Dry Weight(mg/l)



$a_{\text{sys}} 440 \ (\text{m}^{-1})$

Figure 95. Image of the Adriatic (SeaWiFS data) showing the application of the log, 5 input 3 output, version of the algorithm.

2.5.1.4. GKSS Neural Network Algorithm

2.5.1.4.1. Overview of activities

Main objective of the participation of GKSS in the project COAST/OOC was to test an inverse modelling procedure for the retrieval of coastal water constituents from water leaving radiance reflectances derived from earth observation satellite radiance measurements. For this purpose a procedure has been developed which uses the neural network technique as a multiple variable non-linear regression method to determine the inverse relationship between concentrations of water constituents and multispectral water leaving radiance reflectances. This procedure has been tested using data of the imaging spectrometer MOS, which is flying on the Indian remote sensing satellite IRS-1. The selected images are from the same period and areas of the COAST/OOC cruise in May 1998 with RV "Poseidon". Furthermore, a special neural network was developed for data of the airborne imaging spectrometer CASI, which have been used during COAST/OOC parallel to ship measurements.

Other activities within the frame of COAST/OOC:

- measurement of optical properties in the North Sea and during the COAST/OOC cruise with RV "Poseidon" including measurements of above surface radiance reflectances,
- support of the Helicopter campaign,
- support of COAST/OOC by providing in situ instruments (AC-9 beam attenuation and absorption meter, BB-4 backscatterometer, Satlantic downwelling irradiance, upwelling radiance profiler) for most of the campaigns.

Since the budget for our participation in COAST/OOC was small, some of our activities, which are included in this report, were funded through other complementary projects and contracts.

2.5.1.4.2. GKSS team

The following members of the bio-optical laboratory of the GKSS Institute of Hydrophysics have been involved in COAST/OOC (in alphabetic order):

- Wolfgang Cordes (in situ instrumentation)
- Roland Doerffer (surface reflection measurements, radiative transfer simulations, evaluation of MOS data)
- Hans Hakvoort (in situ measurements, data evaluation)
- Kerstin Heymann (processing of water samples, determination of pigments, SPM and Gelbstoff)

*ACRJ - LPCM - SAI - U. Oldenburg
NIOZ - U. Trondheim - FUB - PML - GKSS*

- Helmut Schiller (development and training of neural networks)
- Heinrich Siewers (surface reflection measurements)

2.5.1.4.3. Acknowledgements

We have to thank the Bundesanstalt für Seeschiffahrt und Hydrographie, Hamburg, for the opportunity to take part in cruises with the RV "Gauss", the Alfred-Wegener –Institute for Polar and Marine Research for the opportunity to use the RV "Heincke". Furthermore we had the opportunity to take part in the COAST/OOC cruise of RV "Poseidon". We thank all crew members of the research vessels for their support.

2.5.1.4.4. Overview of field activities

Optical cruises, which have been performed by GKSS within the frame of COAST/OOC, are listed in Table 20. At the beginning of COAST/OOC, H. Hakvoort of GKSS was involved in first Helicopter test flights. Furthermore, our instruments, mainly the AC-9 and the BB-4 were provided to nearly all COAST/OOC field campaigns. Costs for transportation of the instruments were covered by the GKSS COAST/OOC budget.

Cruises

- GAUSS 11.2. - 15.2.1997 North Sea German Bight
- GAUSS 20.5. - 26.5.1997 North Sea German Bight
- GAUSS 24.6. - 30.6.1997 North Sea German Bight
- Heincke 9.3. - 12.3.1998 North Sea German Bight
- Heincke 6.4. - 8.4.1998 North Sea German Bight
- Poseidon 2.5. - 17.5.1998 West Europe (Atlantic, North Sea)
- Participation in Helicopter Flights Mediterranean Sea

Instruments and Samples

- Optical in situ instrument package
 - AC-9 attenuation and absorption meter
 - BB4 backscatterometer
 - SBE CTD
 - Rosette water sampler
- Satlantic profiler E_d and L_u in 13 spectral bands
- Zeiss radiance spectrometer (350 - 950 nm)
- Samples: Pigments, SPM, DOC, POC, gelbstoff absorption

Table 20. Field campaigns within the frame of COAST/OOC.

2.5.1.4.5. Retrieval of water constituents from water leaving radiance reflectances by inverse modelling

The optical properties of most open ocean waters are determined by the concentration of phytoplankton and further constituents, which are associated with phytoplankton. The concentration of this group of covarying substances is expressed as the concentration of chlorophyll *a*, which is the dominating pigment in phytoplankton cells and used here as a proxy variable. For these so called Case I waters, a high correlation exists between the chlorophyll concentration and the ratio of water leaving reflectances at two spectral bands. By determining the regression between chlorophyll and the reflectance band ratio based on simultaneous satellite and in situ observations, this band ratio algorithm is used for determining chlorophyll concentrations from satellite data.

In contrast to open ocean waters, most coastal waters contain a number of different optically active water constituents, which determine the upward directed radiance spectrum by absorption, scattering and fluorescence and which do not co-vary (defined as Case II waters). Simple algorithms, such as band ratios, do not apply to this type of waters or only for cases when the covariance of the constituents is sufficiently high.

There are a number of possibilities to solve this problem, such as multiple linear regression between the reflectances of all spectral bands or their ratios and each of the constituents based on observations, multiple linear regression between the eigenvectors derived from all spectral bands and each of the constituents based on observations or simulations, inversion of a radiative transfer model by a non linear optimisation procedure.

For this project we have chosen the neural network inverse modelling technique, because this procedure has been selected by ESA as the standard case II water algorithm for the Medium Resolution Imaging Spectrometer (MERIS), which is part of the earth observation satellite ENVISAT. This technique has the following advantages: it is based on bio-optical models, the final NN procedure is extremely efficient, any complex radiative transfer model can be used without influence on the data processing time. Disadvantage is the high effort to produce the training and test tables (which depends on the type of radiative transfer model) and to train the neural network.

2.5.1.4.5.1. Outline of the procedure

Input to the algorithm are directional (not normalised) water leaving radiance reflectances together with the solar and observation angles to avoid any assumptions and simplifications for computing normalised reflectances. Thus, the algorithm requires atmospherically corrected radiance reflectances. The multiple non-linear regression procedure, i.e. the NN, is developed from radiative transfer calculations which include a wide range of concentrations to cover Case I and Case II water properties and the solar and observation angles which are relevant for MERIS. The model is a Monte Carlo photon tracing code, which enables the simulation of radiance and irradiance detectors. Using this code, tables of water leaving radiance reflectances are calculated as a function of concentrations of suspended matter, gelbstoff and phytoplankton pigment and the solar zenith angle. In contrast to MERIS, only the nadir reflectance has been used, because of the narrow swath width of MOS . The

*ACRI - LPCM - SAI - U. Oldenburg
 NIOZ - U. Trondheim - FUB - PML - GKSS*

table is the basis for training of a neural network in the inverse order with the water leaving radiance reflectances of the first 6 MOS channels and the solar zenith angle as input and the concentration of the three groups of substances as output. This neural network can directly be used for the operational conversion of MOS data after atmospheric correction. During the training phase the network is tested against an independent test data set to avoid overtraining.

The scheme of the algorithm has three main parts: (1) calculation of a training and test data set using the forward model, (2) design, training and testing of the neural network and (3) implementation and application of the network for the production of concentration data. While the preparation part requires an extensive computational effort, the application part is very fast. In general, this scheme combines a complex forward model, which describes the radiative transfer in a realistic but time consuming way with the high computational speed of the parameterisation of its inverse.

Atmospheric correction for MOS is based on another neural network, which is used to derive the atmospheric transmittance and the atmospheric path radiance for the first 6 bands of MOS-B (408, 443, 490, 520, 560, 615 nm) from top of atmosphere (TOA) reflectances of MOS-B bands 9 (750 nm) and 11 (868 nm). For simulating realistic training data sets for turbid case II waters, not only the concentrations of different aerosols (urban, maritime, continental background, stratospheric) were included in the model, but also different concentrations of cirrus clouds, suspended particles in water and sun glitter.

The computation of training tables is based on independent (non-covarying) concentrations of phytoplankton chlorophyll *a*, non-absorbing suspended matter expressed as SPM dry weight and gelbstoff absorption at 440 nm. The bio-optical model, which describes the relationship between the concentrations of these substances and the optical properties of the water containing these constituents, was based for the tests as described below on the reference model I for MERIS, which is documented in a technical note by ACRI and part of the ATBD 2.3 for MERIS. In this model the optical properties of SPM are described only by scattering while the absorption of gelbstoff has to cover also the absorption of particles.

The concentration range for computing the training table is given in Table 21.

Ranges of independent variables for calculating water leaving reflectances			
Variable	concentration unit	min	max
phytoplankton pigment, chlorophyll <i>a</i>	$\mu\text{g/l}$	0.003	50
mineralic suspended matter	mg/l	0.003	50
gelbstoff, absorption at 440 nm	$\text{a}(440) \text{ m}^{-1}$	0.002	2
solar zenith angle	degree	15	75

Table 21. Ranges of variables for training the NN.

For the simulation of the downwelling radiance distribution as input to the water NN, a realistic atmosphere was implemented in the model with 50 layers, containing standard mixed gas for molecule scattering, aerosols and ozone and a wind roughened sea surface. All computations were performed using a Monte Carlo photon tracing model, which has been developed at GKSS.

Training of the neural network was performed with a program also developed at GKSS, which uses a back-propagation algorithm.

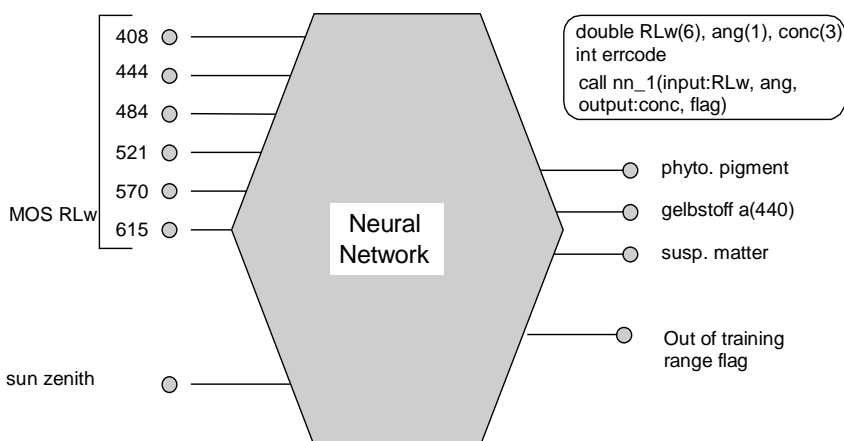


Figure 96. Scheme of NN for retrieving water constituents from MOS water leaving radiance reflectances.

*ACRJ - LPCM - SAI - U. Oldenburg
NIOZ - U. Trondheim - FUB - PML - GKSS*

2.5.1.4.5.2. Results of training

The training results are validated by comparing the concentrations, which were used to compute the water leaving radiance reflectances, with the corresponding concentrations as output of the neural.

The first test case for chlorophyll was set up for the full range of water constituents as used for training of the NN, i.e. up to 50 µg/l chlorophyll, 50 mg/l SPM and a gelbstoff absorption at 440 nm of 2 m⁻¹. The result shows (Figure 97) that the relative accuracy of the retrieval decreases with decreasing concentration of chlorophyll. As expected, this result reflects that the error of the retrieval of a low concentration of one substance increases with increasing concentrations of other substances, a relationship which is true for any algorithm. In this test it means that at SPM concentrations of up to 50 mg/l SPM, chlorophyll concentrations in the range < 1 µg/l can hardly be detected.

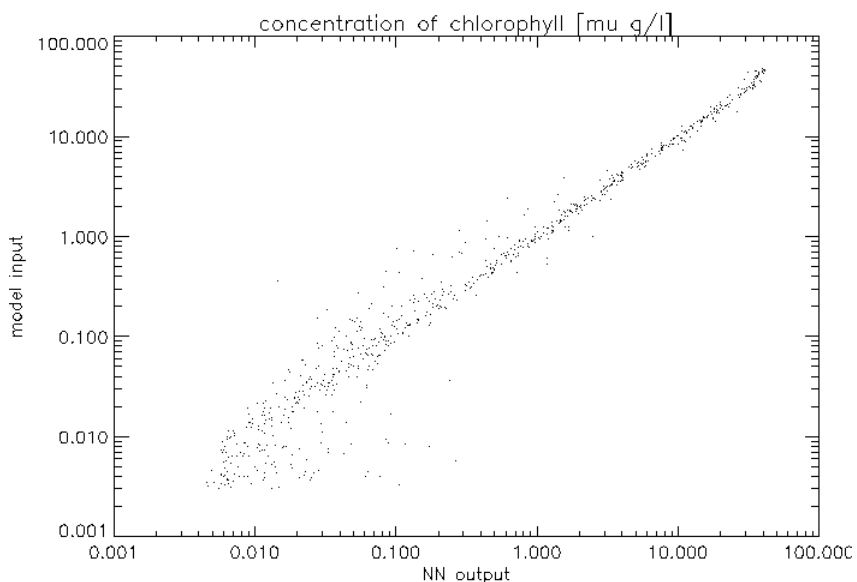


Figure 97. Chlorophyll concentration derived from NN (x-axis) versus the corresponding chlorophyll concentration (y-axis) which were used in the forward model for computing the water leaving radiance reflectances as input to the NN. Concentrations of SPM and gelbstoff float randomly within the full training range

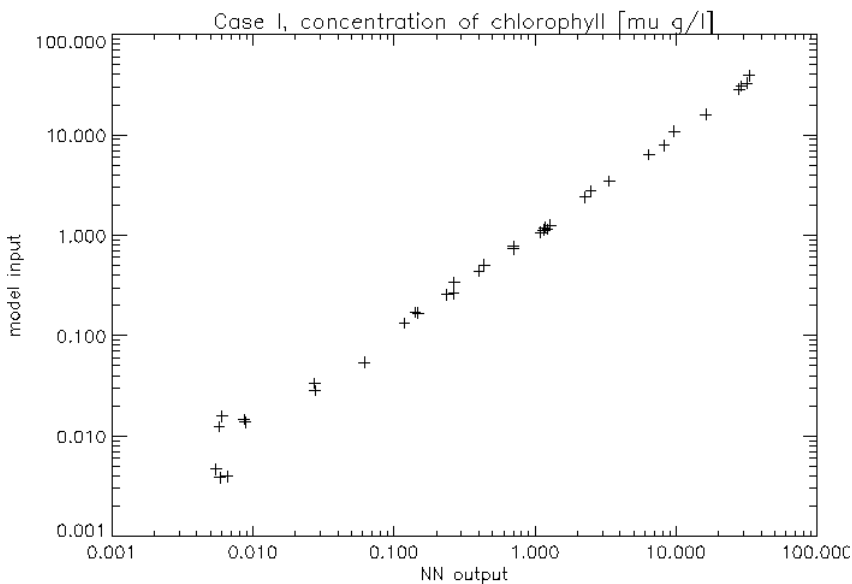


Figure 98. Same as Figure 97, but tested only for cases with SPM concentrations $< 0.6 \text{ mg/l}$ and gelbstoff absorption at $440 \text{ nm} < 0.05 \text{ m}^{-1}$.

The second test with the same NN shows the same result for chlorophyll but for case I water conditions with SPM concentrations $< 0.5 \text{ mg/l}$ and gelbstoff absorption at $440 \text{ nm} < 0.05 \text{ m}^{-1}$. Similar results were found for SPM and gelbstoff when tested in the same way.

The sensitivity of the NN against errors of the input data was validated by deteriorating the reflectances used for testing the NN with random noise for all bands and for each spectral band independently. In general the results show that the output error has the same magnitude as the input error.

2.5.1.4.5.3. Tests using MOS scenes

Six MOS scenes from the same period and area of the COAST/OOC Poseidon cruise were used for testing the NN. Although none of the scenes directly coincide with measurements from the ship (Table 22), the comparison indicate at least if the results are in the same range as expected from the in situ measurements. This assumption is supported by the fact that the weather conditions during the cruise have been stable due to the persisting high pressure with low wind speeds. Table 23 gives an overview about the MOS scenes, time of overflight, time of in situ measurements and the range of concentrations from in situ measurements and the satellite data of the areas, which were visited by ship.

Table 22. MOS scenes from the Poseidon cruise period used for testing the NN algorithm and corresponding dates of ship observations of the same area.

Scene ID	area	Date	ground truth
LEV00008_IP3B27.128	Atlantic, west off Gibraltar	May 8	May 4
LEV00013_IP3B19.129	Bretagne	May 9	May 10
LEV00015_IP3B18.139	Seine, Normandie	May 19	May 11
LEV00015_IP3B16.139	The Wash	May 19	May 14
LEV00019_IP3B15.135	Nordwijk	May 15	May 13
LEV00023_IP3B14.131	German Bight	May 11	May 16

Table 23. Overview of concentrations (mean values or ranges) as determined from water samples and derived from MOS data.

Area	Chlorophyll µg/l	SPM mg/l	Gelbstoff a(440) m⁻¹
Atlantic Ship	0.13	5.1	0.03
Atlantic MOS	0.23	3.8	0.03
Bretagne Ship	0.34	5.3	0.09
Bretagne MOS	0.5	3.8	0.06
Seine Ship	7-25	12	0.1 - 0.2
Seine MOS	0.6 - 2 - 11	5 - 9 - 24	0.0027 - 0.0095 - 0.065

As one example the results of the Seine Bight (west coast of France) with the river plume will be shown. Figure 99 shows the raw image with the transect, which was used for further analysis. Figure 101 shows the concentrations of chlorophyll and SPM and the gelbstoff absorption along this transect as derived using the NN. The area of the Seine plume is clearly visible by the high concentrations of SPM and gelbstoff. In contrast, the chlorophyll concentration is low at the center of the plume. Two explanations are possible. (1) Due to the masking effect of the high SPM concentration it is not possible to detect chlorophyll and (2), most likely, the low chlorophyll concentration is real and the cause for this low concentration at the center of the plume is the high turbidity and thus the low light level for photosynthesis, while at the frontal zone surrounding the

plume optimum conditions occur for phytoplankton growth due to high nutrient input from the Seine river together with low SPM concentration and thus sufficient light.

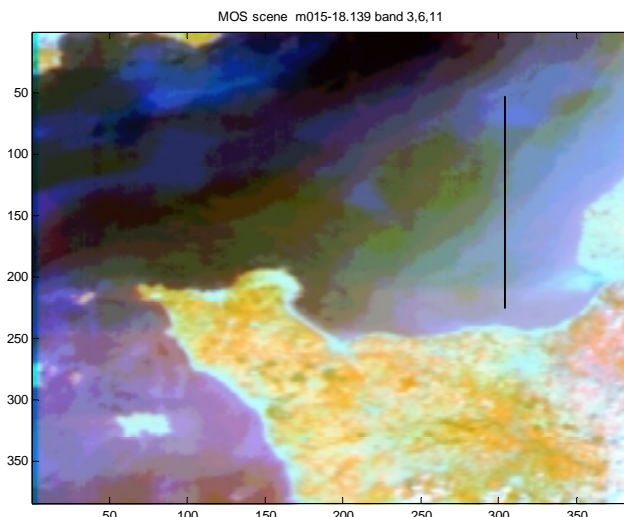


Figure 99. RGB color image of the MOS scene of the Seine Bight. The black line indicates the transect used for further analysis.

Of interest is also to check whether the path radiance determined with the atmospheric correction NN is independent from the SPM concentrations, since both have an effect on the radiance in the bands 750 nm and 868 nm, which are used for atmospheric correction. Figure 102 confirms that the path radiances in the blue to red bands obviously are not affected by backscattering of particles in the plume water, although the radiance at top of atmosphere indicate that the scattering effect of particles influences also the radiances in MOS bands 750 nm and 868 nm (Figure 100).

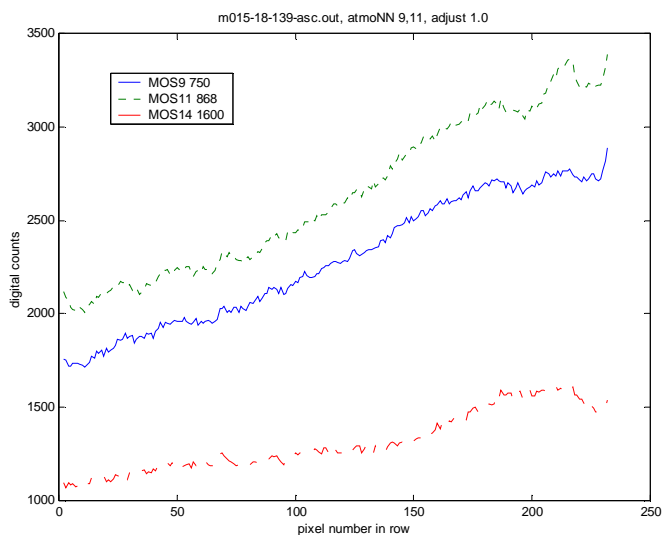


Figure 100. Digital counts (uncalibrated radiances) of MOS bands 750, 868 and 1600 nm along transect.

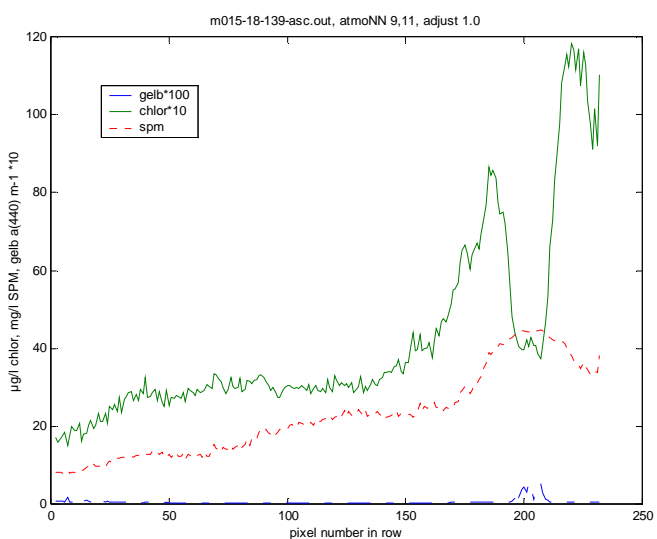


Figure 101. Concentrations of chlorophyll, SPM and gelbstoff derived from MOS along transect.

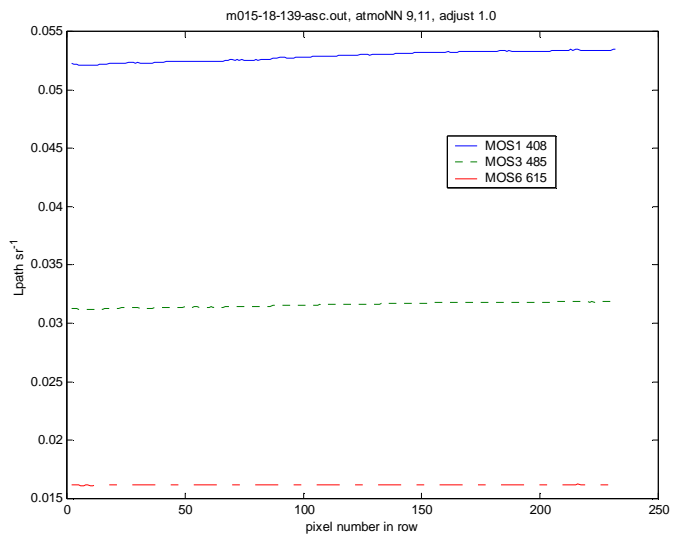


Figure 102. Atmospheric path radiance reflectances of MOS bands 408, 550, 615 nm along transect.

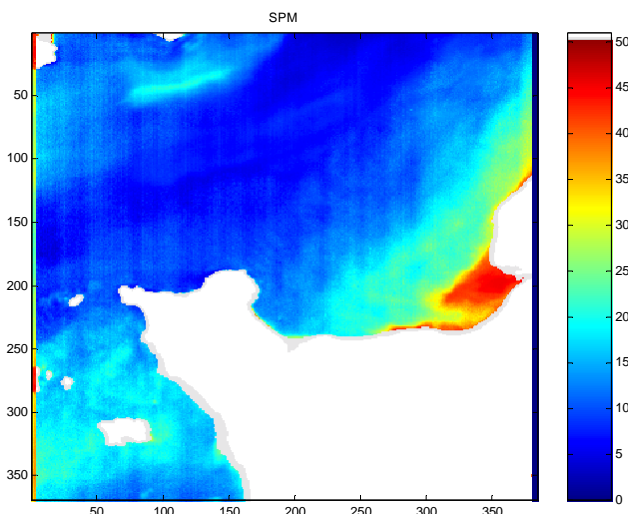


Figure 103. Distribution of SPM derived from MOS, scale in mg/l.

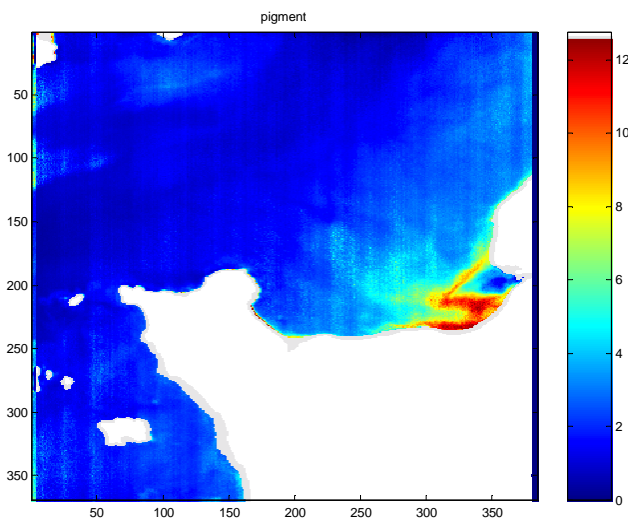


Figure 104. Distribution of chlorophyll derived from MOS, scale in $\mu\text{g/l}$.

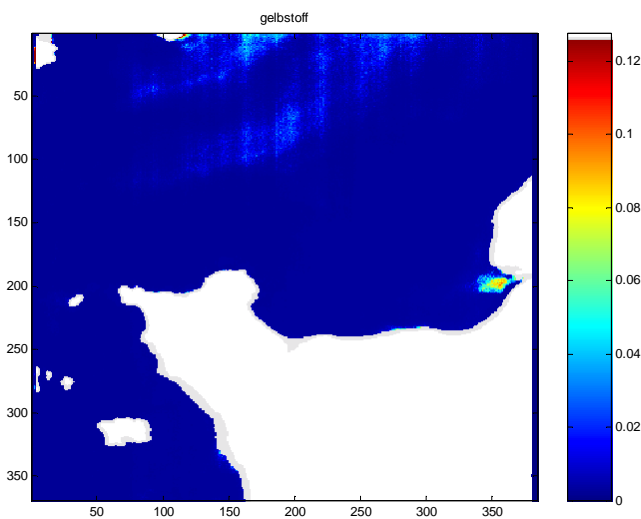


Figure 105. Distribution of gelbstoff derived from MOS, scale in absorption m^{-1} at 440 nm.

2.5.1.4.5.4. Summary and Conclusions

Inverse modelling using neural network as a multiple non linear regression method is one possibility to solve the problem of remote sensing of water constituents in coastal waters. The advantage of this technique is that realistic but time consuming radiative transfer models can be used, which simulate the directional radiance distribution at the sea surface or at top of atmosphere, and that at same hand a very fast and efficient procedure for deriving concentrations from reflectance spectra is achieved. Disadvantage is the high effort for computing training and test data sets and for the training

*ACRJ - LPCM - SAI - U. Oldenburg
NIOZ - U. Trondheim - FUB - PML - GKSS*

itself, which during the experimental phase of the development requires much time and computer resources.

The tests of the NN have demonstrated that for any case II algorithms the concentration accuracy of one substance decreases when the concentrations of other substances are high. Thus, we have to deal with variable errors and with a limited concentration range for which an algorithm can provide useful results. Both facts define the scope of any case II water algorithm. However, preliminary results of a NN algorithm, for which the covariance of water constituents of the COAST/OOC data set was utilized in defining the concentration range for training, indicate a better performance and a much faster training compared to the case where all constituents vary totally independently.

Since the evaluation of all COAST/OOC data and the compilation of the data set was finished close to the end of the project, one open item is to use the bio-optical model based on COAST/OOC data for training of a new NN and test this data with reflectances measured from ship. This work will be completed within the frame of another project.

2.5.1.5. Sun-Induced Chlorophyll Fluorescence algorithm

See Annexes (Section 6.1).

2.5.2. Level 2 ground segment prototype (simulator) adapted to the CASI data

2.5.2.1. CASI operations carried out during the COAST/ OOC campaigns #3, #4, and #6

2.5.2.1.1. Objectives

The objective is here to get *in situ* determinations of water-leaving radiances and of geophysical parameters simultaneously to the corresponding spectral information from CASI. The former can be compared to the same parameters as derived from the CASI spectra by using the MERIS algorithms in a version adapted to aircraft remote sensing; validation of the algorithms is therefore within reach in this case. Another objective was to provide the mission team with a quantitative assessment of several bio-geochemical variables over the whole sampling region, in order to design the next day operations, namely to locate judiciously the stations for optical profiling and water sampling. This is quite important to avoid gaps in sampling, which are prejudicial to algorithm development. This objective has not been reached during COAST/ OOC #6 because of the very bad weather conditions, preventing any planning of the sampling operations from one day to another one (adaptation has been necessary on a daily, even hourly, basis).

*ACRJ - LPCM - SAI - U. Oldenburg
NIOZ - U. Trondheim - FUB - PML - GKSS*

2.5.2.1.2. The “Compact Airborne Spectrographic Imager” (CASI)

CASI is a programmable imaging spectrograph operating between about 400 and 1000 nm. This sensor is based on a two-dimensional CCD. A line across track is imaged by the spectrograph optics onto one axis of the CCD, and the image is spectrally dispersed along the second CCD axis (see Figure 106). A complete spectrum is therefore obtained for each pixel, whatever the way these information are sub-sampled for recording.

The nominal specifications, as given by the manufacturer (ITRES company) are the following : Field of view is 37.8° across track (19° and 14° degrees on each side of nadir) and 0.076° along track, and calibration accuracy is $\pm 2\%$ absolute between 470-800 nm and $\pm 5\%$ absolute between 430-870 nm. The CASI instrument is installed on a stabilising platform allowing minimal geometrical perturbations of the measurements. It is out of the scope of the present document to further describe the instrument, and additional information can be found at URL <http://www.itres.com>.

2.5.2.1.3. Calibration of CASI

Calibration is usually performed by the manufacturer using a radiance standard from the NBS, and allowing radiant sensitivity coefficients to be obtained for each pixel of the CCD. Correct calibration of the “blue bands” of CASI (*i.e.*, $\lambda < 450$ nm) has been a recurrent difficulty, which has been, in principle, corrected by the establishment of new calibration procedures by the FUB’s team (Ivo Keller, Carsten Olbert, Jurgen Fischer). A paper is in preparation about this work, yet it is not already available. In principle, the new calibration procedure that is used should provide radiances with a $+2\%$ absolute accuracy over the 400-900 wavelength range, *i.e.*, something quite close to what is expected from MERIS. The use of CASI for validating the algorithms is therefore pertinent.

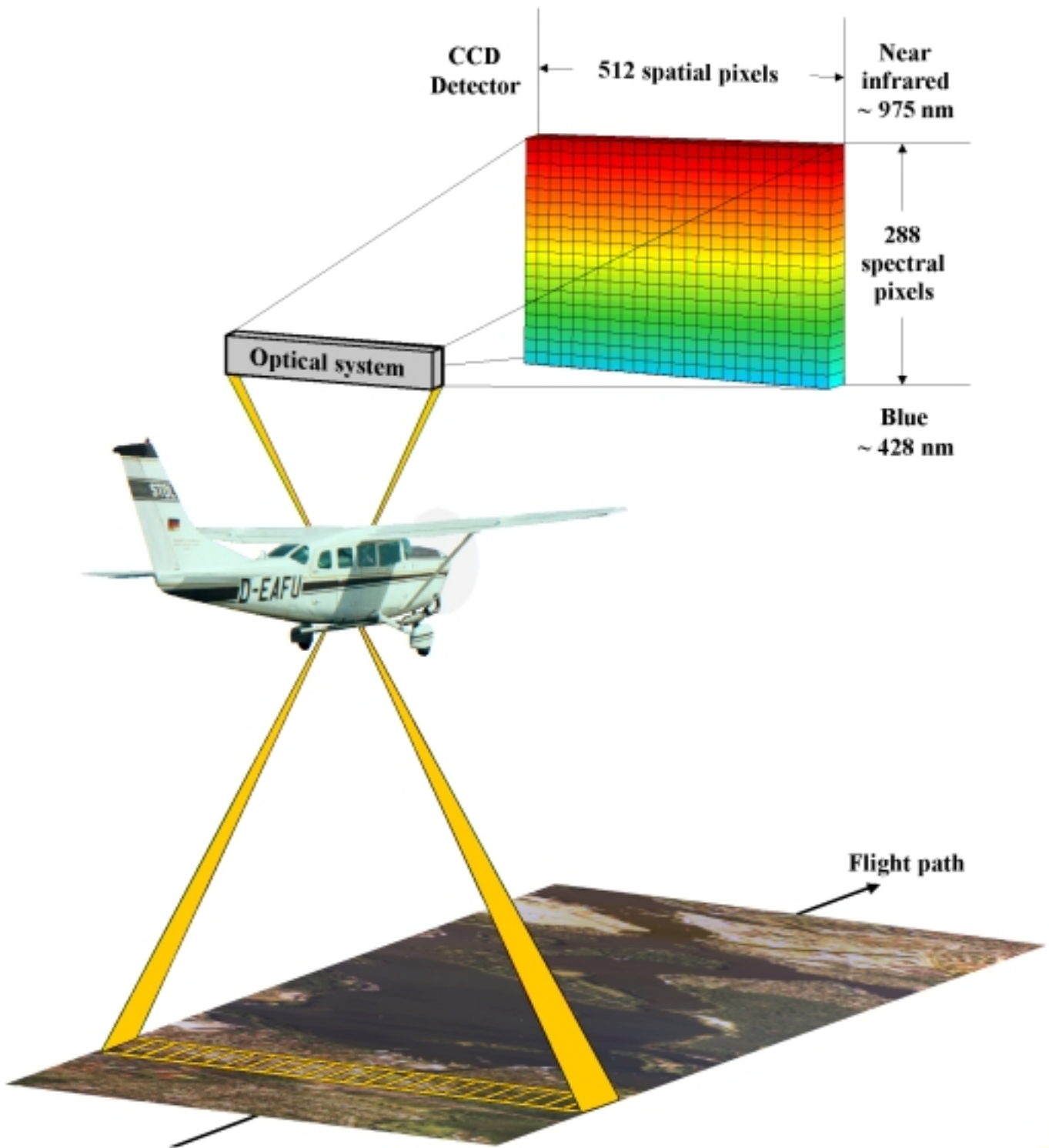


Figure 106. Drawing showing the way CASI performed measurements.

ACRJ - LPCM - SAI - U. Oldenburg
NIOZ - U. Trondheim - FUB - PML - GKSS

2.5.2.1.4. Use of CASI

COAST/OOC #3 and #4 campaigns.

The “full frame mode” operation mode allows the full spectrum to be recorded for 512 pixels across track with a spectral resolution of about 1.9 nm. The “spatial mode”, however, has been used for the present study, providing radiances for selected wavelengths and bandwidths, namely the MERIS bands. The first MERIS band at 412 nm has not been recorded, however, due to the limited spectral range of the CASI instrument used here, and which starts at about 428 nm.

A GPS (reference) is mounted on the system, providing the position of the sub-aircraft point (*i.e.*, the point just below the aircraft, when looking at nadir and whatever aircraft roll and pitch may be).

COAST/OOC #6 campaign.

The “spatial mode” is used as for the other campaigns, while CASI is operated along with a DGPS (reference), providing now the position of the sub-aircraft point with a better accuracy.

Measurements of the downwelling irradiance in the same bands than those programmed on the CASI have been performed by mounting on the aircraft a multi-channel radiometer (the SPMR from the Satlantic company). This instrument is usually used as a surface (air) reference, deployed simultaneously to the in-water instrument that record the in-water downwelling irradiance. With this installation, we dispose of simultaneous measurements of the upwelling radiance and of the downwelling irradiance at the aircraft altitude, allowing the reflectance to be computed. Measuring the downwelling irradiance was actually necessary to get a correct estimate of reflectance when the aircraft flights below overcast skies (for cloudless skies, the reflectance can be computed with respect to the extraterrestrial irradiance, as it is done for a satellite configuration). An uncertainty in this procedure originates from the changes in the spectral quality of the downwelling irradiance, as compared to that of a clear sky; these changes may affect the reflectance spectrum and may introduce artefacts in the atmospheric correction procedure. More serious difficulties arise, however, when the sky above the aircraft is only partly cloudy, because the downwelling irradiance impinging onto the radiometer is not necessarily the irradiance that illuminates the sea surface just below the aircraft, and which determines the radiant intensity escaping water (*i.e.*, the water-leaving radiances that we aim at). The problem is even more critical for low sun elevations, as encountered in September at relatively

high latitudes on the COAST/OOC #6 campaign, and the calculation of the reflectance is biased in such circumstances. In summary, 3 configurations may be encountered :

- (1) Perfectly clear sky : reflectance is computed as

$\rho(\lambda) = \pi L(\lambda) / (F_0(\lambda) \mu_s)$, where $L(\lambda)$ is the radiance measured by CASI, $F_0(\lambda)$ is the mean extraterrestrial irradiance, and μ_s the cosine of the sun zenith angle. This procedure is the same than that used for satellite measurements. In this case, the LUTs used in atmospheric correction are generated by using reflectances calculated following the same equation than above.

- (2) Totally overcast sky (the aircraft flies just below a rather homogeneous cloud layer) :

$\rho(\lambda) = \pi L(\lambda) / E_d(0^+)(\lambda)$, where $E_d(0^+)(\lambda)$ is the downwelling irradiance recorded at the aircraft altitude (temporal matching of CASI and the reference is achieved by synchronising internal clocks of both instruments). Note that LUTs (ρ_r and the ratio ρ_t / ρ_r) have now to be generated for reflectances computed in the same way, *i.e.*, $\rho(\lambda, z) = \pi L(\lambda, z) / E_d(z)(\lambda)$, where z is the altitude considered (and not with respect to F_0 , as made above for clear skies).

- (3) Partly cloudy sky : the problems previously evoked (cloud shadows, etc...) are unavoidable, so that we have to cope with them and accept that some (many) pixels will be unusable. For the remaining ones, reflectance is calculated as in case (1).

2.5.2.1.5. Adaptation of the LPCM MERIS breadboard prototype to CASI specificities

As CASI flights are usually performed at altitudes between 2 km and 3.5 km (*i.e.*, above most of the aerosols), atmospheric correction of the data is necessary. The principle used here is exactly that of MERIS atmospheric corrections, while specific LUTs have been generated for the flight altitudes that we have explored during the COAST/OOC campaigns. These LUTs are generated by keeping the total upward radiance at the relevant altitude (from the outputs of MOMO simulations). The simulations have been performed by keeping the 3-layer structure (Boundary layer from 0 to 2 km, free troposphere from 2 to 12, and stratosphere above 12 km) adopted for MERIS algorithms. Aerosols in the free troposphere and stratosphere and kept unchanged as compared to the basic cases of the MERIS LUTs (*i.e.*, H_2SO_4 in the stratosphere with $\tau_a(550) = 0.005$, and a continental aerosol within the free troposphere with $\tau_a(550) = 0.025$), while only 3 aerosol models have been considered (maritime, rural, and “coastal”, which is the maritime model polluted by a small amount of rural particles; Gordon and Wang, 1994) for 4 values of the relative humidity in the boundary layer (70, 80, 95, and 99%). No tests are performed at 510 and 705 nm to detect the presence of peculiar aerosols. This choice has been motivated by the fact that the CASI flights have been performed mainly above

*ACRI - LPCM - SAI - U. Oldenburg
MIOZ - U. Trondheim - FUB - PML - GKSS*

Case 2 waters, where the relevance of the technique developed for MERIS to identify absorbing aerosols has not been proven.

The geometry of the observation (*i.e.*, solar zenith angle, viewing angle, and azimuth difference between the two half vertical planes containing the sun and CASI and intersecting on the pixel under examination) has been computed for each pixel, under the assumption of a flat Earth (this is a totally acceptable assumption when considering the flight altitude, max. 3.5 km, and the field of view, 38°). The viewing angle is given by the instrument characteristics, the sun zenith angle of the sub-aircraft point has been used for each pixel of a line, and the azimuth difference has been computed for each pixel from the track heading and the solar azimuth (both given in the CASI level 1B data, as degrees from north clockwise).

Therefore, the MERIS atmospheric corrections are applied here nearly in the same way than when they will be applied to real satellite (MERIS) observations. If the conditions permits, the present CASI operations should represent a true opportunity for validation of the MERIS algorithms.

2.5.2.1.6. Integration of the prototypes corresponding to ATBDs 2.5, 2.6, 2.8, and 2.12

In addition to the above adaptation, the LPCM breadboard prototype has been also “increased” by the incorporation of algorithms developed at PML (ATBDs 2.5, 2.6, and 2.8), and at GKSS (ATBD 2.12). It was necessary to add these algorithms, which deal with Case 2 waters, because the COAST/OOC program is devoted to Case 2 waters and the campaigns have been mainly carried out in such waters.

ATBD 2.5 deals with the identification of Case 2 bright waters (*i.e.*, sediment-dominated Case 2 waters). Algorithms described in ATBD 2.6 perform atmospheric correction of the near IR bands over the waters identified by the bright pixel test. ATBD 2.8 presents additional tests designed for identification of Case 2 waters where absorption by yellow substances dominates. Finally, ATBD 2.12 describes the retrieval of chlorophyll, suspended sediments, and yellow substance absorption by a neural network technique.

The ACRI prototypes corresponding to the ATBDs cited here have been provided by ACRI after approval by Dr. Roland Doerffer of GKSS and Dr. Gerald Moore of PML. These prototypes written in C have been successfully included into the FORTRAN breadboard prototype of LPCM. Concerning the neural net technique, however, the absence of the 412 nm band in the measurements compromises the chances to get correct results.

*ACRI - LPCM - SAI - U. Oldenburg
NIOZ - U. Trondheim - FUB - PML - GKSS*

2.5.2.1.7. The problem of surface roughness

When using an instrument such as CASI, with a very small IFOV and flying at low altitude, the pixel size is reduced. It varies between about 1 or 2 meters for the present data set. Therefore, accounting for the effect of surface roughness becomes very difficult, to say the least, because there is no "averaging effect" as with a satellite configuration, where the size of the pixel is large with respect to the typical scale of waves and swells (and more generally of any surface structures). Indeed, with CASI, the surface observed for a given pixel may not be horizontal, as well as it may be entirely contaminated by foam, organic films or any other "material" that totally obscures the optical properties of the water body itself (for the large size of satellite pixels, these effects are often attenuated because the pixel is not entirely concerned).

As a consequence, no correction at all has been attempted for these surface effects. The impact on the results may be sometimes seen in the CASI images (for instance parallel structures in the chlorophyll fields, expressing the effect of swell). It could be difficult, if not impossible, to detect them in the scatter plots where a given parameter, as measured *in situ*, is compared to its value derived from CASI. It is likely that some procedures exist for correcting for the effects evoked here, yet it was out of the scope of our work to attempt such corrections.

2.5.2.1.8. Post-processing of the *in situ* data : from diffuse reflectances to water-leaving radiances

The radiance is the quantity directly measured by CASI. It can be expressed as (see list of notations) :

$$L_w(\lambda, \theta_s, \theta', \Delta\phi) = \varepsilon_c F_0(\lambda) \mu_{s,sensor} t_{\theta_s}(\lambda) \mathfrak{R}(\theta') \frac{R(\lambda, \theta_{s,sensor})}{Q(\lambda, \theta_{s,sensor}, \theta', \Delta\phi)}$$

Several steps are required to derive this value from the parameters measured *in situ*, which are (1) the diffuse reflectance just below the sea surface (R), (2) the chlorophyll concentration (determined by HPLC), (3) the concentration of suspended sediments, (4) the absorption by yellow substance at 440 nm, and (5) some ancillary data.

2.5.2.1.8.1. Accounting for changes in solar elevation

The quantity at our disposal is R at the time of the *in situ* sampling, $R(\lambda, \theta_{s,insitu})$, i.e., $[E_u(0^-) / (E_d(0^+) * 0.96)]$. A first step consists in computing the value it should have for the sun zenith angle corresponding to the time of the CASI track.

*ACRJ - LPCM - SAI - U. Oldenburg
NIOZ - U. Trondheim - FUB - PML - GKSS*

$$R(\lambda, \theta_{s,sensor}) = (f_{1,sensor} / f_{1,in situ}) R(\lambda, \theta_{s,in situ})$$

where $f_{1,sensor}$ is the f factor (here f is defined as $R / [b_b/(a + b_b)]$) for the solar zenith angle ($\theta_{s,sensor}$) at the time of the CASI measurement and at the location of the *in situ* measurement, and $f_{1,in situ}$ is the f factor for the solar zenith angle ($\theta_{s,in situ}$) at the time and location of the *in situ* measurement. This transformation obviously assumes that the IOPs do not change between the time of the *in situ* measurement and the time of the CASI track. The f factors are extracted from a Lookup table (LUT), generated from a series of radiative transfer simulations (see below).

2.5.2.1.8.2. Accounting for the bi-directionality of the diffuse reflectance

The Q factors (Morel and Gentili, 1991, 1993, 1996), which account for the bidirectional character of the diffuse reflectance R, are extracted from a LUT, generation of which is explained below.

The spatial (θ, ϕ) distribution of the water-leaving radiances reflects the spatial distribution of in-water radiances, which in turn is dependent on the inherent optical properties of the water body (IOPs, *i.e.*, absorption coefficient and volume scattering function), on the illumination conditions (sun altitude and sky radiance distribution), and on the characteristics of the air-water interface.

For each station where a reflectance has been measured, we need 2 values of f and a value of Q to compute the water-leaving radiance. In order to consider the wide range of optical properties encountered during the COAST/OOC cruises, and in order to save computational time, we decided to perform radiative transfer simulations where the optical properties are defined through the dimensionless ratios (b/a) and η ($= b_w/b$). These 2 ratios, along with the volume scattering function $\beta(\theta)$, unambiguously define the radiative regime within the water body. This choice allows the wavelength dimension to be omitted, so that the generated LUT is usable for any wavelength, provided that the actual IOPs are included in the (b/a)- η domain considered here. The limitation of such a technique is that trans-spectral processes (*e.g.*, Raman scattering) are not accounted for; their importance for the bidirectionality in Case 2 waters with moderate-to-high chlorophyll concentrations is however totally negligible. On another hand, a unique phase function is used for all computations (Petzold, 1972); this limitation, however, is common to any radiative transfer computation in the ocean, because no other phase function have been measured up to now.

The radiative transfer computations have been performed with the LPCM Monte Carlo code, where the sea surface is considered flat, and the sun zenith angle takes the values 15, 30, 45, 60, and 75

degrees. The upper hemisphere is divided into 360 unequal solid angles, defined by regular angular increments ($\Delta\theta = 3^\circ$, and $\Delta(\Delta\phi) = 15^\circ$).

Two tables are generated from the outputs of these simulations (for Q and for f; f is computed from the relationship $R = f [b_b / (a + b_b)]$). The entries of these tables are the ratios (b/a) and η , the sun zenith angle, and the viewing angle and relative azimuth for the Q table. The wavelength λ , as well as the values of $a(\lambda)$ and $b(\lambda)$ are directly used to estimate the ratios (b/a) and η ; it is then possible to interpolate within the f and the Q LUTs to get the pertinent values for the geometry under examination ($\theta_s, \theta', \Delta\phi$). The 2 coefficients $a(\lambda)$ and $b(\lambda)$ are computed as :

$$a(\lambda) = a_w(\lambda) + a_\phi(\lambda) + a_d(\lambda) + a_y(\lambda)$$

where $a_w(\lambda)$, for pure sea water, is taken from Pope and Fry (1997)

$a_\phi(\lambda)$, for phytoplankton, is modelled as a function of Chl according to Bricaud *et al.* (1995)

$a_d(\lambda)$, for detritus, is modelled as a function of Chl according to Bricaud *et al.* (1999)

$a_y(\lambda)$, for CDOM, = $a_y(440) \exp(-0.014 (\lambda - 440))$

$$b(\lambda) = b_w(\lambda) + b_\phi(\lambda) + b_{SPM}(\lambda)$$

where $b_w(\lambda)$, for pure sea water, = $0.00288(\lambda / 500)^{-4.32}$, from Morel (1974)

$b_\phi(\lambda)$, for phytoplankton, = $(550 / \lambda)^{0.416} \text{ Chl}^{0.766}$ (Loisel and Morel, 1998)

$b_{SPM}(\lambda)$, for sediments, = $(550 / \lambda) b_{SPM}^* SPM$

Where Chl and SPM are the measured concentrations of chlorophyll and sediments, respectively, and $a_y(440)$ is the measured absorption of dissolved coloured matter at 440 nm (measured with the AC9 instrument equipped with a filter). The specific scattering coefficient of sediments, b_{SPM}^* , is taken equal to $0.125 \text{ m}^2 \text{ g}^{-1}$.

2.5.2.1.8.3. Accounting for the surface effects

*ACRJ - LPCM - SAI - U. Oldenburg
 NIÖZ - U. Trondheim - FUB - PML - GKSS*

The geometrical factor $\mathfrak{R}(\theta')$ is given from a table indexed on the refracted viewing zenith angle, θ' . Its values have been computed as

$$\mathfrak{R}(\theta') = \left[\frac{(1 - \bar{\rho})}{(1 - \bar{r} R)} \frac{(1 - \rho_F(\theta'))}{n^2} \right]$$

where

n is the refractive index of water (1.34)

$\rho_F(\theta)$ is the Fresnel reflection coefficient for incident angle θ (Austin, 1974)

$\bar{\rho}$ is the mean reflection coefficient for the downwelling irradiance at the sea surface (0.043)

\bar{r} is the average reflection for upwelling irradiance at the water-air interface (0.489)

2.5.2.1.8.4. The downwelling irradiance above the sea surface

The downwelling irradiance just above the sea surface, $E_d(0^+)$, is the last term that we need to compute to estimate the radiance. In the above equation, it is represented by the product $\varepsilon_c F_0(\lambda) \mu_{s,sensor} t_{\theta_s}(\lambda)$

A question arises here : is it better to fully calculate $E_d(0^+)$ for the time of the CASI pass (meaning that unavoidable uncertainties are introduced in the terms F_0 and t_{θ_s}), or to simply use the value measured during the *in situ* sampling, after correction by the ratio of sun zenith angles and irradiance transmittances $[(\theta_{s,sensor} / \theta_{s,insitu}) * (t_{\theta_s,sensor} / t_{\theta_s,insitu})]$. A third option (actually abandoned) would have been to use the reference measurements made aboard the aircraft, after correction for their attenuation within the atmospheric layer below the aircraft.

2.5.2.1.9. Application to CASI images (COAST/OOC #3, #4, and #6)

Maps of the areas visited during the COAST/OOC campaigns #3, #4, and #6 are displayed in Figure 107 to Figure 112. The CASI flights are shown — Table 24 summarises important information concerning these flights — as well as the *in situ* sampling stations (carried out either from ship, for campaign #3 and #4, or from helicopter, for campaign #6).

The latitude and longitude of each *in situ* sampling station was given by a GPS or DGPS system. The latitude and longitude of each pixel in the CASI image have been calculated from the

*ACRJ - LPCM - SAI - U. OI denburg
NIOZ - U. Trondheim - FUB - PML - GKSS*

latitude and longitude of the sub-aircraft point (also given by a DGPS system), and by considering the altitude of the plane, the viewing angle for each pixel, and the residual roll, pitch, and yaw of the CASI instrument, and the track heading (and assuming a flat surface). Considering that uncertainties are unavoidable for all these parameters, the comparison between *in situ* and CASI-derived geophysical parameters is performed either by looking to the CASI pixel which is the nearest to the *in situ* sampling station, or by comparing the mean value of a 16 by 16 square of pixels in the CASI image (this second way is to avoid too much impact of possible errors in the geo-location of CASI pixels). A precise quantification of the uncertainty in geo-location would require the exact knowledge of the uncertainties in altitude, latitude, longitude, track heading (all from GPS or DGPS), and residual attitude of the platform.

2.5.2.1.10. Mapping of the sampling areas

Figure 113 to Figure 118 show maps of the chlorophyll concentration, as derived from a band ratio algorithm using wavelengths 490 and 555 nm. These maps are constructed by merging several flights, and are shown to provide a rough idea of the characteristics of the visited areas. No data are shown for the COAST/ OOC #6 campaign, because the very bad weather conditions encountered during September 1998 eventually prevented us to process the CASI images and to retrieve meaningful results.

Figure 116 and Figure 117, for the region of the Rhone delta, show that the horizontal distribution of chlorophyll has dramatically changed within a day (from September 29 to September 30), with a clear westward displacement of the Rhone plume. We notice that point here to emphasise that the match-up of *in situ* data with either satellite-derived or airborne-derived parameters requires a tight correspondence in time between both, especially when dealing with Case 2 waters such as those encountered here.

2.5.2.1.11. Results in terms of recovery of the spectral reflectance above the sea surface

Figure 119 and Figure 120 show radiance spectra for two flights in COAST/OOC #4. The data have been acquired on October 1, 1997 (track #5, South to North track), and September 11, 1997 (track #11, East to West track). The results are shown either after atmospheric correction of the CASI observations (black curves), or calculated from the measured diffuse reflectance, and following the two ways indicated in section 1.8.4. The six panels correspond to six *in situ* sampling stations, as displayed in Figure 108. The comparison is not satisfactory, and the reasons for the discrepancies have

*ACRJ - LPCM - SAI - U. Oldenburg
NIOZ - U. Trondheim - FUB - PML - GKSS*



not yet been identified, except perhaps for the flight #11, where contamination of the signal by reflection of the sky is likely among the causes of failure of atmospheric correction.

The differences between the red and green curves (especially for flight #5), emphasise the difficulty of using *in situ* data for validation when they have been gathered with a too important time lag as compared to the CASI pass.

Finally, the shape of the CASI spectra, and particularly its strong and nearly systematic decrease from 490 to 443 nm (not observed in the in-water measurements), seem to indicate that calibration problem still persist in the blue part of the spectrum (*i.e.*, $\lambda < 500$ nm).

2.5.2.1.12. Results in terms of "CASI-derived" *versus in situ* geophysical parameters

Scatter plots of "CASI-derived" *versus in situ* parameters are displayed in Figure 121 and Figure 122, for the flights #5 (October 1, 1997) and #11 (September 29, 1997), respectively. The "best" retrieval of the chlorophyll concentration is obtained by using the Case 1 water algorithm based on the ratio of reflectances at wavelengths 490 and 560 nm (probably because the calibration of the band at 443 nm is not correct). The Suspended matter concentration is relatively well retrieved by the neural network technique.

Flight	start time (GMT)	stop time (GMT)	mean altitude (meters)	mean zenith angle (degrees)	number of lines
Coastloc #3					
970731a2.nc	10:48:19	11:07:45	2922.37	27.3261	22323
970731a3.nc	11:08:49	11:23:50	2855.65	27.0232	17653
970731a4.nc	11:26:07	11:42:32	2860.68	27.3094	19199
970731b1.nc	13:25:00	13:34:50	2887.44	38.4922	11509
970731b2.nc	13:37:15	13:53:17	2873.40	40.8118	18861
970731b3.nc	13:54:56	14:06:25	2862.86	43.2611	13465
970731b4.nc	14:08:07	14:21:10	2662.25	42.4659	15311
970802a1.nc	08:50:55	09:00:50	2800.43	39.7811	11591
970802a2.nc	09:02:37	09:16:10	2849.74	37.8007	15911
970802a3.nc	09:18:09	09:27:42	2799.08	35.9144	11157
970802a4.nc	09:29:17	09:43:03	2816.56	34.1933	16115
970802a5.nc	09:44:53	09:54:11	2813.35	32.5824	10853
970802a6.nc	09:55:50	10:09:20	2788.66	31.1744	15853
970802a7.nc	10:11:24	10:20:35	2860.57	29.9029	10731
970802a8.nc	10:23:44	10:36:10	2859.21	9.80539	14575
970802b1.nc	12:54:05	13:06:56	2672.79	35.3977	15133
970802b2.nc	13:08:34	13:20:24	2653.77	37.2768	12221
970802b4.nc	13:36:15	13:47:58	2714.80	41.2880	12099
970802b5.nc	13:50:14	14:01:44	2687.78	43.4405	11867

ACRI - LPCM - SAI - U. Oldenburg
NIOZ - U. Trondheim - FUB - PML - GKSS

coastlooc #4					
970929a3.nc	10:51:20	11:03:56	2938.71	46.2517	12431
970929a5.nc	11:21:33	11:34:34	2900.53	45.6359	12851
970929a7.nc	11:52:10	12:04:27	2885.65	46.0480	12115
970929a8.nc	12:07:33	12:18:55	2865.05	46.6194	11201
970929a9.nc	12:21:58	12:34:15	2935.01	47.4099	12107
970929ab.nc	12:49:25	13:02:08	2899.22	49.4512	12545
970930a4.nc	10:43:22	10:56:05	3258.36	46.9256	10825
970930a5.nc	10:59:17	11:10:27	3235.78	46.3715	9485
970930a7.nc	11:39:19	11:50:15	3577.78	46.1209	9285
970930aa.nc	12:22:11	12:33:45	3581.21	47.7902	9831
970930ab.nc	12:36:48	12:47:00	3555.64	48.7137	8659
971001b5.nc	11:16:00	11:29:48	3384.96	46.3884	11757
971003b1.nc	13:52:31	13:55:00	3227.08	58.8297	2003
971003b2.nc	13:37:01	13:45:32	3304.36	57.3251	7205
971003b3.nc	13:22:06	13:32:49	3304.35	55.6579	9095
971003b4.nc	13:09:09	13:19:09	3329.43	54.1732	8481
971003b5.nc	12:55:57	13:05:50	3328.50	52.8085	8383
971003b6.nc	12:29:30	12:38:43	3305.16	50.4761	7809
971003b7.nc	12:42:20	12:52:37	3265.86	51.5582	8731
coastlooc #6					
1t0912s.nc	09:45:12	09:56:09	702.178	53.5078	15305
2at0912s_am.nc	09:19:51	09:35:46	691.391	55.4842	22345
2at0912s_pm.nc	17:13:55	17:29:19	1400.21	84.3173	21613
2t0912s.nc	16:48:13	17:06:20	1393.87	80.6115	25595
3t0912s.nc	16:27:23	16:39:17	1392.90	76.8743	16655
11w0917s.nc	08:04:04	08:10:04	1640.91	65.0842	7759
17w0920s.nc	12:45:12	12:52:50	1552.89	55.7535	10755
18w0920s.nc	13:04:58	13:05:37	1528.26	57.1027	845
6w0917s.nc	07:33:04	07:44:10	1760.06	68.7890	15513
7w0917s.nc	12:48:53	12:57:14	1628.77	54.8779	9973
IIIibish0925s.nc	13:00:06	13:04:34	2192.96	60.9763	5595
IIIlh0925s.nc	09:47:46	09:52:09	2262.19	56.7506	6143
IIIh0924s.nc	10:19:43	10:23:38	782.708	55.0817	4821
IVh0925s.nc	13:10:47	13:14:00	2198.59	61.8813	4341
IVh0926s.nc	10:42:52	10:50:32	2149.07	55.6446	10111
Ih0924s.nc	10:28:50	10:33:01	782.914	54.7800	5845
Vh0926s.nc	10:54:49	11:00:26	2156.72	55.7183	7957
bh0925s.nc	09:34:45	09:43:00	2240.86	57.1247	11473
ch0923s.nc	11:19:39	11:28:01	335.304	54.4488	11639
ch0924s.nc	13:30:35	13:38:14	791.278	63.5816	9939
dh0925s.nc	09:25:36	09:30:04	2040.37	57.8029	5577

Table 24. Some information about the CASI flights performed during the COAST/OOC #3, #4, and #6 campaigns

2.5.2.2. Conclusions and perspectives

The COAST/OOC program has provided the opportunity to perform many CASI flights, which were carried out simultaneously to *in situ* sampling (ship or helicopter) of many radiometric (*e.g.*, irradiances), optical (*e.g.*, absorption and scattering coefficients), and “geophysical” (*e.g.*, pigments and sediments) properties. It was therefore legitimate to expect validation of the MERIS algorithms with such a set of concurrent airborne and *in situ* observations. It is, to our knowledge, the first time

ACRJ - LPCM - SAI - U. Oldenburg
NIOZ - U. Trondheim - FUB - PML - GKSS

that CASI measurements are used for validating a series of algorithms designed for the processing of satellite observations. This task has represented a huge amount of work, including gathering of several codes (the breadboard prototypes of PML and GKSS), adaptation and test of an existing code (the LPCM breadboard prototype), generation of a near-real time processing software for use on the spot, data acquisition and post-processing, and so on

Despite this very significant effort, the results presented in the previous sections quite obviously show that the objective of validating MERIS algorithms by using CASI observations has not been reached. One reason is the very bad weather conditions encountered during COAST/OOC #6, which explain why the results are nearly unexploitable. For the COAST/OOC #4 campaign, the conditions were more favourable and the flight altitude was higher, so that results are exploitable.

The following recommendations are therefore put forward here, if future airborne operations are planned for validation of satellite algorithms :

- If the airborne operations are performed during a mission whose objectives are wider than the sole flights, then devote at least a few days to these operations, which should become the priority during this period. This should allow to more closely match the *in situ* sampling and the aircraft measurements.
- If a mission is entirely devoted to aircraft operations, plan it for a period and a location where very nice weather is likely.
- Perform the flights at the highest possible level (even the 10000 feet max altitude of the Cessna plane used here seems insufficient). This is important to minimise surface effects, to maximise the atmospheric contribution (in order to be close to a satellite configuration), and to minimise geo-location difficulties (it is easier to match *in situ* measurements with larger pixels, in principle). It is an error to believe that low altitude flights will allow to directly test the “in-water” algorithms (*e.g.*, chlorophyll retrieval from reflectance ratio), because the data are too much contaminated by surface effects.
- Avoid flying with the sun on one side of the aircraft (problems due to specular reflection becoming too important), but rather with the sun behind it or just in front. If matching with *in situ* data is aimed at, this constraint should be difficult to meet, because the position of water sampling would have to be adjusted as a function of the flight hour.
- Obviously perform the best possible calibration of the instrument.

*ACRJ - LPCM - SAI - U. Oldenburg
NIOZ - U. Trondheim - FUB - PML - GKSS*



Final Report
ENV4-CT96-0310
03 January 2000

Page: 183

- Introduce the minimum modifications in the algorithms, as compared to the satellite algorithms, otherwise there is no longer the possibility of validating anything but the airborne algorithms themselves !!
- If possible and proven to be useful, perform the same flight track at several altitudes from the highest one down to near the surface (verification of the atmospheric correction).

In summary, if CASI is probably suited for performing algorithm validation experiments, the way to deploy it for a successful processing and interpretation of data remains to be improved.

*ACRJ - LPCM - SAI - U. Oldenburg
NIOZ - U. Trondheim - FUB - PML - GKSS*

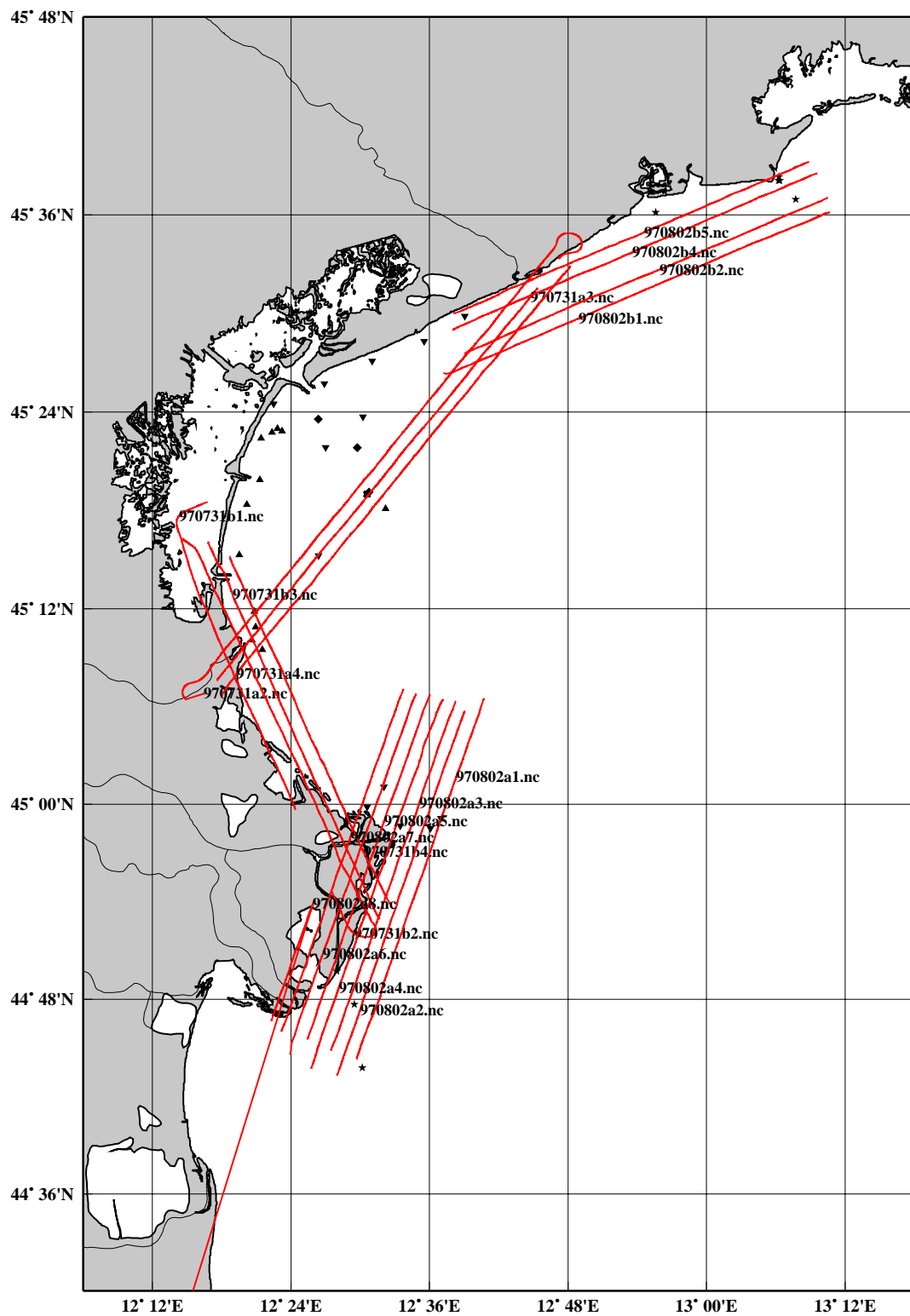


Figure 107. Location of flight tracks during COAST/OOC #3, along with in situ sampling sites (symbols).

ACRJ - LPCM - SAI - U. Oldenburg
NIOZ - U. Trondheim - FUB - PML - GKSS

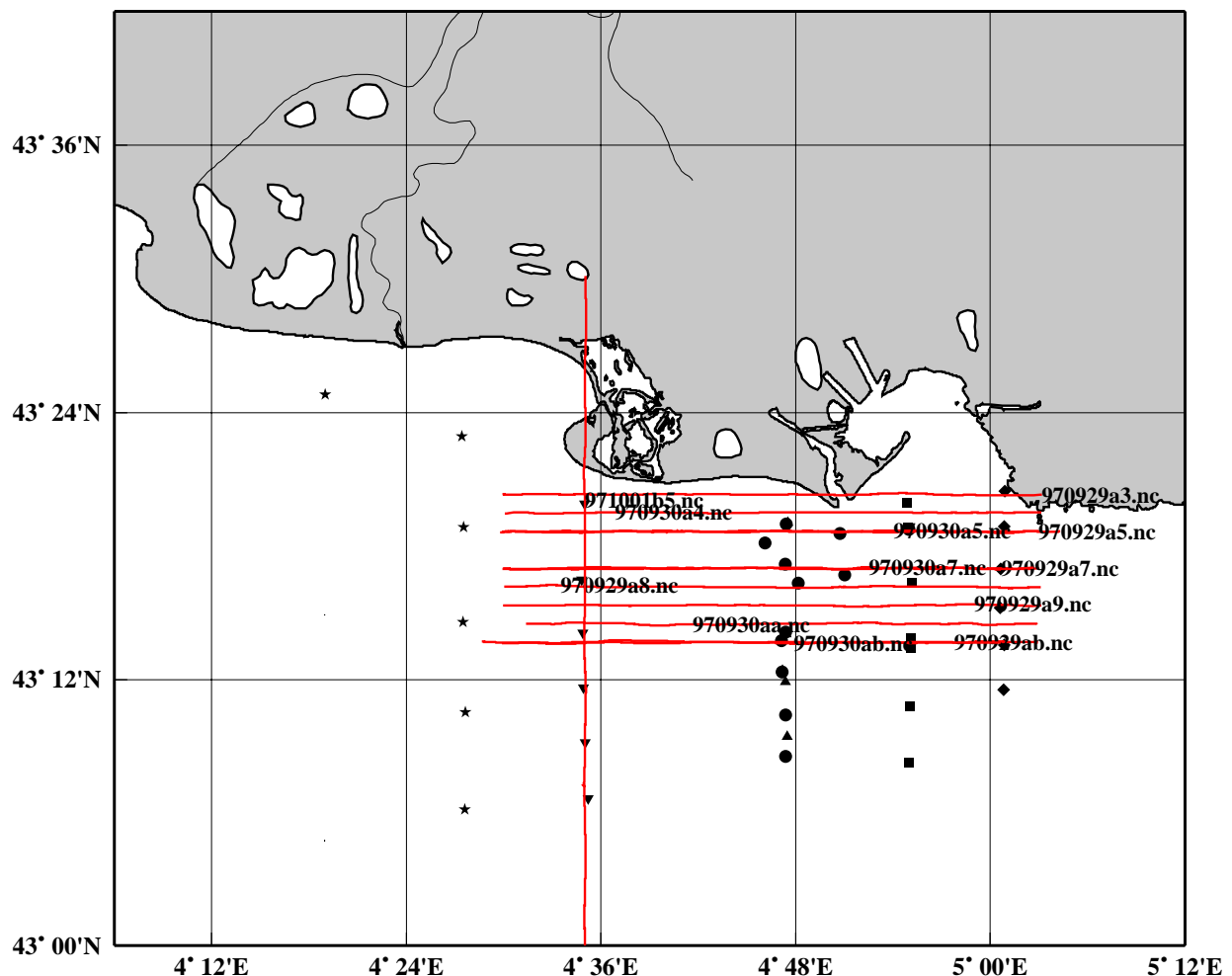


Figure 108. Location of flight tracks during COAST/ OOC #4 (Rhône delta), along with in situ sampling sites (symbols).

ACRJ - LPCM - SAI - U. Oldenburg
NIOZ - U. Trondheim - FUB - PML - GKSS

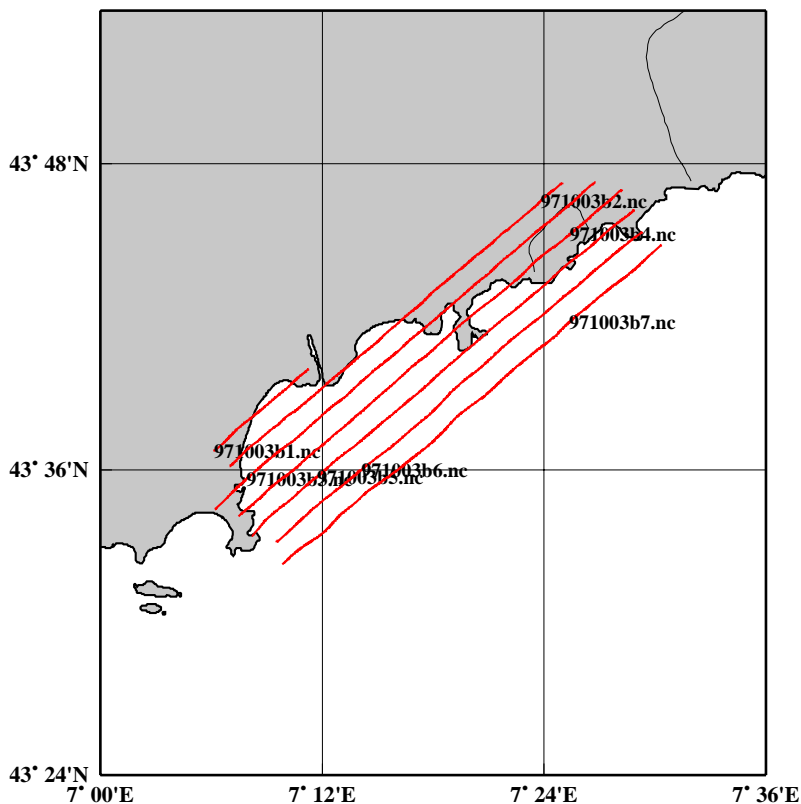


Figure 109. Location of flight tracks during COAST/ OOC #4 (Nice area), along with in situ sampling sites (symbols).

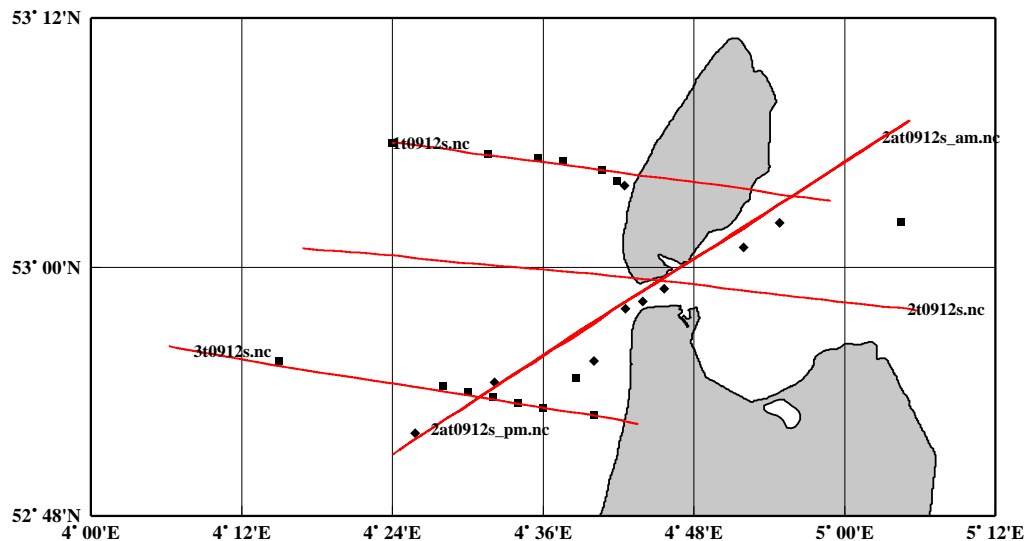


Figure 110. Location of flight tracks during COAST/ OOC #6 (Tessel site), along with in situ sampling sites (symbols).

*ACRJ - LPCM - SAI - U. Oldenburg
NIOZ - U. Trondheim - FUB - PML - GKSS*

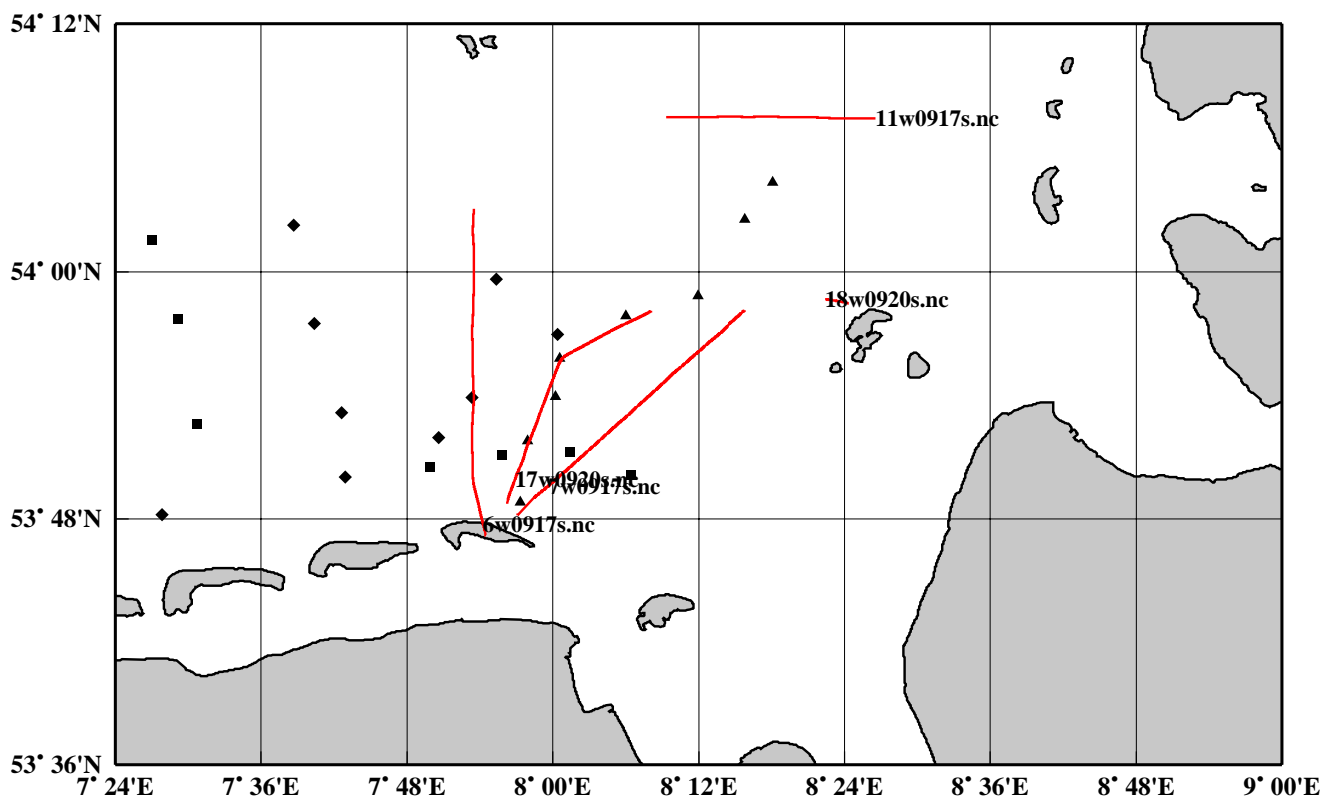


Figure 111. Location of flight tracks during COAST/ OOC #6 (Wilhelshaven), along with in situ sampling sites (symbols).

ACRJ - LPCM - SAI - U. Oldenburg
NIOZ - U. Trondheim - FUB - PML - GKSS

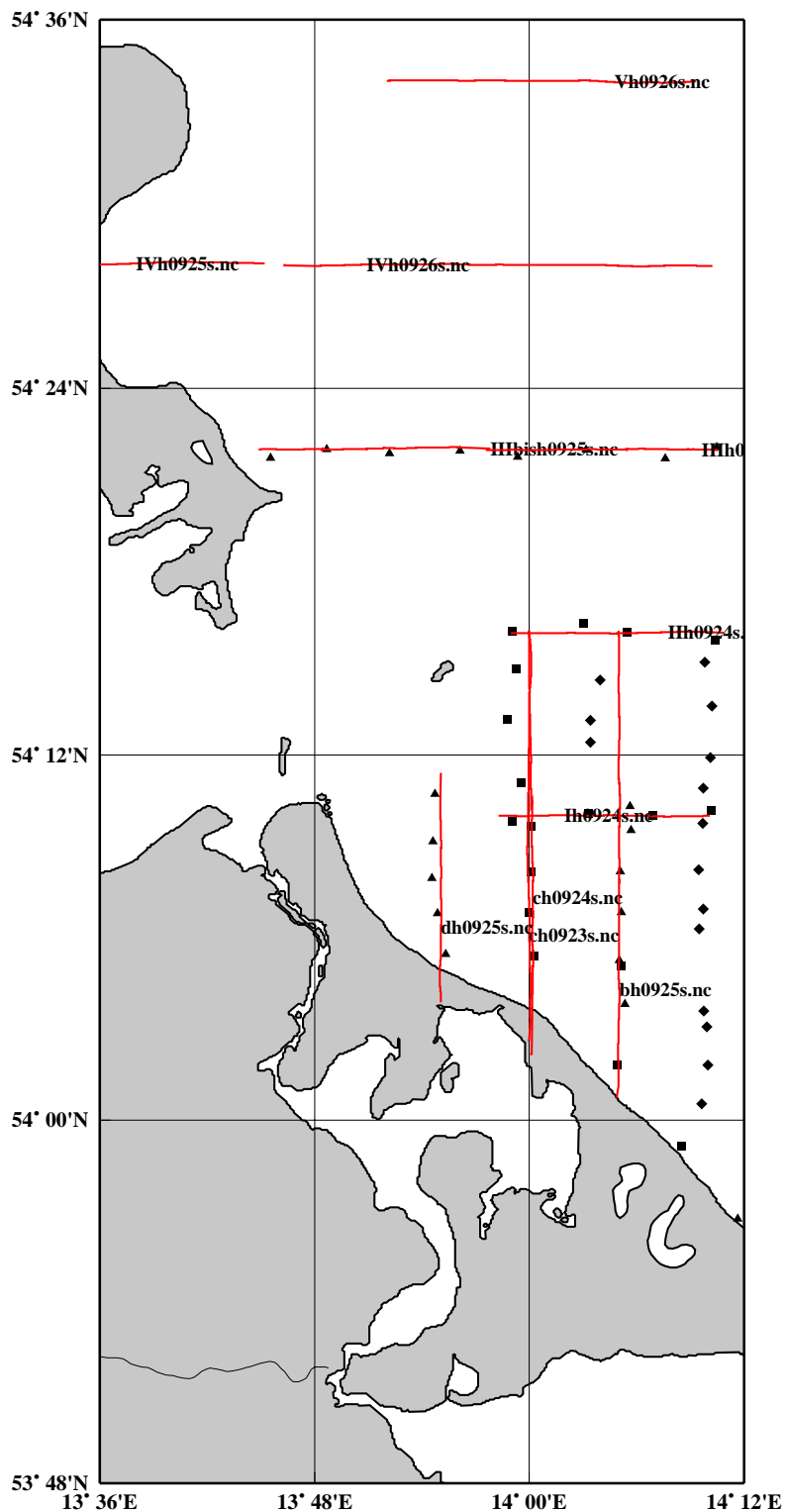


Figure 112. Location of flight tracks during COAST/OOC #6 (Heringsdorff), along with in situ sampling sites (symbols).

ACRJ - LPCM - SAI - U. Oldenburg
NIOZ - U. Trondheim - FUB - PML - GKSS

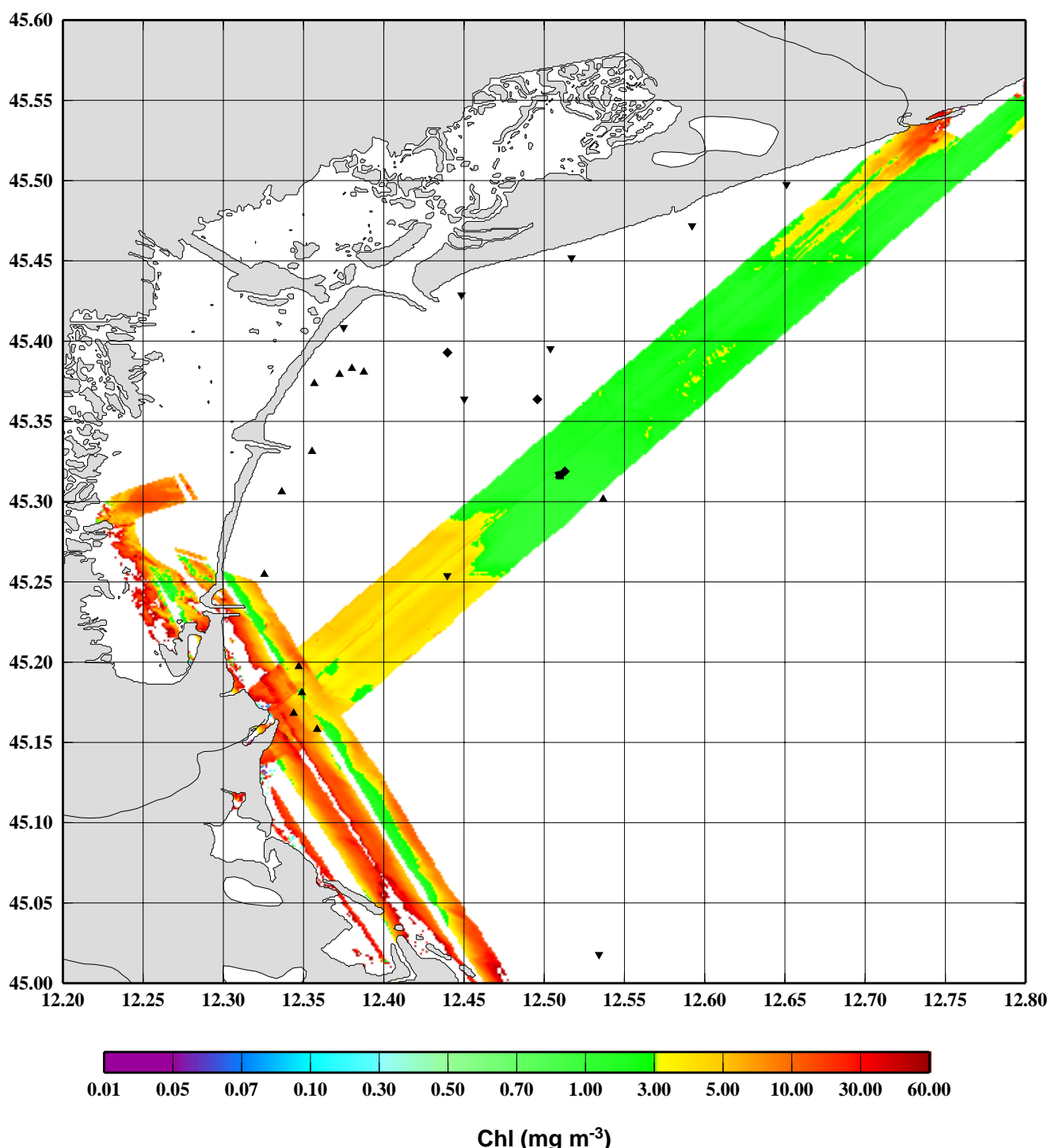


Figure 113. Chlorophyll concentration in the Adriatic (July 31, 1997).

ACRJ - LPCM - SAI - U. OI denburg
NIOZ - U. Trondheim - FUB - PML - GKSS

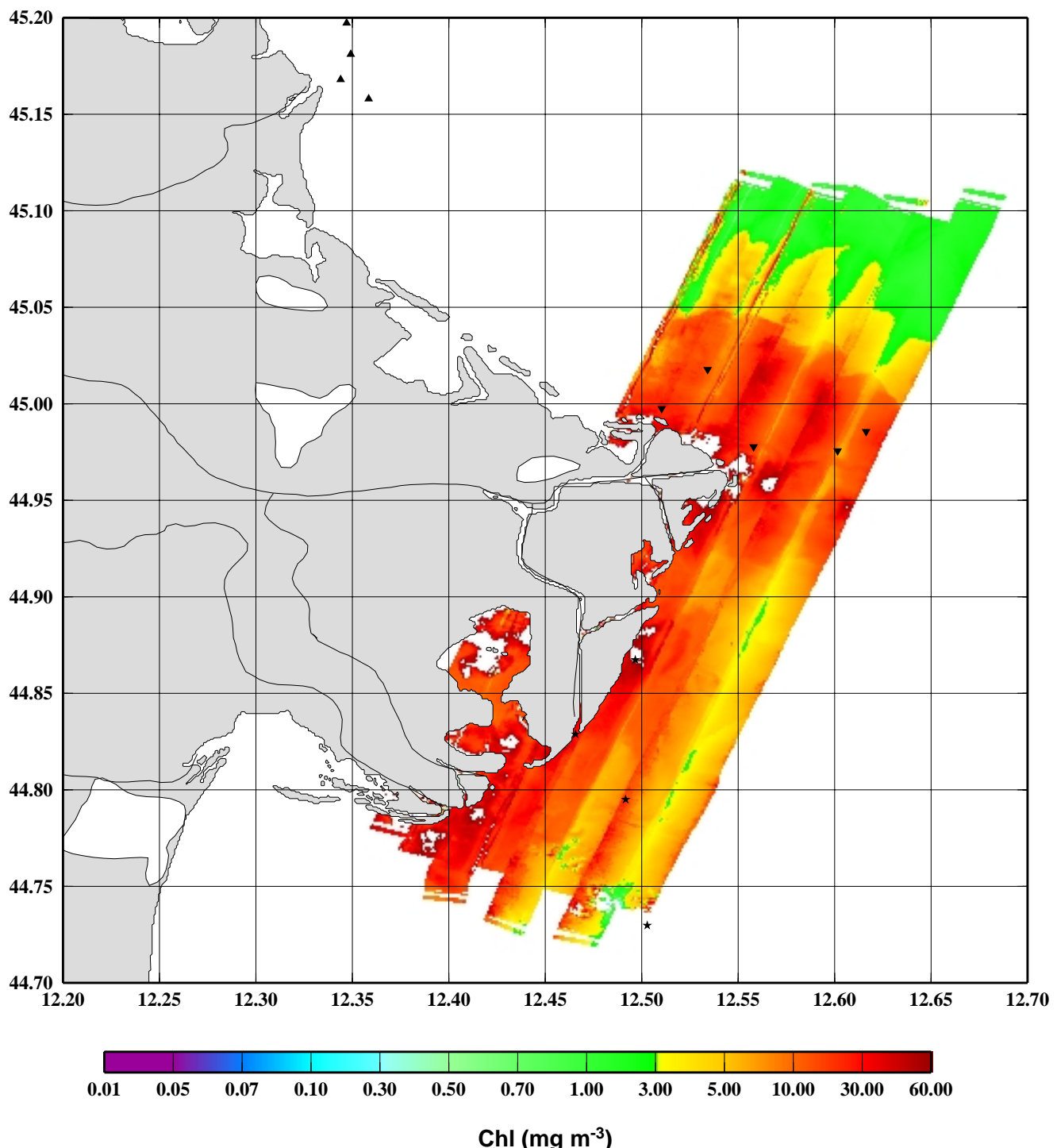


Figure 114. Chlorophyll concentration in the Adriatic (August 2, 1997).

ACRJ - LPCM - SAI - U. Oldenburg
NIOZ - U. Trondheim - FUB - PML - GKSS

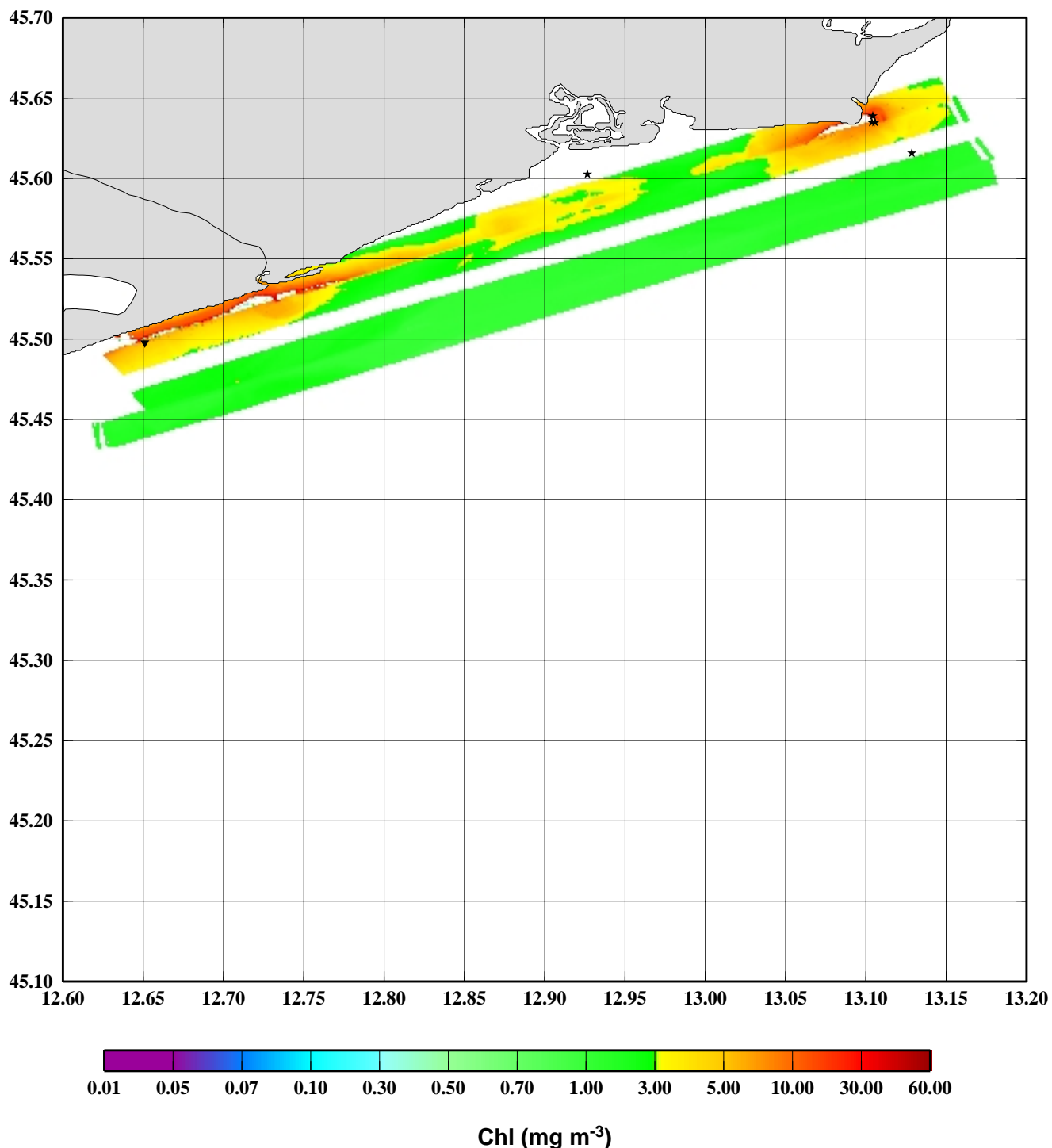


Figure 115. Chlorophyll concentration in the Adriatic (August 2, 1997).

*ACRJ - LPCM - SAI - U. Oldenburg
NIOZ - U. Trondheim - FUB - PML - GKSS*

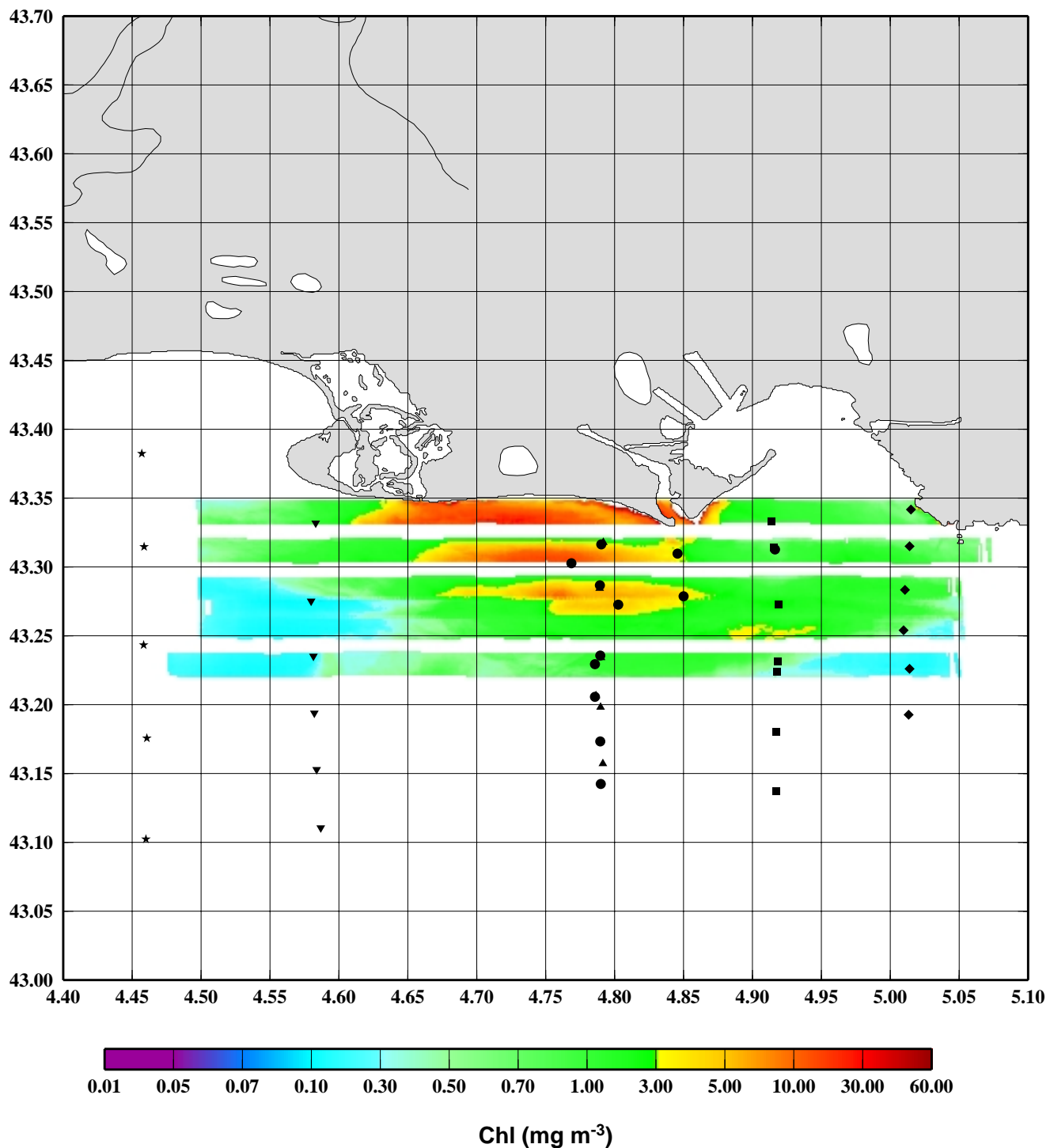


Figure 116. Chlorophyll concentration off the Rhône delta (September 29, 1997).

*ACRJ - LPCM - SAI - U. Oldenburg
NIOZ - U. Trondheim - FUB - PML - GKSS*

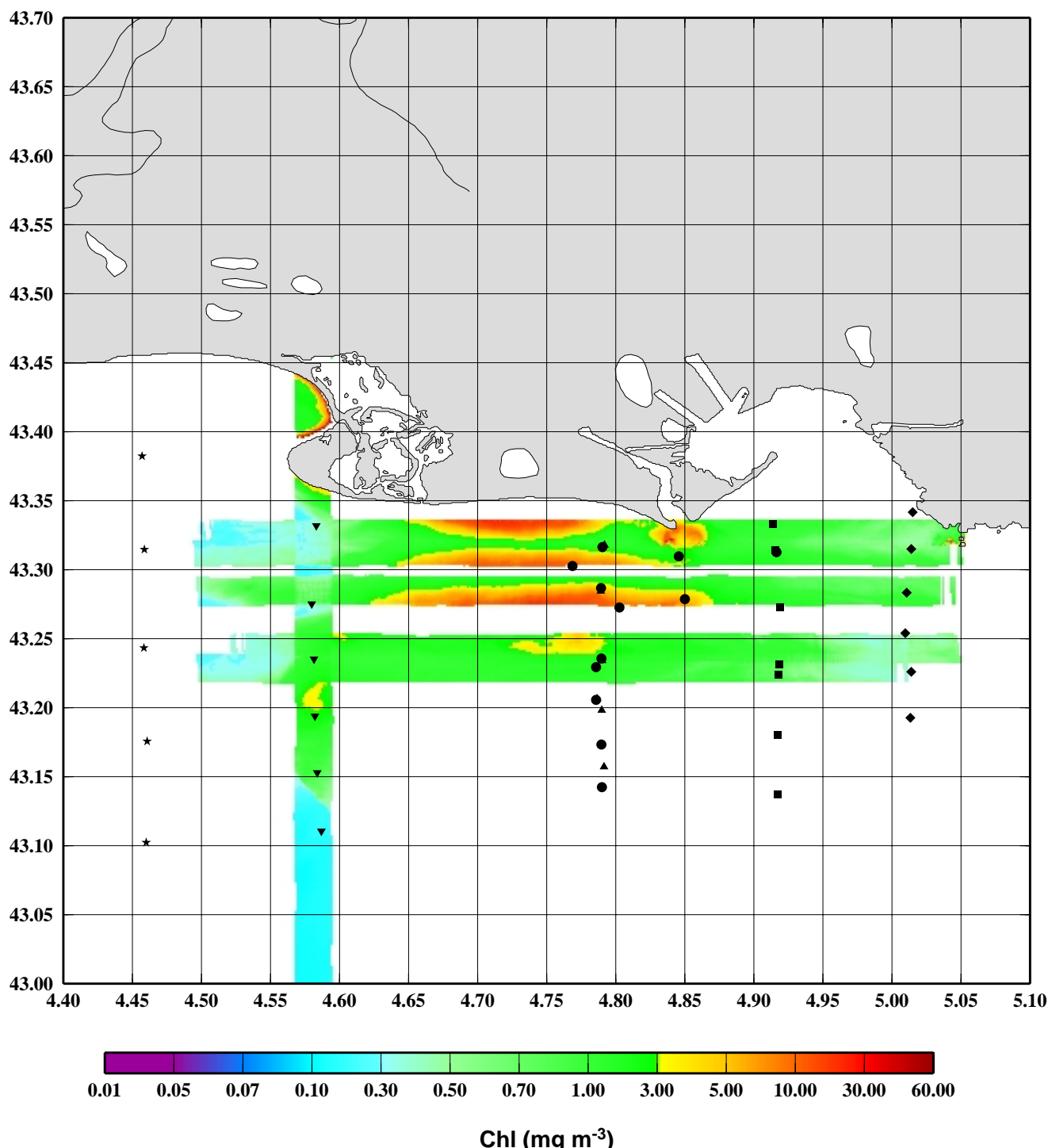


Figure 117. Chlorophyll concentration off the Rhône delta (September 30 and October 1, 1997).

*ACRJ - LPCM - SAI - U. Oldenburg
NIOZ - U. Trondheim - FUB - PML - GKSS*

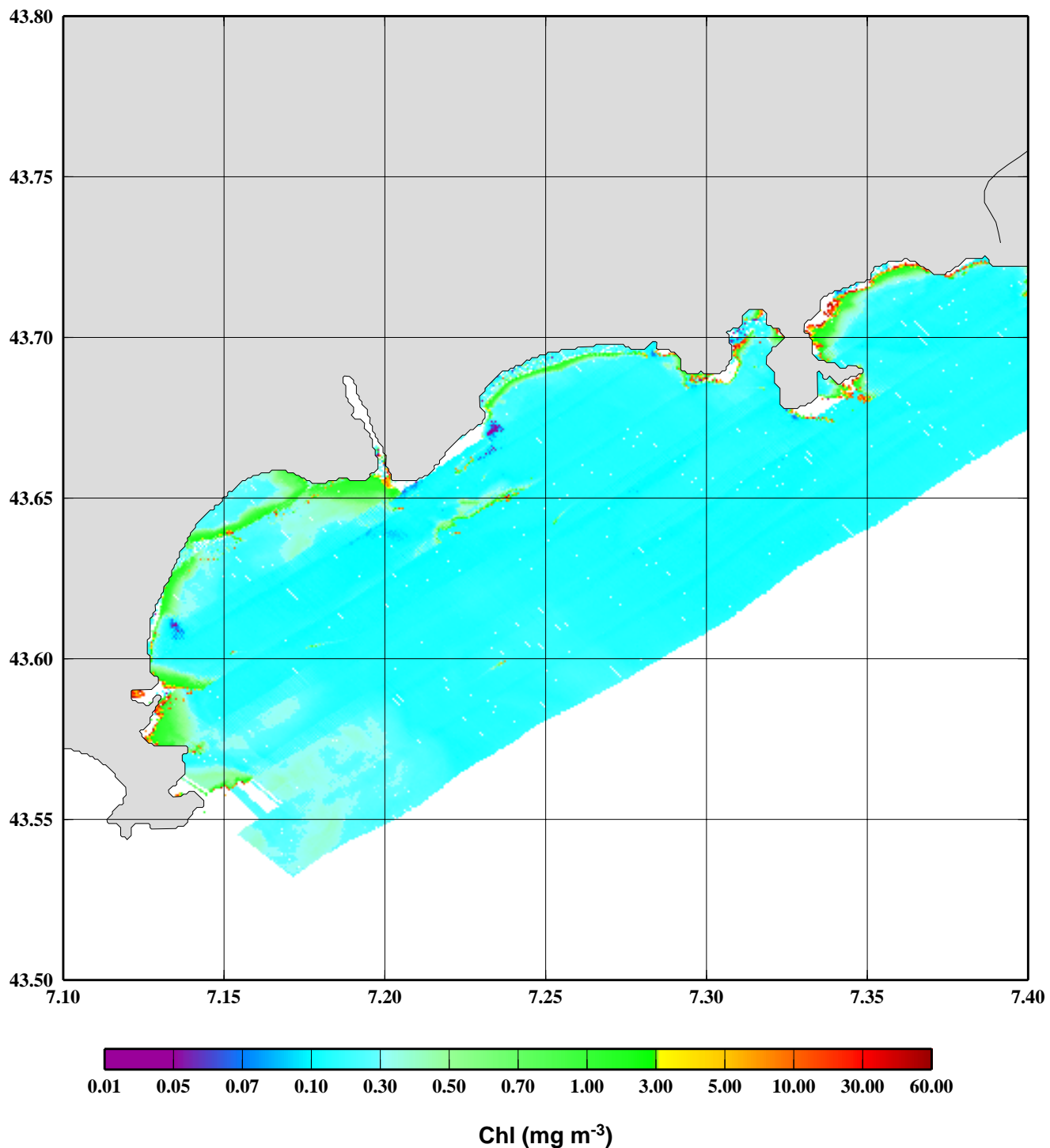


Figure 118. Chlorophyll concentration off the French Riviera, from Antibes to Menton (October 3, 1997).

*ACRJ - LPCM - SAI - U. Oldenburg
NIOZ - U. Trondheim - FUB - PML - GKSS*

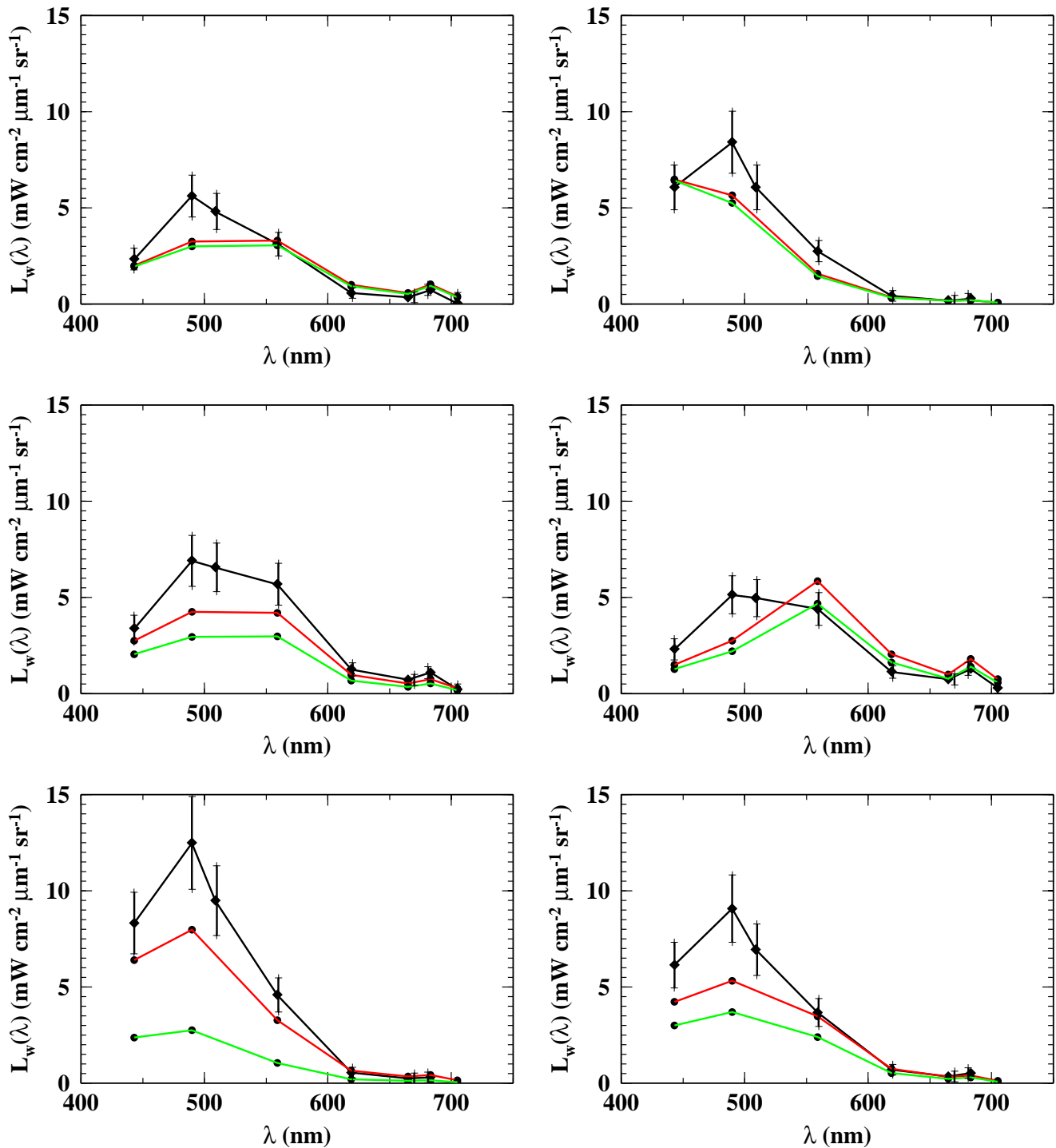


Figure 119. Water-leaving radiance spectra, either obtained after CASI observations have been atmospherically corrected (black curves, the vertical bars are $\pm 1\sigma$ in a 16x16 pixel square centred on the right position), or calculated from *in situ* information (red curve is when the downwelling irradiance is fully calculated, and the green curve is when it is derived from its measured value,

after correction; see text, section 1.8.4). The data are for the flight #5 (COAST/OOC #4, October 1, 1997).

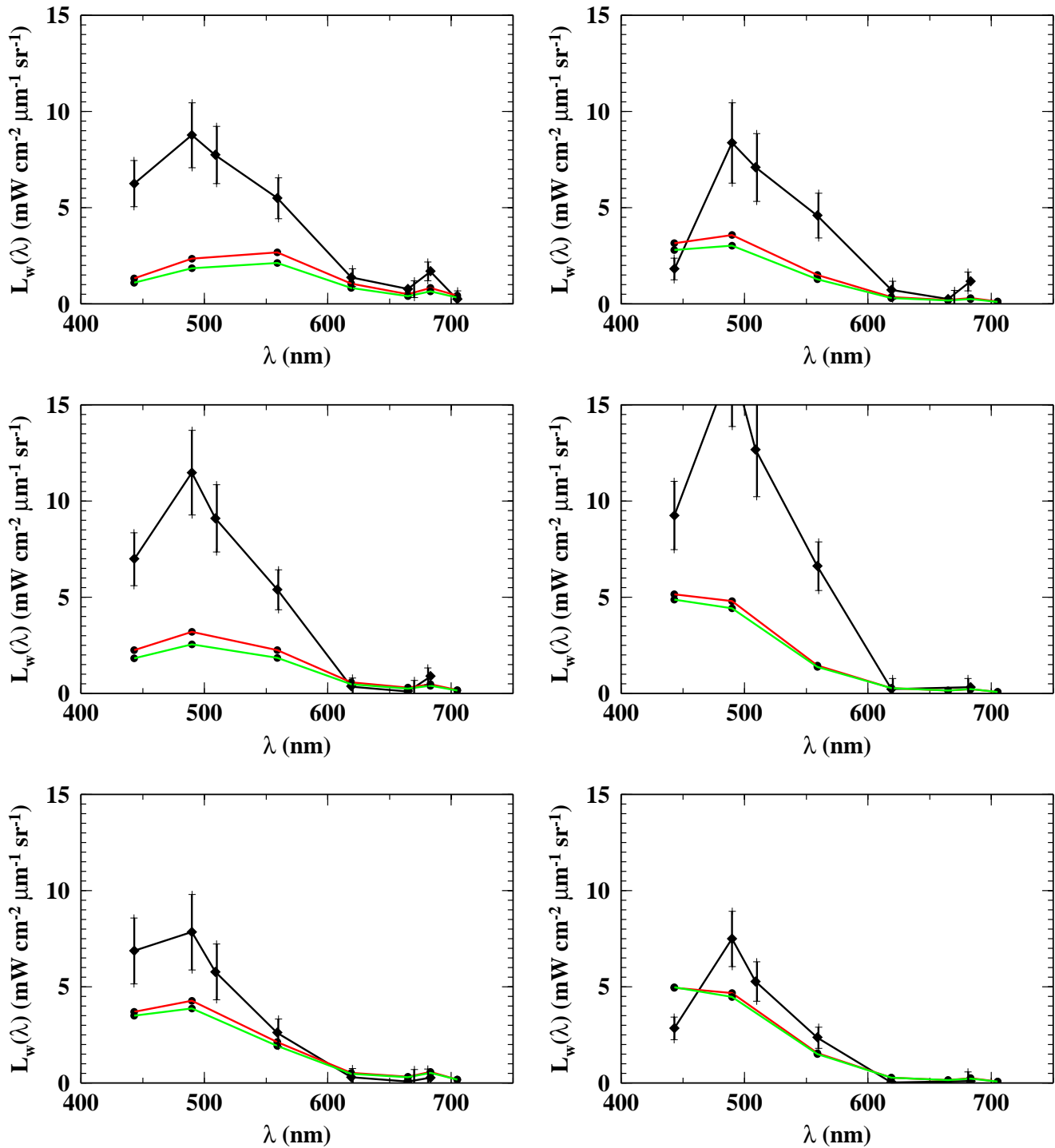


Figure 120. As in Figure 119, but for the flight #11 (COAST/OOC #4, September 29, 1997).

*ACR] - LPCM - SAI - U. Oldenburg
NIOZ - U. Trondheim - FUB - PML - GKSS*

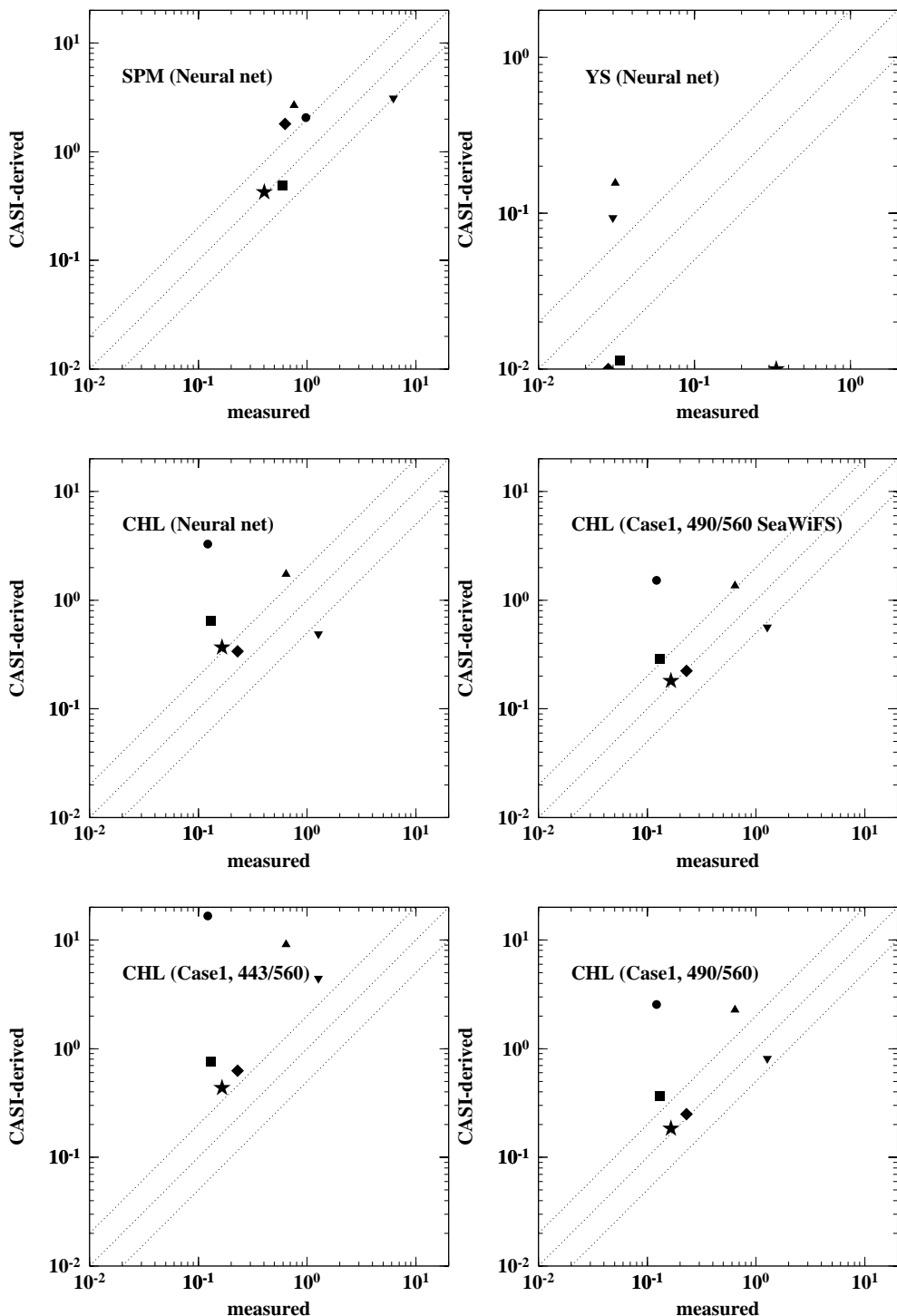


Figure 121. Scatter plots of some parameters, as derived from the CASI processing (vertical axis), and as a function of the value measured *in situ* (horizontal axis). Units are mg m^{-3} for chlorophyll (CHL), g m^{-3} for suspended sediments (SPM), and m^{-1} for yellow substance absorption (YS). The

*ACRJ - LPCM - SAI - U. Oldenburg
NIOZ - U. Trondheim - FUB - PML - GKSS*

data are extracted from the flight #5 on October 1, 1997. The 1:1, 2:1, and 1:2 ratios are shown as dotted lines.

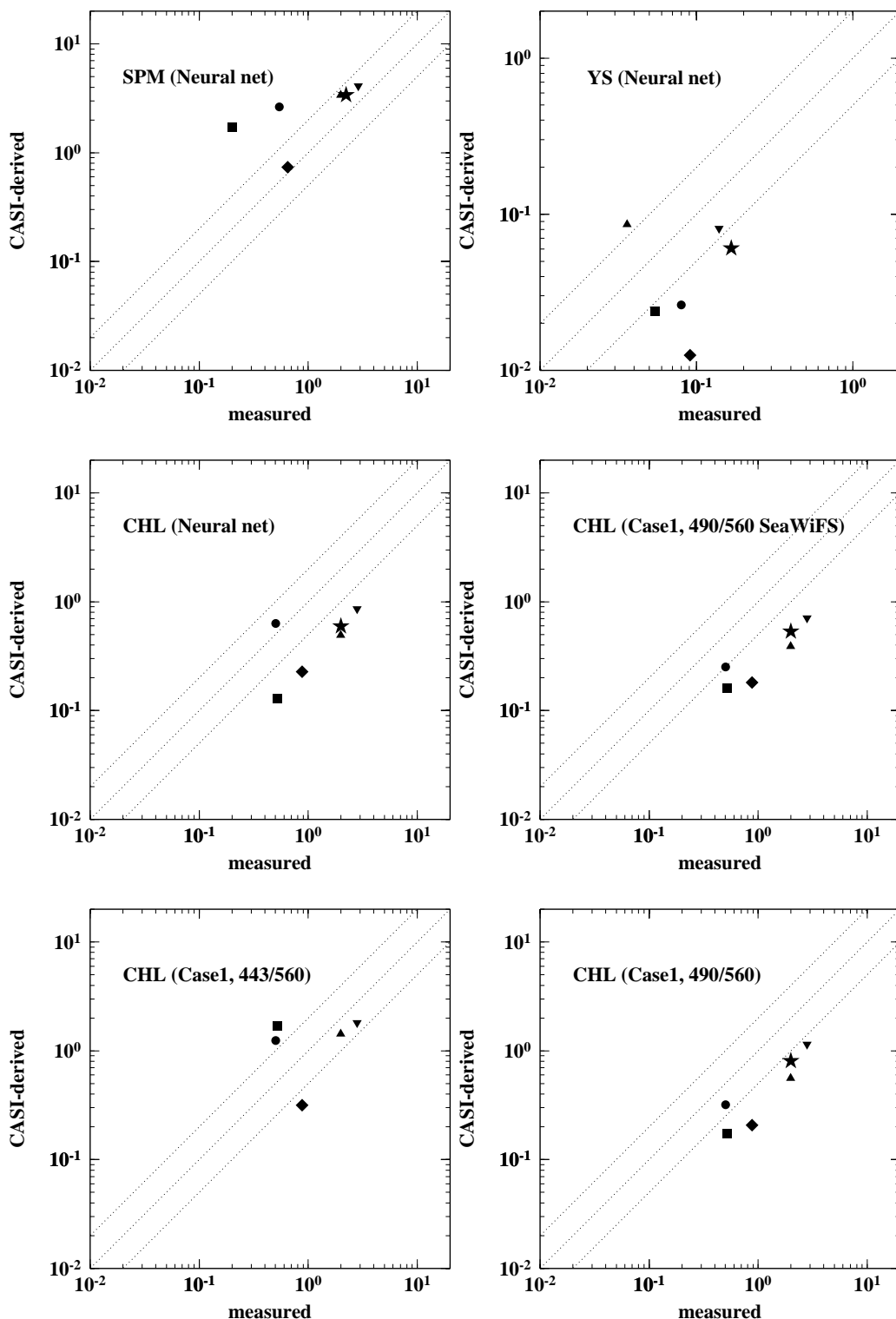


Figure 122. As in Figure 121, but for the flight #11 on September 29, 1997.

*ACRJ - LPCM - SAI - U. Oldenburg
NIOZ - U. Trondheim - FUB - PML - GKSS*



Final Report
ENV4-CT96-0310
03 January 2000

Page: 199

2.5.2.3. Notations

λ : wavelength; nm

$[L_w]_N(\lambda, \theta_s, \theta', \Delta\phi)$: Normalised water-leaving normalised radiance; mW cm⁻² sr⁻¹ μ⁻¹

F_0 : Solar irradiance; mW cm⁻² μ⁻¹

ε_c Correction factor applied to $F_0(\lambda)$, and accounting for the changes in the Earth-sun distance. It is computed from the eccentricity of the Earth orbit, $e = 0.0167$, and from the

$$\text{day number } D, \text{ as } \varepsilon_c = \left(1 + e \cos\left(\frac{2\pi(D-3)}{365}\right)\right)^2$$

$\Re(\theta')$: Term accounting for all the reflection and refraction effects at the air-sea interface; dimensionless

$E_d(\lambda)$: Downward irradiance; W m⁻² μ⁻¹

$E_u(\lambda)$: Upward irradiance; W m⁻² μ⁻¹

$Q(\lambda, \theta_{s,\text{sensor}}, \theta', \Delta\phi)$; ; Q factor (*i.e.*, E_u/L_u) sr

$f_{1,\text{sensor}}$; dimensionless

$f_{1,\text{in situ}}$; dimensionless

$R(\lambda, \theta_{s,\text{in situ}})$: Measured reflectance just below sea surface, *i.e.* $[(E_u(0^-) / (E_d(0^+)) * 0.96)]$, with a solar zenith angle $\theta_{s,\text{insitu}}$; dimensionless

$a(\lambda)$: Absorption coefficient (measured with WetLabs AC9 instrument); m⁻¹

$b(\lambda)$: Scattering coefficient (measured with WetLabs AC9 instrument); m⁻¹

$b_w(\lambda)$: Pure sea water scattering coefficient; m⁻¹

$\eta(\lambda)$: molecular to total scattering ratio

$\theta_{s,\text{in situ}}$: solar zenith angle at the time of the COAST/OOC measurement (cosine is $\mu_{s,\text{insitu}}$); degree

ACRJ - LPCM - SAI - U. Oldenburg - NIÖZ - U. Trondheim - FUB - PML - GKSS



Final Report
ENV4-CT96-0310
03 January 2000

Page: 200

$\theta_{s,\text{sensor}}$: solar zenith angle at the time of the SeaWiFS measurement (cosine is

$\mu_{s,\text{sensor}}$); degree

θ_v : Satellite viewing zenith angle (cosine is μ_v); degree

θ' : $\theta' = \arcsin(\sin(\theta_v) / 1.34)$, degree

$\Delta\phi$: Relative azimuth difference angle,; degree

day: day number in the year (from 1 to 365)

$\tau_a(\lambda)$: Aerosol optical thickness

$\omega_a(\lambda)$: Aerosol single scattering albedo (ratio of scattering to extinction)

$p_a(\lambda, \gamma)$ Aerosol phase function (sr^{-1})

where γ^\pm is the scattering angle

$$\cos(\gamma^\pm) = \pm \cos(\theta_s) \cos(\theta_v) - \sin(\theta_s) \sin(\theta_v) \cos(\Delta\phi)$$

P Actual atmospheric pressure (hPa)

P_0 Standard atmospheric pressure = 1013.25 hPa

$t_{\theta_s}(\lambda, \theta_s)$ Irradiance transmittance for a sun zenith angle θ_s dimensionless

$t_{\theta_s}(\lambda, \theta_s) = E_d(0^+) / (\mu_s \epsilon_c F_0)$, where $E_d(0^+)$ is the

downwelling irradiance just above the sea surface

We compute it from Gregg and Carder (1991).

$t_d(\lambda, \theta)$ Diffuse transmittance for angle θ dimensionless

$$t_d(\lambda, \theta) = L_{TOA}(\lambda, \theta_s, \theta_v, \Delta\phi) / L_{0+}(\lambda, \theta_s, \theta_v, \Delta\phi)$$

*ACRJ - LPCM - SAI - U. Oldenburg
NIOZ - U. Trondheim - FUB - PML - GKSS*

2.5.2.4. References

- Bricaud, A., M. Babin, A. Morel, and H. Claustre, 1995, Variability in the chlorophyll-specific absorption coefficients of natural phytoplankton : analysis and parameterisation, *Journal of Geophysical Research* **100**, 13321-13332.
- Bricaud et al., 1999
- Gordon, H. R., and Wang, M., 1994, Retrieval of water-leaving reflectance and aerosol optical thickness over the oceans with SeaWiFS : a preliminary algorithm, *Applied Optics* **33**, 443-452.
- Gregg W.W. and K.L. Carder, 1990. A simple spectral solar irradiance model for cloudless maritime atmospheres. *Limnol. Oceanogr.* **35**, 1657-1675.
- Loisel, H., and A. Morel, 1998, Light scattering and chlorophyll concentration in Case 1 waters : a reexamination, *Limnology and Oceanography* **43**, 847-858.
- Morel, A., and Gentili, B., 1991, Diffuse reflectance of oceanic waters : its dependence on sun angle as influenced by the molecular scattering contribution, *Applied Optics* **30**, 4427-4438.
- Morel, A., and Gentili, B., 1993, Diffuse reflectance of oceanic waters. II. Bidirectional aspects, *Applied Optics* **32**, 6864-6879.
- Morel, A., and Gentili, B., 1996, Diffuse reflectance of oceanic waters. III. implication of the bidirectionality for the remote sensing problem, *Applied Optics* **35**, 4850-4862.
- Pope, R.M., and E. S. Fry, 1997, Absorption spectrum (380-700 nm) of pure water, II, Integrating cavity measurements, *Applied Optics* **36**, 8710-8723.

3. DELIVERABLES

COAST/OOC deliverables are the following:

- Database including apparent and inherent optical properties of European coastal waters, together with data processing tools
- Database including water leaving reflectance data measured from an airborne platform simultaneously with *in situ* measurements of optical properties
- IOPs parameterisations for coastal waters
- Reflectance models
- Ocean colour Band-ratio and inverse modelling algorithms valid for European waters

- Simulator of ocean colour satellite sensors including algorithms developed previously during the present study
- A new sampling platform
- Dissemination and training

4. DEPARTURE FROM THE WORK PLAN

In the Work Plan, work packages were stated as follows:

Workpackage 1: *In situ* measurements and reflectance modelling

Activity A: *In situ* measurements

Activity B: Reflectance modelling

Activity C: Red tides detection

Workpackage 2: Validation of the reflectance model from airborne operations

Activity A: Airborne surveys

Activity B: Validation of the reflectance model (See details in Workpackage #1)

Activity C: Detection of red tides (See details in Workpackage #1)

Workpackage 3: Simulations

Activity A: Implementation of the reflectance model into an ocean colour simulator

Activity B: Determination of algorithms

Workpackage 4: Network development

Activity A: Implementation of an ocean colour video server

To simplify and rationalise the presentation, these activities are gathered within the 6 following themes:

1. *In situ* measurements (WP 1-Act. A in Work Programme)
2. Airborne measurements (WP 2-Act. A)
3. Reflectance modelling (WP 1-Act.B, WP 2-Act.B)
4. Red tides detection (WP 1-Act.C, WP 2-Act.C)

*ACRJ - LPCM - SAI - U. Oldenburg
NIOZ - U. Trondheim - FUB - PML - GKSS*

5. Simulator and algorithms (WP 3)

6. Video Server (WP 4)

1. In situ measurements (WP 1-Act. A) *In situ* measurements operations have been successfully completed in September 1998. Relatively to the objective initially stated (5 areas with 150 stations / area), the geographical coverage actually achieved is larger (see Figure 2) while *ca.* 60% of the aimed number of station was achieved. 55% of the stations were sampled using helicopter; the remaining was done onboard ships. The completion of *in situ* sampling was late relatively to the initial schedule. In fact, it was decided during the kick-off meeting that the effort on this activity would be spread over 2 years. Globally, the *in situ* measurements activity has been highly successful. An unique data set has been developed using an innovative approach (helicopter). However, the effort deployed for this activity was larger than initially planned. This is partly due to difficulties encountered in the development of the helicopter approach. A first version of the *in situ* data set has been delivered on an optical Compact Disk to the partners in January 1999, by the co-ordinator. It includes all data from the *in situ* profilers and a file containing results from analyses performed on surface water samples, together with surface measurements from optical profilers. An updated CD is delivered with the present report.

2. Airborne measurements (WP 2-Act. A) In the frame of the Workpackage 2, Activity A, it was initially planned to conduct airborne measurements using a passive colour sensor (CASI) and an active sensor (LIDAR). The first one is used to simulate an ocean colour sensor while the latter is supposed to provide sea truth (in fact proxies of chlorophyll, coloured dissolved organic mater and sediment concentrations). CASI measurements were performed during the three helicopter campaigns over sites simultaneously visited for *in situ* measurements. CASI was set to mimic MERIS channels in the visible and near-IR. A total of 70 flight hours were spent for measurements and transits. LIDAR could not be flown. The foreseen instrument, which belongs to the German Department of Environment, was not available during our campaigns; it was more difficult than expected to obtain flight time. Nevertheless, it must be stressed that the comparison between CASI and *in situ* measurements was by far the most important achievement of this activity, which has been highly successful until now.

3. Reflectance modelling (WP 1-Act.B, WP 2-Act.B) Reflectance modelling represented the largest effort during the last year of the project. Reflectance modelling is a permanent activity for several of the COAST/OOC partners: LPCM, JRC, GKSS, PML. The COAST/OOC data set was a master piece in the progress of reflectance modelling. It started being used as soon as the first version was delivered (Version 0.0 in January 1999). The CASI data have started being used in December 1998 for the validation of ocean colour algorithms dedicated to the ESA sensor MERIS. These activities allowed to deliver a new reflectance model valid for European coastal waters.

4. Red tides detection (WP 1-Act.C, WP 2-Act.C) One COAST/OOC objective was to examine the possibility of detecting red tides with ocean colour remote sensing. This objective was relying upon the opportunity to measured sea water optical properties during red tide events. Such an event was not encountered during COAST/OOC. Therefore, this objective could not be fulfilled. The main reason why we were not successful in observing red tides is that the first COAST/OOC objective was: “To

*ACRI - LPCM - SAI - U. Oldenburg
NIOZ - U. Trondheim - FUB - PML - GKSS*

produce a large data set of the inherent optical properties of the main classes of optically active substances in European coastal waters ... the most extensive sampling grid ...". On contrary, red tide tracking implies a specific strategy ("standby" approach) on well identified sites and period known for red tide occurrence. During COAST/OOC we tried to cover the largest area along European coasts. We worked on sites known to be representative of a region in terms of phytoplankton, organic matter and sediments. The working zone had to be close to the laboratories of one of the COAST/OOC partners for logistic purposes. Thus, constraints of COAST/OOC first objective and of red tide detection were not compatible or, at least, could not be merged in an optimal way.

5. Simulator and algorithms (WP 3) A simulator of the MERIS ground segment, developed by the MERIS Expert Support Laboratory (co-ordinated by ACRI and to which take part LPCM, PML, FUB and GKSS), was developed for processing the CASI data. This simulator allowed:

- To apply atmospheric correction to CASI data
- To test the algorithms developed in the frame of COAST/OOC
- To test the MERIS ground segment prototype

6. Video Server (WP 4) It was initially plan in the frame of COAST/OOC to develop a WWW video server in order to disseminate ocean colour images and products. This task was mostly motivated by the possibility of developing a commercial product from the COAST/OOC activities. Since then, such kind of server has emerged, based on data provided by the ocean colour sensors MOS (DLR), OCTS (NASDA), POLDER (CNES) and SeaWIFS (NASA). Data are often delivered for free or, if one must pay for, they are delivered directly by the data provider (space agencies, sensor owners or reception station) at low cost. We therefore believe that this COAST/OOC objective is obsolete. We do not believe anymore that such a video server could be profitable. It was thus quitted.

Although some of the initial COAST/OOC objectives have been quitted (red tide detection and video server), the initial budget asked for was nevertheless fully justified. In terms of *in situ* sampling effort, the fact of not sampling red tides changed nothing.

The effort that was dedicated to the development of the video server, mostly by ACRI (the co-ordinator), has been diverted to data processing and the development of the data archive. These two tasks complemented those initially attributed to ACRI: co-ordination and "design of the image processing frame". ACRI has developed specific codes for processing and merging data from the optical profilers. These tasks were not identified in the Work Programme and were essential to the project.

5. CONCLUSIONS & EXPLOITATION PLAN

The COAST/OOC project has highly contributed to improve our knowledge on coastal waters optical properties. The data gathered during this project allowed to attempt successfully

*ACRI - LPCM - SAI - U. Oldenburg
NOZ - U. Trondheim - FUB - PML - GKSS*

parameterisations of coastal waters IOPs, to develop reflectance models (forward models) valid for European waters, and to improve ocean colour algorithms for coastal waters. COAST/OOC allowed to prepare the ground for the development of operational algorithms. The COAST/OOC data revealed some regional specificities in IOPs. Regional algorithms will certainly be more efficient than global ones in coastal zones. To develop regional algorithms, specific sampling efforts will be necessary to derive trends in IOPs with very small scatter.

COAST/OOC has been especially successful in supporting the development and improvement of ocean colour algorithms dedicated to coastal waters. The most concrete benefit for users will be the availability of coastal products derived from the processing of the ESA MERIS sensor, which will be launched on June 2001 (see <http://envisat.estec.esa.nl/>).

The COAST/OOC data set will be made available to the public on October 1st, 2001. The ocean colour algorithms improved using COAST/OOC data will be definitively implemented within the MERIS processing during year 2000. Meanwhile, all COAST/OOC partners will be involved in the publication of their work.

The COAST/OOC data base will certainly be an important research tool during the next years for the whole international community working on coastal ocean colour remote sensing. This contribution makes COAST/OOC a very successful project.

6. ANNEXES

6.1. SUN-INDUCED CHLOROPHYLL FLUORESCENCE ALGORITHM

**The potential of sun-induced chlorophyll fluorescence
for the remote retrieval of phytoplankton in
European coastal and open ocean waters**

Frank Fell¹

*Freie Universität Berlin, Institut für Weltraumwissenschaften,
Fabeckstraße 69, 14195 Berlin, Germany
fell@amor.met.fu-berlin.de*

Marcel Babin and Hervé Claustre

*CNRS et INSU, Laboratoire de Physique et Chimie Marines,
BP 08, 06238 Villefranche-sur-mer Cedex, France
marcel@obs-vlfr.fr, claustre@obs-vlfr.fr*

Massimo Ferrari

*Joint Research Center, SAI, 21020 Ispra, Italy
massimo.ferrari@jrc.it*

Vincent Fournier-Sicre and Grigor Obolensky

*ACRI S.A., BP 234, 06904 Sophia Antipolis, France
go@acri.fr, vfs@acri.fr*

Running head: Remote retrieval of phytoplankton from SICF

¹ _____ corresponding author

Acknowledgments

This work was supported by the Commission of the European Communities (CEC) through a Training and Mobility of Researchers (TMR) scholarship for FF. The COASTIOOC programme was financed by CEC through the contract ENV4-CT96-0310. The ALMOFRONT 2 campaign was funded by the *Centre National de Recherche Scientifique* (CNRS) in the frame of the French contribution to the Joint Global Ocean Fluxes (JGOFS) programme.

Ship time was made available by the CNRS (*N/O Thétys 2*), by Ifremer (*N/O L'Atalante*) and by *Reedereigemeinschaft Forschungsschiffahrt GmbH* (*FS Victor Hensen* and *FS Poseidon*). The authors would like to thank the crews of the research vessels as well as the helicopter team of the *Commerc'air* company combining professional excellence with a very decent sense of humour which made all work a real pleasure. The assistance of the Plymouth Marine Laboratory (PML), the *Nederlandse Instituut voor Onderzoek der Zee* (NIOZ) and the *Universität Oldenburg* regarding the collaboration with local authorities is gratefully acknowledged.

Abstract

During a number of oceanographic campaigns performed in 1997 and 1998 in different European coastal and open ocean waters, measurements of the in-water light field and chemical analyses on simultaneously collected surface water samples were combined to derive an algorithm relating the sun-induced chlorophyll fluorescence to the combined concentration of chlorophyll-*a* and phaeophytin. The algorithm allows the remote retrieval of these pigments using airborne or spaceborne measurements of the ocean colour for water types ranging from clear case-I waters to turbid case-II waters.

Introduction

The spaceborne determination of the water constituents in the upper ocean layer is based on the information contained in the spectral signature of the water leaving radiance. For water the so-called "case-I" waters, the optical properties of which are essentially determined by phytoplankton and their degradation products, empirical or semi-empirical algorithms are successfully used to relate the water leaving radiance at two or more wavelengths to the chlorophyll concentration [11,7,14]. These algorithms fail in so-called "case-II" waters, where the water colour is additionally influenced by sediments or coloured dissolved organic matter (CDOM) of exogenous origin.

In the near future, spaceborne measurements of the ocean colour in the spectral range of the chlorophyll-*a* fluorescence will become available through a new generation of instruments such as NASA's Moderate Resolution Imaging Spectroradiometer (MODIS) [1], ESA's Medium Resolution Imaging Spectrometer (MERIS) [8] or NASDA's Global Imager (GLI) [12]. First attempts to exploit measurements of the sun-induced chlorophyll fluorescence (SICF) in terms of the chlorophyll concentration were made in the late seventies [13] using baseline techniques to extract the fluorescence signal from measured radiance or irradiance spectra. Due to the chlorophyll-*a* absorption band around 675 nm in the vicinity of the chlorophyll-*a* fluorescence maximum around 685 nm, the main difficulty with these techniques is the choice of an appropriate baseline. Theoretical studies using radiative transfer simulations have been performed with the aim to find the optimal baseline [5]. However, as stated in the latter reference, the baseline technique may give poor re-

sults in extremely turbid waters. This is confirmed by a recent study [8]. Besides, the established relationships between the SICF and the chlorophyll content do often not account for the natural variability of the chlorophyll fluorescence efficiency, the spectral absorption of algae and intracellular re-absorption, which may in reality span over about one order of magnitude [3].

Despite the above mentioned difficulties, measurements of the SICF are a promising method towards a more accurate spaceborne determination of chlorophyll-*a* in case-II waters. In contrast to the existing methods, we try to explicitly consider all processes governing the amount of upward directed SICF just below the sea surface. In order to derive the parameterisations required for such purpose, a measurement programme was initiated with the aim to gather the relevant *in situ* data. The measurements took place in different European waters in 1997 and 1998 covering wide concentration ranges of phytoplankton, non-chlorophyllous particles and CDOM. The measurements are used to derive an algorithm relating the SICF to the combined chlorophyll-*a* and phaeopigment content in the topmost water layer. Reasons for the natural variability of the SICF are investigated and the range of applicability of the presented algorithm is indicated.

1 Study sites

The data presented in this work stem from seven major ship- and helicopter-based oceanographic campaigns carried out between spring 1997 and autumn 1998 in the North Sea, English Channel, North Eastern Atlantic Ocean, Baltic Sea, Adriatic Sea, Lions Gulf and Eastern Alboran Sea (Figure 1). During the mentioned cruises, a total of about 460 stations have been visited in different seasons of the year (Table 1). At each station, radiometric *in situ* measurements have been performed which were complemented by *in vivo* and *in vitro* laboratory measurements on simultaneously taken surface water samples. The sampling strategy was such as to cover the broadest possible range of the natural variability within the test areas at the respective season.

*ACRJ - LPCM - SA1 - U. Oldenburg
NIOZ - U. Trondheim - FUB - PML - GKSS*

2 Methods

2.1 Modelling the sun-induced chlorophyll fluorescence

The sun-induced chlorophyll fluorescence (SICF) is an inelastic scattering process where a portion of the light absorbed by chlorophyll molecules or accessory pigments is shortly thereafter re-emitted at wavelengths around 685 nm. The rate of sun-induced chlorophyll-*a* fluorescence dF [Quanta m⁻² s⁻¹] emitted by a thin layer of seawater of the geometrical thickness dz into the upper hemisphere can be expressed as [3,4]:

$$dF_{up} = 0.5 \text{ PAR} [Chl_a] \bar{a}_{ph}^* Q_a^* f_{PS2} \phi_F dz, \quad (1)$$

where PAR is the photosynthetically available radiation [Quanta m⁻² s⁻¹], $[Chl_a]$ is the concentration of chlorophyll-*a* [mg m⁻³], \bar{a}_{ph}^* is the mean specific absorption coefficient of phytoplankton [m² (mg Chl_{*a*})⁻¹], Q_a^* is a dimensionless factor accounting for the intracellular re-absorption of chlorophyll fluorescence, f_{PS2} is the fraction of absorbed light transferred into photosystem 2, and ϕ_F is the quantum efficiency of fluorescence [Quanta emitted (Quanta absorbed)⁻¹]. Here, it is assumed that the SICF is isotropic and therefore half of the SICF generated inside dz is emitted into the upper hemisphere. This assumption is reflected by the factor 0.5 in Eq. (1). In order to obtain the SICF signal just below the sea surface, a vertical integration of Eq. (1) is required. In this work, we assume all quantities except PAR as independent with depth. The depth dependence of PAR is represented by:

$$\text{PAR}(z) = \text{PAR}(0^-) \exp\{-K_{\text{PAR}} \times z\}, \quad (2)$$

where $\text{PAR}(0^-)$ is the photosynthetically available radiation just below the sea surface and K_{PAR} is the diffuse attenuation coefficient for PAR. Upward directed SICF generated at the depth level z is attenuated on its way towards the sea surface according to:

$$dF_{up}(0^-) = dF_{up}(z) \exp\{-K_F \times z\}, \quad (3)$$

*ACRJ - LPCM - SAI - U. Oldenburg
 NIÖZ - U. Trondheim - FUB - PML - GKSS*

where K_F is the diffuse attenuation coefficient for SICF. Introducing Eqs. (2) and (3) into Eq. (1) and performing the integration over the whole water column gives:

$$F_{up}(0^-) = PAR(0^-) [Chla] \bar{a}_{ph}^* Q_a^* f_{PS2} \phi_F \frac{0.5}{K_{PAR} + K_F} \quad (4)$$

Of all quantities in Eq. (4), only $F_{up}(0^-)$ and $PAR(0^-)$ are directly accessible to airborne or spaceborne measurements. However, the other quantities are equally required to allow the remote determination of the chlorophyll-*a* concentration using the SICF. We therefore propose simple parameterisations of these quantities based as far as possible on measurements, or, where these are not available, on previously published results.

2.2 Definitions

2.2.1 SICF effective depth

Even for a vertically homogenous ocean, the two parameters \bar{a}_{ph}^* and K_{PAR} in Eq. (4) are depth dependent. In order to derive simple parameterisations for these parameters, an effective depth has to be defined at which these parameters are determined. Here, we propose the depth

$$z_{685} = [K_d(685)]^{-1} \quad (5)$$

as representative for the quantities \bar{a}_{ph}^* and K_{PAR} .

2.2.2 Photosynthetically available radiation

The photosynthetically available radiation (PAR) is defined as the number of photons in the spectral range between 400 nm and 700 nm per unit time on a spherical unit area:

$$PAR(z) = \int_{400}^{700} \dot{E}_Q(z, \lambda) d\lambda, \quad (6)$$

where $\dot{E}_Q(z, \lambda)$ is the spectral scalar irradiance expressed in Quanta $m^{-2} s^{-1} nm^{-1}$. The PAR is obtained by transforming the measured spectral scalar irradia-

ances in $\text{W m}^{-2} \text{ nm}^{-1}$ into the corresponding number of photons:

$$PAR(z) = \frac{1}{hc} \int_{400}^{700} \overset{\circ}{E}(z, \lambda) \lambda d\lambda, \quad (7)$$

where $\overset{\circ}{E}(z, \lambda)$ is the spectral irradiance expressed in $\text{W m}^{-2} \text{ nm}^{-1}$, $c = 3.00 \times 10^8 \text{ m s}^{-1}$ is the speed of light and $h = 6.34 \times 10^{-34} \text{ J s}$ is Planck's constant.

2.2.3 Mean specific absorption coefficient of phytoplankton

The mean specific absorption coefficient of phytoplankton \bar{a}_{ph}^* states how much of the incident light energy is stored by the cell per unit PAR and unit chlorophyll concentration:

$$\bar{a}_{ph}^*(z) = \frac{\int_{400}^{700} a_{ph}^*(\lambda) \overset{\circ}{E}_Q(\lambda, z) d\lambda}{PAR(z)} \quad (8)$$

Since it depends on the spectral distribution of phytoplankton absorption and PAR, its value changes with depth.

2.3 Intracellular re-absorption

A portion of the SICF is internally re-absorbed before leaving the cell. The probability of internal re-absorption inside the cell depends on the geometrical distribution and pigment content of the chloroplasts. In order to quantify the intracellular re-absorption, a dimensionless factor Q_a^* is introduced indicating the fraction of the SICF which finally leaves the cell. According to its definition, Q_a^* may theoretically adapt values from 0 to 1.

2.4 Light transfer into photosystem 2

Chlorophyll fluorescence is produced in photosystem 2. The fraction of absorbed light transported from photosystem 1 to photosystem 2 is given by the dimension-

ACRJ - LPCM - SAI - U. Oldenburg
 NIÖZ - U. Trondheim - FUB - PML - GKSS

less factor f_{PS2} . In this work, we have assumed a constant value of

$$f_{PS2} = 1.0 , \quad (9)$$

since the probability of light transport from photosystem 1 to photosystem 2 is implicitly contained in the quantum efficiency of *in vivo* chlorophyll-*a* fluorescence ϕ_F .

2.5 Quantum efficiency of chlorophyll fluorescence

The quantum efficiency of *in vivo* chlorophyll-*a* fluorescence ϕ_F is below its maximal value due to photochemical and non-photochemical quenching processes. The variations of ϕ_F observed in the marine environment may span over an order of magnitude[9,2].

3 Data processing

3.1 Radiometric measurements

In situ profiles of the upward and downward vector irradiances in the water column as well as measurements of the vector irradiance incident on the sea surface have been performed with the SPMR profiler and SMSR surface reference (SN 0006) of Satlantic Inc. (Halifax, Canada), respectively. Both instruments measure at 13 spectral channels of 10 nm full bandwidth between 412 nm and 865 nm. Included is a channel centred at 683 nm to measure the SICF. A number of ancillary instruments is connected to the profiler: a high precision pressure sensor of Paroscientific Inc. ($\Delta p \approx 1$ cm), a conductivity and a temperature probe as well as an altimeter to determine the height above the ocean ground. Internal sensors measure the tilt of the profiler and the surface reference. Data are taken at a rate of 6.0 Hz. Assuming a vertical speed of 0.5 m/s, the obtained vertical resolution is on the order of 0.1 m. The profiler was deployed from a ship either using a winch (COASTIOOC 1 and 4), or in the free-falling mode (ALMOFRONT 2 and COASTIOOC 5), or using a helicopter as sampling platform (COASTIOOC 2, 3 and 6). The helicopter has proven to be a very suitable platform for radiometric measurements in coastal

zones. If flown sufficiently high (between 15 m and 100 m above the sea surface depending on the wind speed), the measurements are neither disturbed by shadowing nor by the effects of the rotor downwind on the sea surface. The radiometer is in a vertical position from the beginning of the cast and not only in depths from about 1-2 m as is the case in the free-falling mode. Besides, the helicopter allows a rapid displacement between the stations. During one flight of about 2.5 h, we were in the average able to visit 10 to 12 stations. Details on the experimental set-up of the helicopter-based measurements will be published elsewhere by Babin *et al.* (*in prep.*)

3.2 Processing of radiometer raw data

The processing of the radiometer raw data is done in several steps. First, raw values are transformed into physical values using the calibration coefficients provided by the manufacturers. The dark currents for each channel were derived from measurements taken in large water depths and subsequently subtracted. Since the calibration coefficients of some channels showed a considerable temporal shift between the manufacturers' calibration, correction factors were derived for each campaign by comparing irradiance measurements taken in air on bright sunny days with radiative transfer simulations.

3.2.1 Extrapolation towards the sea surface

In order to obtain accurate values of the water leaving irradiance, measurements taken in the topmost water layer are extrapolated towards the sea surface. This is done by applying an exponential model for the depth dependence of the measured spectral irradiance values. A by-product of the surface extrapolation is the diffuse attenuation coefficient K_u for upwelling irradiance. The exponential model for the vertical dependence of the light field is only valid a) in a homogeneously mixed ocean, b) in spectral domains not considerably influenced by inelastic scattering (see below), c) during stable incident irradiance conditions, d) far enough above the ground to avoid bottom effects, and e) far enough from the ship to avoid ship shadowing or similar effects. Besides, the radiometer must keep its vertical orientation during the profile in order to collect light from the same solid angle. In order to identify (and reject) measurements that do not meet the quality requirements, a suite of appropriate checks were automatically applied when processing the radio-

metric measurements. An additional visual control was applied in order to identify (and eventually reject) outliers that were not trapped by the operationally applied tests.

3.2.2 Surface extrapolation in the presence of inelastic scattering

The decrease of the upward radiance with depth can not *a priori* be approximated by an exponential in the presence of inelastic scattering processes. The upward light field for wavelengths larger than approx. 600 nm contains a non-negligible contribution of Raman scattered light, even "close" to the sea surface. In order to properly account for the effects of inelastic scattering when extrapolating towards the sea surface, we initially attempted to fit the upward irradiance measurements to a sum of two exponentials, representing the contributions of elastically scattered and inelastically scattered light, respectively. This approach worked well only when applied to measurements taken during favourable external conditions, but often failed in the presence of noise or outliers. It therefore was not applied to the operational data processing. On the other hand, radiometric profiles that passed the quality checks mentioned above showed only minor deviations from the exponential depth dependence at the considered wavelength interval between 650 nm and 710 nm sufficiently "close" to the surface. In the indicated wavelength range, "close" to the surface was defined as depth above 4 m.

3.2.3 Extracting the water fluorescence signal

In this work, a baseline technique is used to separate the chlorophyll fluorescence signal from the irradiance background. The baseline is obtained by fitting an exponential function through the water leaving irradiance values at 664 nm and 704 nm. In order to determine the total yield of the upwelling subsurface chlorophyll-*a* fluorescence, the fluorescence signal in energy-based units is converted into the corresponding spectral density of light quanta. This value is used to normalise a Gaussian distribution centred at 685 nm with $\sigma=10.6$, representing the spectral distribution of chlorophyll-*a* fluorescence[6]. The spectral distribution of fluorescence is finally integrated over the spectral range from 660 nm to 710 nm to give the contribution of the chlorophyll-*a* fluorescence in Quanta s⁻¹ m⁻² to the upward subsurface irradiance.

3.3 Calculating PAR on the sea surface

The energy available in the ocean for photosynthesis is equivalent to the downward PAR on a horizontal surface just above the sea surface minus the portion reected at the air-sea interface[10]. It has been derived from the irradiance measurements taken in air by:

$$PAR(0^-) = 0.94 \frac{1}{hc} \sum_{n=1}^N E(0^+, \lambda_n) \lambda_n \Delta\lambda_n , \quad (10)$$

where the λ_n corresponds to the spectral channels of the radiometer used for the measurements and the $\Delta\lambda_n$ are chosen such that the sum in (10) represents the wavelength interval from 400 nm to 700 nm. The factor 0.94 accounts for the loss of downwelling irradiance due to reection of direct and diffuse radiation at the sea surface. This value is a compromise for a wide range of solar zenith angles, atmospheric aerosol loads and wind speeds. However, for large solar zenith angles or high wind speeds, the loss of downwelling radiation at the sea surface is under-estimated.

3.4 Parameterisations

3.4.1 Mean specific absorption coefficient of phytoplankton

In the frame of the present study, we have determined $\bar{\alpha}_{ph}^*$ at the depth z_{685} for all stations and derived a parameterisation of $\bar{\alpha}_{ph}^*$ as function of the combined Chl-*a* and phaeophytin concentration (Figure 2):

$$\bar{\alpha}_{ph}^* = 0.022 [Chl_a]^{-0.376} . \quad (11)$$

This parameterisation agrees rather well with the one published by Babin *et al.* [3], where $\bar{\alpha}_{ph}^* = 0.0161 [Chl_a]^{-0.257}$.

ACRJ - LPCM - SA1 - U. Oldenburg
 NIÖZ - U. Trondheim - FUB - PML - GKSS

3.4.2 Intracellular re-absorption

In the frame of this study, we have used a parameterisation of the intracellular re-absorption factor Q_a^* given by Babin *et al.* [3]:

$$Q_a^* = 0.549 [Chl_a]^{-0.173}. \quad (12)$$

The above parameterisation for Q_a^* may be applied to values of $[Chl_a]$ between 0.03 mg m^{-3} and 30 mg m^{-3} .

3.5 Quantum efficiency of chlorophyll uorescence

The quantum efficiency of chlorophyll uorescence ϕ_F was not determined during the COASTIOOC campaign, neither exists there an agreed parameterisation. It is commonly known that ϕ_F experiences a significant diurnal course [3]. However, since most of the COASTIOOC data have been obtained around local noon, the full range of diurnal variations was not observed. Nevertheless, it should be kept in mind that a portion of the observed SICF variability may be due to temporal variations in ϕ_F .

3.5.1 Diffuse attenuation coefficient s

The SICF just below the sea surface depends both on the vertical distribution of PAR and the diffuse attenuation coefficient k_F at the chlorophyll uorescence wavelengths.

Measurements of the downward irradiance have been used to determine K_F . This is because the upward irradiance is strongly influenced by SICF and therefore does not properly describe the attenuation of upward irradiance at the chlorophyll uorescence wavelengths. Measurements taken in the topmost water layer were used to obtain k_F via an exponential fit.

The vertical distribution of PAR was determined from measurements of both upward and downward irradiance. In turbid waters, the upward irradiance may significantly contribute to the PAR and may therefore not be neglected. Due to the spectral dependence of the diffuse attenuation coefficient, k_{PAR} decreases with depth. In



this study, we obtain a representative value of k_{PAR} by considering the attenuation of PAR between the sea surface and the depth z_{685} :

$$PAR(z_{685}) = PAR(0^-) \exp\{-K_{PAR} \times z_{685}\}, \quad (13)$$

where $PAR(z_{685})$ is calculated from the upward and downward spectral irradiance at z_{685} .

In the frame of the present study, we have derived parameterisations of the diffuse attenuation coefficient s , K_{PAR} and K_F as functions of the combined Chl-*a* and phaeophytin concentrations. Improved parameterisations based on reectance measurements in one or more spectral channels might become available in the near future.

3.6 Laboratory analyses

The following parameters with relevance to the present study were routinely measured on surface water samples:

- spectral absorption of phytoplankton and non-chlorophyllous particles using the NaClO bleaching technique of Tassan and Ferrari [15].
- Concentration of pigments using the HPLC protocol of Vidussi et al. [16]
- SPM concentration from ltration of sea water through 0.7 μm Whatman pre-weighted GF/F filters.

4 Results

4.1 Corrected Relative Chlorophyll Fluorescence

In order to account for the processes identified as inuencing the SICF, we have introduced a new quantity, the Corrected Relative Chlorophyll Fluorescence (CRCF), dened by:

$$CRCF = \frac{F(0^-) (k_F + k_{PAR})}{0.5 \bar{a}_{ph}^* Q_a^* f_{PS2} PAR(0^-)}. \quad (14)$$

ACRJ - LPCM - SAI - U. Oldenburg
NIOZ - U. Trondheim - FUB - PML - GKSS

The CRCF may be related to the concentration of Chl-*a* via a power law:

$$CRCF = \alpha [Chl_a]^\beta , \quad (15)$$

where the coefficients α and β account for the quantum efficiency of chlorophyll fluorescence ϕ_F and other systematic effects that have eventually not properly been parameterised (geometrical effects, multiple scattering effects, etc.).

4.2 A simple SICF algorithm

When introducing the *in situ* measurements of $F(0^-)$ and $PAR(0^-)$ as well as the parameterisations of \bar{a}_{ph}^* , Q_a^* , f_{PS2} , k_F and k_{PAR} into Equation (14), and relating the CRCF to the Chl-*a* concentration via Equation (15), one obtains (Fig. 3):

$$CRCF = 0.0176 [Chl_a]^{1.245} . \quad (16)$$

The variations observed in Figure 3 result partly from using the parameterisations of the relevant parameters rather than the values directly derived from the measurements. The reason for this approach is that such measurements are not available from remote sensing data.

4.3 Estimating the quantum efficiency of chlorophyll fluorescence

A rough estimate of the quantum efficiency of chlorophyll fluorescence is implicitly contained in Equation (3). Neglecting effects due to multiple scattering and assuming the parameterisations of the other relevant quantities as correct, the value $\alpha=0.0176$ represents ϕ_F for a chlorophyll concentration of $[Chl_a] = 1 \text{ mg m}^{-3}$. This value is well within the range of the published values [2], albeit above the average.

References

- [1] M. R. Abbott and R. M. Letelier. Algorithm Theoretical Basis Document. Chlorophyll fluorescence (MODIS product number 20). Technical Report ATBD-MOD-22, NASA, Goddard Space Flight Center, 1999.

- [2] M. R. Abbott, P. J. Richerson, and T. M. Powell. *In situ* response of phytoplankton fluorescence to rapid variations in light. *Limnol. Oceanogr.*, 27:218–225, 1982.
- [3] M. Babin, A. Morel, and B. Gentili. Remote sensing of sea surface sun-induced chlorophyll fluorescence: consequences of natural variations in the optical characteristics of phytoplankton and the quantum yield of chlorophyll *a* fluorescence. *Int. J. Remote Sens.*, 17(12):2417–2448, 1996.
- [4] M. E. Culver and M. J. Perry. Calculation of solar-induced fluorescence in surface and subsurface waters. *J. Geophys. Res.*, 102:10563–10572, 1997.
- [5] J. Fischer and U. Kronfeld. Sun-stimulated chlorophyll fluorescence, 1: Inuence of oceanic properties. *Int. J. Remote Sens.*, 11(12):2125–2147, 1990.
- [6] H. R. Gordon. Diffuse reectance of the ocean: The theory of its augmentation by chlorophyll *a* fluorescence at 685 nm. *Appl. Opt.*, 18(8):1161–1166, 1979.
- [7] H. R. Gordon, D. K. Clark, J. W. Brown, O. B. Brown, R. H. Evans, and W. W. Broenkow. Phytoplankton pigment concentrations in the middle atlantic bight: Comparison between ship determinations and Coastal Zone Color Scanner estimates. *Appl. Opt.*, 22:20–36, 1983.
- [8] J. F. R. Gower, R. Doerffer, and G. A. Borstad. Interpretation of the 685 nm peak in water-leaving radiance spectra in terms of fluorescence, absorption and scattering, and its observation by MERIS. *Int. J. Remote Sens.*, 20(9):1771–1786, 1999.
- [9] D. A. Kiefer. Fluorescence properties of natural phytoplankton populations. *Marine Biology*, 22:1816–1824, 1973.
- [10] A. Morel. Light and marine photosynthesis: a spectral model with geochemical and climatological implications. *Prog. Oceanogr.*, 26:263–306, 1991.
- [11] A. Morel and L. Prieur. Analysis of variations in ocean colour. *Limnol. Oceanogr.*, 22(4):709–722, 1977.
- [12] NASDA. GLI homepage. <http://www.eorc.nasda.go.jp/ADEOS-II/GLI/index.html>, 1999.
- [13] R. A. Neville and J. F. R. Gower. Passive remote sensing of phytoplankton via chlorophyll *a* fluorescence. *J. Geophys. Res.*, 82(6):3487–3493, 1977.
- [14] J. E. O'Reilly, S. Maritorena, B. G. Mitchell, D. A. Siegel, K. L. Carder, S. A. Garver, M. Kahru, and C. McClain. Ocean color chlorophyll algorithms for SeaWiFS. *J. Geophys. Res.*, 102(C11):24937–24953, 1998.
- [15] S. Tassan and M. Ferrari. An alternative approach to absorption measurements of aquatic particles retaines on lters. *Limnol. Oceanogr.*, 40(8):1358–1368, 1995.



Final Report
ENV4-CT96-0310
03 January 2000

Page: 221

- [16] F. Vidussi, H. Claustre, J. Bustillos-Guzmàn, C. Cailliau, and J.-C. Marty. Rapid hplc method for determination of phytoplankton chemotaxonomic pigments: separation of chlorophyll *a* from divinyl-chlorophyll *a* and zeaxanthin from lutein. *J. Plankton Res.*, 18:2377–2382, 1996.

Table 1

Measurement campaigns providing data for the present study. C1 to C6 stand for COAST-
IOOC 1 to COASTIOOC 6, A2 stands for ALMOFRONT 2.

Campaign	Sampling Platform	Area	Period	Stations
C1	FS Victor Hensen	North Sea, North-East Atlantic Ocean	04/97	46
C2	Helicopter	Lions Gulf	07/97	15
C3	Helicopter	Northern Adriatic Sea	07/97 08/97	40
C4	N/O Thétys 2	Lions Gulf	09/97- 10/97	48
A2	N/O L'Atalante	Eastern Alboran Sea	12/97- 01/98	41
C5	FS Poseidon	Biscay Bay, English Channel, North Sea	05/98	60
C6	Helicopter	English Channel, North Sea, Baltic Sea	09/98	178

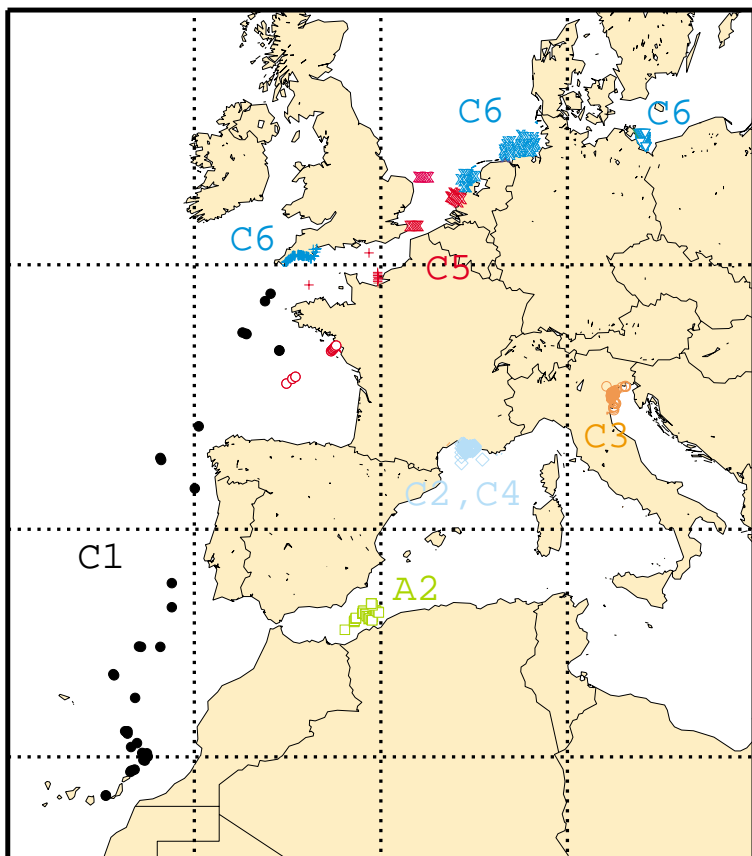


Fig. 1. Geographic location of the stations visited during the oceanographic campaigns COASTIOOC 1 to COASTIOOC 6 (C1-C6) and ALMOFRONT 2 (A2).

¹⁸
ACRJ - LPCM - SAI - U. Oldenburg
NIOZ - U. Trondheim - FUB - PML - GKSS

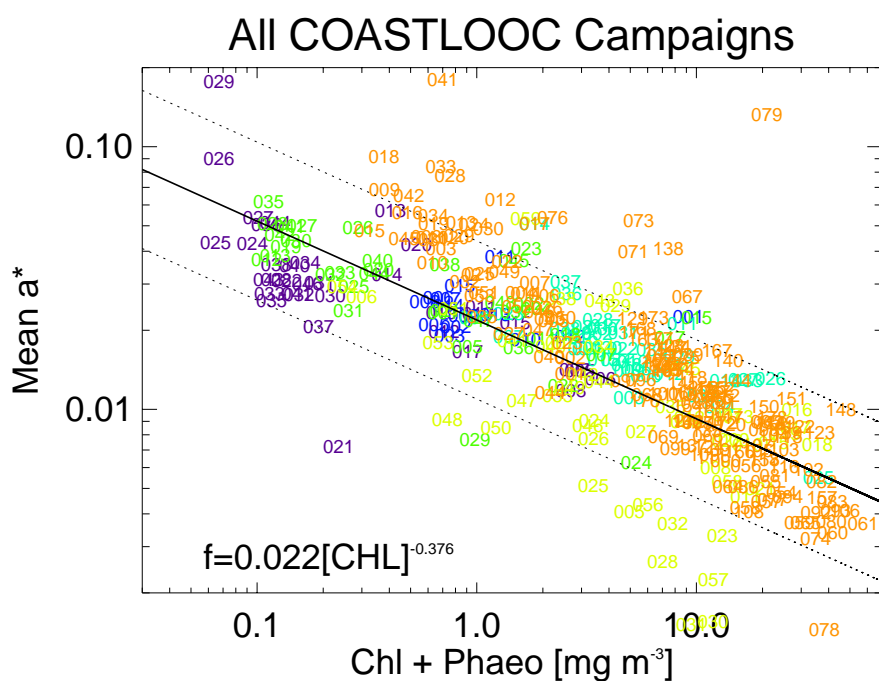


Fig. 2. Parameterisation of the mean specific absorption coefficient \overline{q}_{ph}^* as function of the concentration of Chl_a and phaeophytin obtained from the COASTLOOC campaigns.

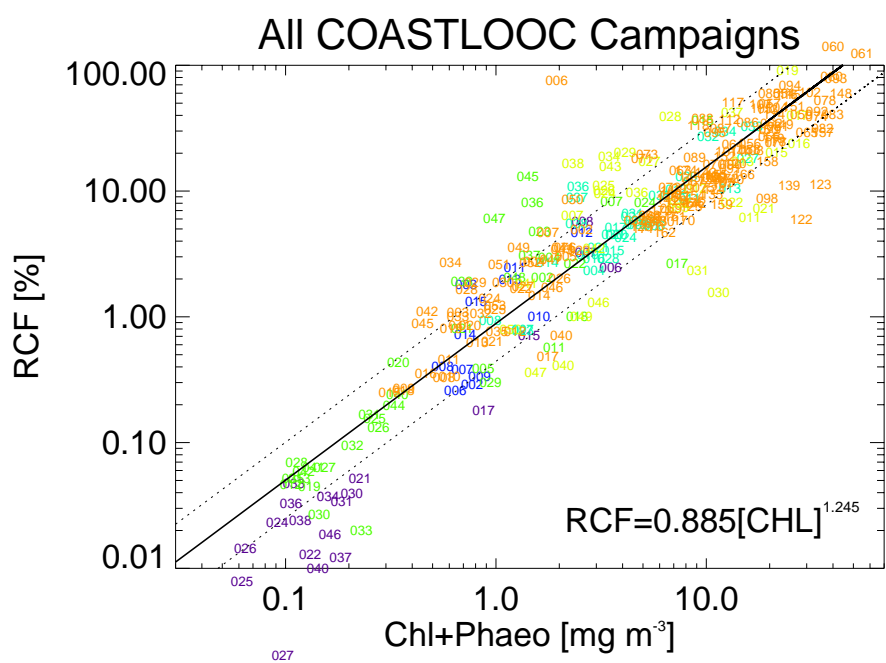


Fig. 3. Algorithm relating the Corrected Relative Chlorophyll Fluorescence (CRCF) to the concentration of *Chla* and phaeophytin.

6.2. COMPARISON BETWEEN MEASUREMENTS PERFORMED WITH THE CORE INSTRUMENT PACKAGE AND THE PML INSTRUMENTS DURING COAST/OOC-6.

6.2.1. Introduction

This report summarises work carried out at Plymouth Marine Laboratory (PML) as part of the European Union funded COAST/OOC project (Coastal Surveillance through Observation of Ocean Colour). PML involvement in COAST/OOC is in two main areas: participation in the *in situ* fieldwork campaign and bio-optical modelling and the development of band-ratio algorithms to retrieve various bio-optical parameters from remotely-sensed ocean colour data of the European coastal region.

6.2.2. In-situ Fieldwork

6.2.2.1. Helicopter Campaign

COAST/OOC fieldwork was conducted from four bases around Europe through September 1998. The first base visited was PML between 30 August and 7 September 1998. PML was responsible for logistic and organisational support of the COAST/OOC team during this period. The COAST/OOC water-analysis and computing equipment were established at the West Hoe site. PML facilitated the flying of the COAST/OOC helicopter to deploy the instrument along the south UK coast between Helford and Exmouth. Despite poor weather, the helicopter flew for 18 hours and 56 stations were visited. At each station, the inherent and apparent optical properties of the water were measured and water samples were collected for analysis of the optically-active constituents.

6.2.2.2. PML Sampling

In order to increase the quantity of *in situ* sampling taken during the helicopter campaign at Plymouth, the PML research vessel *Squilla* worked along the south UK coast during the same period, visiting 16 stations in four days (Table 25). Two scientists used the PML optical profiler to measure inherent and apparent optical properties and analysed water samples for the optically-active constituents. The measurements made at each station were:

- Profiled underwater spectral upwelling radiance (7 band Satlantic radiometer).
- Profiled underwater downwelling irradiance (7 bands Satlantic radiometer).
- Profiled underwater upwelling irradiance (7 bands Satlantic radiometer).
- CTDF (conductivity, temperature, depth and *in situ* chlorophyll fluorescence).
- Profiled attenuation-absorption using a Wetlabs ac-9.
- Phytoplankton pigment concentration by HPLC.

*ACRJ - LPCM - SAI - U. Oldenburg
NIOZ - U. Trondheim - FUB - PML - GKSS*

- Total suspended matter concentration.
- Coloured Dissolved Organic Matter (CDOM) absorption spectrum.
- Organic particulate matter absorption and detrital particulate matter absorption.
- Particle size distribution by Coulter Counter.

Table 25. Summary of sites visited by Squilla during September 1998.

Date	Location	Latitude N	Longitude W	Water depth (m)
01/09/98	Bigbury Bay	50°16.44	03°53.85	12
01/09/98	Salcombe Harbour	50°13.00	03°46.40	11
01/09/98	Mouth of River Dart	50°20.31	03°33.43	11
01/09/98*	Start Bay	50°17.00	04°34.00	20
02/09/98*	Off Dawlish Warren	50°35.00	03°25.00	14
02/09/98	Mouth of River Exe	50°36.09	03°22.14	8
02/09/98	Off Teignmouth	50°32.10	03°28.30	14
02/09/98	Mouth of River Teign	50°32.45	03°28.90	8
03/09/98*	Whitsand Bay	50°19.76	04°14.50	14
03/09/98	Mouth of Looe	50°02.90	04°26.50	10
03/09/98	Off Looe	50°19.85	04°25.14	20
03/09/98*	Off Seaton	50°19.42	04°22.98	20
04/09/98	Plymouth Breakwater	50°20.08	04°08.33	10
04/09/98	Jennycliff	50°20.86	04°07.66	19
04/09/98	West of Drake's Island	50°21.24	04°09.80	30

ACRJ - LPCM - SAI - U. Oldenburg
 NIÖZ - U. Trondheim - FUB - PML - GKSS



Final Report
ENV4-CT96-0310
03 January 2000

Page: 228

04/09/98	King Billy's Statue	50°21.78	04°10.66	30
----------	---------------------	----------	----------	----

Notes: * indicates sampling adjacent to the COAST/OOC helicopter.

6.2.3. PML Data Processing

These data have all been calibrated, processed and delivered to the COAST/OOC data manager for inclusion into the final project database. The Level 1 radiometric data (radiance and irradiance values) have been processed to Level 2 data and submitted to the database. The Level 2 radiometric data are:

- Upwelling radiance just below the sea surface.
- Downwelling irradiance just below the sea surface.
- Diffuse upwelling and downwelling attenuation coefficients.
- Normalised water leaving radiance.
- Remote-sensing reflectance.

Smoothed, quality controlled and 1 m-averaged underwater data have also been submitted.

6.2.4. Comparison between PML and Helicopter Data

The agreement between radiometric measurements made by the PML optical profiler from *Squilla* and adjacent measurements by the COAST/OOC optical profiler from the helicopter are good given the heterogeneity of the water bodies sampled. The spectral diffuse attenuation coefficients differ by an average of 15% in the range 412-555 nm (Figure 123). Irradiance reflectance differs by an average of 24% over the same spectral range (Figure 124). These differences are generally within the range of variation observed during sampling at a given station. The agreement between total suspended matter concentrations and chlorophyll-a concentrations are difficult to quantify given the low number of points (Figure 125), but model-2 regressions fall close to the 1:1 line.

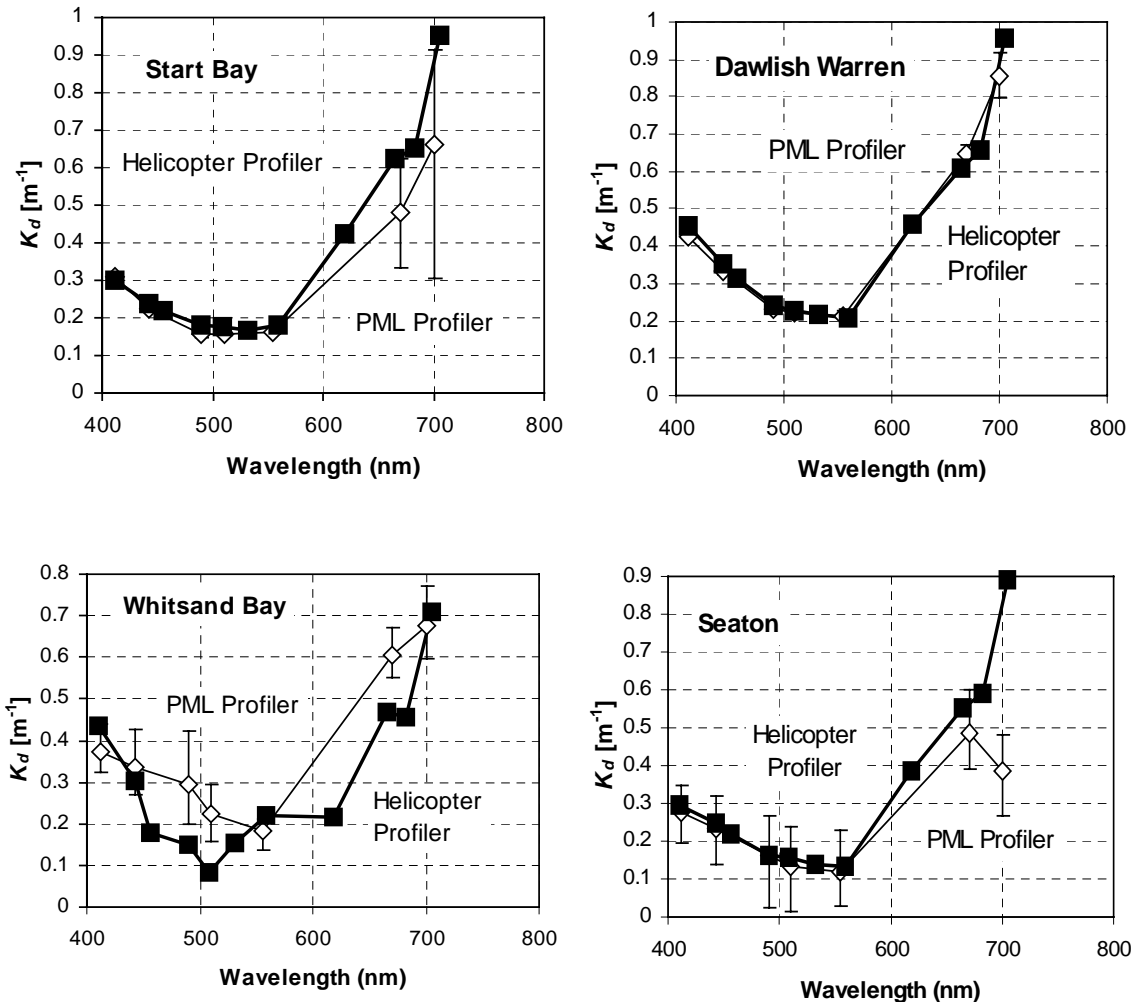


Figure 123. Comparison between adjacent measurements of the diffuse attenuation coefficient from the PML optical profiler from Squilla and the COAST/OOC optical profiler from the helicopter

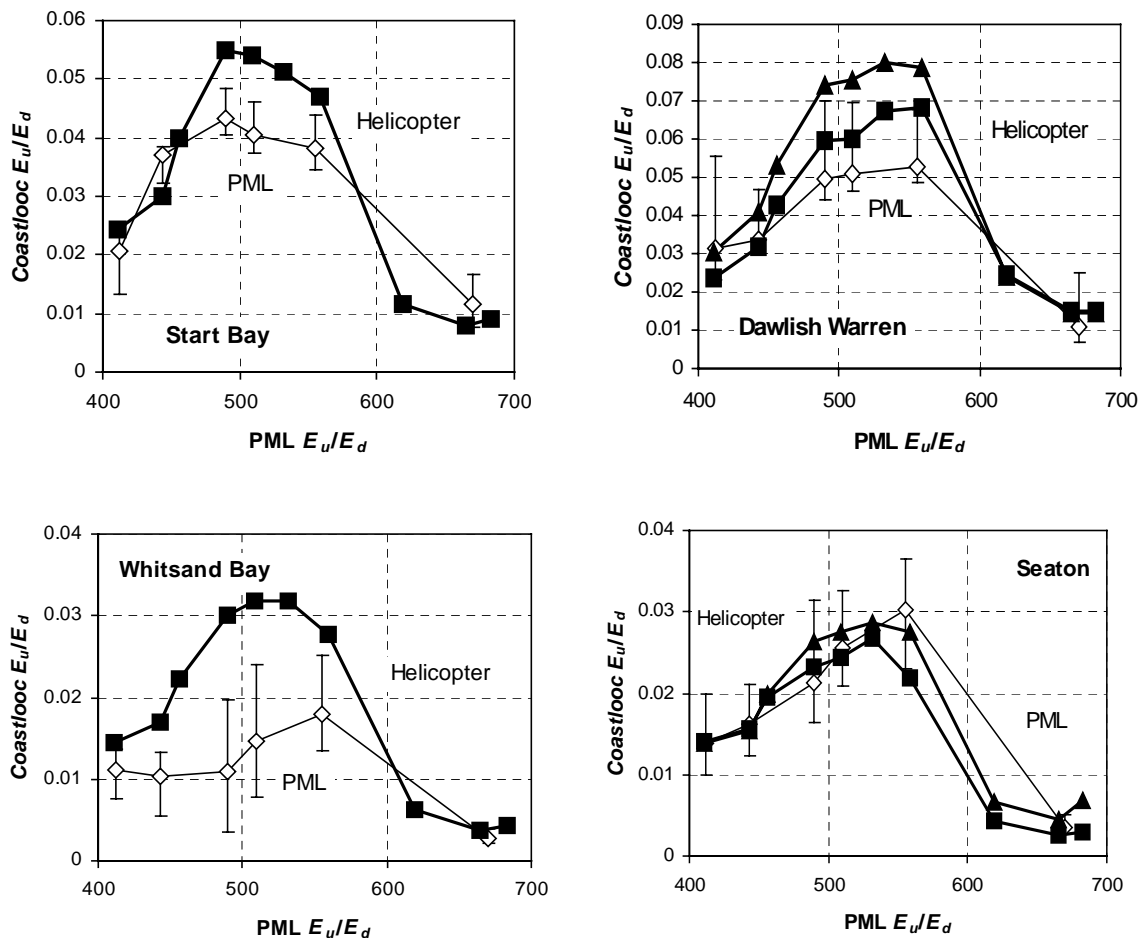


Figure 124. Comparison between adjacent measurements of irradiance reflectance from the PML optical profiler from Squilla and the COAST/OOC optical profiler from the helicopter

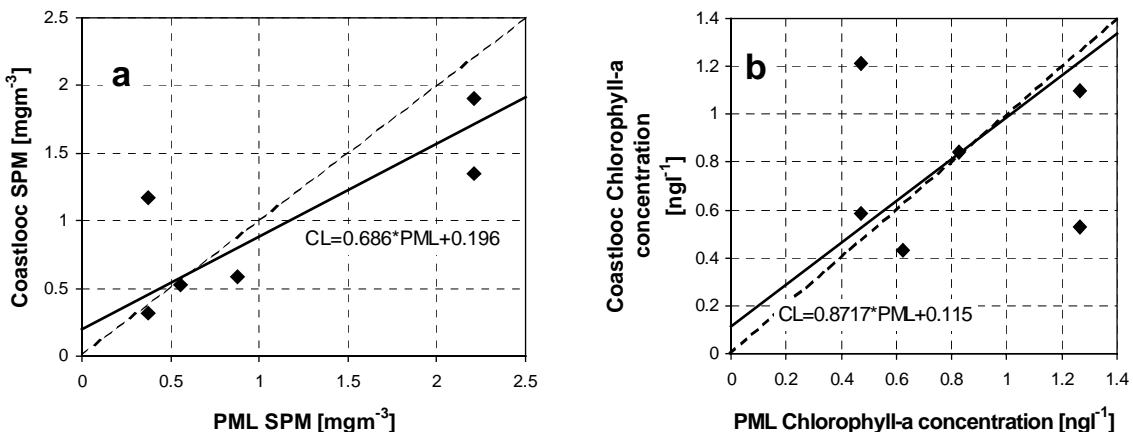


Figure 125. Comparison between adjacent water samples collected from Squilla and analysed at PML and collected from the helicopter and analysed by the COAST/OOC fieldwork team. **a:** Total suspended matter concentration. **b:** Chlorophyll-a concentration.

6.3. PUBLICATIONS

6.3.1. Papers

- Claustre, H., Fell, F., Oubelkheir, K., Prieur, L. Sciandra, A., Gentilli, B. and M. Babin. 1999. Continuous monitoring of surface optical properties across a geostrophic front: biogeochemical inferences. *Limnology and Oceanography, in press*.
- Stelvio Tassan, Giovanni Massimo Ferrari, Annick Bricaud and Marcel Babin. 1999. Variability of the amplification factor of light absorption by filter-retained aquatic particles in the coastal environment. *Journal of Plankton Res. In press*.
- Giovanni M. Ferrari. 2000. The relationship between Chromophoric Dissolved Organic Carbon in European Atlantic Coastal Areas and in West-Mediterranean Sea (Gulf of Lions). *Marine Chemistry, In press*.
- Johnsen, Geir & Samset, O. Bio-optical taxonomy in phytoplankton: Field and laboratory studies of potential harmful algal blooms (in preparation).
- Johnsen, G., Chauton, M. Ferrari, M., Fell, F. Bio-optical and pigment signature as a function fresh water run off and phytoplankton distribution (in preparation).
- Babin, M., Ferrari, M., Fell, F., Obolensky, G., Fournier-Sicre, V. & Claustre H. Parametrerisation of the absorption coefficient in coastal waters. *In preparation*.
- Babin, M., Fell, F., Obolensky, G. & Fournier-Sicre, V. Parametrerisation of the scattering coefficient in coastal waters. *In preparation*.

ACRJ - LPCM - SAI - U. Oldenburg
NIOZ - U. Trondheim - FUB - PML - GKSS

Babin, M., Fell, F., Antoine, D., Ferrari, M., Montagner, F. & Morel, A. A reflectance model for coastal waters. *In preparation.*

6.3.2. Theses

Barth, H. 1999. Substanzspezifische Analyse spektraler Attenuationskoeffizienten und ihr Einfluß auf das Strahlungsfeld im Meer. PhD Thesis, Carl von Ossietzky Universität Oldenburg

Schröder, M. 1999. Beiträge durch Fluoreszenz und Raman- Streuung zum Spektrum des Tageslichtes im Ozean.

Diploma Thesis, Carl von Ossietzky Universität Oldenburg.

Loisel, H. 1999. Contribution à l'étude des propriétés bio-optiques et du transfert radiatif dans l'océan: applications. Doctorate Thesis, Université Pierre et Marie Curie.

Obolensky, G. 1997. Etude du coefficient de rétrodiffusion de l'eau de mer et de ses variations en fonction de la concentration en particules. Diplôme d'Etudes Approfondies, Université Pierre et Marie Curie.

Lemasle, B. 1998. Propriétés optiques des eaux côtières: Bi-directionalité de la réflectance. Diplôme d'Etudes Approfondies, Université Pierre et Marie Curie.

6.3.3. Conference papers and abstracts

Claustre, H., Fell, F., Oubekheir, K., Prieur, L. and A. Sciandra. 1998. Multivariate, bio-optical investigation of a frontal system in the Mediterranean Sea. SPIE Ocean optics XIV, Hawaii, November 1998. (poster + abstract)

Barth, H., Heuermann, R. & Reuter, R. 1977. *In situ* analysis of Water Quality - Spectral Attenuation and Fluorescence; In: Giovanna Gecchi, Thorsten Lamp, Rainer Reuter, Conraddin Weber; Proceedings of Remote Sensing of Vegetation and Water, and Standardization of Remote Sensing Methods; SPIE Proceedings Series Vol 3107; 1997; p. 187 - 194.

Barth, H. 1999. Influence of Gelbstoff, Chl_a and Mineral Particles on the light field in coastal and oceanic waters. EnviroSens (Environmental Sensing and Application). München June 1999.

Conference talks

Fell, F., Babin, M., Ferrari, M. & Obolensky, G. 1999. The potential of chlorophyll fluorescence for the space-borne retrieval of phytoplankton in European coastal and open ocean waters. In IGARSS'99, IEEE International Geoscience and Remote Sensing Symposium, 28 June - 2 July, Hamburg, Germany, 1999.

6.4. FORMATION

The following table indicate the persons that were trained in the frame of COAST/OOC.

NAME	State	Level	Supervisor	Involvement
F. FELL	(DE)	postdoc	LPCM	All postdoc period in the frame of COAST/OOC. He took part to <i>in situ</i> measurements (all campaigns), data processing (development of SADAM, Section 2.2.3.2.1), and data interpretation (paper on the use of the fluorescence signal to detect phytoplankton, Section 0).
E. ROUSSIER	(F)	Ing.	LPCM	He did his Engineer training during COAST/OOC-6, which last 1 month. He took part to <i>in situ</i> measurements and learned basic knowledge on marine optics.
F. LAHET	(F)	Dr.	LPCM	She took part to COAST/OOC-4 and COAST/OOC-5 campaigns, and learned different laboratory analyses. She exploited COAST/OOC data for validating an inversion technique for the estimation of the marine particle refraction index.
H. BARTH	(DE)	Dr.	U. Oldenburg	He did his Ph. D. in the frame of COAST/OOC. He took part to COAST/OOC campaigns n° 1, 4, 5 and 6. He developed an inversion method for the estimation of IOPs (Section 2.2.3.1).
C. OLBERT	(DE)	Dr.	FUB	He supervised and conducted CASI flights, and then performed the Level 1 processing (Section 2.5.2) of CASI data.
G. OBOLENSKY	(F)	M.Sc.	LPCM & ACRI	He took part to most field campaigns and performed many of the laboratory analyses. After his M. Sc., he got a permanent position at ACRI S.A. as junior Engineer. He then supervised the development of the COAST/OOC data base (Section 2.2.3.3).
V. FOURNIER-SICRE	(F)	Ing.	ACRI	As a junior engineer, he took part to several field campaigns (chief scientist during COAST/OOC-4) and developed the processing tool for multiple instrument data acquisition (Section 2.2.3.1). He also took part to the design of the core instrument package and helicopter operations.
K. OUBELKHEIR	(F)	Dr.	LPCM	She took part to COAST/OOC campaigns n° 2 and 3 and learned some of the laboratory analyses.
M. CHAUTON	(NO)	Dr.	U. Trondheim	She took part to the COAST/OOC-5 campaigns and performed all phytoplankton species composition analyses (Section 2.3.2).
M. PINKERTON	(UK)	Dr.	PML	He was in charge of the local organisation of the helicopter surveys and organised simultaneous ship measurements (Section 6.2.4).
M. DOWELL	(UK)	postdoc	SAI/JRC	He used COAST/OOC data for the development of an ocean colour algorithm (Section 2.5.1.3).
H. HAKVOORT	(NL)	postdoc	GKSS	He took part to the COAST/OOC-5 campaigns during which he performed <i>in situ</i> optical measurements.
B. LEMASLE	(F)	M.Sc.	LPCM	He developed an IDL tool for the processing and interpretation of AC-9 and BB-4 vertical profiles (Section 2.2.3.2.2).
D. DOXARAN	(F)	M.Sc.	LPCM	He developed an IDL tool for the processing and interpretation of AC-9 and BB-4 vertical profiles (Section 2.2.3.2.2).

6.5. DATA CDs

A new version of the COAST/OOC data CD is delivered with the current report. See Section 2.2.3.3 for a description of this CD and the different “readme” on the CD.

ACRI - LPCM - SAI - U. Oldenburg
NIOZ - U. Trondheim - FUB - PML - GKSS